UNIVERSIDADE FEDERAL DO RIO DE JANEIRO
Instituto de Química
Programa de Pós-Graduação em Ciência de Alimentos

BIOACTIVE MICRO-STRUCTURED LIPID CARRIERS FOR INCORPORATION IN BIODEGRADABLE FILMS FOR POTENTIAL FOOD APPLICATION

BÁRBARA ELISABETH TEIXEIRA COSTA

RIO DE JANEIRO
2021

BÁRBARA ELISABETH TEIXEIRA COSTA

BIOACTIVE MICRO-STRUCTURED LIPID CARRIERS FOR INCORPORATION IN BIODEGRADABLE FILMS FOR POTENTIAL FOOD APPLICATION

Doctoral Thesis presented to the Graduate Program in Food Sciences, Institute of Chemistry, Federal University of Rio de Janeiro, as requirements for obtaining the title of Doctor of Science (Food)

Advisor: Prof. Dr. Cristina Tristão de Andrade

RIO DE JANEIRO
August, 2021

CATALOG FORM

CIP - Catalogação na Publicação

TT266b
b

Teixeira-Costa, Bárbara Elisabeth
Bioactive micro-structured lipid carriers for incorporation in biodegradable films for potential food application / Bárbara Elisabeth Teixeira Costa. -- Rio de Janeiro, 2021.
232 f.

Orientador: Cristina Tristão de Andrade.
Tese (doutorado) - Universidade Federal do Rio de Janeiro, Instituto de Química, Programa de Pós Graduação em Ciência de Alimentos, 2021.

1. Chitosan-based coacervates. 2. Biobased composite films. 3. Antioxidant food packaging. 4. Coacervates. 5. Food Hydrocolloids. I. Tristão de Andrade, Cristina, orient. II. Título.

Elaborado pelo Sistema de Geração Automática da UFRJ com os dados fornecidos pelo(a) autor(a), sob a responsabilidade de Miguel Romeu Amorim Neto - CRB-7/6283.

APPROVAL SHEET

Bárbara Elisabeth Teixeira Costa

BIOACTIVE MICRO-STRUCTURED LIPID CARRIERS FOR INCORPORATION IN BIODEGRADABLE FILMS FOR POTENTIAL FOOD APPLICATION

Doctoral Thesis presented to the Graduate Program in Food Sciences, Institute of Chemistry, Federal University of Rio de Janeiro, as requirements for obtaining the title of Doctor of Science (Food).

Approved by

Professor Cristina Tristão de Andrade, PhD/UFRJ

Professor Carlos Adam Conte Júnior, PhD/UFRJ

Professor Ana Elizabeth Cavalcante Fai, PhD/UERJ

Professor Anderson Junger Teodoro, PhD/UNIRIO

Professor Edwin Elard Garcia Rojas, PhD/UFF

RIO DE JANEIRO

August, 2021

IN DEDICATION TO

I dedicate this work to the extraordinary and lovely women in my family.

To my grandmother Elisa*, in memoriam*, who was a brave woman, dedicated to her family and graduated in Pedagogy at the age of 43 years old.

To my mother Sheylla, who is a caring mother, always encouraged me to study and to be a dedicated professional and professor like her.

To my sister Nathalia, who is a courageous woman for pursuing her dreams, even when so many have told her otherwise, for being herself and always caring for others.

And, finally, to my dearest daughter Mariana, who is the reason for my life. For her, I want to be a good example of a person, mother, professor, and scientist. That maybe one day she will be as proud as I am of her now. That maybe one day she will be proud to say that her mother is doing science in Brazil in search of a better world.

ACKNOWLEDGMENTS

I acknowledge to my advisor, who encourages, challenges, teaches, and helps me to achieve excellent results. I am pleased to have worked with and learned immensely. Thank you, Professor Cristina T. Andrade, for all your advices.

I would like to thank my family, Valdir and Mariana. You are my world! I could not get done this thesis without your unconditional love, patience, comprehension and support through all difficulties, hours of dedicated study and as well as on every happy times. You have courageously accompanied me in every moment of success and challenges, including going to another country during my international PhD internship. My lovely husband, you never let me chill out on this, you were always pushing me forward. My beautiful daughter, you are so brave! I am so proud of you!

I am grateful to thank my mom, dad, sister and brother. Your support, encouragement and love have guided me to trill a better way. I am here because of your caring motivation. To all my relatives, my carious thanks. You have help me so many times, thus, I was able to dedicate myself to this thesis.

I acknowledge to all my laboratory colleagues who helped me so many times. Guided me on using different softwares, equipments, and techniques, which were important to achieve good results. All of you help me on lab procedures and shared happy times. I am flattered to have worked with you.

I would like to thank my supervisors, Professor Brent Murray and Francisco Goycoolea, at the University of Leeds, Leeds, UK, and to all their other students and lab technician teams. Both of you have always been interested in listening to my achievements. I am very honored to have worked with you and to be part of your team. You guided me in a truly kind way. I learned a lot, and for that I am grateful.

I am honored to be part of the Graduate Program in Food Science at the University of Rio de Janeiro (PPGCAL/UFRJ). I would like to thank all Professors and colleagues from this for a great experience.

I acknowledge to all colleagues at the Federal University of Amazonas for supporting me in carrying out this thesis.

I also would like to thank to Coordenação de Aperfeiçoamento de Pessoal de Nível Superior - CAPES for the scholarship support during my PhD and the international internship at the University of Leeds, through the project CAPES/PRrInt. This study was financed in part by CAPES – Brasil – Finance code 001.

EPIGRAPH

"*You must really understand how I regard art. One must work long and hard to arrive at the truthful. What I want and set as my goal is damned difficult, and yet I don't believe I'm aiming too high. I want to make drawings that MOVE some people... In short, I want to reach the point where people say of my work, that man feels deeply and that man feels subtly. Despite my so-called coarseness — you understand — perhaps precisely because of it. It seems pretentious to talk like this now, but that's why I want to push on."*

From Vincent van Gogh to Theo van Gogh, at The Hague, on 21 July 1882.

PRESENTATIONS AND PUBLISHED WORKS RELATED TO THE THESIS

TEIXEIRA-COSTA, B. E.; PEREIRA, B. C. S.; ANDRADE, C. T. Encapsulación de aceite vegetal de açaí (*Euterpe oleracea*) por coacervación compleja de quitosano y alginato. Abstract published in the **XXIX Congreso Peruano de Química - La química peruana rumbo al bicentenario**, p. 90, Sociedad Química Perú, at the Colegio Químico Farmacéutico del Perú, Surco, Lima, Peru, 16–19th October 2018.

TEIXEIRA-COSTA, B. E.; PEREIRA, B. C. S.; LOPES, G. K.; ANDRADE, C. T. Production and properties of açaí pulp oil microcapsules in crosslinked alginate/chitosan as wall material. Abstract published *in* **Anais do IV Simpósio de Alimentos e Nutrição – SIAN**, at Universidade Federal do Estado do Rio de Janeiro, Rio de Janeiro, RJ, Brazil, 17–18th June, 2019.

TEIXEIRA-COSTA, B. E. Seminar entitled Biodiversity and Sustainability of Amazonian Foods and Products, presented *in* the **Food Science and Nutrition School Seminar Series** at the University of Leeds, Leeds, United Kingdom, 16th October 2019.

TEIXEIRA-COSTA, B. E. Seminar entitled Biodiversity and Sustainability of Amazonian Foods and Products, presented *in* the **Food Science and Nutrition FCB Symposium Seminar Series** at the University of Leeds, Leeds, United Kingdom, 23rd January 2020.

TEIXEIRA-COSTA, B. E.; SILVA PEREIRA, B. C.; LOPES, G. K.; ANDRADE, C. T. Encapsulation and antioxidant activity of assai pulp oil (*Euterpe oleracea*) in chitosan/alginate polyelectrolyte complexes. **Food Hydrocolloids**, 109, 106097, 2020. Available at https://doi.org/10.1016/j.foodhyd.2020.106097.

ABSTRACT

TEIXEIRA COSTA, Bárbara Elisabeth. **Bioactive micro-structured lipid carries to incorporation in biodegradable films for potential food application.** Rio de Janeiro, 2021. Thesis (Doctorate in Food Sciences) — Institute of Chemistry, Federal University of Rio de Janeiro, Rio de Janeiro, Brazil, 2021.

The main goal of this thesis was to obtain active lipid carriers by complex coacervation and incorporate them in biodegradable chitosan-based films plasticized with deep eutectic solvents (DES) based on the mixture of choline chloride:glycerol (ChCl:Gly) to potential food application. Two different systems based on chitosan (CS) and sodium alginate (SA), and CS and pea protein isolate (PPI) were formulated and optimized using the design of experiments (DOE) methodology to encapsulate açaí pulp oil (AO) and extra-virgin olive oil (EvO). The first system was investigated by a central composite design. It was formulated to study the effect of different amounts of AO (0.25 - 0.75%), and calcium chloride ($CaCl_2$) (0 – 1.0%), in the formation of CS:SA polyelectrolyte complexes (PECs). CS:SA complex formation and AO encapsulation were confirmed by optical (OM) and electron scanning microscopy (SEM), as well as infrared spectroscopy (FTIR), thermogravimetric and derivative thermogravimetric analyses (TGA/DTG). In this system, AO and $CaCl_2$ significantly influenced the size and polydispersity index (span) of the PECs, although the encapsulation efficiency (>99%) was not affected. These PECs exhibited a gel-like behavior, consistent with the complexes formation. AO and the optimum PECs (0.5% AO and 0.5% $CaCl_2$) presented high antioxidant activity, >70% by the DPPH scavenging radical. The other microencapsulation system was formulated to study the effect of CS concentration (0.39 - 1.1%) and CS:PPI ratio (0.18 - 2.31) on the formation of PECs to encapsulate EvO using a central composite design. The particles size was significantly influenced by CS:PPI ratio, whereas span was influenced by both, CS and CS:PPI ratio. The results were optimized by response surface methodology (RSM) and desirability function (D), displaying optimum conditions of 0.75% CS, 2.31 CS:PPI ratio and 0.5% EvO, and D = 0.845. The optimized particles had a small size and narrow span, ~3 μm and 2, respectively. FTIR spectra and TGA/DTG curves of the complexes have confirmed the EvO encapsulation. The CS:PPI-EvO complexes exhibited moderate

antioxidant activity, with the highest value ~117 mg Trolox equivalent (TE) L^{-1} by DPPH radical scavenging assay. As to the AO encapsulated in optimum CS/SA, PECs exhibited satisfactory physicochemical and antioxidant properties. Their incorporation in biodegradable films was evaluated. The casting method was used to produce CS-composite films plasticized with 1:2 ChCl:Gly and incorporated with different amounts (0 - 10%) of AO PECs. The OM, SEM and confocal laser scanning microscopy (CLSM) techniques were used to observe their microstructure and to confirm the presence of AO PECs. FTIR and X-ray diffraction patterns revealed interactions between CS, DES and AO PECs in the films by typical and shifted spectral bands, as well as by its decreased crystallinity (8 to 4%), respectively. The films exhibited good mechanical properties, high elongation at break > 100%, low tensile strength and Young's modulus. All films exhibited antioxidant activities by using different assays, although the highest value was determined by DPPH radical scavenging, up to 17 mg TE g^{-1} of film. This could be associated to the higher antioxidant capacity of AO, 101.8 ± 8.2 mg TE L^{-1} oil, also determined by DPPH radical scavenging assay. Furthermore, these results have demonstrated the good structural, mechanical and antioxidant properties of the CS-composite films as a potential active food packaging.

Keywords: Chitosan-based coacervates. Biobased composite films. Antioxidant food packaging.

RESUMO

TEIXEIRA COSTA, Bárbara Elisabeth. **Carreadores micro estruturados de lipídios bioativos para incorporação em filmes biodegradáveis para potencial aplicação em alimentos.** Rio de Janeiro, 2021. Tese (Doutorado em Ciência de Alimentos) — Instituto de Química, Universidade Federal do Rio de Janeiro, Rio de Janeiro, Brasil, 2021.

O objetivo principal desta tese foi obter carreadores lipídicos ativos por coacervação complexa e incorporá-los em filmes biodegradáveis à base de quitosana plastificados com solventes eutéticos (DES) à base de cloreto de colina: glicerol (ChCl: Gly) para potencial aplicação em alimentos. Dois diferentes sistemas baseados nos pares de polímeros quitosana (CS) e alginato de sódio (SA), e CS e isolado de proteína de ervilha (PPI) foram formulados e otimizados usando planejamento de experimentos (DOE) para encapsular o óleo de polpa de açaí (AO) e azeite de oliva extra-virgem (EvO). O primeiro sistema foi formulado para estudar o efeito de diferentes concentrações de AO (0,25 - 0,75%) e cloreto de cálcio ($CaCl_2$) (0 - 1,0%), na formação de complexos de polieletrólitos CS:SA (PECs) usando planejamento composto central. A formação do complexo CS:SA e o encapsulamento AO também foram confirmados por microscopia óptica (OM) e microscopia eletrônica de varredura (MEV), além de espectroscopia de infravermelho (FTIR), análises termogravimétricas e termogravimétricas derivadas (TGA/DTG). Neste sistema, AO e $CaCl_2$ influenciaram significativamente o tamanho e o índice de polidispersão (span) dos PECs, embora a eficiência de encapsulação (> 99%) não tenha sido afetada. Esses PECs exibiram comportamento típico de gel, consistente com a formação dos complexos. AO e os PECs otimizados (0,5% AO e 0,5% $CaCl_2$) apresentaram alta atividade antioxidante, > 70% pelo método de sequestro do radical DPPH. O outro sistema de microencapsulação foi formulado para estudar o efeito da concentração de CS (0,39 - 1,1%) e razão CS:PPI (0,18 - 2,31) na formação de PECs para encapsulação de EvO usando um planejamento composto central. O tamanho das partículas foi significativamente influenciado pela razão CS:PPI, enquanto que o *span* foi influenciado por ambos, CS e razão CS:PPI. Os resultados foram otimizados pela metodologia de superfície de resposta (RSM) e função *desirability* (D), apresentando condições ótimas de 0,75% de CS, 2,31 de razão CS:PPI and 0,5% de EvO, e D igual a 0,845. As partículas otimizadas tinham um tamanho pequeno e *span* estreito, ~ 3

μm e 2, respectivamente. Os espectros de FTIR e as curvas TGA/DTG dos complexos confirmaram a encapsulação de EvO. Os complexos CS:PPI-EvO exibiram atividade antioxidante moderada, com o maior valor ~ 117 mg equivalente de Trolox (TE) L^{-1} pelo ensaio DPPH. Como o AO encapsulado em CS/SA PECs exibiu propriedades físico-químicas e antioxidantes satisfatórias, sua incorporação em filmes biodegradáveis foi avaliada. O método de *casting* foi utilizado para produzir filmes compósitos de CS plastificados com 1:2 ChCl:Gly e incorporados com diferentes quantidades (0-10%) de AO PECs. As técnicas de OM, MEV e microscopia confocal de varredura a laser (CLSM) foram utilizadas para observar sua microestrutura e confirmar a presença de PECs de AO. Os espectros de FTIR e as curvas de difração de raios-X e revelaram interações entre CS, DES e AO PECs nos filmes por bandas espectrais típicas deslocadas, bem como por sua cristalinidade diminuída (8 a 4%), respectivamente. Os filmes exibiram boas propriedades mecânicas, alto alongamento na ruptura > 100%, baixa resistência à tração e módulo de Young. Todos os filmes exibiram atividades antioxidantes por diferentes ensaios, embora o maior valor tenha sido determinado pelo método de sequestro de radical DPPH, ~17 mg TE g^{-1} de filme. Isso pode estar associado à maior capacidade antioxidante de AO, 101,8 ± 8,2 mg TE L^{-1} de óleo, também determinada por DPPH. Esses resultados demonstraram as boas propriedades estruturais, mecânicas e antioxidantes dos filmes compósitos de CS com um bom potencial para ser empregado como embalagem ativa de alimentos.

Palavras-chave: Coacervatos à base de quitosana. Filmes compostos de base biológica. Embalagem antioxidante para alimentos.

LIST OF ILLUSTRATIONS

Continuation - List of Illustrations **Pages**

Continuation - List of Illustrations **Pages**

Continuation - List of illustrations **Pages**

Continuation - List of illustrations **Pages**

LIST OF TABLES

***Continuation* – List of Tables** **Pages**

LIST OF ABBREVIATIONS AND ACRONYMS

ABTS: 2,2'-azino-bis-3-ethylbenzothiazoline-6-sulfonic acid

AcOH: Acetic acid

AcONa: Acetic anhydride-sodium acetate

ANOVA: Analysis of variance

AO: Açaí ou assaí pulp oil

APP: Apple peel polyphenols

ATR: Attenuated total reflectance

BHT: Butylated hydroxytoluene

BTE: Black tea extracts

CAGR: Compound Annual Growth Rate

ChCl: Choline chloride

ChCl-CA: choline chloride-citric acid

ChCl-Gly: choline chloride-glycerol

ChCl-Urea: choline chloride-urea

CLSM: Confocal laser scanning microscopy

CrD: Crystallinity degree

CS: Chitosan

CSPPI-EvO: Microparticles based on chitosan, pea protein isolate and extra-virgin olive oil encapsulated

CSSA-AO: Microparticles based on chitosan, alginate and açaí oil encapsulated

D[4,3]: Particle size expressed as volume mean diameter value

DA: Degree of *N*-acetylation

DES: Deep eutectic solvent

DMA: Dynamic mechanical analysis

DMSO: Dimethyl sulfoxide

DNA: Deoxyribonucleic acid

DOE: Design of experiments

DPPH: 2,2-diphenyl-1-picrylhydrazyl

DSC: Differential scanning calorimetry

DTG: Derivative thermogravimetric analysis

EB: Elongation at break

***Continuation* - List of abbreviations and acronyms**

EC: European Commission

EC_{50}: Half maximal effective concentration

EE: Encapsulation efficiency

EO: Essential oil

ESI: Electrospray Ionization

EvO: Extra virgin olive oil

FDA: Food and Drug Administration

FRAP: Ferric reducing antioxidant power

FTIR: Fourier-transform infrared spectroscopy

GC-MS: Gas chromatography coupled with mass spectrometry detector

Gly: Glycerol

GMO: Genetically modified organisms

GRAS: Generally recognized as safe

GTE: Green tea extracts (GTE)

HAT: Hydrogen atom transfer

HBA: Hydrogen bond acceptor

HBD: Hydrogen bond donor

HDL: High-density lipoprotein cholesterol

ILs: Ionic liquids

LC-MS: Liquid chromatography coupled with mass spectrometry detectors

LC-PDA: Liquid chromatography coupled with photo diode array detectors

LVR: Linear viscoelastic range

M/G: Mannuronic/ guluronic ratio

MUFAs: Monounsaturated fatty acids

Mw: Molecular weight

NMR: Nuclear magnetic resonance

OM: Optical microscopy

OrgMMT: Organoclay nanocomposites

PBAT: Polybutylene adipate terephthalate

PBS: Polybutylene succinate

PCL: Polycaprolactone

Continuation **- List of abbreviations and acronyms**

PE: Polyethylene

PECs: Polyelectrolytes complexes

PEG: Polyethylene glycol

PET: Polyethylene terephthalate

pH: Negative log of the hydrogen ion concentration

pKa: Negative log of the acid dissociation constant

PLA: Polylactic acid

PP: Polypropylene

PPI: Pea protein isolate

PUFAs: Polyunsaturated fatty acids

RH: Relative humidity

RNA: Ribonucleic acid

ROS: Reactive oxygen species

RSM: Response surface methodology

SA: Sodium alginate

SEI: Strength of electrostatic interaction

SEM: Scanning electronic microscopy

SET: Single electron-transfer

SFAs: Saturated fatty acids

SNPs: Silver nanoparticles

TEAC: Trolox equivalent antioxidant capacity

TGA: Thermogravimetric analysis

T_{onset}: Initial degradation temperature

TPC: Total polyphenols content

T_{peak}: Peak degradation temperature

TROLOX: (±)-6-hydroxy-2,5,7,8-tetramethyl-chroman-2-carboxylic acid

TS: Tensile strength

WVP: Water vapor permeability

XRD: X-ray diffraction

YM: Young Modulus

LIST OF SYMBOLS

σ: Tensile strength

$\dot{\gamma}$: Shear rate

η_{sp}: Specific viscosity

M_v: Viscosity average molecular weight

k': Huggins' coefficient

k'': Kraemer's coefficient

η_{rel}: Relative viscosity

$[\eta]$: Intrinsic viscosity

E": loss modulus of the dynamic mechanical analysis

E': storage modulus of the dynamic mechanical analysis

G": Loss modulus

G': Storage modulus

L: Thickness

r: Resistência à tração

R^2: Coefficient of determination

tan δ: Tan-delta

ζ-potential: Zeta potential

η*: Complex viscosity

η: Viscosity

ω: Oscillatory frequency

ε: Elongation at break

C: Chitosan solution concentration

K: Intercept log of the Mark-Houwink-Sakurada relationship

a: equation slope of the Mark-Houwink-Sakurada relationship

SUMMARY

Continuation of Summary

Continuation of Summary

Continuation of Summary

1. INTRODUCTION

The development of biodegradable food packaging has gained great thrust in recent years, dominating markets, and stimulating the research for new products. Campaigns, mainly related to the population's awareness about the reduction of the indiscriminate use of plastic materials and, consequently, about the importance of reducing environmental pollution, are among the most motivating factors for the study of new food packaging materials. The replacement of conventional polymers used in packaging such as polyethylene, polypropylene and polyvinyl chloride is a trend.

Natural polysaccharides, from renewable sources, such as chitosan, alginates, starches, gums, and proteins from milk, soybeans, peas, collagen, and gelatin, appear as good alternatives for this change (AZEVEDO et al., 2017; CAROCHO et al., 2019; RIVERO et al., 2016; SUN, SUN, XIONG, 2013; VITAL et al., 2018). The use of natural materials has great advantages, in addition to reducing the consumption of petroleum-derived polymers and environmental pollution, as they have good bioavailability, biocompatibility, biodegradability, antioxidants, antimicrobials, low toxicity and low allergenicity (MUJTABA et al., 2019; TAMM et al., 2016; TAVASSOLI-KAFRANI, SHEKARCHIZADEH, MASOUDPOUR-BEHABADI, 2016).

Packaging is a fundamental barrier agent to containment, processing, conservation, and extension of the shelf-life of food, and can receive the incorporation of additives to improve these properties. The additives incorporation can also promote interaction with foods, for example, through antioxidant action on their surface, and consequently promoting a higher quality and shelf-life (QUIRÓS-SAUCEDA, et al., 2014). For this, natural and safer bioactive substances, which occur naturally in fruits and other vegetables, have been gaining market preference in substitution for those of chemical origin (DOMÍNGUEZ et al., 2018). Phenolics, carotenoids and polyunsaturated fatty acids are examples of natural compounds that, in addition to preserving action, may also have beneficial properties for health (LAGOS et al., 2015; XIAO et al., 2018).

Among the various Brazilian foods, known as sources of bioactive substances, such as flavonoids, phenolics, anthocyanins, terpenes, and others, we can highlight the fruits of açaí, *Euterpe oleracea* (DEL POZO-INSFRAN, BRENES, TALCOTT, 2004; BATISTA et al., 2016; MERTENS-TALCOTT et al., 2008; RUFINO et al., 2009; SANTOS et al., 2021; YAMAGUCHI et al., 2015). High content of lipids, ~50%, good source of saturated fatty acids (26 to 34%), monounsaturated (57 to 70%) and

polyunsaturated (8 to 16%), and antioxidant properties of açaí pulp oil and extracts contribute to widespread use and international recognition (BATISTA et al., 2016; PACHECO-PALENCIA, MERTENS-TALCOTT, TALCOTT, 2008; MATTA et al., 2020; RUFINO et al., 2011; RABELO et al., 2018).

The efficiency of bioactive substances in promoting health benefits decreases considerably with their exposure to oxidative conditions, such as air, humidity, heat, and light. Thus, encapsulation in biopolymeric matrices represents a good barrier in maintaining its biological activities (DEVI et al., 2017; EGHBAL, CHOUDHARY, 2018). The encapsulation is a process that can confine active substances in biopolymeric matrices of proteins, polysaccharides, and their combinations, on micro or nanoscale (DEVI et al., 2017; EGHBAL, CHOUDHARY, 2018). Different techniques, such as complex coacervation, interfacial polymerization, spray-drying, freeze-drying, ionic gelation, and others, can be used for this purpose (DEVI et al., 2017; OZKAN et al., 2019).

Complex coacervation is the most used technique for encapsulating hydrophobic substances, such as vegetable oils. The latter produces particles or polyelectrolyte complexes (PECs) by forming hydrogen bonds, electrostatic, hydrophobic, and steric interactions between the macromolecule chains (carbohydrate/carbohydrate or carbohydrate/protein) in aqueous solution (DEVI et al., 2017; SANTOS, DA COSTA, GARCIA-ROJAS, 2018; TIMILSENA et al., 2019). The formation of this complex is dependent on the molecular mass, concentration, and proportion of the biopolymers, in addition to the ionic strength, pH and temperature of the solution (OZKAN et al., 2019). Natural polyelectrolytes such as chitosan, alginates, and some proteins such as peas can be used (ELMER et al., 2011; OZKAN et al., 2019; TIMILSENA et al., 2019). These macromolecules contribute to the rheological-structural properties by forming a gelling network and their complexes promote changes in the interfacial structures, stability, and durability of food colloids (EGHBAL, CHOUDHARY, 2018; SHISHIR et al., 2018).

Natural polysaccharides, chitosan, and alginates, have a wide application in food products due to their characteristics of biodegradability, biocompatibility, atoxicity, antioxidant, antimicrobial, and anticancer activities, in addition to the good ability to form stable hydrogels. (ASSAD et al., 2020; AGÜERO et al., 2017; CAZÓN et al., 2017; MOHAMED, EL-SAKHAWY, EL-SAKHAWY, 2020). Chitosan is a linear polymer obtained by alkaline deacetylation of chitin, extracted from crustacean exoskeleton residues. In its polymeric structure it has cationic groups (protonated amines), which

allow electrostatic interactions with anionic polyelectrolytes (carboxylic groups), such as sodium alginate, forming a crosslinked hydrogel in the form of capsules (HAGHIGHI et al., 2020; SANCHEZ-SALVADOR et al., 2021; VAN DEN BROEK et al., 2015). Alginate (SA) is a water-soluble linear anionic polysaccharide of alternating units of α-1,4-L-guluronic acid (G) and β-1,4-D-manurunic acid (M), extracted from brown seaweed (*Laminaria digitata, Macrocystis pyrifera* and *Ascophyllum nodosum*) (AGÜERO et al., 2017; GOH, HENG, CHAN, 2012; TAVASSOLI-KAFRANI, SHEKARCHIZADEH, MASOUDPOUR-BEHABADI, 2016). Its major employment is due to their functional properties, such as notable crosslinking capacity, good gelling and film-forming properties, fine water absorption, thickener, emulsion-stabilizer, pH-sensitivity, mucoadhesiveness and others (AGÜERO et al., 2017; BAYBAŞ, SERDAROĞLU, SEMERCI, 2021).

Plant-derived proteins have gained remarkable attention of food manufactures and consumers in the search for natural food resources and alternative materials to vegetarian, vegan, and food allergy diet restrictions. Protein-based film packaging exhibit extraordinary mechanical and barrier properties, especially to oxygen and carbon dioxide gases, when compared to polysaccharides (MOHAMED, EL-SAKHAWY, EL-SAKHAWY, 2020; QUIRÓS-SAUCEDA et al., 2014). Pea proteins, *Pisum sativum* L. ssp. *sativum*, are predominantly made up of two globulins, legumin (6 subunits of α and β chains covalently linked, 11 S, 350 – 400 kDa) and vicillin (three subunits, 7 S, 150 kDa) (Liu, Low, & Nickerson, 2009) and in a minority due to convicillin (71 kDa) (BARAC et al., 2010; ELMER et al., 2011; MCCARTHY et al., 2016). The pea proteins, as well as other proteins in seeds are considered bioactive proteins, as they can contribute to wellness and health. Nevertheless, the food applications of pea proteins are related to its nutritional value, distinguishable functional properties, low allergenicity, non-GMO status, and biological activities, such as reducing the risk of cardiovascular disease and lowering blood pressure effect (WEI et al., 2020). It has high nutritional value, good emulsifying properties and low allergenicity that value its use in food products. Solubility, water- and lipid-binding capacities, rheological, emulsifying and gel forming properties, can be cited as mostly significant abilities to application in food products.

In the development of biobased films, the hydrophilic character of its natural macromolecules matrix should be considered since water molecules may be a problem to the shelf-life of the product as well as to the physical stability of the packaging. To overcome this issue, hydrophobic or less hydrophilic substances can be incorporated

to the films modifying its physical properties. These substances, denominated plasticizers, are responsible for increasing the matrix free volume and molecular mobility of amorphous biopolymers, competing chain-to-chain H-bonding along the polymers' chains (QUIRÓS-SAUCEDA et al., 2014; RIVERO et al., 2016). The most commonly used plasticizers are glycerol, sorbitol, polyethylene glycols (PEG), lipids and their derivatives, and others. More recently, films plasticization can be performed using deep eutectic solvents (DES), as sustainable solvent systems (ALMEIDA et al., 2018; PEREIRA, ANDRADE, 2017; SOUSA et al., 2014). DESs are obtained by complexation of a hydrogen bond donor (HBD) with a quaternary ammonium salt (hydrogen bond acceptor - HBA), producing liquids with physical and solvent properties analogue to ionic liquids (ILs) (ABBOTT et al., 2011; SMITH, ABBOTT, RYDER, 2014). DESs are chemically and thermally stable, non-flammable, possessing high dissolution ability, lack of flammability, low volatility, low melting point and tailorability, as well as are water neutral, and low- or non-toxic. For plasticizing film packaging the most common DES used are the mixture of choline chloride-citric acid (ChCl-CA), choline chloride-urea (ChCl-Urea) and choline chloride-glycerol (ChCl-Gly), this last one, mainly used for chitosan-based coatings (ALMEIDA et al., 2018; PEREIRA, ANDRADE, 2017; ZDANOWICZ, WILPISZEWSKA, SPYCHAJ, 2018). Particularly, the eutectic mixture of ChCl:Gly at a molar ratio of 1:2 was found to efficiently plasticize starch and starch/zein blends, and chitosan and chitosan/micro-crystalline cellulose/curcumin composites (PEREIRA, ANDRADE, 2017; SOUSA et al., 2014).

2. OBJECTIVES

AIM OF THE THESIS

The main goal of this work was to obtain different active lipid carriers by complex coacervation and incorporate them in biodegradable chitosan-composite films plasticized with deep eutectic solvents. The main motivation was to be able to produce bioactive films based on natural polymers with good barrier and antioxidants properties to potential food application.

SPECIFIC OBJECTIVES

- Obtain and characterize lipid carriers based on complex coacervation between chitosan and sodium alginate.
- Obtain and characterize lipid carriers based on complex coacervation between chitosan and pea proteins isolate.
- Obtain chitosan-based films plasticized with eutectic solvents and incorporate with active lipid carriers.
- Characterize the active films in terms of structure, functionality, and antioxidant activity.

3. LITERATURE REVIEW

3.1. Food packaging

Packaging protects foods from the environment. Over the years, packages have changed to follow the different demands of consumers and the evolution of the food industry. Packaging is responsible to maintain food quality, improve safety and shelf-life, provide label information of the ingredients, and promote world-wide distribution of food products until reach the final consumers (RIBEIRO-SANTOS et al., 2017). From all these, the maintenance of food quality across the whole supply chain is the most critical factor when choosing a packaging material (SOHAIL, SUN, ZHU, 2018).

To fulfill these functions, the materials for the packaging design must have good thermo-mechanical properties, to be properly processed by different means, resist the surrounding aspects through distribution, exhibit an adequate shelf-life for product storage and prevent cross contamination of unwanted substances to their content (KAMDEM, SHEN, NABINEJAD, 2019). Different materials have been used for food packaging, such as glass, metal, paper, and plastic, though, the last two are often utilized for this purpose (CARINA et al., 2021). Moreover, the packaging technology is dynamic and is evolving since ancient times until nowadays following human lifestyle.

3.1.1. Historical background of packaging

It has been exceedingly difficult to study the firstly used materials for packaging food supplies, since so little of it have survived along the centuries. These primarily packaging used by the ancient populations thousands of centuries ago were made from natural materials, like, wooden parts, bamboo, shells, animal skin, leaves, grasses, jute, glass, and ceramic (MILLER, KROCHTA, 1997; RISCH, 2009; TWEDE, 2002; VERMA et al., 2021). Some evidence of primitive pottery and glass used as packaging is dated around 7000 B.C. (MILLER, KROCHTA, 1997; RISCH, 2009).

When visiting museums, is common to find ancient ceramic jars named amphoras, and potteries made from glass, which were frequently used in Mediterranean region as packaging for different goods. Some of these, dating about 1500 B.C. (*before Christ*) to 500 A.D. (*anno Domini*), were used to transport and commercial trade of wine, oil, grains and other foods by Egyptians, Greek and Roman civilizations (RISCH, 2009; TWEDE, 2002). In the other side of the Atlantic Ocean, Latin-America indigenous populations also have used ceramic materials to prepare

and dish their foods during ritual events, dating around 1000 B.C (BARRETO, OLIVEIRA, 2016).

Limestone, sand, soda, and silica were the basic material molded and used to make glass potteries, cups and bowls in the 1200 B.C. (BERGER, WELT, 2005; RISCH, 2009). These ingredients have not changed in the glass-making process since their discovery. However, the molding evolved with the invention of the blowpipe by Phoenicians in 300 B.C., which improved the glass production to make round vessels (BERGER, WELT, 2005). It was only in the 17-18th century that the split molding process was develop allowing the fabrication of irregular shapes and different decorations on glass packaging (BERGER, WELT, 2005). From this period until the early 1900s glass vessels with a wide range of shapes and sizes gained the consumers attention and dominated the packaging market up to the 1960s (BERGER, WELT, 2005). Even with the discovery and use of metals for different purposes during the Iron Age, 500 – 332 B.C., its use as a packaging material was not common until the development of stronger alloys and thinner coatings by the process of tin plating in 1200 A.D. (BERGER, WELT, 2005).

The major packaging evolution occurred during the Industrial Revolution on the 18 – 19th centuries. During this period, an event stamps the beginning of the Modern Packaging Era, the discovery of canning operation by Nicholas Appert, who used this method to preserve food supplied to the French Army of Napoleon Bonaparte (BRODY et al., 2008; PAGE, 2012; RISCH, 2009). The Appert' method allowed that food products were heated during processing, consequently improving their shelf-life and preserving it against microbial contamination (RISCH, 2009). This technology was quickly employed in many places, especially in the USA, where it was placed in a continuous production in the early 1900s (PAGE, 2012).

The development of aluminium cans, that years later were gone to be used to beer and other drinking food, occurred as a result from the tinplate shortage during the World War II (WWII) (PAGE, 2012). Several of these technologies were specially designed to sustain a safe food supply to the armies during the WWII and are used until today. In the 19th century, different materials, such as paper and paperboard, were continuously improved, folded into smaller packages, cartons, and corrugated boxes and used to food packaging (RISCH, 2009). Additionally, the first plastics derived from a cellulose-based and petroleum-based polymer were discovered in the 1800s (BRODY et al., 2008; MILLER, KROCHTA, 1997). The petroleum-based plastics were firstly employed to protect munition during the WWII and then became packages used

for cereals and biscuits (BRODY et al., 2008). The development of various polymers in the early 1900s, such as polypropylene, polyester, and ethylene vinyl alcohol, pushed the plastic packaging industry increasingly forward letting the metal, glass, and paperboard industries back (BRODY et al., 2008; RISCH, 2009).

The use of edible materials as food coating has also few historical reports. Back in the ancient age, edible packaging was used in the production of sausages, preserving meat by stuffing it in animal intestines, a process developed by Sumerians in Mesopotamia around 3000 B.C., and by Chinese settlers in China around 580 B.C (MKANDAWIRE, ARYEE, 2018). A particular type of edible thin film made from the skin of boiled soy milk was used in Japan during the 15th century to cover different foods (PAVLATH, ORTS, 2009). In China and Europe, during the 16th century animal grease (lard) and wax were used to coat fruits and other food products to its conservation and later consumption (MILLER, KROCHTA, 1997; PAVLATH, ORTS, 2009). And later, back on the 19th century, a coating made from gelatin was patented by USA and used in meat products (PAVLATH, ORTS, 2009). As the synthetic plastic dominated the packaging market after the WWII, the use of edible resources to packaging were left behind until recently.

After the WWII, the synthesis of different plastic materials and their development to food packaging was significantly high. The plastic industry has profoundly expanded in the 21st century. With a quick look in some aspects of our daily life is possible to identify many different types of plastics surrounding us. In the food industry, this expansion was also intense, mainly because the use of these materials has improved food preservation and extended the storage of a wide range of products. Many advantages have contributed to this extensively use of plastics in food packaging, such as low cost, good resistance and processability, flexibility, lightweight, easiness to mold in different sizes and shapes, and others (VERMA et al., 2021). In the 1960s, more than 25% of bread sold was packaged in low-density polyethylene bags (RISCH, 2009). It was estimated that in the period of 1950 to 2015 the cumulative production of plastics reached more than 7.5 billion metric tons, and only in 2018 the global production of these materials has risen to 360 million tons (KAMDEM, SHEN, NABINEJAD, 2019; SOARES et al., 2021). Around 40% of the petrochemical-based plastics are used for packaging purposes and closely to 60% of plastic packaging are used to pack food and beverages (GROH et al., 2019).

Mainly, conventional packaging made from synthetic plastic polymers are items of one-time use and are discarded after using. About 95% of plastic packaging are

wasted after a single-use cycle and ended up in the ecosystem, where it can be break down into micro or nanoplastics (JÄGER, PISCICELLI, 2021; SOARES et al., 2021). These microplastics are carried out by oceans currents and can be ingested by the sea-wild life and birds, in which can accumulate in its digestive system, modify their health, and end up in the food chain (RAI et al., 2021).

Other issue that negatively affects the plastic packaging production is concern about the human occupational health, since different hazardous chemicals added intentionally and unintentionally are used during processing (GROH et al., 2019). Moreover, during manufacturing of synthetic petroleum-based plastics, greenhouse gases and particulates are released in the environment, also contributing to world pollution (KAMDEM, SHEN, NABINEJAD, 2019). In addition to all this, packaging manufacturers face a new market challenge due to consumer demand for biobased resources for food packaging as has been an effort to reduce plastic waste and as is well known about the negative impact of these materials on the world environment (KAMDEM, SHEN, NABINEJAD, 2019; MARKUS, RAMANI, 2021). Thus, all these circumstances have been stimulating the search for new biobased materials and the development of biodegradable packaging from renewable sources as strategies to mitigate pollution and sustain the planet.

Giant food industries and packaging companies have announced commitments to the reduction of plastics waste and to practice a circular economy for them. For example, Unilever®, the owner of the food brands Ben & Jerry's® and Lipto®, have declared on October 2019 an ambitious commitment with the reduction of the use of plastic packaging in more than 100,000 tons and use at least 25% of recycled plastic packaging until 2025 (UNILEVER, 2019). In Brazil, the actions of the group are supported by a long-running partnership with the retailer Grupo Pão de Açúcar®, which helps in the waste collection through drop-off stations (UNILEVER, 2019). Dasani®, a brand of bottled water commercialized by The Coca-Cola Company® in USA, has announced the first fully recyclable polyethylene terephthalate (PET) bottle 50% plant-based, HydridBottle™ (COCA-COLA, 2019). The Coca-Cola Company® has announced to make 100% of its packaging recyclable by 2025 and use at least 50% recyclable materials in their packaging by 2030 (COCA-COLA, 2021). Other food companies, such as Keurig Dr Pepper®, PepsiCo® and Mondelez®, also have agreed to reduce the use of virgin plastic for its rigid plastic packaging (AS YOU SOW, 2021). According to the non-profit organization As You Sow (2021), Keurig Dr Pepper® used

208,00 metric tons of plastic packaging in 2018, and the company have planned to cut by 20% the use of virgin plastics by 2025.

Innovative packaging designed to food products with differentiated characteristics, such as high moisture content, high pressure and modified atmosphere, natural and fresh foods, among others, and with an environment-friendly approach are a challenge for the research and development in the packaging industry (CAMPOS, GERSCHENSON, FLORES, 2011). Moreover, these materials should be from renewable sources, recyclable and have low greenhouse gas emissions in the ecosystem (KAMDEM, SHEN, NABINEJAD, 2019).

3.1.2. Trends in food packaging

In response to the challenges that the plastic packaging industry is facing due to pollution, the growing demands for new environmentally friendly materials and the need for a sustainable industrial commitment, there is a great opportunity for the development of novel food packaging. In this context, biobased, biodegradable, compostable, edible, active and intelligent packaging are innovative trends in the field.

Biobased packaging contains wholly or partly materials from biological origin (IMRE et al., 2019; ISO, 2015). Materials from biological sources, such as from plants, animal, microorganisms, seafood, woods, and agricultural residues are naturally biodegradable and compostable. These materials when used to packaging can be degraded by the action of living organisms upon disposal and converted to CO_2, CH_4, H_2O, inorganic compounds, or biomass, returning to nature (CARINA et al., 2021; DHALL, ALAM, 2020; GROSS, KALRA, 2002; MARKUS, RAMANI, 2021). Once made by biological resources, like proteins, polysaccharides and microbial polyesters, packaging materials can be named as biobased plastics. To Siracusa and Lotti (2018), biobased materials are obtained from renewable carbon resources, as plants or biomass, such as chitosan, starch, cellulose, hemicellulose, or vegetable oils, and biodegradable materials can be made from both fossil and renewable resources (CARINA et al., 2021; SIRACUSA, LOTTI, 2018).

Biobased, biodegradable, and composting plastics are terms frequently misunderstood and cannot be considered synonymous (DHALL, ALAM, 2020; VAN DEN OEVER et al., 2017). Not all biobased material is biodegradable and otherwise, not all biodegradable material is derived from biological sources (HAGHIGHI et al., 2020). Different institutions and experts have diverted about a unique definition for the term

biodegradable. According to the standard designation, D 996–04, from the American Society for Testing and Materials, biodegradable and compostable can be defined as

> *Biodegradable, Adj* — capable of undergoing decomposition into carbon dioxide, methane, water, inorganic compounds, or biomass in which the predominant mechanism is the enzymatic action of micro-organisms, that can be measured by standardized tests, in a specified period of time, reflecting available disposal conditions (ASTM, 2004, p. 2).

> *Compostable, Adj* — capable of undergoing biological decomposition in a compost site as part of an available program, such that the material (that is, feedstock) is not visually distinguishable and breaks down to carbon dioxide, water, inorganic compounds, and biomass, at a rate consistent with known compostable materials (ASTM, 2004, p. 3).

The biodegradability rate of biobased materials is intrinsically linked to its chemical structure. For example, the biobased polypropylene (PP) and polyethylene (PE) (vinyl polymers) obtained from the sugar cane processing are non-biodegradable materials and are used similarly to the fossil-based PP and PE (HALONEN et al., 2020). It is critical to underline that biodegradability do not imply a short time process and this should be expected to happen on a specific ecosystem at a particular time (DHALL, ALAM, 2020). Different biodegradable materials and their sources are displayed in the Figure 1.

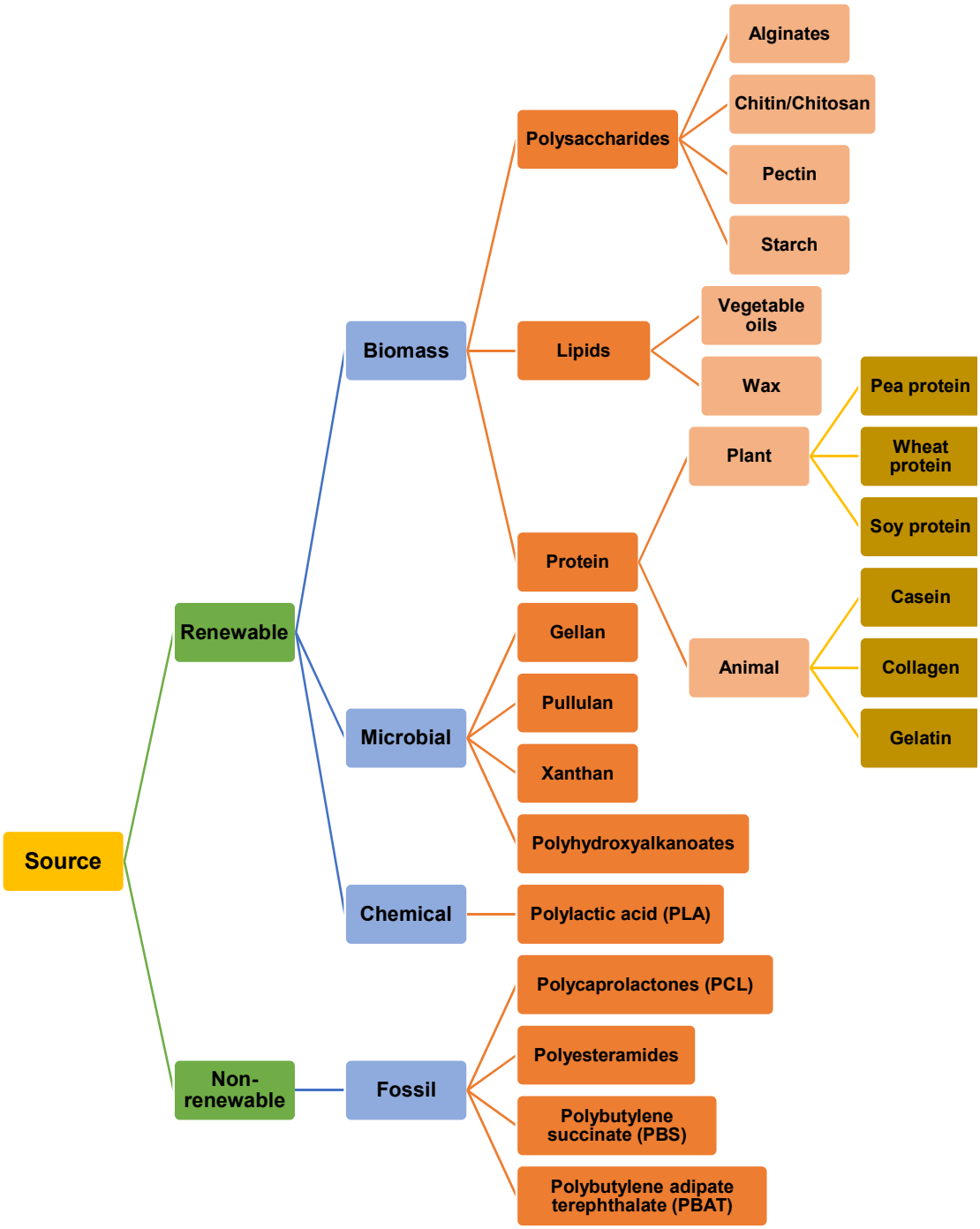

Figure 1. Classification of biodegradable materials. Adapted from Dhall and Alam, 2020; Haghighi et al., 2020.

Nowadays, the global production of bioplastics, considered low, has reached a total of 2.11 million tons in 2020 and is expected to grow in 15% until 2024 (HALONEN et al., 2020). According to the report published in November 2020 by Intrado Globe Newswire (2020), the world bioplastic market has generated more than U$ 4.5 billion in 2019 and has an estimative to reach more than U$ 13 billion until 2027 in business. To them, the starch-based bioplastics market should achieve U$ 561 million up to

2023, with an annual growth rate (CAGR) of more than 3.5%. The major contribution to the bioplastic market was from the Asia-Pacific regions and Europe should have the highest CAGR, more than 16%, until 2027 (INTRADO GLOBE NEWSWIRE, 2020). The distribution by sector of the bioplastics global production market in 2020 are presented in Figure 2. Thus, the plastics and packaging markets are witnessing a significant increase on demand for material from renewable resources.

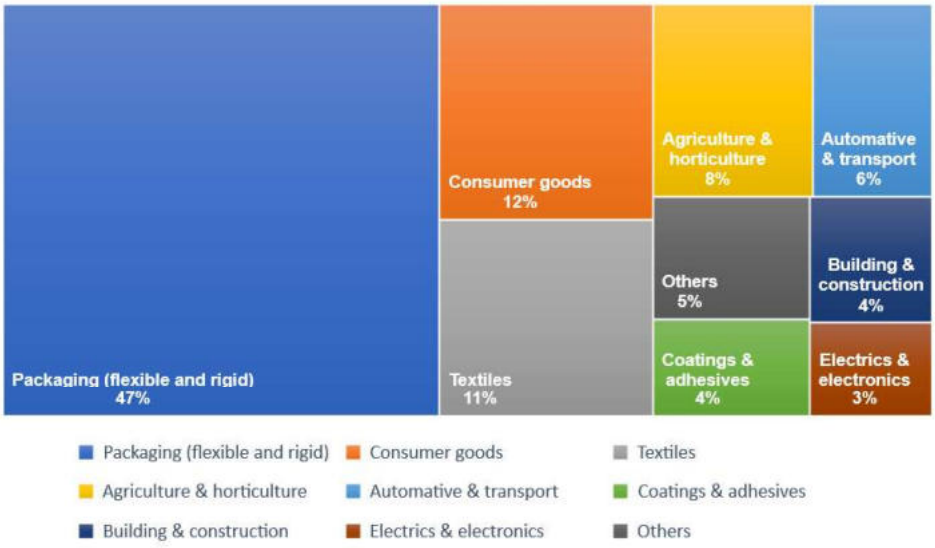

Figure 2. Distribution by sector of the bioplastics global production market in 2020 (total of 2.11 million tons). Adapted from European Bioplastics Org (2020).

Even with this high demand for biobased materials, some challenges must be overcome, such as:

- Improvement of national and international legislation to correctly establish the concepts and required standards related to bioplastics.
- Revision of industrial facilities to the processability of these materials while maintaining optimized and efficient performance.
- Maintaining the adequate quality of its products and ensuring its biodegradability and compostability.
- Adjustments of the waste management system of each country/ region to the collection of biobased plastics since each city has its own program.

3.2. **Edible films and coatings**

Edible films can be defined as a thin layer of a material coating or placed between foods, in which act as a barrier ad that can be consumed without any health risk (QUIRÓS-SAUCEDA et al., 2014; PETKOSKA et al., 2021). It is primary packaging made from edible natural materials. These films should be composed only by food-grade components, GRAS (generally recognized as safe), including any additives, such as plasticizers (OTONI et al., 2017). As any other packaging, the edible films and coatings must protect the food integrity, maintaining quality, controlling mass and volatile losses, extending its shelf-life, preventing surface contamination, offering mechanical protection, and improving its sensory properties (Figure 3) (OTONI et al., 2017; PETKOSKA et al., 2021; SILVA-WEISS et al., 2013). Although, it is not expected that the edible films can replace completely all conventional packaging, they can be used to significantly reduce the use of petroleum-based plastics, decrease food losses, and reduce the environment pollution in a long-term.

Figure 3. Main purposes of an edible food packaging.

Edible films and coatings may have on their composition two main based materials, a biomacromolecule-based matrix, and additives, such as plasticizers, cross-linkers, other reinforcements substances and functional ingredients (MKANDAWIRE, ARYEE, 2018). These materials can be used alone or blended. As the edible packaging is composed by natural-based materials, it can be classified as a subgroup of biobased and biodegradable packaging (PETKOSKA et al., 2021).

Generally, polysaccharides, proteins, lipids, and their mixtures are used for the development of edible films and coatings. The classification and some examples of these natural materials commonly used for this purpose are presented in Table 1.

Table 1. Natural materials used in edible films and coatings.

Biomacromolecules	Raw Materials	References
Polysaccharides	Agar	SOUSA et al., 2014
	Alginate	VITAL et al., 2018.
	Cellulose	KOWALCZYK et al., 2021
	Chitosan	MUJTABA et al., 2019.
	Gums	SHARMA, RAO, 2015
	K-carrageenan	HAMZAH et al., 2013
	Pectin	JAHROMI et al., 2020
	Pullulan	ZHOU et al., 2021
	Starch	MORENO, ATARÉS, CHIRALT, 2015
Proteins	Casein	CHEVALIER et al., 2018
	Collagen	JIANG et al., 2020
	Corn zein	SUN et al., 2020
	Gelatin	KOWALCZYK et al., 2021
	Pea protein	ACQUAH et al., 2020
	Sodium caseinate	JAHROMI et al., 2020
	Soy protein	MARYAM ADILAH; JAMILAH; NUR HANANI, 2018.
	Wheat gluten	ANSORENA; ZUBELDÍA; MARCOVICH, 2016
	Whey protein	AZEVEDO et al., 2017
Lipids	Candelilla wax	LEÓN-ZAPATA et al., 2015
	Bee wax	ROCCA-SMITH et al., 2016
	Vegetable oils	RODRIGUES et al., 2016
Composites	Blends	AZEVEDO et al., 2017; CHEVALIER et al., 2018; JIANG et al., 2020; KAMDEM, SHEN, NABINEJAD, 2019; ZHOU et al., 2021.
	Residues and by-products from agriculture	GARRIDO et al., 2014; FERREIRA et al., 2016; MUNHOZ et al., 2018
	Fruit pulps	ESPITIA et al., 2014

Edible films and coatings even though to be similar due to the barrier function, are different. The first are solid laminates, separately prepared, dried, processed and then used to cover food surface, placed between food parts, or used as an edible sealed bag (MOHAMED, EL-SAKHAWY, EL-SAKHAWY, 2020; SILVA-WEISS et al., 2013). In a different way, the edible coatings are prepared as a forming-solution directly sprayed or dipped on the food surface and then dried (OTONI et al., 2017). Thus, coatings can be considered as a part of the food product since it is not made to be removed (PETKOSKA et al., 2021). Moreover, films can be prepared as a mono, bi or multilayers. The last ones provide a better water barrier to food but are less commonly used as they need two or more processing steps of casting and drying (MOHAMED, EL-SAKHAWY, EL-SAKHAWY, 2020).

Edible coatings can be used to decrease the weight loss, color changing, inhibit ethylene production and delay softening related to the postharvest ripening of fruits (TAVASSOLI-KAFRANI, SHEKARCHIZADEH, MASOUDPOUR-BEHABADI, 2016). Different natural polymers, such as chitosan, carrageenan, alginates, gums, starches, their blends, and a wide range of additives can be used to prepare edible coatings and to be applied on fruits, as listed in Table 2.

Moisture and oxygen absorption as well as lipids, flavor and odor change due to degradation or migration between packaging, food and the environment are important factors that impacts on food quality. These aspects are tightly correlated to the mass transfer phenomena during shelf-life of food products and cannot be dissociated from packaging properties (PETKOSKA et al., 2021). Because of this, films and coatings should be developed accordingly to its application purpose, e.g., layers for fruits should have lower water vapor permeability to reduce weight loss and reduce respiration.

The investigation of the water vapor permeability (WVP) of edible films are a valuable information to comprehend the mass transfer phenomenon since it implies diffusion and solubility of water moieties through the polymeric matrix. WVP represents the amount of water that infiltrates per unit of area of the film and time (kg m^{-1} s Pa), considering the film thickness and differential pressure (CAZÓN et al., 2017). Usually, polysaccharide-based films and coatings exhibit higher values of WVP than petroleum-based plastics. Natural polysaccharide-based films may present WVP value ranging from 6.6 x 10^{-13} to 1.7 x 10^{-8} than synthetic polymers, ranging from 1.1 x 10^{-14} to 0.5 x 10^{-11} (BASTARRACHEA, DHAWAN, SABLANI, 2011; CAZÓN et al., 2017). The

addition of lipids, plasticizers, and emulsifiers are a useful method to overcome higher values of WVP in edible films and coatings since this may decrease hydrophilicity.

Table 2. Edible coatings applied on fruits.

Matrix	Concentration	Additives	Food product	Reference
Carboxymethyl chitosan/ pullulan	Different mixing ratio of 5:0, 4:1, 3:2, 2.5:2.5, 2:3 and 1:4 (w/w)	8% galangal essential oil and 20% glycerol (w/w)	Mangoes	ZHOU et al., 2021.
Chitosan	1% (w/v)	40 mmol L^{-1} of ascorbic acid	Plums (*Prunus salicina*)	LIU et al., 2014.
K-carrageenan	0.2 – 0.8% (w/v)	0-1% glycerol (w/v)	Papaya (*Carica papaya*)	HAMZAH et al., 2013.
Sodium alginate	0, 1 and 3% (w/v)	20% glycerol (v/v)	Plum (*Prunus salicina*)	VALERO et al., 2013.
Sodium alginate	1.5% (w/v)	*Ficus hirta* extract, 0.7% citric acid and 1.0% sucrose ester (w/v)	Nanfeng mandarin (*Citrus reticulata*)	CHEN et al., 2016.
Starch/ chitosan	2% / 0.5-1.0% (w/v)	2% glycerol (w/v)	Apples Fuji cultivar	COSTA et al., 2020.
Starch/gelatin	3 - 5%/ 10% (1:1)	10% sorbitol	Red Crimson grapes	FAKHOURI et al., 2015.
Xantham gum	2.5 g L^{-1}	1.0 g L^{-1} cinnamic acid	Pears (*Pyrus pyrifolia* and *P. communis*)	SHARMA, S.; RAO, 2015.

Differently from polysaccharides, proteins-based films exhibited better mechanical and optical properties, as well as good barrier against gases permeability, especially O_2 and CO_2. The use of protein in food packaging provides a wide range of interactions and chemical reactions with other substances, through covalent (peptide and disulfide) and non-covalent (ionic hydrogen and van der Waals) bonds (QUIRÓS-SAUCEDA et al., 2014). They can be prepared as a mono or multilayer food packaging and blended with other polymers as a composite film. Some of the most used proteins in edible films are collagen, zein, gelatin, soy protein, milk protein and pea protein (DUBEY, DUBEY, 2020).

The processing methods used to obtain films or coatings will be influenced by many factors, such as the matrix composition, solubility, thermal behavior, flexibility, as well as their compatibility and cohesion forces, e.g., ionic, covalent and H-bonding, between polymer chains, and presence of additives (PETKOSKA et al., 2021; QUIRÓS-SAUCEDA et al., 2014; SILVA-WEISS et al., 2013). Coatings can be applied on foods using methods, such as dipping, spraying, fluidized bed processing, brushing, and panning. For the films production, mainly two types are used, wet and dry process. In the wet process, also known as casting, the polymers are solubilized and dispersed onto a flat surface, then dried under specific conditions until the film formation. In the dry processing, different methods, extrusion, injection, blow-molding, and heat-pressing, can be used without the use of liquid solvents, and process high viscous polymers (PETKOSKA et al., 2021). In the dry method, thermoplastic materials are transformed in films using thermomechanical techniques, which may be advantageous when compared to the wet process because do not need solvents. However, the dry method could not be used in the case of thermosensitive substances to be present in the matrix composition.

A composite edible film packaging commonly will consist of a blend two or more hydrocolloids aiming to improve their individual properties and application (CHAKRAVARTULA et al., 2019). In this, protein and lipid can be supported on a polysaccharide matrix, or the lipid material may be encapsulated on hydrocolloids and dispersed on the polysaccharide film matrix (PETKOSKA et al., 2021). This conformation may be used to improve mechanical properties and to overcome some processing limitations. Furthermore, the incorporation of natural or chemical additives, such as plasticizers, may also contribute to improve mechanical, functional, sensorial, and nutritional features of edible films (PARREIDT, MÜLLER, SCHMID, 2018).

3.3. **Natural and renewable polymers sources**

A wide range of natural polymers from renewable sources have been used in the development of a biobased food packaging. The main natural sources to this purpose are derived from polysaccharides, proteins, lipids, or blends of these macromolecules (CAZÓN et al., 2017; LIANG et al., 2017) (Figure 4). The utilization of these natural materials is partly linked to its biodegradability and renewability. However, some other advantages are expected when used to food packaging, e.g., as they can act as carriers of functional substances adding well-being benefits, incorporating flavorings

and colorings aspects, enhancing organoleptic characteristics, improving mechanical and barrier resistance, and others (PETKOSKA et al., 2021).

Polysaccharides are known to possessing good oxygen barriers and having great hydrogen bonding, which can be used to the incorporation of functional substances, e.g., coloring, flavoring, and antioxidants agents. On the other hand, these materials do not have good barrier to water vapor, which can be overcome blending it with other hydrophobics macromolecules, such as lipids (MOHAMED, EL-SAKHAWY, EL-SAKHAWY, 2020; PETKOSKA et al., 2021). Polysaccharides, such as pectin, cellulose, starch, carrageenan, pullulan, xanthan, alginate, and chitosan, have been used to develop natural-based packaging (CAZÓN et al., 2017; MOHAMED, EL-SAKHAWY, EL-SAKHAWY, 2020).

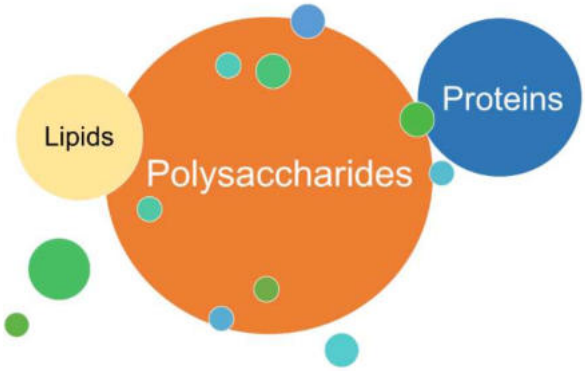

Figure 4. Major natural biological materials used in food biobased packaging.

3.3.1. Chitin and chitosan

Chitosan is a natural polysaccharide derived from chitin. These are the most abundant biopolymers from animal source (HAGHIGHI et al., 2020). Chitin is an important structural component of the invertebrate exoskeleton of insects and other terrestrial arthropods (e.g., beetles and locusts), crustaceans (e.g., crab, shrimp, and krill), that can be extracted from it or produced by microorganisms (e.g., fungi, and some algae) (HAGHIGHI et al., 2020; SANCHEZ-SALVADOR et al., 2021).

The earliest reports on chitin are from the early 19th century, when Antoine Odier extracted an alkaline-insoluble fraction from the insects' exoskeleton and named it *Khiton*, which in Greek means tunic or an envelope. The first works with chitosan dates from the 1850s, when Charles Rouget reported that obtained a novel *chitine modifiée* after treating chitin with a concentrated alkaline solution under reflux, making this modified chitin soluble in organic acids (CRINI, 2019). Many years later, back in the 1890s, shells from crabs, scorpions and spiders were treated by Felix Hoppe-Seyler

with a solution of potassium hydroxide at 180°C, obtained a product and dissolved in an acid solution, naming it as chitosan (CRINI, 2019; HAGHIGHI et al., 2020). Up to the 1950s, chitin and chitosan gained considerable attention due to the increasing exploitation of natural polymers.

Chitin is a linear polymer of mainly *β*-(1→4)-2-acetamido-2-deoxy-*D*-glucopyranose units and low amounts of *β*-(1→4)-2-amino-2-deoxy-*D*-glucopyranose residues (Figure 5) (SANCHEZ-SALVADOR et al., 2021; VAN DEN BROEK et al. 2015). In solid state, it can be found in three different crystalline polymorph structures, anti-parallel *N*-acetylglucosamine chains or α-chitin, parallel chains of N-acetylglucosamine or β-chitin and two parallel chains alternated with a single anti-parallel one, forming the γ-chitin (HOELL, VAAJE-KOLSTAD, EIJSINK, 2010; KHAYROVA, LOPATIN, VARLAMOV, 2021). The first two forms are the most frequent in nature and these arrangements may contribute to its mechanical properties (HOELL, VAAJE-KOLSTAD, EIJSINK, 2010).

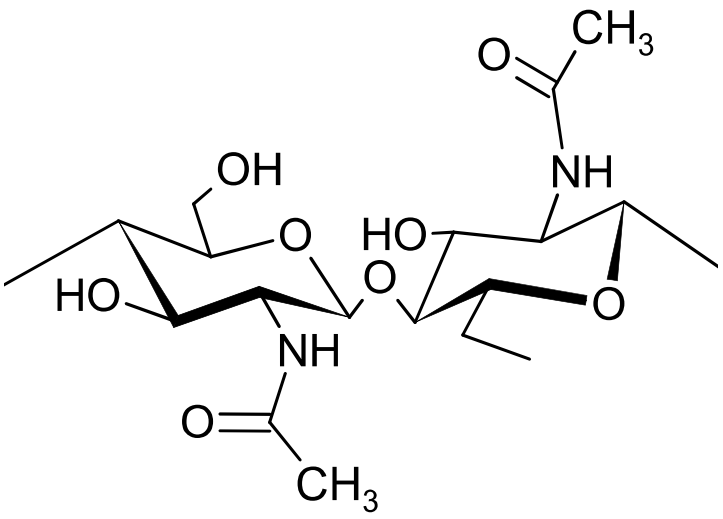

Figure 5. Chemical structure of chitin.

Reports from FAO (FAOSTAT, 2021) have listed that the world production of crustacean in 2013 was 12,607.540 tons, of which Asia was the biggest producer (81.4%), followed by Americas (13.7%), Europe (3.5%), Africa (1.1%) and Oceania (0.3%). A substantial amount of waste is produced during seafood processing, making the extraction of chitin from this residue a good opportunity to add value to this market and to reduce the environment contamination. About 20 to 30% of chitin, as well as proteins, minerals, and pigments, can be extracted from shrimp shell waste (ABDEL-RAHMAN et al, 2015). Researchers have investigated the transformation of

crustaceans' shells into a more valuable compound and a potential source of ingredients to food industry (BASTOS et al., 2010). Japan have been dominating the chitin/chitosan market since the 1980s until nowadays, being responsible for more than 35% of its industrialization in 2015 and consuming more than 800 tons per year (MORIN-CRINI et al., 2019). Even though, chitin is an underutilized biomass resource, being mostly used to the chemical production of chitosan.

Chitin is insoluble in many organic and inorganic solvents, due to its high intra and intermolecular hydrogen bonds. Its dissolution is essential to estimate the molecular weight (M_w), however the presence of aggregates in chitin solution trickles the measurements by light scattering falling on this calculation (YOUNES, RINAUDO, 2015). To bypass this, some green solvents as ionic liquids and deep eutectic solvents, e.g., 1-allyl-3-methylimidazolium bromide, 1- ethyl-3-methylimidazolium alkanoates and others, have been recently used to chitin solubilization (KHAYROVA, LOPATIN, VARLAMOV, 2021). As chitin is a polymer highly acetylated and insoluble in water, traditional methods, as chemical deacetylation, or enzymatic hydrolysis, are most commonly used to make it less hydrophobic, which results in the production of chitosan (HOELL, VAAJE-KOLSTAD, EIJSINK, 2010; MUXIKA et al., 2017; VAN DEN BROEK et al. 2015). Its chemical deacetylation involves an alkaline treatment at high temperatures. Different factors, such as alkali concentration, processing time, chitin:alkali ratio, temperature, and chitin source, can affect the degree of *N*-acetylation (DA) of chitosan.

Chitosan is a versatile natural polymer with a broad range application in food products, mainly due to its biodegradability, biocompatibility, nontoxicity, and bioactive properties, such as antioxidant, antimicrobial, and anticancer activities (MUJTABA et al., 2019). It is a linear random copolymer of *N*-acetyl-*D*-glucosamine (*A*-units) and deacetylated *D*-glucosamine (*D*-units) units connected by *β*-1,4 glycosidic linkages (Figure 6), obtained from the chemical alkaline deacetylation of chitin (MUJTABA et al., 2019; MUXIKA et al., 2017). In each repeating chitosan molecule three functional groups are present, i.e., primary, and secondary hydroxyl groups and amine groups, which allow chemical changes under pronation, and influence in its biological, mechanical, and physical-chemical characteristics, including solubility, hydrophilicity, and crystallinity (KHAYROVA, LOPATIN, VARLAMOV, 2021; MUJTABA et al., 2019). The amine groups, NH_2, located on C-2 of the rings on the *D*-glucosamine repeated units pronate and induce the changes of CS to a polyelectrolyte polysaccharide under

acidic environment, acquiring a polycationic characteristic (BASTOS et al., 2010; MUJTABA et al., 2019).

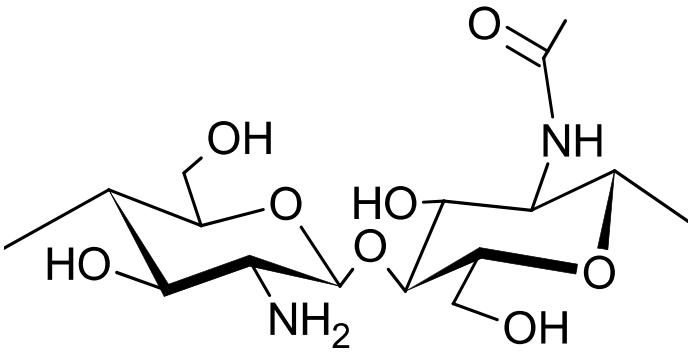

Figure 6. Chemical structure of chitosan.

The properties of chitosan in solution depends on its degree of acetylation (DA), the chain length, and distribution of acetyl groups along the chain (HOELL, VAAJE-KOLSTAD, EIJSINK, 2010). The DA is given by the ratio between its acetylated and deacetylated units and expressed as molar percentage (mol%). The DA can range between 0.05 – 0.30 and below 50% makes chitosan soluble on aqueous acidic media (MUXIKA et al., 2017; VAN DEN BROEK et al., 2015). The chitosan origin may influence on its DA as well as on its M_w. Generally, microbial chitosan exhibited a lower DA than those extracted from the exoskeleton of crustaceans (PHILIBERT, LEE, FABIEN, 2017). Heterogenous deacetylation played on solid state chitin may produce block-wise distribution of acetyl groups causing chain linkage and consequently affecting its dissolution and M_w quantification (YOUNES, RINAUDO, 2015). The DA and the M_w are the most important factors contributing to the physical-chemical identity of chitosan and influence its structure-properties relationships, e.g., solubility, viscosity, and gelling abilities, among others (GONZÁLEZ-ESPINOSA et al., 2019; KASAAI, 2008).

The main characterization of chitosan starts with the determination of its M_w in solution, followed by the DA quantification and finally the distribution of acetyl groups along the backbone chain (by nuclear magnetic resonance - ^{13}C-NMR) (YOUNES, RINAUDO, 2015). Various methods have been used to quantify the M_w of chitosan, e.g., viscometry, light scattering, osmometry, size exclusion chromatography and more recently the multi-detection asymmetric flow-field flow fractionation (GONZÁLEZ-ESPINOSA et al., 2019). The DA determination for chitosan can be realized by infrared spectroscopy, potentiometric titration, and elementary analysis, although, the ^{1}H liquid state and solid state ^{13}C-NMR spectroscopy have been favored (KASAAI,2008;

YOUNES, RINAUDO, 2015). Besides these parameters, the intrinsic viscosity [η] also is an important factor to be considered on chitosan characterization. The η may be determined by double extrapolation to zero concentration of Huggins' and Kraemer equations, Equation 1 and Equation 2 (BASTOS et al., 2010).

$$\frac{\eta_{sp}}{C} = [\eta] + k'[\eta]^2 C \qquad (1)$$

$$\frac{(Ln\ \eta_{rel})}{C} = [\eta] + k''[\eta]^2 C \qquad (2)$$

where η_{rel} and η_{sp} are the relative and specific viscosities, k' and k'' are the are the Huggins' and Kraemer's coefficients, respectively, and C is the chitosan solution concentration.

The intrinsic viscosity is essential to determine the viscosity average molecular weight, M_v, using the Mark-Houwink-Sakurada relationship as expressed in the Equation 3 (BASTOS et al., 2010; YOUNES, RINAUDO, 2015).

$$[\eta]\ (mL\ g^{-1}) = K M_v^a \qquad (3)$$

where $[\eta]$ is the intrinsic viscosity, K is the intercept log and a is the equation slope, both are constants, and M_v is the viscosity average molecular weight for chitosan.

Brugnerotto et al. (2001) characterized chitosan by steric exclusion chromatography with different DA (0.5 to 25 mol%) and found values to the K and a constants varying from 0.080 to 0.068, and 0.796 to 0.800 (random coil), respectively, when the used solvent was AcOH 0.3 M/ AcONa 0.2 M at 25 °C. High values (>0.800) of a coefficient indicates a semi-rigid feature of the polysaccharide with a very stiff chain, and when a presents a low value (<0.650) is an indication that the chain is compact sphere, which can affect their hydrodynamic volume, dimensions and viscometry (YOUNES, RINAUDO, 2015). However, the most frequent values reported for the constant a ranged between 0.7 and 1.0, indicating that chitosan behaves like a flexible or linear conformation depending on the solubilization solvents (KASAAI, 2007).

It is an eco-friendly biopolymer as it is biodegradable on various environments (Figure 7). Chitosan is a versatile material being used to a wide range of applications. To environmental purposes, CS can be used to water purification, membrane filtration,

flocculation/coagulation of dyes and proteins, and wastewater treatments, as it is a competent sorbent material for heavy metals, pesticides, and dyes (ANNU, RAJA, 2020; HOELL, VAAJE-KOLSTAD, EIJSINK, 2010; MORIN-CRINI et al., 2019; MUXIKA et al., 2017). In agricultural production, CS can be applied as micro/nanoparticles acting as fertilizer carriers aiming to mitigate deleterious effects to plants and human health (MUXIKA et al., 2017; OLIVEIRA et al., 2016). It can be used in the development of electrochemical sensors in combination with conducting materials, ionic liquids, green solvents, and carbon nanotubes, and many other purposes are given in the chemistry industry (ANNU, RAJA, 2020; MORIN-CRINI et al., 2019).

Figure 7. Biodegradability of chitosan and other natural polymers on various environments. Adapted from Nova-Institute, 2021.

Chitosan greatest utilization is on the pharmaceutical, cosmetic, nutrition and food markets, mainly due to its classification as a safe substance, GRAS - generally recognized as safe, by regulatory agencies over many countries. In the United States, CS is classified as a preservative and antioxidant substance by the Environmental Protection Agency (EPA, 2021) and in Brazil, is approved as a functional health ingredient to food products by National Health Surveillance Agency of Brazil, *Agência Nacional de Vigilância Sanitária* (ANVISA, 2019). In the food and nutrition field, CS has a significative market in Asia, mainly Japan, China, and South Korea, followed by USA in North America and Europe, which reached more than 2000 metric tons in 2018 (MORIN-CRINI et al., 2019). This demand is mostly related to utilization of CS as a nutraceutical/functional ingredient in dietary supplements and as a natural additive with a wide range of functions in food products.

It is well documented the countless biological activities of chitosan, such as antioxidant, antimicrobial, antifungal, anti-inflammatory, wound healing, immunostimulant, prebiotic (LOPEZ-SANTAMARINA et al., 2020; MORIN-CRINI et al., 2019; MUXIKA et al., 2017; PHILIBERT, LEE, FABIEN, 2017). Chitosan is non-digestible in the upper gastrointestinal tract, influencing/ blocking the absorption of carbohydrates, fats, and cholesterols in this, and contributing to a faster intestinal transit time. Additionally, it is reported that CS could increase the excretion of atherogenic saturated fatty acids, which could lead to a reducing risk of developing a chronic disease (PHILIBERT, LEE, FABIEN, 2017). Furthermore, as a dietary fiber, chitosan can be considered as a prebiotic material, due to the improvement of gut microbiota (LOPEZ-SANTAMARINA et al., 2020). For this reason, CS has been commonly used as a dietary product as part of an effective body weight regimen and control of fat mass, even though, this effect is not completely unanimous in the literature.

A recent single-blinded, placebo controlled and random clinical study (500 mg of CS, five/day) for body weight reduction found that CS from fungal origin reduced the average body weight up to 3 kg after 90 days, promoted an improvement in body composition, and anthropometric parameters (TRIVEDI et al., 2016). In another work that performed a systematic review of CS consumption through a meta-analysis of 15 randomized controlled trials found a significant reduction ($p<0.05$) in body weight and body fat of the overweight/obese participants that received CS supplementation (HUANG et al., 2020). Even though, studies aiming to investigate this question may differ in their results because there is different sources and types of chitosan, the dosage often varies as well as the dosage timing, different methodologies to assess end points (weight loss *vs* fat loss), lack of well-constructed clinical trials, and others affecting conclusion (PREUSS, KAATS, 2006).

Another common utilization of CS by food industry can be pointed out due to its excellent antimicrobial/antioxidant properties. To this purpose, CS can be used in many different forms and applications, e.g., as solution, powders, gels, beads/particles, fillers, films and casting or sprayed coatings, and its blends. The use of chitosan for preservative purposes of foods as an antimicrobial/antifungal agent has been well reported by Friedman and Juneja (2010); Ma, Garrido-Maestu, Jeong (2017); Muñoz-Bonilla, Cerrada, Fernández-García (2014); Sahariah and Másson, (2017); Verlee, Mincke, Stevens (2017). A summary of the broad chitosan application is listed in Table 3.

Table 3. Broad application of chitosan to different purposes.

Application	Purpose	Product	Reference
Nutraceutical/functional ingredient	Body weight reduction	Oral capsules	HUANG et al., 2020
Additive in food products	Texture controlling agent	Rice noodles; meat product	KLINMALAI et al., 2017; HAN et al., 2018.
	Emulsifying/gelling agent	Films; microparticles	PEREDA, AMICA, MARCOVICH, 2012; MORELLI, HOLDICH, DRAGOSAVAC, 2016.
		Pastes	MUXIKA et al., 2017.
Biological, antimicrobial or antioxidant activity	Preservation agent in powder	Rice	RACHTANAPUN et al., 2015.
	Film/coatings	Fish fillet	BONILLA et al., 2018.
		Chicken fillet	MENCONI et al., 2013.
		Meat cutlets	RAJAEI et al., 2017.
		Fruits	DUAN et al., 2019; ZHOU et al., 2021.
	Nanofibers	Active food packaging	HAI et al., 2020.
	Hydrogels	Delivery of enzymes	WU et al., 2018.
	Liposomes	Delivery of bioactive substances	YAROSLAVOV, et al., 2021.

Mainly, the physical state as well as chitosan solubility are the most significant factors that affects its antimicrobial activity, since it was observed that its microbial inhibition action is only observed in acidic medium, in which is soluble and has net positive charge (SAHARIAH, MÁSSON, 2017). Other environment factors, such as molecular weight, DA, positive charge density, pH, ionic strength, and temperature, also can influence on its antimicrobial activities (MA, GARRIDO-MAESTU, JEONG, 2017; MUÑOZ-BONILLA, CERRADA, FERNÁNDEZ-GARCÍA, 2014). Even, it is not completely elucidated, antimicrobial, antifungal, and antiviral properties have been correlated to interaction with chitosan protonated groups, which involving electrostatic

stacking at cell surface, chelation of essential trace elements and metalloenzymes, protonation forms and cell membranes disruption, and blockage of RNA transcription from DNA when chitosan molecules are inside cell's nucleus (CAZÓN et al., 2017; FRIEDMAN, JUNEJA, 2010; PHILIBERT, LEE, FABIEN, 2017; VAN DEN BROEK et al., 2015). Thus, its antimicrobial activity is restricted to the target microorganism. Although chitosan possesses a wide range of inhibition activity against numerous microorganisms, fungi seem more susceptible to its action than bacteria (MUÑOZ-BONILLA, CERRADA, FERNÁNDEZ-GARCÍA, 2014). Furthermore, chitosan easily forms quaternary ammonium salts at low pH values. Thus, organic acids, such as acetic, formic, and lactic acids can dissolve it (ABDEL-RAHMAN, et al., 2015). Acetic acid, generally at 1% concentration, is the most common organic acid used to chitosan dissolution (DUAN et al., 2019). When chitosan is dissolved in an acidic media, generally below pH 6.5, its amino groups in the main chain protonate and turns in to a cationic polysaccharide. This positively charged groups, protonated amines, allow the interaction with a wide range of negative charged molecules forming complexes. Some of these negative charged substances are anionic synthetic or natural polymers, dyes, lipids, fats and cholesterol, metals ions, enzymes, biological cells, DNA and RNA (KHAYROVA, LOPATIN, VARLAMOV, 2021).

3.3.1.1. Chitosan-based films

Chitosan is among the most studied polysaccharides for the development of film/coating packaging. This is justified by its versatility, good physical-chemical and biological properties. Mechanical properties are affected by the chitosan DA, solvent, pH, concentration, viscosity, and molecular weight (MUJTABA et al., 2019). Moreover, chitosan is generally less expensive and commercially available when compared to other biopolymers (VAN DEN BROEK et al. 2015). The first reports of chitosan films are from the mid-1930s, when George W. Rigby patented it (CRINI, 2019). Since there, the employment of chitosan as films, coatings, or composites, to different products were extensively increased. Recent works on the sustainable application of chitosan-based films for food packaging were reviewed by Haghighi et al. (2020) and Mujtaba et al. (2019).

Films based on chitosan are environmental-friendly materials and can be degraded by microorganisms (LIANG et al., 2017). Leceta et al (2013) have studied the environmental assessment between two different food packaging systems, polypropylene, and chitosan films, during different life cycle stages. For them, from

about 1 kg of chitosan-based film waste, 20% can be considered as compost and the remaining 80% are degraded as organic matter by microorganisms. Furthermore, these authors found that the highest positive impact of chitosan-based films is related to the end-of-life scenarios, especially associated to composting and carcinogens, when compared to polypropylene films, which can provide a reduction on environmental pollution generated by food packaging industry. In another work, the biodegradability of chitosan-based films on three different soils, industrial compost, commercial garden soil, and soil from a vineyard, was evaluated. The authors found that the properties of chitosan-based film deteriorate in less than 3 days and its biodegradation occurred in all tested soils after 14 days (OBERLINTNER et al., 2021). Moreover, when these films were incorporated with *Quercus* polyphenol extract its active properties in compost and garden soil occurred in 6 days, while total biodegradation process was not completed in the vineyard soil during the 14 days. These authors also found that adding of water to the soil decreased the rate of biodegradation from the chitosan film on terrestrial environment. These findings are relevant to confirm the biodegradability of chitosan films when using it as a sustainable alternative food packaging.

Pure chitosan films can only be prepared via solvent casting. In this process, chitosan is dissolved using enough solvent, mainly, acidified water, placed in a flat surface and let to dry until constant weight. Generally, these pure films are reported to exhibit a smooth, continuous, and compact surface, but are brittle and fragile possessing low mechanical properties (HAGHIGHI et al., 2020; LIU et al., 2013; VAN DEN BROEK et al., 2015). To overcome the low mechanical performance and high sensitivity to water, the addition of plasticizers and other different approaches have been indicated. Some of these are using crosslinking, complexation, graft copolymerization, surface coating, filler incorporation and others (HAGHIGHI et al., 2020). Blending chitosan with other polymers to form composite films could also be a strategy.

In the mechanical properties, the tensile strength (TS) and elongation at break (EB) are two of the most important characteristics for film applications (VAN DEN BROEK et al., 2015). TS is related to the maximum tensile stress that a film can hold up (SUN et al., 2020). Moreover, TS of chitosan films with high and low M_w was described as dependent on storage time due to the conformational changes of chitosan molecules by the free volume reduction (KERCH, KORKHOV, 2011). The type of solvent acid used to prepare chitosan-starch composite films also influenced TS

according to the following order: lactic acid < malic < acetic acid (ZHONG, LI, 2011). In another work, chitosan film displayed a significantly lower TS, 18.252 MPa, but a higher EB, ~40%, than gelatin and composite films (WANG et al., 2021). In the development of chitosan-zein composite films, Sun et al. (2020) found that TS was influenced by different plasticizers, sorbitol < glycerol and PEG-400, which can be explained by more hydroxyl groups in sorbitol making it bind more water molecules. The TS values may also decrease when the increase of pH because of a lower chitosan dissociation (CAZÓN et al., 2017). Furthermore, in chitosan composite films with quinoa protein, it was observed that TS and EB were influenced by the presence of protein in the films (ABUGOCH et al., 2011).

Water vapor and oxygen barrier are relevant factors to consider in the development of food packaging since both can influence the food quality and shelf-life. The evaluation water vapor permeability (WVP) of polysaccharide-based films provides information of diffusion and solubility of water molecules through the polymeric matrix and will be influenced by its composition. In this way, Kerch and Korkhov (2011) investigated the WVP of films of high and low M_w chitosan and found that the high M_w chitosan films exhibited higher permeability. The addition of a natural phenolic antioxidant, protocatechuic acid, significantly decreased the WVP of chitosan composite films (LIU et al., 2017). Furthermore, the addition of vegetable olive and corn oils displayed a significant effect decreasing the WVP by the diminution of the hydrophilic content of the film (GIANNAKAS et al., 2017). Depending on the chitosan M_w, solvent, plasticizer content, film composition, and pH, different results are reported to the mechanical and barrier properties, which makes more challenging the values comparison. Some application examples of chitosan-based films are listed in the Table 4.

Table 4. Broad application of chitosan-based films and their main results.

Film matrix	Composited ingredient	Application	Main results	Reference
Chitosan/Zein	Glycerol, PEG-400, and sorbitol	Potential food application	- Permeability increased with higher plasticizer concentration. - PEG-400 promoted better barrier performance.	SUN et al. (2020)
Chitosan	Aloe vera gel and silver nanoparticles (SNPs)	Potential biomedical applications	- SNPs decrease the crystallinity of the films. - SNPs affected the structure and viscoelastic behavior of chitosan films.	MADIAN, MOHAMED, 2020.
Chitosan	Glycerol	Strawberries	- Protection of the fruit against fungi - Maintenance of flavor, appearance, texture, and aroma.	PAVINATTO et al., 2020.
Chitosan	Apple peel polyphenols (APP)	Potential bio-composite food packaging material	- APP significantly increased the thickness, density, solubility, opacity, and swelling ratio of the films. - APP decreased the moisture content, water vapor permeability, TS and EB pf the films.	RIAZ et al., 2018.
Chitosan/ organoclay nanocomposites (OrgMMT)	Olive oil and corn oil as plasticizers	Potential food packaging applications	- OrgMMT significantly reduced the EB of all oil containing samples acting as stress concentrator upon deformation. - Corn oil was a less effective as plasticizer than olive oil.	GIANNAKAS et al., 2017.
Chitosan/Gelatin	Red grape seed extract and *Ziziphora clinopodioides* essential oil	Potential food packaging applications	- The addition of Red grape seed extract and *Ziziphora clinopodioides* essential oil improved total phenolic content, antibacterial and antioxidant activities, thickness, and water vapor barrier property.	SHAHBAZI, 2017.

Continuation of Table 4. Broad application of chitosan-based films and their main results.

Chitosan/Corn starch	Glycerol as plasticizer	Potential food / pharmaceutical applications	- The WVP and moisture content of films increased with an increase of chitosan concentration. - Incorporation of chitosan increased solubility, total color differences, TS, and EB of the films.	REN et al., 2017.
Chitosan	Propolis extract	Potential food packaging applications	- All chitosan/ Propolis extract films inhibited bacteria on contact surface underneath the film. - Mechanical properties, oxygen and moisture barrier, antioxidant and antimicrobial properties were improved by the addition of Propolis extract into the films.	SIRIPATRAWAN, VITCHAYAKITTI, 2016.
Chitosan	Clove oil (*Syzygium aromaticum*)	Cooked pork sausages	- The shelf-life of cooked pork sausages increased from 14 to 20 days with the chitosan/clove oil films.	LEKJING, 2016
Chitosan/Gelatin	Glycerol as plasticizer	Beef steaks	- Myoglobin oxidation during retail display was reduced and the percentage of deoxymyoglobin increased with the gelatin content of the film.	CARDOSO et al., 2016

3.3.2. Alginate

Alginate is a natural anionic polysaccharide from marine origin. This biopolymer is widely used in the food, and pharmaceutical/cosmetic industries because of its biodegradability, biocompatibility, bioavailability, nontoxicity, and low price (AGÜERO et al., 2017; BAYBAŞ, SERDAROĞLU, SEMERCI, 2021). Although, the major contribution to its employment is due to their functional properties, such as notable crosslinking capacity, good gelling and film-forming properties, fine water absorption, thickener, emulsion-stabilizer, pH-sensitivity, mucoadhesiveness and others (AGÜERO et al., 2017; HAMEDI et al., 2017; TAVASSOLI-KAFRANI, SHEKARCHIZADEH, MASOUDPOUR-BEHABADI, 2016). Moreover, alginic acid and its salts are classified by the U.S. Food and Drug Administration (FDA) and European Commission (EC) as a food grade additive and approved to be used as a gelling, emulsifier, and thickener agent (PARREIDT, MÜLLER, SCHMID, 2018).

Alginates are largely isolated from different brown seaweeds, such as *Laminaria digitata*, *Macrocystis pyrifera* e *Ascophyllum nodosum,* being the most important of them (GOH, HENG, CHAN, 2012). These diverse seaweed sources can influence on the properties of alginate. Although, it can be obtained from microbial origins, employing microorganisms from *Azotobacter* and *Pseudomonas* genus, is not economically feasible (AGÜERO et al., 2017; DRAGET, SMIDSRØD, SKJÅK-BRÆK, 2005). Furthermore, the algae origin is mainly used to commercialize it as sodium alginate, a salt from alginic acid (AGÜERO et al., 2017; HAMEDI et al., 2017).

Alginates can be extracted from seaweeds by extraction with a hot alkali solution, usually sodium carbamate. Afterwards, alginates dissolves as sodium alginate forming a very dense slurry, which may contain undissolved algae cellulose parts, and need to be diluted and press filtered. Finally, the alginate is precipitated from the filtered solution, eighter as alginic acid or calcium alginate. To improve this process, to obtain a less colored product and reduce the loss of viscosity, an acid pretreatment can be performed (GOH, HENG, CHAN, 2012; TAVASSOLI-KAFRANI, SHEKARCHIZADEH, MASOUDPOUR-BEHABADI, 2016). The monovalent salts from alginic acid are sodium alginate, potassium alginate, ammonium alginate and calcium alginate. From these, the sodium alginate, potassium alginate and ammonium alginate are soluble in water, while the other are not (PARREIDT, MÜLLER, SCHMID, 2018). It can be highlighted that sodium alginate is the most used salt from alginic acid.

The industry of seaweed hydrocolloids, which include alginate, agar, and carrageenan, has been growing in the order of 2-3% per year, mainly in Asia region (PORSE, RUDOLPH, 2017). China is the major manufacturing market of seaweeds reaching 10 million tons in 2014, especially of *Laminaria (Saccharina) japonica*, followed by Indonesia and Philippines in Asia (BUSCHMANN et al., 2017; PORSE, RUDOLPH, 2017).

In Americas and Europe, the seaweed market is dominated by Chile (*Lessonia spp.* and *Macrocystis*), with more than 20,000 dry tons in 2015 and Norway and France (*Laminaria ssp.* and *Ascophyllum ssp.*), respectively, with a production of more than 32,000 dry tons in 2015 (PORSE, RUDOLPH, 2017). Besides this market is expanding, only a small fraction of the global biomass supply of seaweeds are produced. Some researchers suggests that the cultivation of seaweeds offshore could provide an alternative source of biomass leading to a sustainable production of food, chemicals, and biofuels (BUSCHMANN et al., 2017).

The utilization of seaweeds to food and feed by mankind has an ancient history. The earliest written report was tracked in China and dated from about 1700 years ago (BUSCHMANN et al., 2017). For many centuries, the harvesting and consumption of seaweeds were linked to costal inhabitants, until its scaleup industrial utilization in the 19th century. The first extraction reports of alginic acid extracted from kelps are from the 1880s, by the British chemist Edward C. Stanford (DRAGET, SMIDSRØD, SKJÅK-BRÆK, 2005). He patented and published a paper with his discovery in 1883 at The Chemical News and Journal of Physical Science (1883: Jan.-June, v.47, p. 254-257), entitled as '*On Algin: A new substance obtained from some of the commoner species of marine algae'.* Later, alginate was firstly used as a food gelling agent to the production of artificial cherries in 1946 (QIN et al., 2018). Since there, alginates have been widely used in different industries, such as in textile, pharmaceutical, cosmetic, food and other fields. Some examples of the utilization of alginate to different purposes are listed in Table 5.

Table 5. Some recent application of alginate to diverse purposes.

Function	Application form	Purpose	Reference
Physical properties	Composite gel	Improvement of rheological properties of food products	PEÑA-CHÁIDEZ et al., 2021.
	Films	Improvement of water barrier	NEHCHIRI, AMIRI, RADI, 2021.
		Evaluate the effect of crosslinking and M/G ratio	COSTA et al., 2018.
Quality and antimicrobial properties	Edible coating	Shelf-life of chicken fillet	HAMEDI et al., 2017
		Shelf-life of fish fillet	VITAL et al., 2018.
	Food ingredient	Fortified wheat noodles	HONG et al., 2021.
Biological activities	Composite hydrogel as micro/nano particles	Potential drug design	BAYBAŞ, SERDAROĞLU, SEMERCI, 2021
		Release of bioactive immobilized substances	OSMOKROVIC et al., 2018.
		Design of encapsulation systems	PRAVINATA et al., 2016.
		Acrylamide removal from coffee	BEDADE, SUTAR, SINGHAL, 2019.
	Hydrogel films	Wound healing	PEREIRA et al., 2013.
	Food ingredient	Salt-adsorbing materials	FUJIWARA et al., 2021.
		Fat mass reduction by the bread intake	HOUGHTON et al., 2019.

Alginate is a linear co-polymer of alternating units of α-1,4-L-guluronic acid (G) and β-1,4-D-mannurunic acid (M), forming 3 different regions (Figure 8) (AGÜERO et al., 2017). The molecular weight of alginate varies from 32 to 400 kDa according to its source, species, and processing methods (HU et al., 2021). In the 1960s, different researchers using partial hydrolysis were able to separate the alginic acid in three fractions, where two of them contained units of G and M, while the last fraction contained balanced proportions of both blocks, MG dimers residues. Later on, it was

elucidated that alginate have no regular repeating unit and that the monomers distribution along the backbone chain cannot be predicted by statistical analysis, Markov or Bernoullian's model (DRAGET, SMIDSRØD, SKJÅK-BRÆK, 2005). These models were used to assign the bacterial composition to a post-polymerization epimerization pathway, though, it does not fit for ascribing the algal monomer sequences (GOH, HENG, CHAN, 2012).

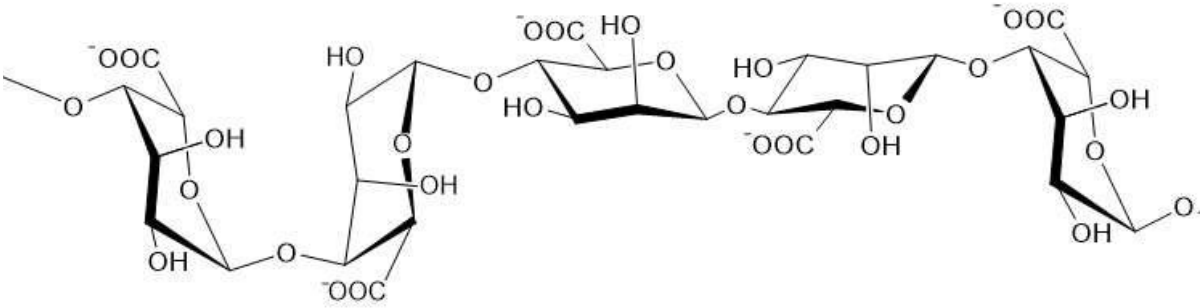

Figure 8. Chemical structure of alginate in chain conformation.

The G and M units forms homopolymeric blocks, whilst MG residues forms the heteropolymeric blocks, and the distribution of these 3 regions on the polymer chain differ from its extracted source and influences the physical properties of alginate. M/G rations lower than 1 are an indication of higher amounts of guluronic acid, which influences the gels strength for its ability of form stronger linkages. For this, high G blocks alginates are greatly recommended for microcapsules formation (QIN et al., 2018). Some of these, such as greater gel strength and solubility in acid media, have been linked to the proportions of G and MG blocks on the polymer chain (TAVASSOLI-KAFRANI, SHEKARCHIZADEH, MASOUDPOUR-BEHABADI, 2016). Although the composition of these blocks can influence alginate physical properties, its molecular weight is also a significant factor to this (GOH, HENG, CHAN, 2012; HU et al., 2021).

Sodium alginate, a polyanion polymer, is soluble in water, in which it forms a viscous sol with volume swelling 10 times after water absorption, and insoluble in organic solvents (HU et al., 2021). Alginate solubility depends on 4 main factors, G and M distribution blocks, solvent pH, ionic strength, and presence of gelling ions. It can go through sol-to-gel transformation by inotropic gelation, resulted of the addition of multivalent ions that will act as crosslinking agents, e.g., calcium, magnesium, aluminium, manganese, and iron, or by lowering the pH below the pK_a value of the guluronic residue (CONZATTI et al., 2017; GOH, HENG, CHAN, 2012). Alginate is

greatly sensible to pH changes due to the presence of carboxylic acids along its chain. At pHs <3.4 (below pK_a to M = 3.38 and G = 3.65), the carboxylic groups are nonionized (−COOH) making alginate insoluble, whereas, at a pH > 4.4, then became ionized ($-COO^-$), resulting on the chain expansion by the electrostatic repulsion of these negative charges, reaching the highest point at pH 7.4 (AGÜERO et al., 2017).

The alginate affinity for divalent ions decreases in the following order: trivalent cations > Pb^{2+} > Cu^{2+} > Cd^{2+} > Ba^{2+} > Sr^{2+} > Ca^{2+} (AGÜERO et al., 2017; TAVASSOLI-KAFRANI, SHEKARCHIZADEH, MASOUDPOUR-BEHABADI, 2016). Even though, all these ions can react with alginate, the calcium ions are commonly used as crosslinking agents. This predilection can be linked to the formation of Ca-alginate network gel, as well as to the biocompatibility of calcium with human organism, which is an advantage when using it in the intake of medicines/nutraceuticals. Besides, the use of Pb^{2+}, Cu^{2+} and Cd^{2+} is restricted due to their toxicity (AGÜERO et al., 2017). To the alginate gels formation, a three-dimensional network is diaxially formed by the interaction of carbonyl groups from the G blocks with multivalent cations, such as calcium, resulting in the formation of a cavity or binding site, commonly named as “egg-box” conformation or zipping mechanism (GOH, HENG, CHAN, 2012; JURIĆ et al., 2021; TAVASSOLI-KAFRANI, SHEKARCHIZADEH, MASOUDPOUR-BEHABADI, 2016). Preparation, characteristics, and binding mode of alginate with different ions were critically reviewed by HU et al. (2021).

The Ca-alginate crosslinking was proposed to occur in three successive steps, firstly the ion interacts with a single G unit forming monocomplexes; in the second stage happens the formation of the egg-box dimers binding mechanism by zipping intra-cluster association of it; and finally, a lateral association of the egg-box takes place to generate multicomplexes by Ca^{2+} and Na^+ mediated interactions (Figure 9) (HU et al. 2021). Furthermore, this crosslinking model are in constant update, since studies are proposing new arrangements (WANG et al., 2018).

As it is known that calcium ions favorites binding sites in the guluronic segments, alginates with high M blocks, such as from *Laminaria digitata*, show lower affinity, consequently affecting its physical properties (GOH, HENG, CHAN, 2012). Thus, chemical composition, source, as well as the molecular weight and M/G ratio of guluronic blocks of alginate will affect the gelling properties quality, mainly gel strength. High G alginates trend to form a rigid and brittle matrix, while low G alginates may produce more elastic gels (GOH, HENG, CHAN, 2012). Furthermore, alginate blocks

interact differently with cations. In M blocks, cations are externally bind near to carboxylate groups, whilst, in G blocks, the ions are linked by the egg-box sites. In the MG blocks, cations are joined in a concave structure formed by M-G pairs (TAVASSOLI-KAFRANI, SHEKARCHIZADEH, MASOUDPOUR-BEHABADI, 2016).

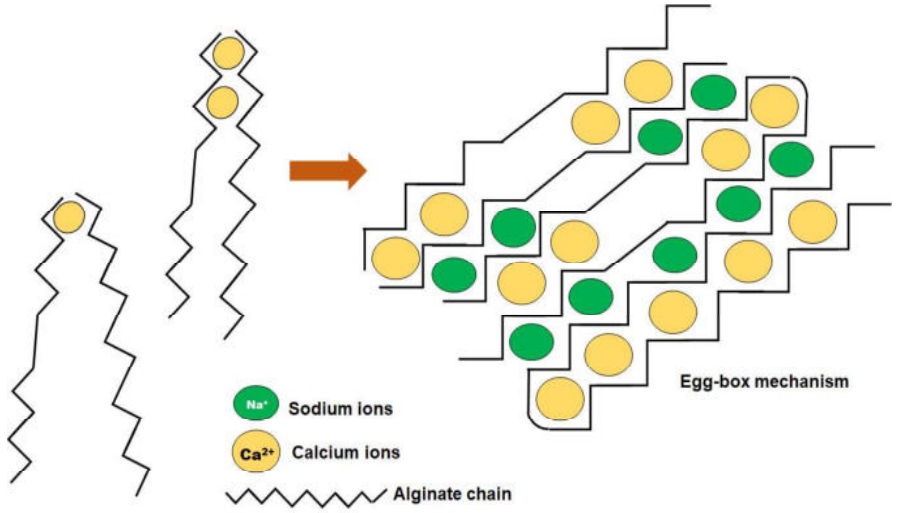

Figure 9. Schematic representation of the calcium-alginate binding mechanism by the formation of egg-box structure. Adapted from Hu et al. (2021).

The flexibility of alginate matrices can be increasingly influenced by its segment blocks according to the following order: MG > MM > GG (GOH, HENG, CHAN, 2012). Besides this interchain interactions, it is known that alginate as an anionic polyelectrolyte can be combined with a cationic polyelectrolyte, such as chitosan via complexation of their opposite charges, complex coacervation, aiming the formation of micro/nanoparticles to encapsulate bioactive substances (JURIĆ et al., 2021).

3.3.3. Pea protein

Plant-derived proteins have gained remarkable attention of food manufactures and consumers in the search for natural food resources and alternative materials to vegetarian, vegan, and food allergy diet restrictions. Protein-based film packaging exhibit extraordinary mechanical and barrier properties, especially to oxygen and carbon dioxide gases, when compared to polysaccharides (MOHAMED, EL-SAKHAWY, EL-SAKHAWY, 2020; QUIRÓS-SAUCEDA et al., 2014). Besides being an eco- friendly material, these films can nutritionally improve food quality and preservation. Moreover, the amphiphilic attribute of proteins contributes to its utilization as emulsifiers by stabilizing oil/water interface due to changes in interfacial tension (BURGER, ZHANG, 2019). Nowadays, a great variety of plant proteins have been

used in food industry and packaging, such as from soybean, wheat, corn, sunflower, and pea (ASSAD et al., 2020).

Pea, *Pisum sativum* L. ssp. *sativum*, is a notable grain legume that belongs to Fabaceae (or Leguminosae) and Papilionoïdeae botanical families, like soybean (FISCHER, CACHON, CAYOT, 2020). It is known by several common names such as common pea, green pea, garden pea, field pea, yellow field pea, spring pea, English pea, and Austrian winter pea (*Pisum sativum* L. ssp. *sativum* var. *arvense*) (TULBEK et al., 2017). Pea is a cool-season pulse crops largely cultivated for protein and feed purposes, being one of the most important food harvests, reaching around 11 Mt per year worldwide (FISCHER, CACHON, CAYOT, 2020). The major producers in 2014 were Canada and USA in Americas, France in the European Union, Russia at Eastern European, and Australia in Oceania regions (TULBEK et al., 2017). However, nowadays, with the major producing areas, in the ascending order, are Asia, Europe, Africa, Americas, and Oceania, reaching more than 21 million tons of green pea worldwide production in 2019 (FAO, 2020).

Up to 30% of proteins can be found in peas, which contains 65-80% of globulins and up to 20% of albumins (BURGER, ZHANG, 2019). Moreover, peas exhibit a good-balanced amino acid profile, highlighting higher amounts of lysine, around 6% and tryptophan than cereal grains, and deficient in methionine and cysteine than cereal grains (MCCARTHY et al., 2016; SHEVKANI et al., 2015; WEI et al., 2020). Five proteins fractions can be found in peas, though, the major fractions are from globulins (up to 70%) and albumins (around 25%), and the remaining are prolamins, glutelin and residue protein (DJEMAOUNE, CASES, SAUREL, 2019; TULBEK et al., 2017). Albumins are water-soluble metabolic and enzymatic proteins involved in cytosolic functions, unlikely, globulins are salt-soluble proteins which are used on seeds germination to provide nutrients for plant growing (MCCARTHY et al., 2016).

The major storage proteins found in pea seeds are globulins, which consists of legumin (11S, M_w ~380 kDa) and vicilin (7S, M_w ~60 kDa) and convicilin (7S). Legumin is a hexameric molecule containing six subunits held together by noncovalent interactions, that contains 4–5 acidic (α) (40 kDa) and 5–6 basic (β) (20 kDa) polypeptides from several gene families' precursors, linked by disulfide bonds. Vicilin is a trimeric protein containing three subunits each 50 kDa in size, that lacks cysteine residues and cannot form disulfide bonds. Convicilin, a third major storage protein in peas, has a subunit of ~71 kDa and a M_w in its native form of 290 kDa (BARAC et al.,

2010; ELMER et al., 2011; MCCARTHY et al., 2016). The variations in content, composition, and structure of both globulins, vicilin and legumin, reflects in their nutritional and functional properties, e.g., higher globulins content may result in greater emulsification properties (BURGER, ZHANG, 2019)

The pea protein, as well as other protein in seeds are considered bioactive proteins, as they can contribute to wellness and health. Nevertheless, the food applications of pea proteins are related to its nutritional value, distinguishable functional properties, low allergenicity, non-GMO status, and biological activities, such as reducing the risk of cardiovascular disease and lowering blood pressure effect (WEI et al., 2020). The extraction methods used to obtain pea proteins have a significant impact on its functionalities. A diverse number of methods have been used to extract plant proteins, which can be classified as conventional (solvent and alkali-based), physical (ultrasound, microwave, high-pressure and pulse electric field-assisted extraction), and green extraction technologies (single and concoction of enzymes) (KUMAR et al., 2021).

For pea protein isolation two processes, dry or wet extractions, can be used. The dry process is based on air classification, in which the pea seeds are milled into a flour, and separated in light and heavy fractions, protein and starch-rich respectively, by the application of a spiral air stream. For the wet process, the proteins are extracted according to their solubility in solutions, alkaline or saline, and further isolated by dialysis, micellar precipitation, or ultrafiltration (TULBEK et al., 2017; YANG et al., 2021). Recent studies have found that the methods used to pea protein recovery influence its composition and gelling properties, e.g., ultrafiltration and dialysis let to greater albumin fraction, while alkaline-isoelectric and micellar precipitation resulted in the retention of globulins (YANG et al., 2021). In this work, gels formed by pea proteins with higher compressive strength resulted from micellar precipitation and ultrafiltration extractions. Although, when considering yield protein isolates and protein solubility, the highest results can be achieved by salt extraction-dialysis, followed by alkali extraction/isoelectric precipitation and micellar precipitation, as found by Stone et al., (2015). In this same work, the authors found that salt-extracted isolates displayed greatest oil holding capacities and lowest water holding capacities. Additionally, pea protein isolate (PPI) is commonly obtained using isoelectric precipitation with pH around 4.5 followed by membrane separation, e.g., ultrafiltration or diafiltration, to increase protein concentration (MCCARTHY et al., 2016). Thus, the technological

understanding involving pea protein extraction and composition helps to achieve their better functional physicochemical properties and meticulously design of formulated products based on it.

Generally, functional properties of proteins can be categorized as related to: a) hydration (absorption of water and lipids, solubility, wettability, and thickening); b) structure and rheological behavior (adhesiveness, viscosity, elasticity, gelation and aggregation); c) protein surface (emulsification, foaming, whipping and formation of protein-lipid-based films) (SHEVKANI et al., 2015). From these, solubility, water- and lipid-binding capacities, rheological, emulsifying and gel forming properties, can be cited as mostly significative abilities for application in food products.

Beyond processing factors, environmental conditions, e.g., temperature, pH, ionic strength, and type of solvent, can significantly affect the functional properties of pea protein, especially its solubility. The solubilization of pea protein isolate is deeply influenced by pH variation, presenting minimum solubility between pH 4-6 (MCCARTHY et al., 2016). In another work, at neutral pH, pea protein exhibited the highest surface hydrophobicity value, low surface, and low solubility, resulting in a lower emulsion capacity when compared to chickpea, faba bean and lentil proteins produced by isoelectric precipitation and salt extraction (KARACA, LOW, NICKERSON, 2011). To overcome these issues, the use of polysaccharides forming stable complexes with proteins have gained interest. It prevents proteins aggregation and precipitation and improve functionalities. Furthermore, protein-polysaccharides plays important roles controlling food systems stability and forming film/coating and composite packaging materials.

3.4. **Plasticizing biodegradable films**

In the development of biobased films, the hydrophilic character of its natural macromolecules matrix should be considered since water molecules may be a problem to the shelf-life of the product as well as to the physical stability of the packaging. To overcome this issue, hydrophobic or less hydrophilic substances can be incorporated to the films modifying its physical properties. These substances are denominated plasticizers and are generally of low molecular weight. Plasticizers are responsible for increasing the matrix free volume and molecular mobility to amorphous biopolymers, competing chain-to-chain H-bonding along the polymers chains (QUIRÓS-SAUCEDA et al., 2014; RIVERO et al., 2016). They are often used to reduce the brittleness by

reducing the polymer interchain interactions by putting themselves between the polymers molecules, although they do not chemically bind to it (MKANDAWIRE, ARYEE, 2018).

The most commonly used plasticizers are glycerol, sorbitol, polyethylene glycols (PEG), lipids and their derivatives, such as fatty acids, phospholipids, lecithin, oils, and waxes, low molecular weight sugars, e.g., fructose-glucose syrups and honey, and others (MKANDAWIRE, ARYEE, 2018; QUIRÓS-SAUCEDA et al., 2014). Crosslinkers and micro/nano-reinforcements can be incorporated in film packaging aiming a superior tensile, gas and water barrier properties. Nevertheless, the improvement of cohesive strength of the coatings can be achieved by application of physical treatments, i.e., irradiation, by crosslinking formation (QUIRÓS-SAUCEDA et al., 2014). More recently, films plasticization can be performed using deep eutectic solvents (DES), as sustainable solvent systems (ALMEIDA et al., 2018; PEREIRA, ANDRADE, 2017; SOUSA et al., 2014).

DESs are obtained by complexation of a hydrogen bond donor (HBD) with a quaternary ammonium salt (hydrogen bond acceptor - HBA), producing liquids with physical and solvent properties analogue to ionic liquids (ILs) (ABBOTT et al., 2011; SMITH, ABBOTT, RYDER, 2014). Ionic liquids are liquid solvents with melting point below 100 °C and are formed from systems composed primarily of one type of discrete anion and cation. Initially, the DES were extensively used to decrease the temperature for molten salt applications, although nowadays it has been used to a wide range application, from lubrication of steel to synthesizing drug solubilization vehicles (ABBOTT et al., 2004; SMITH, ABBOTT, RYDER, 2014).

DESs contain large asymmetric ions of the HBA that have low lattice energy and so, low melting points, caused by hydrogen bonding formation. A wide range of mixture of substances can form DES, which were critically reviewed by Smith, Abbott, Ryder (2014). For plasticizing film packaging the most common DES used are the mixture of choline chloride-citric acid (ChCl-CA), choline chloride-urea (ChCl-Urea) and choline chloride-glycerol (ChCl-Gly). The latter has been used mainly for chitosan-based coatings (ALMEIDA et al., 2018; PEREIRA, ANDRADE, 2017; ZDANOWICZ, WILPISZEWSKA, SPYCHAJ, 2018). Particularly, the eutectic mixtures of ChCl:Gly at a molar ratio of 1:2 were found to efficiently plasticize starch and starch/zein blends, and chitosan and chitosan/ micro-crystalline cellulose/curcumin composites (PEREIRA, ANDRADE, 2017; SOUSA et al., 2014).

Many advantages can be pointed out from using DES as they are much cheaper, safer and easier to manufacture than ionic liquids. Moreover, DES are chemical and thermal stable, non-flammable, possessing high dissolution ability, lack of flammability, low volatility, low melting point and tailorability, as well as are water neutral, and low- or non-toxic. The DES toxicity, including cytotoxicity and phytotoxicity, is highly depended on the testing species used on the mixture and their responses, as well as their physicochemical properties, concentration, and salt's counteranion species (ZDANOWICZ, WILPISZEWSKA, SPYCHAJ, 2018). In the work of Mbous et al. (2017), the toxicity of some DES was tested, and they found that pure ChCl exhibited lower cytotoxic values than its aqueous solutions (EC_{50} 30 ≥ $ChCl_{aq}$ ≤ 40 mM), suggesting that ChCl did not dissociate after crossing the cellular membrane, implying a nontoxic profile of ChCl-based DES, although this should be further encountered *in vivo* or *in vitro* (MBOUS et al., 2017). As they are often biodegradable, they can be considered green solvents. DESs are appropriate to biobased packaging processing and application. To the preparation of polysaccharide films, DES mixture should be separately prepared and incorporated to the matrix materials or can be formed *in situ* after heat homogenization with other components (ZDANOWICZ, WILPISZEWSKA, SPYCHAJ, 2018).

3.5. **Incorporation of natural bioactive substances**

The incorporation of bioactive agents into packaging films is a growing strategy that aims to extend shelf-life, to increase lipid and microbial stability and safety when it is applied to food products. Furthermore, the use of active packaging to extend the food shelf-life and safety is an emerging and dynamic technology in food processing, since this coating can actively interact with the food surface and the environment based on the intrinsic property of their constitutional biopolymers or incorporated additives (SALGADO et al., 2015). Moreover, using natural bioactive compounds have become a good alternative for traditional packaging and replace synthetic additives commonly used in it, i.e., butylated hydroxytoluene (BHT) (DOMÍNGUEZ et al., 2018). Besides this, the addition of bioactive substances has been associated to microbial and physical improvements in film properties as well as health beneficial activities, such as antioxidant and probiotic, to consumers intake (NOGUEIRA et al., 2020). Some uses of different bioactive substances on chitosan-based films are listed in Table 6.

Table 6. Incorporation of bioactive substances in chitosan-based films.

Additives	Biological properties	Main results	Reference
Maqui berry extracts	Antimicrobial and antioxidant	- Effective against seven bacteria species. - Higher antioxidant activity.	GENSKOWSKY et al., 2015.
Grape seed extract and *Ziziphora clinopodioides* essential oil		- Improvement of total phenolic content, antibacterial and antioxidant activities, thickness, and water vapor barrier property.	SHAHBAZI, 2017.
Propolis extract		- Inhibition all tested bacteria on contact surface. - Tensile strength, elongation at break, total phenolic content and antioxidant activity increased.	SIRIPATRAWAN, VITCHAYAKITTI, 2016.
Apple peel polyphenols		- Improved the physical properties of the film. - Antioxidant and antimicrobial activities were significantly increased.	RIAZ et al., 2018.
Zataria multiflora Boiss EO and grape seed extract	Antioxidant	- Wettability of the surface, total phenol and antioxidant activity increased.	MORADI et al., 2012.
Green tea (GTE) and black tea extracts (BTE)		- GTE films presented stronger antioxidant activity than that of BTE films in all food simulants.	PENG, WU, LI, 2013.
Carvacrol	Antibacterial activity	- Incorporation of carvacrol was not effective against bacterial activity.	KAMDEM, SHEN, NABINEJAD, 2019.

Natural bioactive materials can be obtained from plants, animals, marine organisms, and microorganisms using biotechnological methods (QUIRÓS-SAUCEDA et al., 2014). Plant-based bioactive substances are widely found in nature and is mainly secondary metabolites that presents inherent biological functions. They can be obtained from renewable plant parts, such as, leaves, flowers, fruits, seeds, grains,

roots, and other vegetable portions, as extracts, resins, essential oils, or vegetable oils and fats. In these materials, a wide number of natural phytochemicals, such as phenolic acids, carotenoids, flavonoids, vitamins, isoflavones, indoles, saponins, monoterpenes, bioactive peptides, phytosterols, essential fatty acids, and others can be categorized as bioactive compounds (XIAO et al., 2018).

Natural bioactive substances present many advantages to food preservation when added into packaging, although, some disadvantages, such as off-flavors, thermosensitivity and early loss of functionality, that may take place during its processing and storage. Furthermore, the bioactive efficiency decreases when exposed to oxidative conditions of the surrounding environment, such as air, humidity, heat, light, oxygen, and others (LAGOS et al., 2015). Thus, encapsulation of bioactive substance onto biopolymeric matrixes follow by incorporation of these active particles in the food packaging is an effective strategy, which can improve durability and maintenance of biological properties (DEVI et al., 2017; EGHBAL, CHOUDHARY, 2018).

Furthermore, vegetable oils are a feasible source of essential fatty acids and sterols, particularly, alpha-linolenic acid and linoleic acid fatty acids and phytosterols, which are related to health benefit effects in reducing the risks of heart diseases, displaying antioxidant activity and others associated to their incorporation in food products (COMUNIAN, FAVARO-TRINDADE, 2016). Besides, it is from renewable source, edible, effortlessly available, generally display low cost, non-toxic, non-depletable and non- volatile. Lipid materials can be used to promote a desirable smooth effect, improve water, and gas barrier, as well as enhance cohesivity when incorporated in biobased films (SALGADO et al. 2015; QUIRÓS-SAUCEDA et al., 2014).

The functionality of these bioactive materials may be different, as each component introduces a wide range of properties to the matrix. Besides, functionality depends not only on intrinsic characteristic of each component, but significantly on their compatibility and cohesivity. Different approaches to this can be pursued, e.g., incorporation of the encapsulated particles on the external surface of films or in the interface between the film and the food and dispersed among the film (QUIRÓS-SAUCEDA et al., 2014). It is expected that these incorporated active compounds will be released from the package or absorb substances from food and surrounding environment, as well as make changes in food composition and sensorial

characteristics (SALGADO et al., 2015). Some examples of the incorporation of lipid materials onto different hydrocolloid matrixes are listed in Table 7.

Table 7. Incorporation of lipids onto different hydrocolloid matrixes.

Hydrocolloids	Lipids	Form	Application	Reference
Gelatin and gum Arabic	Methyl oleate	Microcapsules by complex coacervation	Functional lipids and lipophilic food ingredients	MA et al., 2019.
Gluten and gelatin plasticized with glycerol or sorbitol	Fatty acids	Incorporated in edible films	Biobased packaging	FAKHOURI et al., 2018.
Mesquite seed gum	Palm fruit oil	Emulsion edible film	Biobased packaging	RODRIGUES et al., 2016.
Chitosan/xanthan or chitosan/pectin	Palm oil	Microcapsules by complex coacervation	Yogurt preparation	RUTZ et al., 2017.
Chitosan/sodium tripolyphosphate or chitosan/carboxy methyl cellulose	Palm oil and β-carotene	Microcapsules by complex coacervation	Food systems under gastrointestinal simulant conditions	RUTZ et al., 2016.
Chitosan plasticized with glycerol	Olive oil	Emulsion film	Biobased packaging	PEREDA, AMICA, MARCOVICH, 2012.

3.5.1. Encapsulation

Encapsulation is a technique widely used to entrap of coat active substances (core) into polymer matrices (shell or wall) for different applications on food, cosmetic and pharmaceutical fields. The biopolymer shell acts as a physical barrier protecting the encapsulated core material from the direct contact with the environment (RODRÍGUEZ et al., 2016; TIMILSENA et al., 2017). Thus, this process shields susceptible substances against degrading factors, such as oxygen, light, heat, pH, humidity, and others (EGHBAL, CHOUDHARY, 2018; RODRÍGUEZ et al., 2016; SHISHIR et al., 2018). Furthermore, the incorporation of encapsulated compounds into foods can improve its biological activity, nutritional content, shelf-life, and stability,

masking off-flavors, reducing the evaporation of volatiles, preserves sensorial properties, permits the controlled release of bioactive substances, and enhance solubility (AUGUSTIN, HEMAR, 2009; RODRÍGUEZ et al., 2016; SHISHIR et al., 2018).

Solid, liquid or gas substances can be encapsulated in different wall materials to form micro or nanocapsules (AUGUSTIN, HEMAR, 2009; OZKAN et al., 2019). The classification of capsules based on its size may diverge, though, it is well established that nanocapsules have less than hundred nanometers in diameter, submicron-capsules have more than a hundred nanometers to one micrometer, and microcapsules are in the micrometer range (1 – 1000 μm) (AUGUSTIN, HEMAR, 2009; CAMPOS et al, 2013; OZKAN et al., 2019 SHISHIR et al., 2018; ZANETTI et al., 2018). Microencapsulation is commonly used in food industries to preserve and release sensible substances such as polyunsaturated oils, fats, aromatic and volatile compounds, antioxidants, vitamins, proteins and enzymes, dyes, probiotics, and others (MOSCHAKIS, BILIADERIS, 2017; RODRÍGUEZ et al., 2016; RUTZ et al., 2017).

A broad range of natural or synthetic polymers can be used as shell matrix in encapsulation process depending on the required properties of the final product (AUGUSTIN, HEMAR, 2009; SHISHIR et al., 2018). For food application, the encapsulating materials are food-grade based and “generally recognized as safe” (GRAS) (AUGUSTIN, HEMAR, 2009; DEVI, KAKATI, 2013; SHISHIR et al., 2018). Natural polymers have been used to fabrication of delivery systems based on their nature, edibility, stability, renewable source, processability, biodegradability and low toxicity.

Carbohydrates, proteins, and lipids are the major food-grade materials used in the encapsulation process (AUGUSTIN, HEMAR, 2009; SHISHIR et al., 2018). These biopolymers should have good emulsification and dissolution properties, as well as a reasonable ability to form gel networks (AUGUSTIN, HEMAR, 2009; SHISHIR et al., 2018). Generally, more than one type of biopolymer is used in the encapsulation process, because a single material may not have all the necessary characteristics for this purpose (RUTZ et al., 2017). The choice of these biomaterials depends not only on the type of encapsulated core or process method, but it is also based on several other factors that will be better explained in the following sections. Besides, it is important to establish the aim of encapsulation, which will guide the design of the

experiments, the appropriated material selection, the optimization of the process and the achievement of the desired goal (AUGUSTIN, HEMAR, 2009).

3.5.2. Encapsulation by complex coacervation process

Polysaccharide-polysaccharide and polysaccharide-protein interactions behaves importantly in controlling food and biomaterials functions, such as structure, texture, and stability. These interactions can occur either by segregative or associative liquid–liquid phase separation. The segregative or depletion interaction arises when the biopolymers repeal each other, leading to a liquid-liquid separation in two phases, i.e., a rich phase in protein and other rich in polysaccharide. Otherwise, if the biopolymers have opposite charges, an associative phase behavior or coacervation, inducing interbiopolymer complexation via electrostatic interaction. In this case, the separation in two phases leads to the precipitation of the biopolymer complexes in a lower phase, and forms an upper phase containing the solvent used (EGHBAL, CHOUDHARY, 2018; ELMER et al., 2011; SANTOS, DA COSTA, GARCIA-ROJAS, 2018).

Historically, ‘coacervate’ derived from the Latin word ‘*acervus’* meaning aggregate and its prefix ‘*co*’ is correlated to the association of two reactants and has been commonly used to design a metastable suspension of macro ion-rich drops (DEVI et al., 2017). The first reports using the term coacervation is dated from 1911 by F.W.Z. Tiebackx, then the process was investigated by Dutch chemists Bungenberg de Jong and Hugo R. Kruyt (1929). These researchers observed electrostatic interaction between gelatin (negatively charged) gum acacia (positively charged) by changing pH and adding NaCl (EGHBAL, CHOUDHARY, 2018; SANTOS, DA COSTA, GARCIA-ROJAS, 2018; TIMILSENA et al., 2019). Since then, coacervation have been used in colloidal industry to denote associative phase separation process.

Two types of coacervation processes, simple or complex, can occur based on the reaction between the involved macromolecules and the phase separation. Simple coacervation occurs with a solo biopolymer when changing environment conditions, such as adding micro-ions, a desolvation solvent, changing temperature and pH, causes its dehydration and forms the phase separation. This can be achieved per example to the coacervation of gelatin when sodium sulfate (Na_2SO_4) or ethanol is added into its solution (DEVI et al., 2017; TIMILSENA et al., 2019). The complex coacervation, on the other hand, is formed by the electrostatic interactions between

two oppositely polyelectrolytes, proteins, and surfactants in a solvent media, resulting in the formation of polyelectrolytes complexes (PECs) that separates in a dense coacervation phase, and another liquid diluted phase formed by solvent (KAYITMAZER, 2017; QUIRÓS-SAUCEDA et al., 2014).

These polyelectrolytes are macromolecules carrying active functional groups that are charged or can become charged under specific conditions, i.e., chitosan turns in a cationic macromolecule under acidic medium, pH below 6.5 (LUO, WANG, 2014; MUXIKA et al., 2017). The complex coacervation happens in low biopolymers concentration (< 4%) and ionic strength (<400 mM) (SANTOS, DA COSTA, GARCIA-ROJAS, 2018). The complex coacervation process is majorly driven by electrostatic interaction among the charged polyelectrolytes, although, other interactions, e.g., van der Waals intermolecular force, hydrophobic interaction in dipolar proteins and nucleic acid conformation changes due to intermolecular hydrogen bonding, may occur (TIMILSENA et al., 2019).

Complex coacervation is one of the most effective used methods to encapsulation of lipids and thermosensitive ingredients to food application, although it also can be used to formation of packaging films, production of emulsions and microgels, and development of biomimetic and delivery systems. It has been frequently used in encapsulation of food ingredients due to is simple processing, low cost, good scalability, and reproducibility, as well as a higher loading capacity, which can reach up to 99%, and reduced thermal degradation (EGHBAL, CHOUDHARY, 2018; TIMILSENA et al., 2019). Furthermore, this technique is compatible in releasing the active materials, requires no sophisticated equipment, and can be considered a green methodology, as uses non-toxic solvents (OZKAN et al., 2019).

Encapsulation by this method involves the deposition of the biopolymers (shell) around the active ingredient (core) in four basic steps: (a) preparation of aqueous solution of two or more biopolymers or an emulsification; (b) homogenization to produce a stable coacervation system; (c) changing of pH and temperature to induce coacervation and promote phase separation or gelation; and (d) hardening using elevated temperature, a desolvation agent, or crosslinker. The soluble, aggregated, or precipitated PECs are recovery by filtration or centrifugation, followed by washing with an appropriate solvent and drying it (OZKAN et al., 2019; TIMILSENA et al., 2019).

PECs can be formed instantaneously in solution by mixing oppositely charged macromolecules even without the addition of any crosslinker agent. However, the

coacervation can be run by lowering temperature and changing pH, or either by dilution or adding a salt or crosslinking agent. It is possible to visually observe the coacervates formation by the changes in turbidity, that should be highest on the greatest electrostatic interactions between the biopolymers. If the coacervation goes on, the coalescence of microparticles turned into larger particles, which leads to a higher particles density and resulting a visible phase separation (Figure 10).

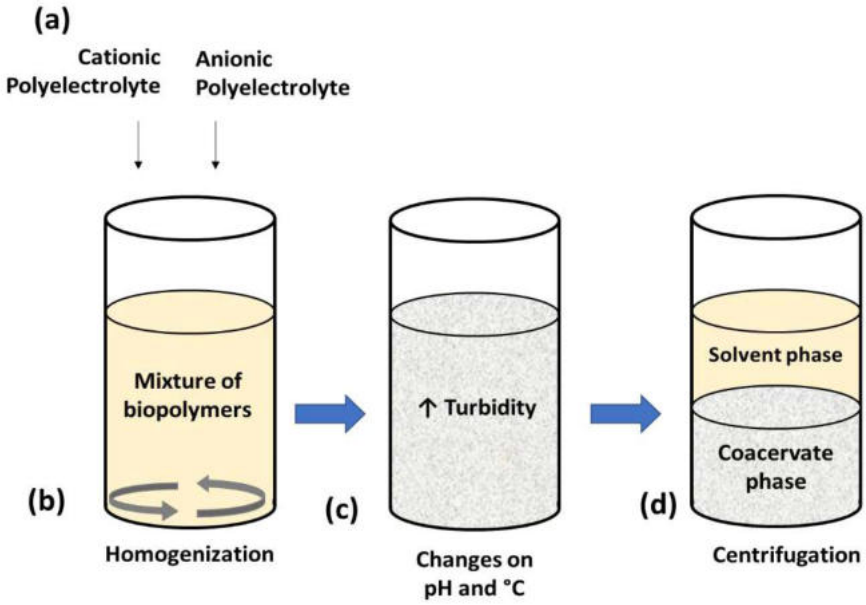

Figure 10. Complex coacervation process: a) solutions of two oppositive polyelectrolytes, b) homogenization of biopolymers solution, c) induction of coacervation by changes in pH or temperature resulting in increase of turbidity and d) phase separation and centrifugation to obtain precipitated PECs. Adapted from Ozkan et al, 2019 and Timilsena et al., 2019.

Generally, the complex coacervation process can be considered highly adaptable-dynamic, as it forms and segregates particles in a reversible way, being modified according to the environmental conditions. For this, biopolymer reorganization and rearrangements, i.e., changing charge distribution, and chain mobility, can take place until its free energy are optimized, resulting in a well-defined structure. These rearrangements may happen along time at a slow rate (MOSCHAKIS, BILIADERIS, 2017). The processing conditions can produce different particles size and morphology, although, particles can be either mononucleated or polynucleated (TIMILSENA et al., 2019). The microstructure of these particles was well studied using different microscopy techniques, such as light microscopy, phase contrast microscopy, scanning electron microscopy, transmission electron microscopy, atomic force microscopy and recently by confocal laser scanning microscopy (GÅSERØD,

SMIDSRØD, SKJÅK-BRÆK, 1998; GHASEMI et al., 2018; NATRAJAN et al., 2015; PHOEUNG et al., 2017; ZHAO et al., 2019). A wide range of biopolymers, polysaccharide-based or polysaccharide-protein-based systems, can be combined via complex coacervation, e.g., chitosan and alginate, chitosan and pea protein, and others (DEVI et al., 2017; JURIĆ et al., 2021; HARDY et al., 2018; TIMILSENA et al., 2019). A list of complex coacervate systems based on different biopolymers is displayed in Table 8.

Table 8. Complex coacervate systems based on different biopolymers.

Biopolymers		Core material	Particle size	Reference
Gelatin	Octenyl succinic anhydride modified kudzu starch	Astaxanthin dissolved in soybean oil	Not measured	ZHAO et al., 2019.
Chitosan	Sodium alginate	Citral	Not measured	AFZAL, MASWAL, DAR et al., 2018.
Gum Arabic	Ovalbumin	Without core material	Not measured	NIU et al., 2018.
Pectin	Whey protein	D-limonene	100 nm	GHASEMI et al., 2018.
Sodium alginate	Beta-lactoglobulin and bovine serum albumin	Without core material	Not measured	GORJI et al., 2018.
Chitosan	Soy protein	Algal oil	< 70 µm	YUAN et al., 2017.
Chitosan	Carboxymethylcellulose	Palm oil and soybean oil	Not measured	RUTZ et al., 2017.
Collagen	Pectin/ alginate	Avocado extract, nisin and soybean oil	< 105 µm	CALDERÓN-OLIVER et al., 2017.
Chitosan	Pea protein	Without core material	Not measured	ELMER et al., 2011.
Chitosan	Calcium alginate	Protein-stabilized lipid droplets	<100 nm	LI, MCCLEMENTS, 2011.

The interactions between the polyelectrolytes are important to texture, structure, compatibility, stability, and functional properties of the coacervates. Many of the factors influencing the complex coacervation systems are inherent to each polyelectrolyte composition and to the surrounding environment. These forces will affect morphology and size of the polyelectrolyte complexes particles, thus, understanding it is essential to achieve a better coacervation and efficient encapsulation. As coacervation is dependent on the interaction between oppositive charges ions, its main driving factor is the reduction in the free electrostatic energy of the reaction system (TIMILSENA et al., 2019). Thus, the maximum coacervation yield can occur under charge neutralization, i.e., charge stoichiometry of 1:1 between biopolymers, although, this depends on the other factors as well (MOSCHAKIS, BILIADERIS, 2017).

Factors, such as, pH and ionic strength of medium, temperature, concentration and mixing ratio of macromolecules as well as its charge distribution, M_w, charge density, order of reacting the polyelectrolytes, type of homogenization, have significant influences on the complex coacervation process (KAYITMAZER, 2017; LUO, WANG, 2014; MOSCHAKIS, BILIADERIS, 2017). The optimization of the polyelectrolyte complexes can be pursued by surface charge density, also named as zeta potential (ζ-potential, mV), and turbidity (absorbance a.u.) as a function of pH and polymers ratio. The surface charge density of biopolymers gives important information correlated to its interaction properties, which explains part of the (+/-) stoichiometry conditions for coacervation and is extremely sensitive to changes on environment conditions, especially to pH variation (CROGUENNEC, TAVARES, BOUHALLAB, 2017).

In other words, the ζ-potential can be correlated to the electrokinetic potential of the particle with its own ionic radiance and surrounding medium. Furthermore, the strength of the electrostatic interaction (SEI) between oppositely charged biopolymers is equivalent to the absolute value of ζ-potential of both macromolecules at each pH values. As a result, highest SEI values suggest the pH range of strongest biopolymer attractions (DUCEL et al., 2004). Wang et al. (2000) suggest that at very low charge density, coacervation can be suppressed, otherwise, at very high charge density, precipitation may occur, although this behavior is specific for each polyelectrolyte and their complexes. When the ζ-potential is close to zero, the protein-polysaccharide polyelectrolytes complexes were aggregated, due to neutralization charges between -COO^- and -NH_3^+ moieties, reaching maximum coacervation yield (ESPINOSA-ANDREWS et al., 2013; GULÃO et al., 2015).

3.6. **Açai berry**

A fruit from the Brazilian Amazon rain-forest region, açaí or assaí fruit, *Euterpe oleracea* can be point out as an important source of bioactive substances. This berry-like fruit has been recognized as a 'super-fruit' by researchers and consumers (YAMAGUCHI et al., 2015). This recognition is mainly due to the health benefits and biological activities, mainly related to anthocyanins, polyphenols, essential mineral elements, and polyunsaturated fatty acids, that were investigated by scientific works (BATISTA et al, 2016; DEL POZO-INSFRAN, BRENES, TALCOTT, 2004; MERTENS-TALCOTT et al., 2008; RUFINO et al., 2009; SANTOS et al., 2021; SILVA et al., 2019). Açaí belongs to the *Euterpe* genus that is widely spread in Central and South America, mainly distributed through Amazon region. *Euterpe oleracea*, *E. edulis* and *E. precatoria* are palm trees, that most frequently occurs in this area. Different biological activities are linked to these fruit species since they diverse on its nutritional and chemical composition.

Açaí berries from *Euterpe oleracea* are globular fruits with a rounded shape, sizing up to 20 mm in diameter and weighing about 2.5 g, that display a dark violet color (peel and pulp) when reach maturity. The fruit contains a single seed that constitutes close to 85% of the fruit (ODENDAAL, SCHAUSS, 2014; SANTOS et al., 2021). To the Amazonian communities, açaí fruit is an important food in the day-to-day diet. From the pulp fruit can be extracted a nutritious juice, which is traditionally consumed in Brazil as a sweet viscous juice or as a salt soup, as well as a processed into a diverse product, e.g., ice-cream-like and popsicles, jams, pulp in powder, energetic drinks, fermented beverages, cakes, pastry, sweetmeats, in chocolate bars, and others. The consumption of açaí by national and international markets, such as USA, China, Japan and Europe, has grown significantly (PALA et al., 2018; YAMAGUCHI et al., 2015). Brazil is the major producer and exporter of açaí, reaching around 9 billion dollars per year in business, which exceeds the commercialization of soybeans and Brazil nuts per ton (MATTA et al., 2020).

The proximate composition of the açaí fruit pulp reveals higher proportion of moisture, up to 88% (wet basis), followed by lipids (20-54%), fibers (7-32%), carbohydrates (3.6-27.2%), proteins (6.2-11%) and ashes (2-5%) (dry basis) (COSTA, SILVA, VIEIRA, 2018; RUFINO et al., 2011). The açaí pulp is known for high concentrations of bioactive compounds, such as anthocyanins, which is linked to its intense purple color. These are the major phenolic compound found in the fruit pulp,

mainly cyanidin 3-glucoside and cyanidin 3-rutinoside, although other phenolic compounds, such as rutin, orientin, homoorientin, catechin, epicatechin, ferulic acid, vanillic acid, gallic acid, p-hydroxybenzoic acid and syringic acid have been extensively reported (CARVALHO et al., 2017; YAMAGUCHI et al., 2015).

This phytochemical composition of açaí suggests that it could be involved in modulation of cholesterol metabolism and antioxidant defenses through several mechanisms, mainly due to the polyphenols' composition. In the last case, these compounds can act directly by removing reactive oxygen species (ROS) or indirectly by modulating intracellular pathways (PALA et al., 2018). The antioxidant activity of the açaí pulp and oil determined by using ABTS and DPPH radical scavenging assays were ~438.0 μmol Trolox equivalent g^{-1} and ~336.0 μmol Trolox equivalent g^{-1}, and <15.3 μmol Trolox equivalent g^{-1} and <7.4 μmol Trolox equivalent g^{-1}, respectively (MATTA et al., 2020). Furthermore, the intake of açaí pulp for four weeks may improve redox metabolism and lipid transfers to high-density lipoprotein (HDL) cholesterol, which is important parameters in this lipoprotein metabolism (PALA et al., 2018). Açaí pulp is also known for presenting good amounts of essential mineral elements, especially Ca, Cu, K, Mg, and Mn, that have a bioaccessibility value above 75%, and less availability of zinc, up to 50%, and iron, up to 25% (SANTOS et al., 2021).

Açaí is a highly oil fruit, which contains major monounsaturated fatty acids (MUFAs) as oleic acid (up to 70%), as well as around 34% of saturated fatty acids (SFAs), i.e., palmitic acid, and up to 16% of polyunsaturated fatty acids (PUFAs) mainly represented by linoleic acid (RUFINO et al., 2011). In the study of Batista et al (2016), an açaí oil extract from the lyophilized pulp was obtained using different supercritical CO_2 extraction conditions. The authors found that the highest oil yield was obtained using the conditions of 70 °C and 490 bar, which achieved the greatest proportion of MUFAs, ~70.5%, and around 30% of SFAs. These same authors evaluated the phenolic compounds and anthocyanin content in the CO_2 extracts. They found that the highest levels of phenolics, up to 800 mg 100 g^{-1}, were obtained under 70 °C and 350 bar, and solvent density of 900 kg m^{-3}, and of anthocyanins were around 140 mg 100 g^{-1}, at 50 °C and 220 bar, and solvent density of 700 kg m^{-3}. Furthermore, due to its hydrophilic nature, anthocyanins should not be retained in açaí oil during its processing, although phenolics and flavonoids may remain in it at different proportions than the pulp, which can be linked to a significative antioxidant capacity of the oil (PACHECO-PALENCIA, MERTENS-TALCOTT, TALCOTT, 2008).

3.8. **Olives**

Olives are fruits from the *Olea europaea* tree (*Oleaceae* family), an evergreen shrub native species from the Mediterranean region, although its cultivation is not limited to this (FOSCOLOU, CRITSELIS, PANAGIOTAKOS, 2018; GUO et al., 2018; WANI et al., 2018). These trees have been cultivated for more than 5000 years and are historic-culturally linked to Mediterranean populations (FOSCOLOU, CRITSELIS, PANAGIOTAKOS, 2018; GUO et al., 2018). Olives are a drupaceous fruit, with different sizes (2 – 3 cm), weigh from 3 to 10g, contains a single seed, and an oily mesocarp (GUO et al., 2018). The major constituents of olive fruits are water (<75%), lipids, from 10 to 25%, and lower carbohydrates, 2–5%, though this may change depending on its variety and harvesting period (GUO et al., 2018). The major fatty acids found out in olive oil are the oleic acid, followed by palmitic, linoleic, and stearic acids, which depends on the maturation stage (WANI et al., 2018).

The main use of olives by food industries is to olive oil production, and 93% of all its global processing undertaken by the European Union (ESPADAS-ALDANA et al., 2019). The intake of olive oil as food have been recommended since Aristotle and Hippocrates ages because of its associated health benefits (FOSCOLOU, CRITSELIS, PANAGIOTAKOS, 2018; LIOUPI, NENADIS, THEODORIDIS, 2020). The nutritional properties of the olive oil vary according to their subtypes, e.g., pomace; refined, virgin and extra-virgin olive oil. Extra-virgin olive oil is extracted using non-chemical low temperature pressing from fresh olives, usually within 24h after their harvesting, and usually have an acidity index below 0.8% (FOSCOLOU, CRITSELIS, PANAGIOTAKOS, 2018). Similarly the virgin olive oil is also extracted from the first olives pressing, while its acidity are usually higher than the extra-virgin olive oil, up to 2% (FOSCOLOU, CRITSELIS, PANAGIOTAKOS, 2018).

The biological properties of the olive oil are linked to a high content of unsaturated fatty acids, α-tocopherol and phenolic compounds, such as derivatives oleuropein and ligstrosides (LIOUPI, NENADIS, THEODORIDIS, 2020; LOZANO-SÁNCHEZ et al., 2011). A health claim related to protection of blood lipids from oxidative stress by the polyphenols of extra-virgin olive oil (EvO) was approved by the European Food Safety Authority in 2011 (SIANO, PICARIELLO, VASCA, 2021). Both, EvO, and virgin olive oil exhibits relevant content of hydrophilic polyphenols, however, the first one has been associated to a much higher amount of it, around 55 mg 100 g^{-1}, than the second, as being around 21 mg 100 g^{-1} (FOSCOLOU, CRITSELIS, PANAGIOTAKOS, 2018).

4. MATERIAL AND METHODS

4.1. Materials

Açaí pulp oil (AO) (from *Euterpe oleracea*) with 99,95% of purity, acidity (expressed as oleic acid) of ≤ 3.0% and peroxides of ≤ 10 mEq O_2 kg^{-1}, as quality indices, was donated from Beraca Ingredientes Naturais S.A. (Ananindeua, PA, Brazil). The extra-virgin olive oil (EvO) from a commercial brand was purchased in a local market in city of Leeds (United Kingdom). The AO and EvO were used as encapsulated material.

Medium molecular weight CS was purchased from Sigma Aldrich Brazil Ltd. (São Paulo, SP, Brazil). The degree of acetylation (DA), around 15%, and the viscosity average molecular weight ($\bar{M}_v \sim 2.97 \times 10^5$) of the CS were previously determined by 1H NMR spectrometry in D_2O/DCl at 65ºC and using the Mark-Houwink equation, $[\eta] = K\bar{M}_v^a$, respectively, by Gonçalves et al. (2017).

Sodium alginate (SA) with medium viscosity were purchased from Sigma Aldrich Brazil Ltd. (São Paulo, SP, Brazil). The molecular weight of SA (similar sample from Sigma Aldrich and same batch) was reported as being between 80,000 and 120,000 Da and having a mannuronic (M)/ guluronic (G) ratio of 1.56 by Osmokrovic et al. (2018).

The pea protein isolate (PPI) (NUTRALYS® S85F, 85% on a dry basis extracted from *Pisum sativum*) was donated by Roquette Frères Group (Geneva, IL, USA). The materials, CS, SA and PPI were used as encapsulating agents.

The chemicals, Folin-Ciocalteau's phenol reagent, 2,2'-azino-bis-3-ethylbenzothiazoline-6-sulfonic acid (ABTS), 2,2-diphenyl-1-picrylhydrazyl (DPPH), gallic acid and (±)-6-hydroxy-2,5,7,8-tetramethyl-chroman-2-carboxylic acid (Trolox), 2,4,6-Tris(2-pyridyl)-s-triazine (TPTZ), Nile Red (9-(diethylamino)benzo[*a*]phenoxazin-5(5*H*)-one) and ChCl were purchased from Sigma–Aldrich (Milan, Italy). Other analytical grade reagents, calcium chloride ($CaCl_2$), acetic acid, ethanol, methanol and glycerol, were purchased from Vetec Química Fina Ltda. (Rio de Janeiro, RJ, Brazil). Ultrapure water from a Millipore Direct-Q 3 UV system was used. The $C_{15:0}$ - methyl pentadecanote, as internal standard for the gas chromatography (GC) analysis, and 37-Component FAME Mix (methyl esters of fatty acids ranging from C_4 to C_{24} CRM47885) were purchased from Supelco (from Sigma–Aldrich, Milan, Italy). All the other chemicals used in this study were of analytical grade.

4.2. Methods

This thesis was organized in three main experimental sections. The first section is related to the development, optimization and characterization techniques of the microencapsulated systems based on chitosan (CS) and sodium alginate (SA) to encapsulation of açaí oil (AO). The second is related to the development, optimization and characterization techniques of the microencapsulated systems based on chitosan (CS) and pea protein isolate (PPI) to encapsulation of extra-virgin olive oil (EvO). And the third part is related to development and characterization of CS-composite films plasticized with deep eutectic solvents and incorporated with the optimized microparticles of CS:SA-AO obtained in the first section. The main schematic representation of this sections is displayed in Figure 11.

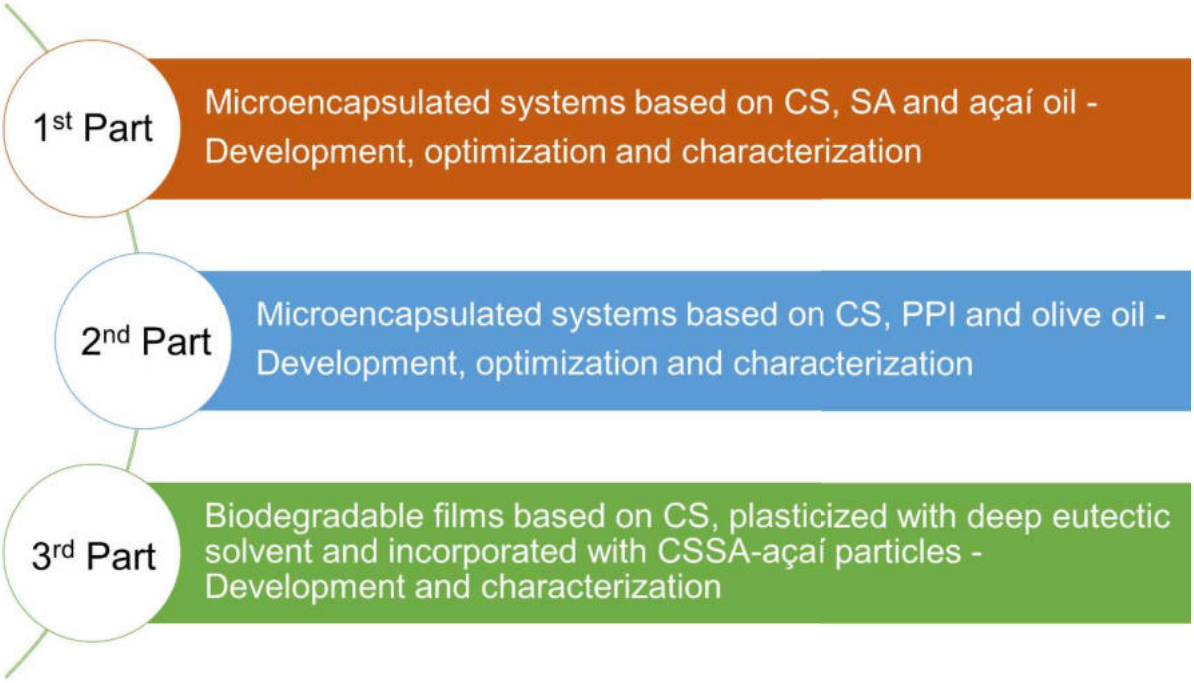

Figure 11. Schematic representation of the sections on this thesis.

A more detailed scheme of the methods used in each part is presented in the following Figures. In Figure 12 is presented the schematic representation of the methods used in the 1st section of this thesis.

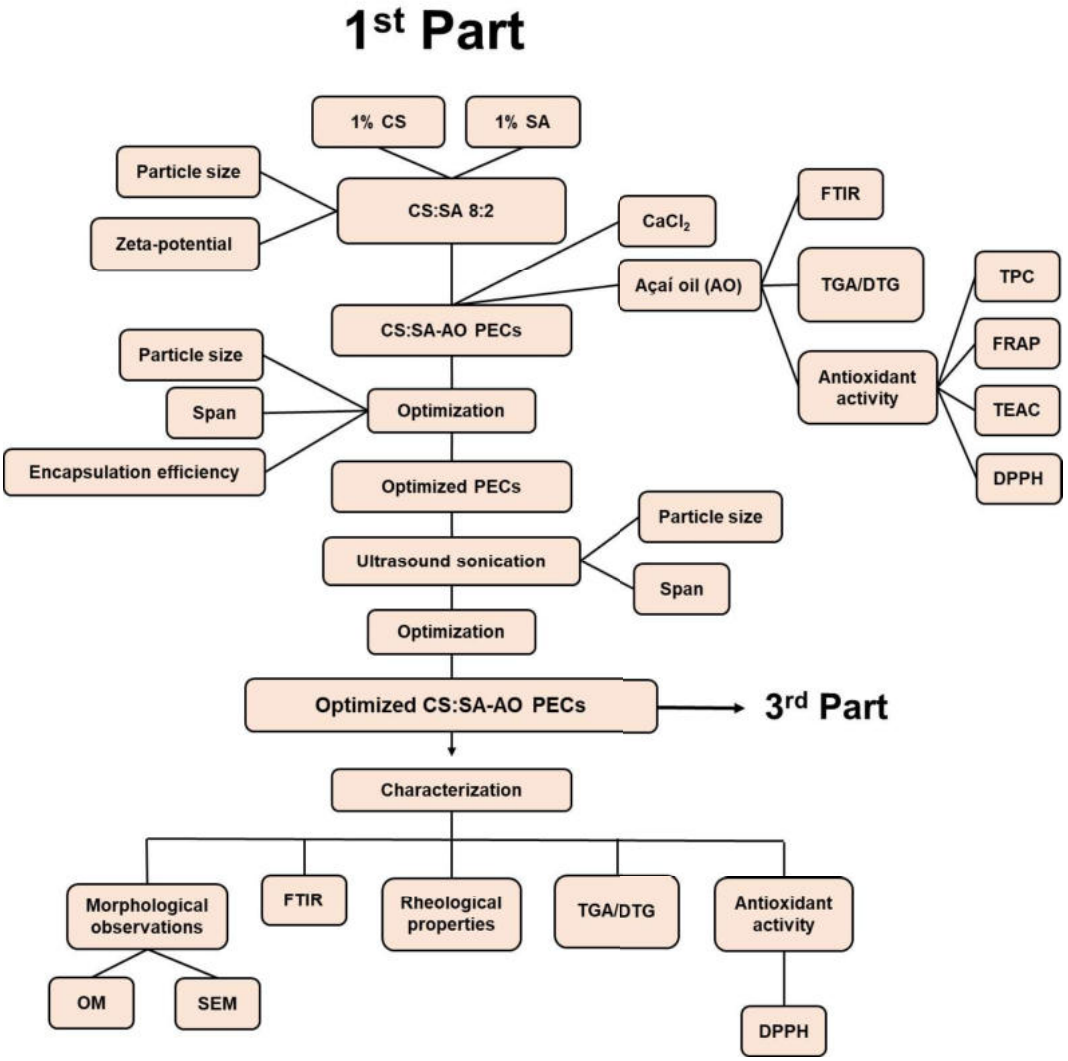

Figure 12. Schematic representation of the methods used in the 1st section of this thesis.

In Figure 13 is presented the schematic representation of the methods used in the 2nd section of this thesis.

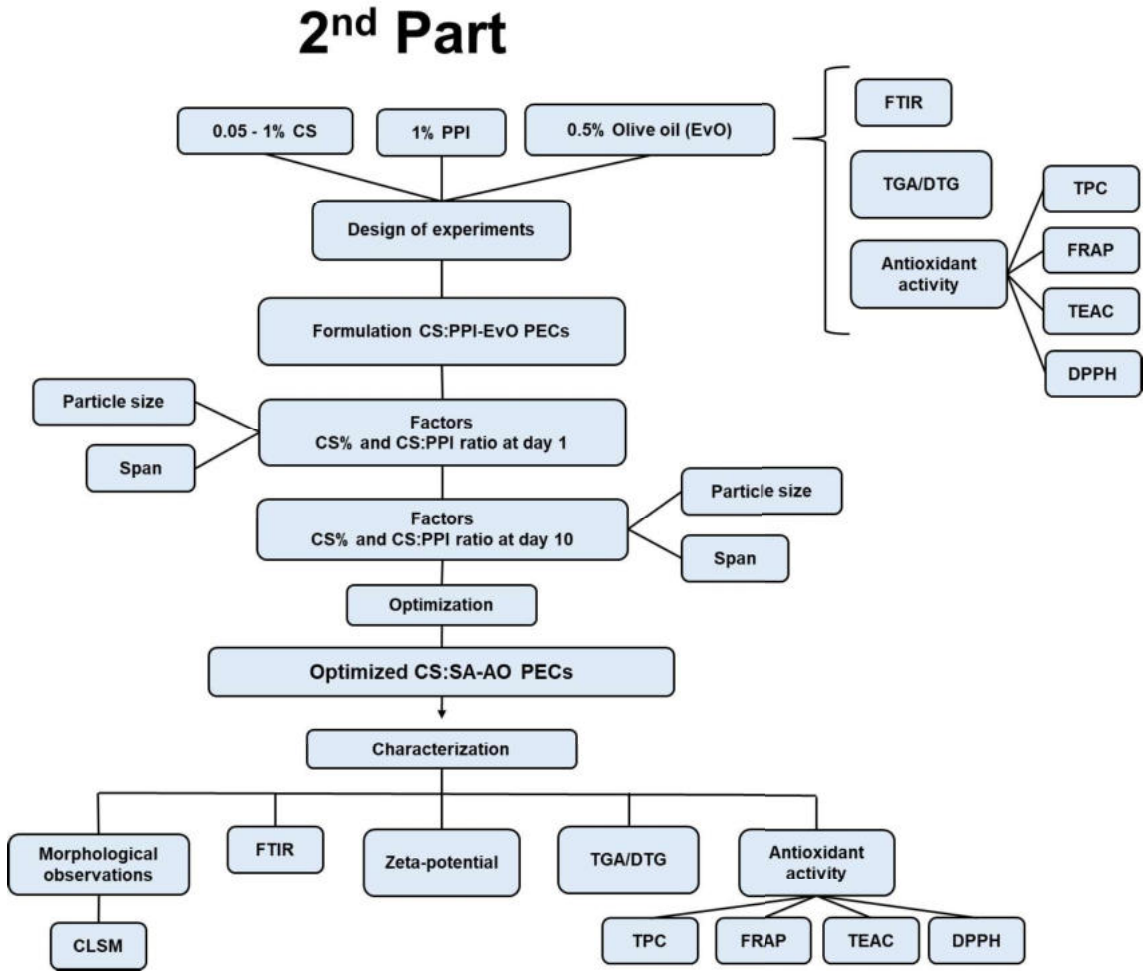

Figure 13. Schematic representation of the methods used in the 2nd section of this thesis.

In Figure 14 is presented the schematic representation of the methods used in the 3rd section of this thesis.

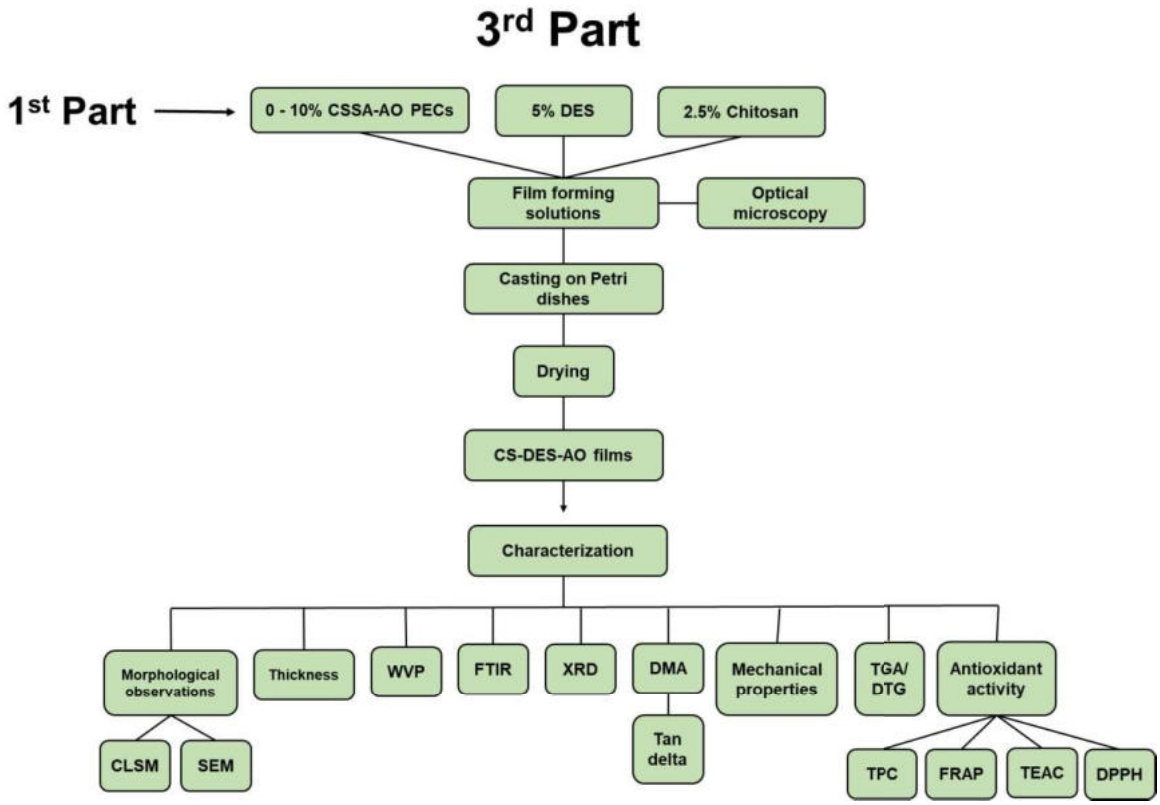

Figure 14. Schematic representation of the methods used in the 3rd section of this thesis.

4.2.1. Microencapsulation systems based on CS:SA and CS:PPI

4.2.1.1. Preparation of biopolymers stock solutions

Stock solutions at 1% (v/v) of SA in pure water and 1% of PPI in a pH 7.0 aqueous sodium phosphate buffer (0.36 M Na_2HPO_4 and 0.24 M NaH_2PO_4) were prepared at room temperature, under stirring for 12 h using a magnetic stirrer. The CS stock solution at different concentrations (0.5, 0.75, 1 and 1.10%) in 1% (v/v) acetic acid were also prepared at room temperature, under over-night stirring using a magnetic stirrer. The initial pH of the solutions was measured using a Q400MT pH meter (Quimis Aparelhos Científicos, SP, Brazil) and adjusted with 0.25 M NaOH and 0.25 M HCl, to obtain a pH 6.5 for SA, pH 6.0 to PPI and pH 4 for CS.

4.2.1.2. Zeta-potential and pH of CS, SA and PPI stock solutions

The zeta-potential (ζ – potential) for CS and SA stock solutions was determined by dynamic light scattering with a Zetasizer Nano (Nano-ZS, Malvern Instruments, Worcestershire, UK). The ζ–potential of these solutions as a function of their

concentration and different pH (ranging from 4.0 to 10.0) was evaluated. The pH of these solutions was measured using a benchtop pH meter (Orion Star A215, Thermo Fisher Scientific, Waltham, MA, USA) and adjusted with 0.25 M NaOH and 0.25 M HCl, under constant stirring using a magnetic stirrer. An aliquot of the solutions, ~ 1 mL, was placed in a DTS1070 cuvette and the analyses were conducted in triplicate.

4.2.1.3. Preparation of CS:SA based microparticles

Different ratios (1:1, 2:8, 3:7, 7:3 and 8:2 m/m) of CS and SA solutions at a 1% final concentration were used to prepare the microcapsules. The average size of these microcapsules was determined in preliminary tests as the following description and the CS:SA system that presented the smallest size was used to optimize the AO encapsulation.

The CS:SA (8:2) microcapsules were prepared according to the methodology previously reported (YUAN et al., 2017), with modifications. AO (0.0 - 0.75% w/w) was added to the SA solution (15 g) and homogenized at 8,000 rpm for 5 min with an Ultra-Turrax model T25 (Ika Works, Wilmington, NC, USA), leading to an oil emulsion (SA-AO). The CS solution (60 g) was added by dripping with a peristaltic pump model 202 (Milan Equipamentos Científicos, Colombo, PR, Brazil) into the SA-AO emulsion. The resulting mixture was homogenized at 8,000 rpm for 10 min and the pH was adjusted to 6.0 to initiate the PEC formation and the preparation of the microcapsules. The systems were treated with a $CaCl_2$ (0.0 – 1.0% w/v) solution (crosslinking agent) at room temperature, under constant stirring for 3 h.

The samples were dried using two different methods, a desiccator under vacuum, and using a freeze-dryer. The first one was adapted from the desiccant method (ASTM-E096M-16) ASTM (2016). In this method, the dispersions of samples were separated by filtration, weighed in a glass Petri dish, and then dried at room temperature under vacuum in a desiccator containing anhydrous calcium chloride (~25% RH) until constant weight. The dried PECs were stored under refrigeration for further analyses.

Another part of the samples was dried using a LT1000 freeze-dryer (Terroni Equipamentos LTDA, São Carlos, SP, Brazil). For this method, the samples were priorly weighed, placed in Falcon tubes, and centrifuged in a Himac CR22GII high-speed refrigerated centrifuge (Hitachi Koki Co., Katsuta, Okayama, Japan) for 60 min at 5000 rpm. Then, its supernatant liquid was discarded, and the centrifuged PECs

were placed cooled to -12 °C in a domestic freezer (Brastemp, Brasil Temperatura Ltda, São Bernardo do Campo, SP, Brazil) for 48 h. After this, the frozen samples were placed in the freeze-dryer under 2000 μHg with condenser temperature of -40 °C for 72h. The freeze-dried PECs were stored under refrigeration for further analyses.

4.2.1.4. Preparation of CS:PPI based microparticles

The CS:PPI based coacervates to encapsulation of EvO were prepared using two steps mixing: first, using a Jet Homogenizer (School of Food Science and Nutrition, University of Leeds, Leeds, UK) and then, an Ultra Turrax T25 homogenizer (Ika Works, Wilmington, NC, USA). The Jet Homogenizer uses compressed air to mix the solutions that are placed in two different cylindrical chambers as can be visualized in Figure 15. These chambers have different volume capacities and are connected via fixed thin capillary tubing to an outlet via very small hole of 0.5 mm diameter, drilled into a stainless-steel disk.

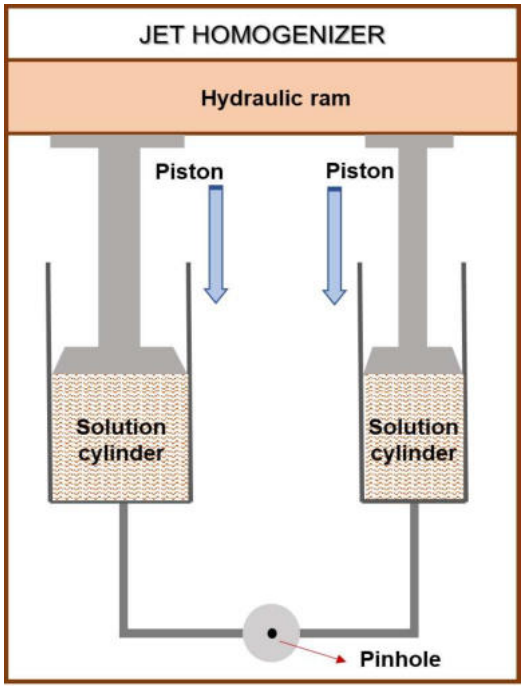

Figure 15. Schematic diagram of the Jet Homogeneizer. Adapted from Pravinata et al. (2016).

A compressed air pushes the hydraulic ram on the pistons placed in the top of each chamber (solution cylinder) to force the liquids out of the chambers and through the pinhole. The fluid velocities generated through the hole can be extremely high (> 300 m s^{-1}), creating highly turbulent flow with Reynolds number > 10^5 as described by

Pravinata et al. (2016). In this experiment, CS was gently mixed with EvO using a magnetic stirrer, prior placing it in one chamber, and PPI was placed in the other one. The pressure applied was of approximately 300 bar and the time process was shortly, less than 1s. Each sample was passed through the Jet Homogenizer three times prior the following procedure.

In the second mixing step, the samples were mixing using the Ultra Turrax T25 homogenizer at 10,000 rpm for 5 min. The PPI solution at 1% concentration and 0.5% of EvO (w/w) were maintained constant for all systems. Different concentrations of CS solution were used to prepare the coacervates as is presented in the following optimization section (item 4.2.2.3). The initial pH of the dispersions was measured and adjusted to 6.0 to initiate the complex coacervate formation and the preparation of the microcapsules. The dispersions were kept under magnetic stirring for 1h at room temperature to stabilize the complexes formation.

The CS:PPI coacervates were dried using a VirTis Sentry 2.0 bench top freeze-dryer (SP Scientific, Inc., PA, USA). For this method, the samples were placed in Falcon tubes, and centrifuged in an Avanti J-30I high-speed refrigerated centrifuge (Beckman Coulter Inc., Indianapolis, United States) for 20 min at 20,000 rpm. Then, its supernatant liquid was discarded, and the centrifuged PECs were placed cooled to -80 °C in an ultra-freezer for 24 h. After this, the frozen samples were placed in the freeze-dryer under 2000 μHg with condenser temperature of -98 °C for 96h. The freeze-dried coacervates were stored under refrigeration for further analyses.

4.2.2. Optimization of the microencapsulated systems

4.2.2.1. CS:SA based microparticles

A two-level-two-factors central composite design (cube plus star) with 4 axial points, 4 face centered star points and 5 central replicate points, and the response surface methodology, were used to study the effect of AO as the core material (X1) and $CaCl_2$ as the crosslinking agent (X2) in the characteristics of the CS:SA microcapsules. The samples were named according to the coded level, A = –1, B = +1 and C = 0, of the factors AO and $CaCl_2$ and the overview of the experimental conditions are shown in Table 9. A sample without açaí encapsulated oil and without cross-linker was used as the control. The experimental data was fitted according to the following second-order polynomial (Equation 4).

$$Y = \beta_0 + \sum_{i=1}^{k} \beta_i X_i + \sum_{i=1}^{k-1} \sum_{j=2}^{k} \beta_{ij} X_i X_j + \sum_{i=1}^{k} \beta_{ii} X_i^2 + e_i \quad (4)$$

where values of X_i and X_j are the independent variables affecting the Y responses. β_0 is the model intercept, β_i, β_{ii} and β_{ij} are regression coefficients of the linear, quadratic and interaction terms from the model, respectively, and k is the number of variables (SABERI et al., 2016).

Table 9. Overview of the experimental conditions for the CS:SA microparticles.

Factors	**Low value**	**Center point**	**High value**
AO (%)	0.25	0.5	0.75
$CaCl_2$ (%)	0	0.5	1.0
Sample	**Coded levels**		**Factors**
	X_1	**X_2**	**AO (%)**	**$CaCl_2$ (%)**
AA	–1	–1	0.25	0
BA	+1	–1	0.75	0
AB	–1	+1	0.25	1.0
BB	+1	+1	0.75	1.0
AC	–1	0	0.25	0.50
BC	+1	0	0.75	0.50
CA	0	–1	0.50	0
CB	0	+1	0.50	1.0
CC*	0	0	0.50	0.50

* Five replicas in the central point.

4.2.2.2. Ultrasound sonication of the optimized CS:SA microparticles

Sonication was used to investigate its effect on the size reduction of CS:SA PECs using methodology adapted from Ren et al. (2019). The equipment, an ultrasonic processor, 750-Watt model (Sonics & Materials Inc., Newtown, CT, USA), operating at 20 kHz, and equipped with a standard probe of 13 mm in diameter was used for this experiment (GOUVÊA et al., 2021). The parameters were pulsed on-time/off-time, time ranging from 1 to 3 min, amplitude ranging from 20 to 30%. The temperature of the sample was maintained around 25 °C by using an ice bath. About 15 mL of the dispersion of CS:SA açaí oil PECs, CC sample, were used. This treatment was applied on the particles before and after the addition of the crosslinking agent, $CaCl_2$.

For this, a two-level-two-factors central composite design (cube plus star) with 4 axial points, 4 face centered star points and 3 central replicate points, and the response surface methodology, were used to study the effect of time (min) and amplitude (%) as factors, X_{US1} and X_{US2} on the size of the microparticles. The samples were named according to the factors, as CCT-A, where CC represents that the particles used were the CC PECs (0.50% AO and 0.50% of $CaCl_2$), T and A represents the time and amplitude applied by the ultrasound sonication, respectively. An overview of the experimental conditions is shown in Table 10. A sample without the ultrasound sonication treatment was used as the control.

Table 10. Overview of the experimental conditions for the ultrasound sonication of CC microparticles.

Factors	**Low value**		**Center point**	**High value**
Time (min)	1		2	3
Amplitude (%)	20		25	30
Sample	**Coded levels**		**Factors**	
	X_{US1}	**X_{US2}**	**Time (min)**	**Amplitude** (%)
CC1-20	–1	–1	1	20
CC3-20	+1	–1	3	20
CC1-30	–1	+1	1	30
CC3-30	+1	+1	3	30
CC1-25	–1	0	1	25
CC3-25	+1	0	3	25
CC2-20	0	–1	2	20
CC2-30	0	+1	2	30
CC2-25*	0	0	2	25

* Three replicas in the central point.

The experimental data was fitted according to a second-order polynomial (Equation 4). After this procedure, the optimized particles were used to incorporation on the CS-based films, which are described in the following sections.

4.2.2.3. CS:PPI based microparticles

A two-level-two-factors central composite design with 4 axial points, 4 face axial points and 5 central replicates points was used to study the effect of % CS concentration (X1) and the CS:PPI ratio (w/w) (X2) on the EvO encapsulation and in

the formation of the coacervates complexes. The PPI solution at 1% concentration and 0.5% of EvO (w/w/) were maintained constant for all systems. The samples were named according to the coded level, D = –1, E = +1, F = -1.41, G = +1.41 and H = 0, of the factors CS and CS:PPI ratio and the overview of the experimental conditions are shown in Table 11. The experimental data was fitted according to a second-order polynomial equation (Equation 4).

Table 11. Overview of the experimental conditions for the CS:PPI coacervates.

Factors	**Low value**	**Center point**	**High value**
CS concentration (%)	0.5	0.75	1.0
CS:PPI ratio (w/w)	0.5	1.25	2.0

Sample	**Coded levels**		**Factors**	
	X1	**X2**	**CS (%)**	**CS:PPI ratio (w/w)**
DD	-1	-1	0.5	0.5
ED	+1	-1	1.0	0.5
DE	-1	+1	0.5	2.0
EE	+1	+1	1.0	2.0
FH	-1.41	0	0.39	1.25
GH	+1.41	0	1.10	1.25
HF	0	-1.41	0.75	0.18
HG	0	+1.41	0.75	2.31
HH*	0	0	0.75	1.25

* Three replicas in the central point.

4.2.3. Effect of pH on the formation of microparticles

The ζ – potential and turbidity measurements were determined to verify the effect of pH on the formation of CS:SA and CS:PPI microparticles, according to the methodology of HUANG et al. (2012). The ζ – potential was determined using dynamic light scattering based Zetasizer Nano equipment (Nano-ZS, Malvern Instruments, Worcestershire, UK). Samples (~1 mL) were placed in a DTS1070 cuvette and the ζ – potential analyses were conducted in triplicate. To analyze the microcapsules systems, their dispersions were diluted at 0.1% (v/v) with ultra-pure water, when necessary, and gently stirred prior analyses.

The turbidity measurements were determined using a Specord 210 Plus UV-Vis spectrophotometer (Analytik Jena GmbH, Jena, Germany), using an adapted method from GULÃO et al. (2015). The pH of the microparticles' solutions was measured and adjusted with 0.25 M NaOH and 0.25 M HCl, to achieve a pH ranging from 4.0 to 10.0. The microparticles solutions were left for 10 min to stabilize, then were gently poured into the 1 cm cuvette without stirring and the turbidity was then rapidly measured with a UV/Vis spectrophotometer at 600 nm. The equipment was calibrated with deionized water to 100% of Transmittance. The turbidity was defined through the Equation 5:

$$T = -\ln\left(\frac{I}{I_0}\right) \quad (5)$$

where *I* is the intensity of the incident light and I_0 is the intensity of the light that has passed through the sample volume. The maximum turbidity was related to the maximum biopolymer interaction and could result in highest particle yield (%).

4.2.4. Morphological observations of microparticles

The morphological aspects of the microparticles were observed by optical microscopy (OM), scanning electron microscopy (SEM) and confocal laser scanning microscopy (CLSM). These methodologies are described as follow.

4.2.4.1. OM observations

The dispersions of microparticles were observed by OM with a BX50 U-SPT Olympus binocular phototube microscope (Olympus Corporation, Tokyo, Japan) using an adapted methodology from Ifeduba and Akoh (2016). One drop of the dispersion was placed on glass slides with a drop of distilled water and glass covered for observation. The complexes were viewed using different magnification lens, 10x, 20x and 40x objectives. The images were captured with a coupled microscope digital camera HDCE-50B (E) using the Micrometrics Image Software.

4.2.4.2. SEM observations

The morphology of the microparticles was observed by SEM. Freeze-dried samples were sprinkled onto pieces of double-sided adhesive tape, attached to circular specimen stubs, coated with gold or silver under 6 x 10^{-1} mbar ultrapure argon vacuum (Baltec, SCD 005 Sputter Coater, Balzers, Liechtenstein) for 150s, examined with an

accelerating voltage of 5 kV and photographed using a scanning electron microscope (TM3030 Plus, Hitachi, Tokyo, Japan).

4.2.4.3. CLSM observations

Microscopy images of the microparticles were performed according to adapted methodology from Sadahira et al. (2018) with some modifications, using a LSM880 Airyscan Zeiss Confocal Laser Scanning Microscope (Zeiss, Oberkochen, German). The fluorescent dye, Nile Red, was used to dye the hydrophobic phase (oil) encapsulated on the PECs. The drop of the samples dispersion was placed on concave microscope glass slides, stained with 2 drops of a 1 mg mL^{-1} Nile Red solution in dimethyl sulfoxide (DMSO) and covered with glass coverslips. To observe encapsulated oil phase in the loaded microparticles, the fluorescence of Nile Red was examined by exciting an argon laser at 488 nm and the applied magnification varied from 10 to 63x. For optimum image resolution the microscope pinhole was set up to 1 Airy unit (AU) and the range indicator tool on the Zen Image Software (Zeiss, Oberkochen, German) was used to adjust the proper red pixels saturation, and images recorded.

4.2.5. Determination of particle size

The particle size of microcapsules was determined by laser diffraction. For the CS:SA PECs the particle size was measured using a Malvern Mastersizer 2000 (Malvern Instruments, Malvern, UK). For particle size of the CS:PPI coacervates, a Mastersizer 3000 Hydro (Malvern Instruments, Malvern, UK). In both equipment, the measurements procedure is the equal. Approximately 1 – 5 mL of the microparticles dispersions (depending on the measured obscuration value for each sample) were diluted in distilled water (dispersant liquid) and stirred at 2000 rpm to keep the samples suspended and homogenized. Five replicates were made for each sample. The average particle size, expressed as D[4,3] (μm), and the span value, which indicates the polydispersity of the particles, were determined. For the CS:PPI microparticles the particle size was measured after 10 days of storage to evaluate its changing.

4.2.6. Evaluation of encapsulation efficiency (EE%)

The encapsulation efficiency of the CS:SA PECs was determined by the UV–vis spectrophotometric method reported by Khoshakhlagh et al. (2017) with

modifications. A standard curve for AO in heptane solutions (0.01 – 0.1%, w/v) was prepared. The absorbance of these solutions was measured within the 200 – 500 nm range with a Cary 100 spectrophotometer (Agilent Technologies Inc., Santa Clara, CA, USA). *N*-heptane was used as blank. The methodology was performed in two steps. The first step was to determine the amount of free AO and then to calculate the encapsulated oil by difference. The free AO was extracted with n-heptane. The absorbance of this solution was determined at 294 nm and the amount of free AO was calculated by Equation 6.

$$Free\ AO\ (\%) = \left(\frac{W_2}{W_1}\right) \times 100 \qquad (6)$$

where W_1 is the mass of AO used to produce the microcapsules and W_2 is the mass of the non-encapsulated AO. The amount of AO encapsulated was determined by the difference between the total oil mass added in the systems and that of non-encapsulated AO. The encapsulation efficiency (EE) was calculated by Equation 7.

$$EE\ (\%) = \left(\frac{W_4}{W_3}\right) \times 100 \qquad (7)$$

where W_4 is the encapsulated AO mass, and W_3 is the AO mass used for microcapsule production. Two replicates were made for each sample.

4.2.7. Determination of total polyphenols and antioxidant activity

The *in vitro* determination of biological activities of the AO, EvO, and loaded PECs was performed by different assays, total polyphenol content, DPPH radical scavenging activity, Trolox equivalent antioxidant capacity and ferric reducing antioxidant potential. Priorly, for the AO and EvO, about 10 µg, was added in 1mL of ethanol, and for the PECs, an aliquot of approximately 10 µL of its dispersions was added in 1 mL of 60% ethanol:water. These samples were vigorously mixed for 1 min and centrifuged for 5 min in a mini-centrifuge (C1008-B-E MyFuge, Benchmark Scientific, NJ, USA) and the assays were performed as follow.

4.2.7.1. Total polyphenols content (TPC)

The Folin-Ciocalteu assay has been widely used to investigate the total polyphenols content in food matrixes, however it also can be applied to study antioxidant activity, since its action mechanism is based in an oxidation/reduction reaction (PRIOR, WU, SCHAICH, 2005).

The TPC of AO, EvO and the loaded PECs was analyzed by the the Folin-Ciocalteu assay as reported by Singleton, Orthofer, Lamuela-Raventós (1999). An aliquot of 10 µL of the supernatant solution of the samples was mixed in a 96-well plate with 40 µl of Folin-Ciocalteu reagent and 150 µl of a 4% sodium carbonate solution and incubated for 30 minutes at room temperature in the dark. Subsequently, the absorbance was read at 765 nm in a plate-reader spectrophotometer (Spark 10M, Tecan Trading AG, Switzerland). Ethanol and distilled water were considered as blank for the oils, AO and EvO, and for the PECs, respectively. All samples were analyzed in triplicate. The results were expressed in µg of gallic acid equivalent antioxidant capacity per mL of sample ($\mu g\ GAE\ mL^{-1}$).

4.2.7.2. DPPH radical scavenging activity

The free radical scavenging activity for AO, EvO and the loaded PECs was determined by the 2,2-diphenyl-1-picrylhydrazyl (DPPH) radical• method, adapted from Brand-Williams, Cuvelier, Berset (1995). An aliquot of the samples' supernatant solutions (10 mg mL^{-1}) was mixed in a 96-well plate with 300 µl of DPPH reagent and incubate at 25°C for 0, 30, 60 and 120 min in a dark room. The absorbance was read at 517 nm in a plate-reader spectrophotometer (Spark 10M, Tecan Trading AG, Switzerland). Ethanol and distilled water were considered as blank for the oils, AO and EvO, and for the PECs, respectively. The results were compared with a Trolox standard curve (0 – 250 mg L^{-1}) and expressed in mg of Trolox equivalent antioxidant capacity per mL of sample (mg TE L^{-1}). The $DPPH\ scavenging\ capacity$ can also be expressed as percentage (%) of inhibition and calculated according to the Equation 8.

$$DPPH\ scavenging\ capacity = \frac{A_B - A_S}{A_B} \times 100 \qquad (8)$$

where A_B is the absorbance of the blank and A_S is the absorbance of the sample.

4.2.7.3. Trolox equivalent antioxidant capacity (TEAC)

The TEAC assay was used to investigate the *in vitro* antioxidant activity of the samples, according to the methodology from Re et al. (1999). An aliquot of the supernatant solution (10 mg mL^{-1}) was mixed in a 96-well plate with 300µl ABTS solution. The absorbance was read after 6 min at 734 nm using a plate-reader spectrophotometer (Spark 10M, Tecan Trading AG, Switzerland). Results were compared with a Trolox standard curve (0 – 250 mg L^{-1}) and expressed as mg TE L^{-1}

4.2.7.4. Ferric reducing antioxidant potential (FRAP)

The antioxidant activity of samples was measured as FRAP according to the methodology adapted from Lotito and Frei (2004). In this method, an aliquot of supernatant solution (10 mg mL^{-1}) was mixed in a 96-well plate with 300 µl of FRAP reagent (containing a 10:1:1 mixture of 300 mM sodium acetate pH 3.6: 0.8 mM TPTZ: 1.7 mM $FeCl_3$), and incubated for 15 min at 37°C. The absorbance was read at 593 nm in a plate-reader spectrophotometer (Spark 10M, Tecan Trading AG, Switzerland). Results were compared with a Trolox standard curve (0 – 250 mg L^{-1}) and expressed as mg TE L^{-1}.

4.2.8. Characterization of raw materials and PECs by infrared spectroscopy

Fourier transform infrared spectroscopy (FTIR) analyses were carried out using a Perkin Elmer spectrometer, Frontier 98737 model (Waltham, MA, USA) at ambient temperature, equipped with a Universal Attenuated Total Reflectance (ATR) cell device, in the 4000 – 400 cm^{-1} range. All spectra were registered by averaging 60 scans with a resolution of 4 cm^{-1} in transmission mode.

4.2.9. Rheological properties

The rheological properties for the dispersions of microcapsules were investigated at 25ºC with a controlled stress rheometer AR G2 (TA Instruments, New Castle, DE, USA), equipped with cone-and-plate geometry (40 mm in diameter, 2º cone angle and a gap of 50 µm). Strain sweep tests were conducted as the variation of complex modulus at 6.28 rad/s to determine the linear viscoelastic range. The storage modulus (G'), the loss modulus (G''), and the complex viscosity (η*) values were measured within the viscoelastic region, whereas the angular frequency varied from 10^{-1} to 4 $x10^2$ rad s^{-1} at a constant strain of 0.1%. The steady state flow was performed from 10^{-1} to 4 $x10^2$ s^{-1} shear rates, first in increasing order and then in decreasing order of applied torque.

4.2.10. Thermogravimetric analysis (TGA)

TGA was used to investigate the thermal stability of the raw materials and PECs. The experiments were carried out with dried samples under nitrogen atmosphere in a TA Instrument, model Q-500 (New Castle, DE, USA). Approximately, 10 mg of sample were heated from 25°C to 700°C at a 10°C min^{-1} rate.

4.2.11. Analysis of differential scanning calorimetry (DSC)

The thermal properties of PECs were investigated using a DSC Q-1000 Differential Scanning Calorimetry equipment from TA Instruments (New Castle, DE, USA). About 5.0 ± 0.5 mg of samples were sealed in an aluminum pan with a pinhole and subjected to a 50 mL min^{-1} flow rate nitrogen atmosphere. The first ramp was equilibrated at -50 °C and heated until 250 °C at 10 ºC min^{-1} rate. An isothermal ramp kept the temperature at 250 °C for 1 min, then a swiftly cooling ramp was played to equilibrate the temperature at -50 °C. All consecutively measurements were heated, cooled, and reheated from -50 °C to 250 °C at 10 ºC min^{-1} rate. The DSC profile was analyzed with the Universal Analysis software version 4.2 (TA instruments, New Castle, DE, USA), and the resulting curves were graphically edited in the Origin software (OriginLab, 2021).

4.2.12. Chitosan composite films

4.2.12.1. Preparation of the CS stock solution

CS powder at 2.5% (w/v) was dissolved in a 1% (v/v) acetic acid solution under constant magnetic stirring over night at room temperature.

4.2.12.2. Preparation of the deep eutectic solvent

The DES was prepared by mixing the ChCl powder (hydrogen bond acceptor) with Gly (hydrogen bond donor) at the molar ratio of 1:2 (w/w) (ALOMAR et al., 2016), under constant magnetic stirring at 80°C to obtain a homogenous mixture. The DES mixture was left to cool down and stored at room temperature until further analysis.

4.2.12.3. Preparations of the CS-DES-PECs films

The 2.5% CS solution gently mixed with the DES at 0 and 5% (v/v) and stirred overnight at 25 °C until full homogenization. The optimized açaí CS:SA microcapsules (8:2 chitosan: sodium alginate PECs incorporated with 0.5% of açaí oil and crosslinked with 0.5% of $CaCl_2$) were prepared as previously described in item 4.2.2.1 and incorporated at different concentrations from 0 to 10% (v/v) into the CS-DES solution to obtain the film-forming mixture, as listed Table 12.

Table 12. Formulation of the CS composite films incorporated with CS:SA-AO PECs.

Sample	DES (%, v/v)	CS:SA-AO PECs (%, v/v)
F0/0	0	0
F5/0	5	0
F5/0.25	5	0.25
F5/0.5	5	0.50
F5/1	5	1
F5/2	5	2
F5/5	5	5
F5/10	5	10

The film-forming solutions were casted in glass Petri dishes and dried at 60°C in an oven for 24h. Then the dried films were kept at room temperature in a desiccant apparatus under vacuum containing a modified atmosphere of anhydrous calcium chloride, ~25% of relative humidity (RH), until constant weight (5 days), which resulted in the formation of thin CS-DES-PECs films. The thickness of the films was controlled by casting the same weight (~15g) of film-forming solutions in each plate. Finally, the films were stripped off from glass plates, stored at room temperature and a modified atmosphere (~25% of RH) until further analysis.

4.2.12.4. Characterization of the chitosan composite films

4.2.12.4.1. Microstructural observations

The morphological aspects of the films were observed by optical microscopy (OM), scanning electronic microscopy (SEM) and confocal laser scanning microscopy (CLSM). The film-forming solutions, prior drying, were observed by OM with a BX50 U-SPT Olympus binocular microscope (Olympus Corporation, Tokyo, Japan) at 10x and 40x magnification. One drop of the film-forming solutions was placed on glass slides with a drop of distilled water and glass covered for observation.

For the SEM observations, the dried films were priorly immersed in liquid nitrogen and cracked into small pieces, then sprinkled onto double-sided adhesive tape, attached to circular specimen stubs, coated with carbon under 6 x 10^{-1} mbar ultrapure argon vacuum from Baltec (SCD 005 Sputter Coater, Balzers, Liechtenstein) for 150s, examined at 5 kV and photographed (TM3030 Plus, Hitachi, Tokyo, Japan).

The CLSM assessments were performed according to Shi et al. (2016) with some modifications, using a LSM880 Airyscan Zeiss confocal microscope (Zeiss, Oberkochen, German). The fluorescent dye, Nile Red, was used to dye the hydrophobic phase (açaí oil) of the PECs dispersed in the CS-DES films. The film samples (~ 20 x 20 mm) were placed on concave microscope glass slides, stained with 2 drops of a 1 mg mL^{-1} Nile Red solution in dimethyl sulfoxide (DMSO) and covered with glass coverslips. To observe the presence of the açaí PECS loaded in the CS-DES-PECs films, the fluorescence of Nile Red was examined by exciting an argon laser at 488 nm and the applied magnification varied from 10 to 63x. For optimum image resolution the microscope pinhole was set up to 1 Airy unit (AU) and the range indicator tool on the Zen Image Software (Zeiss, Oberkochen, German) was used to adjust the proper red pixels saturation.

4.2.12.4.2. Measurement of the films thickness

The films thickness (*L*) [mm] were measured with a digital micrometer model 13101-25 with a 0.001 mm resolution (PANTEC®, Rio Grande do Sul, Brazil). For the calculation of the water vapor permeability of the films, five random measurements were taken on each testing sample at different points. For the determination of the tensile strength of the films, the thickness was measured along the length of each film strips. The results were expressed as mean ± standard deviation.

4.2.12.4.3. Water vapor permeability (WVP)

The WVP of the films was determined gravimetrically based on the E96/E96M assay from the Standard Test Method for Water Vapor Transmission of Materials (ASTM, 2016). Film with no visual physical defects, such as bubbles or cracks, were chosen for the WVP tests. Samples squares with ~20 × 20 mm were tightly sealed to the top of a plastic permeation cell with a pinhole of ~6 mm of diameter. The permeation cell contained distilled water (100% of RH) at a ¾ level from the film. Paraffin was used to seal the films in the cells and to make sure that the water vapor permeation goes only through the films. The permeation cells were weighed, placed in a desiccator containing granular anhydrous calcium chloride (~25% of RH) at room temperature and applied vacuum atmosphere, providing a relative humidity gradient through the films. The cells were periodically weighed to evaluate the changes of weight every 24h

for 14 days. The tests were carried out in duplicate for each film sample and the WVP in g m^{-1} s^{-1} Pa^{-1} was obtained from Equation 9.

$$WVP = (\Delta m \times L)/(A \times \Delta t \times \Delta p) \quad (9)$$

where *Δm* is the weight change (g), *L* is the film thickness (m), *A* is the area (0.006 m^2) of the film exposed to water vapor permeation for a time Δ*t* (s) to a partial water pressure Δ*p* (Pa).

4.2.12.4.4. Fourier transform infrared (FTIR) spectroscopy

FTIR analyses were carried out using a Frontier 98737 model spectrometer, (Perkin Elmer, Waltham, MA, USA) at room temperature, equipped with a Universal Attenuated Total Reflectance (ATR) cell device, in the 4000 – 400 cm^{-1} range. All samples spectra were registered by averaging 60 scans with a resolution of 4 cm^{-1} in transmission mode. The spectra resulting curves were graphically edited in the Origin software (OriginLab, 2021).

4.2.12.4.5. X-ray diffraction (XRD)

The XRD analysis of the films were performed using the Ultima IV X-ray diffractometer (Rigaku Corporation, Tokyo, Japan) in continuous scanning mode with CuK*α* radiation generated at 40 kV and 20 mA. The data were collected over the angular region of 2º to 50º (2*θ*) at 0.05º per second (2*θ*). The crystallinity degree (CrD) of the films was estimated from peak deconvolutions executed with *Fytik*® (an open-source software) using the following Equation 10, according to Ferreira and Andrade (2015). The resulting curves were graphically edited in the Origin software (OriginLab, 2021).

$$CrD\ (\%) = \frac{H_C}{(H_C + H_A)} \times 100 \quad (10)$$

where H_c is height of the crystallinity reflection related to the crystalline area and H_A is the height of the amorphous halo at the same angle.

4.2.12.4.6. Dynamic mechanical analyses (DMA)

Compression molded samples with (14.0) mm x (8.0) mm x (0.3) mm in dimensions were analyzed in a Q800 DMA (TA Instruments, New Castle, DE, USA) using film clamp at 1 Hz, under multi frequency-strain mode, from –50 to 310°C, at a heating rate of 3°C min^{-1} (FERREIRA, ANDRADE, 2015). A total of two measurements

was taken for each sample. The results were presented as loss factor (tan δ), given by the ratio between the loss modulus (E") and the storage modulus (E'), as a function of temperature. The resulting curves were graphically edited in the Origin software (OriginLab, 2021).

4.2.12.4.7. Mechanical properties

Tensile tests were carried out at 21 °C in a Q-800 DMA equipment (TA Instruments, New Castle, DE, USA) according to the adapted method from Jost and Langowski (2015). The films were previously conditioned at 21 °C, and 50% relative humidity, for a period of at least 48 h, then cut off in rectangular stripes measuring approximately 14.0 mm x 8.0 mm x 0.3 mm. The samples were placed between a fixed and a moveable film clamp, and the experiments were performed in tensile mode. The tensile strength (σ), Young's modulus (YM), and elongation at break (ε) were measured, in triplicate. The resulting curves were graphically edited in the Origin software (OriginLab, 2021).

4.2.12.4.8. Thermogravimetric analysis (TGA)

The TGA were performed in a Q500 TGA equipment (TA Instruments, New Castle, DE, USA) under nitrogen flow. Samples weighing approximately 10 mg were heated from 25 to 700 °C, at a heating rate of 10 °C min^{-1}. Curves from the derivative thermogravimetric (DTG) analysis were used to measure and compare the peak temperatures. The resulting curves from TGA and DTA were graphically edited in the Origin software (OriginLab, 2021).

4.2.12.4.9. Antioxidant activity of CS-composite films

The *in vitro* biological activities of the CS-DES based films incorporated with the microstructured açaí PECs were determined by different antioxidant tests, as previously described in item 4.2.7, total polyphenols content, TEAC, DPPH radical scavenging and FRAP assays. To all antioxidant analyses, a film extract was obtained by adding ~10 mg of film samples in Eppendorf vials containing 1mL of 60:40 ethanol: distilled water solution, vigorously mixed for 1 min and then centrifuged. An aliquot of this supernatant solution was then combined in a 96-well plate with the appropriate reagents.

4.2.13. Determination of fatty acids profile of açaí pulp oil by GC-MS

The composition of fatty acids (FAs) from the AO was determined using the following methodology. The lipids were priorly converted to fatty acid methyl esters (FAMEs) through methylation, which allowed subsequently determine the FAs profile by gas chromatography (GC). The FAMEs were prepared in two steps, digestion and separation, using a MARS 6 Express 40 position Microwave Reaction System (CEM Corporation, Matthews, NC, USA) according to method described by Brunton, Mason, Collins (2015). For FAMEs digestion, the lipids samples weighing, approximately 1g, were placed into the reaction vessel with 10 mL of a 2.5% methanolic potassium hydroxide solution, a 10 mm magnetic stirrer and sealed with a cap. The capped vessels were placed in the turntable and introduced into MARS6 microwave. The samples were heated to 90 °C for 5 minutes and held at this temperature for 10 minutes. Then, the reaction vessels were removed from the turntable and cooled on cold water until reached room temperature before opened. The procedure was carried out by adding 15 mL of HCl in the reaction vessels, tightly closed and placed again in the MARS6 microwave to a ramp of 120 °C for 5 min and held it in this temperature for another 6 minutes. Afterwards, the vessels were removed from the equipment and led to cool down until it reached 25 °C. For FAMEs separation, 10 mL of pentane was added in the vessels and sealed, to be slowly inverted and brought back vertical once. Then, 15 mL of a saturated aqueous sodium chloride solution was added. The top layer comprising the pentane layer with the FAMEs was transferred into an amber glass vial containing small amounts (~ 0.5mg) of anhydrous sodium sulfate and 2 µL of the internal standard ($C_{15:0}$ - methyl pentadecanote). The samples were stored at –18°C until required for analysis. The samples were prepared in duplicate.

The GC-MS analysis were performed on a Varian Star CP3800 gas chromatograph (Varian, Walnut Creek, CA, USA) coupled with a Saturn 2000 Mass Spectrometer, equipped with a Supelco SP-2560 column (dimensions: 100 m length x 0.25 mm Internal diameter, 0.2 µm of a polar non-bonded biscyanopropyl siloxane phase). Samples (1 µL) were injected in a split mode 1:10 (Injector temp: 250°C), using Helium as carrier gas (0.5 mL min^{-1}). The oven temperature was programmed from a 5 min isotherm at 140°C to 240°C, at a rate of 4°C/minute, followed by a final 15 min isotherm. MS analysis were performed in Electron Impact (EI) mode (70 eV) and a scan range of 90-650 m/z.

4.2.14. Analysis of phenolics from açaí pulp oil by LC-PDA and LC-MS

4.2.14.1. Extraction of phenolic compounds from açaí oil

To perform the analysis of phenolic compounds from açaí oil by liquid chromatography coupled with ultraviolet (LC-PDA) and mass spectrometry (LC-MS) detectors, extracts were prepared according to the adapted methods from Slatnar et al., 2014 and Wang et al., 2017. Oil samples, about 2 g were weighed into a centrifuge tube. Then, 10 mL of *n*-hexane and 2 mL of CH_3OH/H_2O (60:40, v/v) were added. The mixture was stirred for 2 min using a vortex apparatus, and subsequently centrifuged at 2000 rpm for 10 min at 4 °C. The methanol layer was removed, and the operation was repeated three times. The methanolic extracts were combined and washed two times with 2 mL of *n*-hexane. Then, the *n*-hexane layer was discarded. The extracts were rotary-evaporated under reduced pressure at 40 °C (water bath). Then, the residue was re-dissolved in methanol/water (50:50, v/v) solution to achieve 1.0 mg mL^{-1} and 2.0 mg mL^{-1} of extract concentration. The samples were filtered through a 0.20 µm filter prior to LC-MS injection. Samples were stored the samples in amber vessels and refrigerated until analysis.

4.2.14.2. Analysis of açaí oil extracts by LC-PAD and LC-MS

The LC analysis were performed on a Prominence High Performance Liquid Chromatograph (Nexera modular HPLC, Shimadzu Scientific Instruments Corp., Columbia, USA), equipped with a Phenomenex Gemini C18 column (dimensions: 4.6 mm x 250 mm x 5 µm) in an oven at 25 °C. Using an automatic injector (Reodyne), 30 µL of methanolic solution were injected. Using a flow rate of 0.6 mL/min, the HPLC grade eluents (all of them acidified with formic acid at 0.1%) were: (A = H_2O, and B = methanol or C = acetonitrile). The chromatographic analysis was initiated with 95% of A, following and increasing content of B (or C), as following: 0 - 1 min (5% B); 2 min (10% B), 30 min (30% B), 50 min (80% B), 60 - 80 min (95% B), and 85 - 86 min (5% B). LC-PDA detection system ranged from 200 to 800 nm. The MS analysis (LCMS-2020 mass spectrometer detector) were performed in Electrospray Ionization (ESI), in mode positive and negative, with a scan range of 100-1000 m/z.

4.2.15. Statistical analysis

The results were statistically analyzed using the Statistica 7.0 (StatSoft, Inc., Tulsa, OK, USA) software and Minitab version 18.1 (Minitab, Inc, Coventry, UK). The adequacy of the models and the response surface methodology were determined based on the lack of fit and the coefficient of determination (R^2). These same programs were used for the analysis of variance (ANOVA) and Tukey's test, at a significance level of 95% ($p < 0.05$).

5. RESULTS AND DISCUSSION

In this section, the results from the development and characterization of microencapsulated systems based on the pair of natural biopolymers, CS and SA, and on CS and PPI, are presented. The obtained CS:SA PECs were incorporated on DES plasticized CS-composite films, which were also characterized by different methods. Part of these study, mainly the results related to CS:PPI system, which were obtained during an international internship at the University of Leeds, Leeds, UK, between October 2019 and March 2020. For this reason, some techniques used to the particles characterization can differ from each other.

5.1. Microencapsulation systems based on CS:SA

Systems using CS and SA were developed and studied aiming the encapsulation of AO. Different techniques were used in the formulation as well as to the characterization of the microparticles. To study the ideal ratio of CS and SA in the microparticles formulation, the different proportions between these biopolymers were investigated. For this, the determination zeta-potential of the stock solutions, size and polydispersity index of their respective PECs were explored. After chosen the ideal CS:SA ratio, the system was optimized using statistical tools, the response surface methodology and the desirability function, to evaluate significant factors affecting AO encapsulation on PECs and to find an optimum condition to it.

Subsequently, the optimized CS:SA AO PECs were submitted to an ultrasound sonication to study the effect of this on the size reduction. The response of this step was also optimized to achieve the smallest possible size and span. The raw materials, AO, CS and SA, as well as the formulated PECs were observed using microscopy techniques to examine its morphological aspects, and characterized by physical-chemical methodologies, such as laser diffraction, Fourier transform infrared spectroscopy, rheological measurements, thermogravimetric analysis, and spectrophotometric analysis of antioxidant properties. The results from all these determinations are following presented.

5.1.1. Determination of the zeta-potential of stock solutions

The concentration of biopolymers and their ratio influence the formation of PECs. For this reason, the concentration of biopolymers used for the preparation of all

microcapsules systems was kept at 1.0% (w/v). The ζ-potential for the CS and SA solutions at 1.0% concentration changed with the solution pH, as can be observed in Table 13.

Table 13. ζ-potential of stock solutions as function of pH.

pH	ζ-potential (mV)	
	1% CS	1% SA
4.0 ± 0.2	+17.2 ± 2.4[a]	–14.9 ± 0.5[c]
5.4 ± 0.2	+19.4 ± 3.1[a]	–6.2 ± 0.9[b]
6.4 ± 0.4	+13.8 ± 4.6[a,b]	–5.6 ± 0.6[a]
7.2 ± 0.1	+2.6 ± 0.6[b]	–1.4 ± 0.1[a]

Results are expressed as mean ± standard deviation. Means followed by different superscript lower-case letters in the same column differ statistically by Tukey's post-hoc test ($p<0.05$).

Positively charged ζ-potential values were observed for CS solutions, due to the positive charges of –NH3+ groups on glucosamine units. On the other hand, a negative charge was determined for SA solutions at all pH values studied, due to the charge of carboxylate groups in the chain. As expected, when the pH was increased from 4 to 7, a decrease in the ζ-potential for the CS solution and an increase in the ζ-potential for the SA solution were observed. This behavior may be attributed to deprotonation of amino groups and protonation of carboxylate groups in CS and SA, respectively.

A second-order polynomial regression was plotted with the ζ-potential results as a function of pH for both biopolymers solutions and a coefficient of determination (R^2) was calculated. The ζ-potential for 1.0% CS and SA solutions at different pH can be expressed by Equation 11 and Equation 12:

$$\zeta - \text{potential } 1.0\% \text{ CS} = -1.449 \times pH^2 + 11.483 \times pH - 4.10 \quad [R^2 = 0.9438] \qquad (11)$$

$$\zeta - \text{potential } 1.0\% \text{ SA} = -1.218 \times pH^2 + 17.842 \times pH - 66.99 \quad [R^2 = 0.9897] \qquad (12)$$

The ζ-potential for a 0.1% CS solution in the formation of a PEC with hsian-tsao gum was studied by You, Liu, Zhao (2018). The authors observed a decrease in the ζ-potential from ~ 60 to 10 mV as the pH increased from 4 to 7. Other researchers also reported changes in the ζ-potential for a 0.1% SA solution under pH variation (GORJI

et al., 2018). These authors found that the ζ-potential for SA decreased from -19.05 to -46.24 mV as the pH was varied from 4.80 to 2.80.

5.1.2. Determination of the CS:SA ratio

The positively charged CS (ζ-potential of 17.2 ± 2.4 mV at pH 4.0 ± 0.2) and negatively charged SA (ζ-potential of −5.6 ± 0.6 mV at pH 6.4 ± 0.4) solutions were mixed at different ratios, 2:8, 3:7, 1:1, 7:3 and 8:2, to obtain microcapsules. The ζ-potential, particle size and polydispersity index (span) for these systems were evaluated and are shown in Table 14. The ζ-potential for CS:SA PECs presented values ranging between the values for CS and SA solutions alone. This result is an indication of the interaction between their opposite charges in the mixed systems (YOU, LIU, ZHAO, 2018). A substantial shift in the ζ-potential values, from 9.2 to −6.80 mV ($p < 0.05$) was observed, when the PECs were in excess of CS (8:2) and SA (2:8), respectively. When the ratio between CS and SA was < 1 (excess of SA) the PECs were larger in size. Thus, the size of the microcapsules was influenced by the increase in SA in the PEC composition, as can be seen in Table 1.

Table 14. ζ-potential and particle size of microcapsules under pH 6.5.

CS:SA ratio	ζ-potential (mV)	D[4,3] (μm)	Span
2:8	–6.8 ± 0.8^{d}	506.5 ± 1.9^{b}	1.16 ± 0.01^{b}
3:7	–1.4 ± 0.5^{c}	507.8 ± 11.9^{b}	1.16 ± 0.04^{b}
1:1	–1.7 ± 0.6^{c}	468.4 ± 13.7^{a}	1.37 ± 0.05^{a}
7:3	+1.6 ± 0.3^{b}	463.9 ± 8.0^{a}	1.26 ± 0.03^{c}
8:2	+9.2 ± 0.7^{a}	387.7 ± 1.5^{c}	1.55 ± 0.02^{d}

Results are expressed as mean ± standard deviation. Means followed by different superscript lowercase letters in the same column differ statistically by Tukey's post-hoc test ($p<0.05$).

The order in which CS and SA were mixed together may have also influenced this result, as has been previously reported (SÆTHER et al., 2008). These authors found that the order of mixing a polyanion in a polycation solution, or contrarywise, could affect the size, ζ-potential and other properties of the PECs. In this work, it was found that the 8:2 CS:SA microcapsules were significantly different ($p<0.05$) from the other systems, presenting the smallest size and the highest ζ-potential. As particle size is known to influence several properties, such as solubilization, mechanical and optical

properties of polymeric films, the 8:2 CS:SA composition was selected for the following encapsulation experimental design.

In Figure 16 is presented the visual aspects of the CS:SA 8:2 PECs dispersion under different pH values.

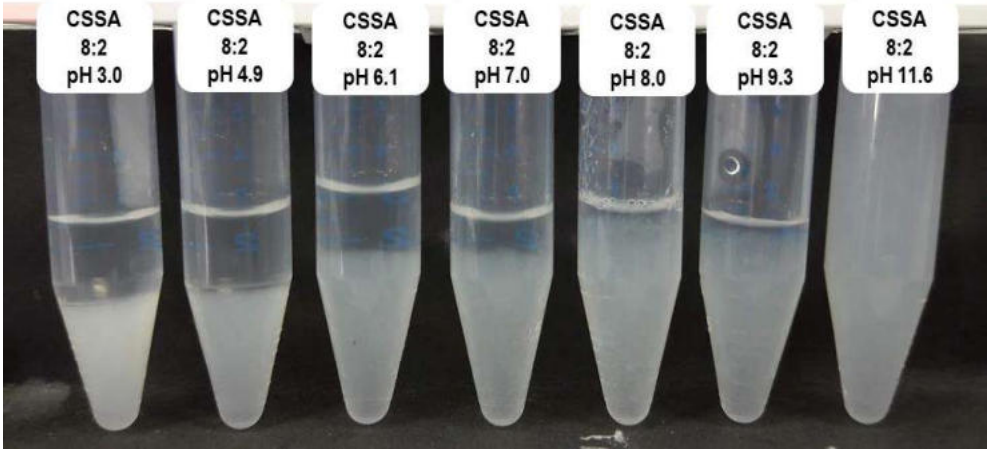

Figure 16. Visual aspects of the CS:SA 8:2 dispersion under different pH values.

5.1.3. Optimization of the 8:2 CS:SA microencapsulated systems

Several parameters can affect the encapsulation process, such as the concentration and ratio of biopolymers used as the wall material, the pH, the amount of core material, the use and type of crosslinking agents, the homogenization rate among others (EGHBAL, CHOUDHARY, 2018). Some of these parameters were optimized using a central composite design (cube plus star) in order to verify their influence on the characteristics of microcapsules based on CS and SA. The overview of the experimental conditions for the encapsulation of AO (X_1) in CS:SA (8:2) microcapsules crosslinked with $CaCl_2$ (X_2), with the respective results for the particle size (D[4,3]), span and encapsulation efficiency (EE) are shown in Table 15.

The PECs presented a large size, above 340 μm, and polydispersity index of 1.47. The largest size, ~ 435 μm, was observed for the sample BB, which was prepared with the maximum content of AO and $CaCl_2$. The increase in size as a result of the increase in the amount of those factors also corroborates the results of encapsulation efficiency. This effect may also be related to the largest amount of calcium salt added to the PECs, which promoted alginate gelation and allowed the diffusion of chitosan molecules through the particle, which consequently promoted the increase in its volume (GÅSERØD, SMIDSRØD, SKJÅK-BRÆK, 1998). All systems presented an encapsulation efficiency above 99.5%. This result is in accordance with reports from

the literature, in which a high EE% is one of the advantages of obtaining microcapsules by complex formation (EGHBAL, CHOUDHARY, 2018).

Table 15. Overview of the experimental conditions and responses for the AO encapsulation in CS:SA microcapsules crosslinked with $CaCl_2$.

Sample	Coded levels		Parameters		Responses		
	X_1	X_2	AO (%)	$CaCl_2$ (%)	D[4,3] (μm)	Span	EE (%)
AA	–1	–1	0.25	0	374.5 ± 1.6^{b,c}	1.73 ± 0.00^{b,c}	99.91 ± 0.02^{a}
BA	+1	–1	0.75	0	397.8 ± 1.0^{a,b}	1.61 ± 0.00^{e}	99.90 ± 0.01^{a}
AB	–1	+1	0.25	1.0	369.1 ± 1.7^{b,c}	1.68 ± 0.01^{d}	99.90 ± 0.03^{a}
BB	+1	+1	0.75	1.0	435.9 ± 1.8^{a}	1.47 ± 0.02^{f}	99.89 ± 0.03^{a}
AC	–1	0	0.25	0.5	360.8 ± 0.5^{b,c}	1.87 ± 0.01^{a}	99.58 ± 0.05^{b}
BC	+1	0	0.75	0.5	383.9 ± 1.5^{b,c}	1.68 ± 0.00^{d}	99.88 ± 0.04^{a}
CA	0	–1	0.5	0	346.1 ± 1.9^{c}	1.76 ± 0.03^{b}	99.51 ± 0.01^{b}
CB	0	+1	0.5	1.0	384.2 ± 3.6^{b,c}	1.73 ± 0.01^{b,c}	99.50 ± 0.03^{b}
CC*	0	0	0.5	0.5	367.7 ± 1.0^{c}	1.72 ± 0.1^{c}	99.95 ± 0.01^{a}

Results are expressed as mean ± standard deviation. *Central point with five replications. Means followed by different superscript lower-case letters in the column differ statistically by Tukey's post-hoc test ($p < 0.05$).

The responses, size (D[4,3] μm), polydispersity index (span) and encapsulation efficiency (EE%) were modelled by fitting a second-order polynomial Equations 13 - 15.

$$Size\ D[4,3] = 363.9 + 18.7\beta_1 + 10.96\beta_2 + 16.17\beta_{11} + 8.95\beta_{22} + 10.46\beta_{12} \quad (13)$$

$$Span = 1.75 - 0.09\beta_1 - 0.04\beta_2 - 0.03\beta_{11} - 0.06\beta_{22} - 0.02\beta_{12} \quad (14)$$

$$EE = 99.87 + 0.05\beta_1 - 0.01\beta_2 + 0.08\beta_{11} - 0.15\beta_{22} - 0.002\beta_{12} \quad (15)$$

Where β_1, β_2 are the linear regression coefficients, β_{11} e β_{22} quadratic regression coefficients and β_{12} are the interaction coefficients for the AO (%) and $CaCl_2$ (%) factors, respectively.

The results for the regression coefficients and the variance analysis (ANOVA) of this experimental design are listed in Table 16. The results for the linear regression coefficients show that the size of the particles was significantly affected by AO and $CaCl_2$ and the span was influenced only by AO ($p \leq 0.05$).

Table 16. Results for regression coefficients and analysis of variance (ANOVA) for dependent variables of the experimental design.

Coefficients	D[4,3] (μm)	Span	EE (%)
Mean			
β_0	363.9*	1.75*	99.87*
Linear			
β_1	18.7*	-0.09*	0.05
β_2	10.96*	-0.04	-0.01
Quadratic			
β_{11}	16.17*	-0.03	0.08
β_{22}	8.95	-0.06	-0.15
Interactions			
β_{12}	10.46	-0.02	-0.002
R^2	0.867	0.768	0.210
$F_{calculated}$	9.13*	4.66*	0.37

*Significant factors ($p \leq 0.05$). β1, β2 are the regression coefficients for the AO (%) and $CaCl_2$ (%) factors, respectively.

On the other hand, it is possible to infer that the EE% was not affected by the studied factors. The quadratic responses for EE% and span were not statistically influenced by the interaction of the factors AO and $CaCl_2$. However, this response was statistically different in relation to the particle size. The models were used to calculate the response surface for each variable response. The estimated contours of the response surface are shown in Figure 17 and 18.

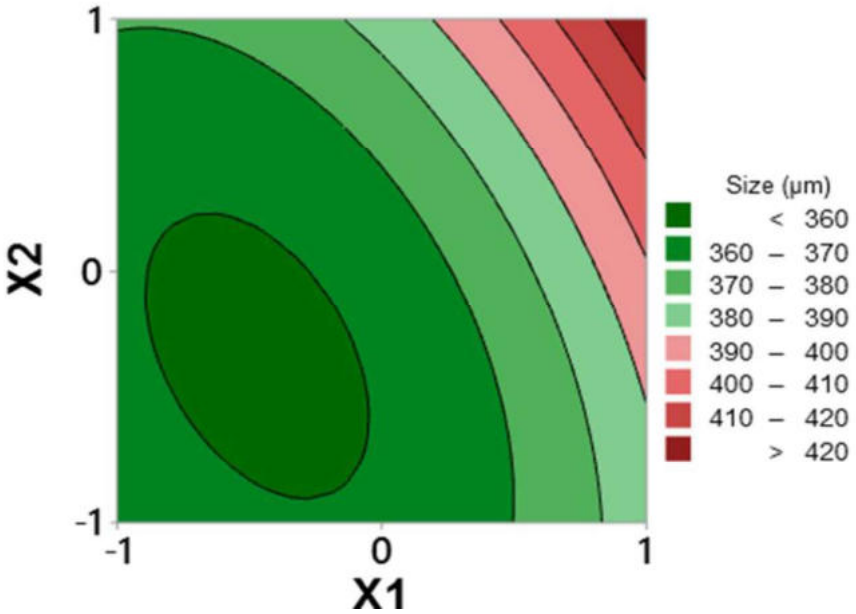

Figure 17. Response surface contours for size estimated from the interactions between X_1 (AO) and X_2 ($CaCl_2$) for the optimized PECs.

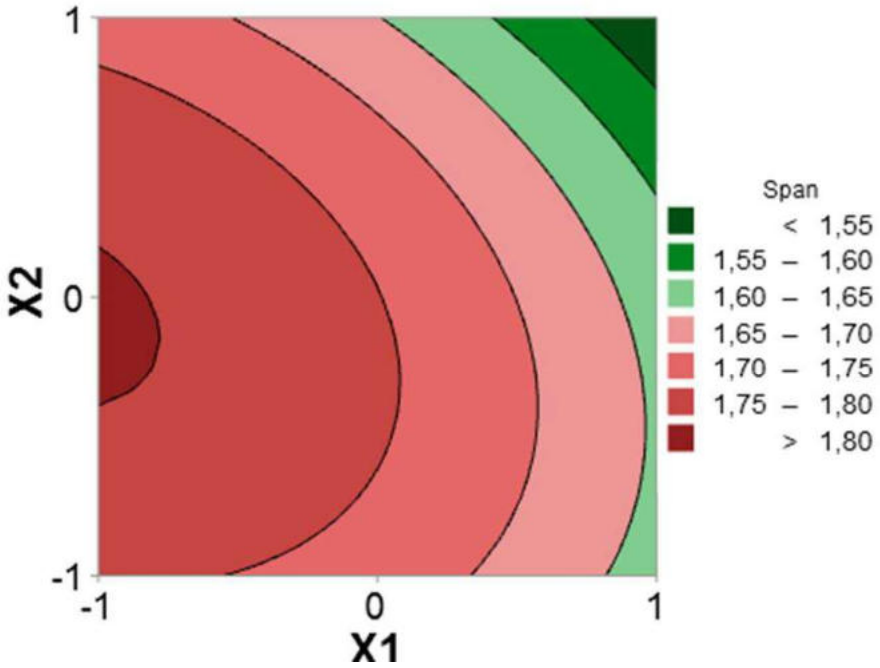

Figure 18. Response surface contours for span estimated from the interactions between X_1 (AO) and X_2 ($CaCl_2$) for the optimized PECs.

The desirability function was added to the response surface to optimize the response parameters. Limits were set for each parameter aiming to minimize size and span, and to maximize EE%. The maximum desirability of 0.74 can be visualized in Figure 19, which was reached by the combination of 0.5% AO and 0.5% $CaCl_2$.

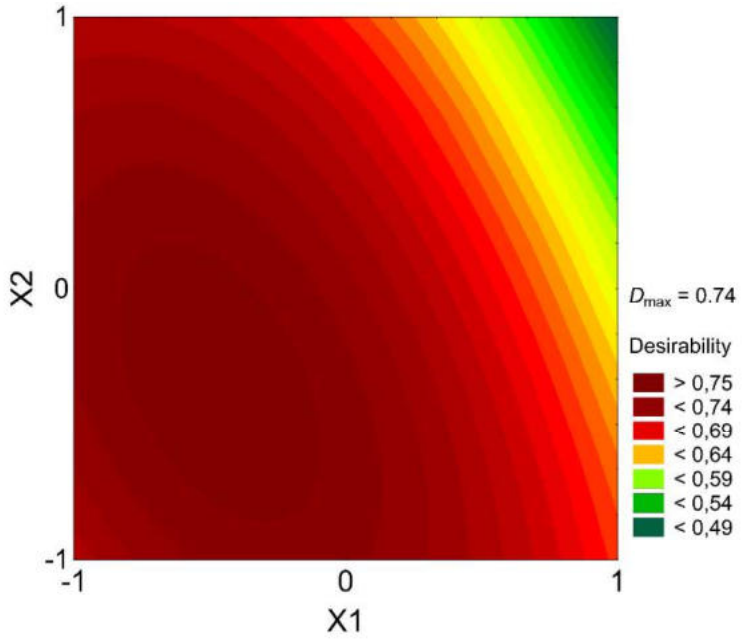

Figure 19. Desirability surface contour for the optimized PECs.

Thus, the CC system produced under the selected conditions (0.5% AO and 0.5% $CaCl_2$) was further characterized by FTIR, as well as for its rheological, thermal stability and antioxidant properties to be used as an optimized encapsulation system for a bioactive vegetable oil.

5.1.4. Ultrasound sonication of the CS:SA microencapsulated systems

The sonication technique by using an ultrasound was applied to investigate its effect on the reduction of particle size of the CS:SA açaí oil PECs (system CC). The experimental conditions, time (T) and amplitude (A) of ultrasound sonication ranged from 0-3 min and 0-30%, respectively. These parameters were applied on the CC particles before and after the addition of the crosslinking agent, $CaCl_2$. The overview of those parameters as well as their responses for the ultrasound sonication before crosslinking are presented in Table 17.

It was notable that size reduced from ~370 to 300 μm, while the span factor increased from around 1.8 to 2.2 with the application of ultrasound sonication. The smallest particle size and the highest span was achieved with the highest sonication conditions, 3 min (T) and 30% (A). The increase in the span factor is an indication that the sonication produced smaller particles resulting on a higher polydispersity, which can be related to a broader size distribution.

Table 17. Two-level-two-factors central composite design (cube plus star) from ultrasound sonication before the addition of crosslinking on PECs, and their respective responses.

Sample	Factors				Responses	
	Time (min)	Amplitude (%)	Coded factors		Before crosslinking	
			X_{US1}	X_{US2}	D[4,3] (μm)	Span
Control	0	0	0	0	373.36 ± 3.33	1.78 ± 0.01
CC1-20	1	20	-1	-1	343.90 ± 3.25	1.85 ± 0.01
CC2-20	2	20	0	-1	337.88 ± 0.57	1.88 ± 0.01
CC3-20	3	20	+1	-1	328.64 ± 0.98	1.95 ± 0.01
CC1-30	1	30	-1	+1	331.31 ± 2.69	1.95 ± 0.01
CC2-30	2	30	0	+1	328.03 ± 2.07	2.02 ± 0.00
CC3-30	3	30	+1	+1	303.43 ± 4.07	2.24 ± 0.02
CC1-25	1	25	-1	0	333.97 ± 3.75	1.93 ± 0.01
CC2-25*	2	25	0	0	333.27 ± 2.97	1.95 ± 0.01
CC3-25	3	25	+1	0	325.44 ± 2.35	2.00 ± 0.01

Results are expressed as mean ± standard deviation. *Central point with three replications.

The influence of ultrasound sonication before PECs crosslinking on the particle size ($D[4,3]$) and span were fitted by a second-order polynomial equation (Equation 16 and 17).

$$D[4,3] = 332.16 - 8.61T - 7.94A - 3.92\,T^2 - 0.67A^2 - 3.16(TA) \quad (16)$$

$$Span = 1.9391 + 0.0767T + 0.0883A + 0.0345T^2 + 0.0195A^2 + 0.0475(TA) \quad (17)$$

where, T and A are the factors, time (min) and amplitude (%), respectively, used for ultrasound sonication experiment.

In Table 18 are listed the significant factors of this experiment and its respective responses. The use of sonication prior crosslinking significantly affected size and span. The results for the linear regression coefficients show that the size and span of the particles were significantly affected by time and amplitude of sonication ($p<0.05$). While the quadratic coefficients had no significant effect on the responses.

Table 18. Results for regression coefficients and analysis of variance for dependent variables of the experimental design for ultrasound sonication before PECs crosslinking.

Coefficients	D[4,3] (μm)	Span
Mean		
β_0	332.16*	1.9391*
Linear		
β_1	-8.61*	0.0767*
β_2	-7.94*	0.0883*
Quadratic		
β_{11}	-3,92	0.0345
β_{22}	-0.67	0.0195
Interactions		
β_{12}	-3.16	0.0475*
R^2	0.8948	0.9309
$F_{calculated}$	11.91*	18.85

*Significant factors by ANOVA ($p \leq 0.05$). β1, β2 are the regression coefficients for the time (T, min) and amplitude (A, %) factors, respectively.

The models were used to calculate the response surface for each variable response. The estimated response surface contours are shown in Figures 20 and 21.

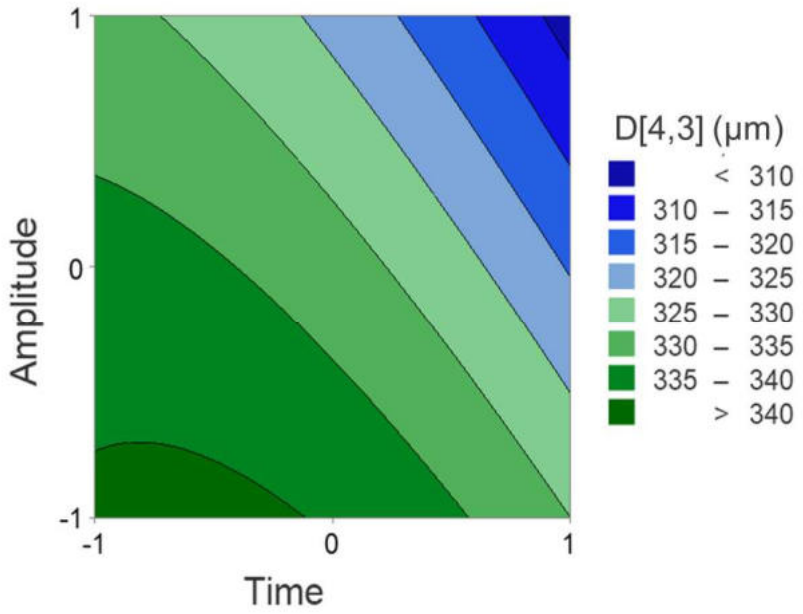

Figure 20. Response surface contours for estimated size [D4,3] (µm) from interactions between time and amplitude (coded factors) using ultrasound sonication prior crosslinking of the CC PECs (0.5% AO and 0.5% $CaCl_2$).

It can be noted that the smallest particle size can be found using the highest time and amplitude factors, 3 min and 30%, respectively (Figure 20). While the narrowest span can be produced using low down time and amplitude, 1 min and 20% (Figure 21).

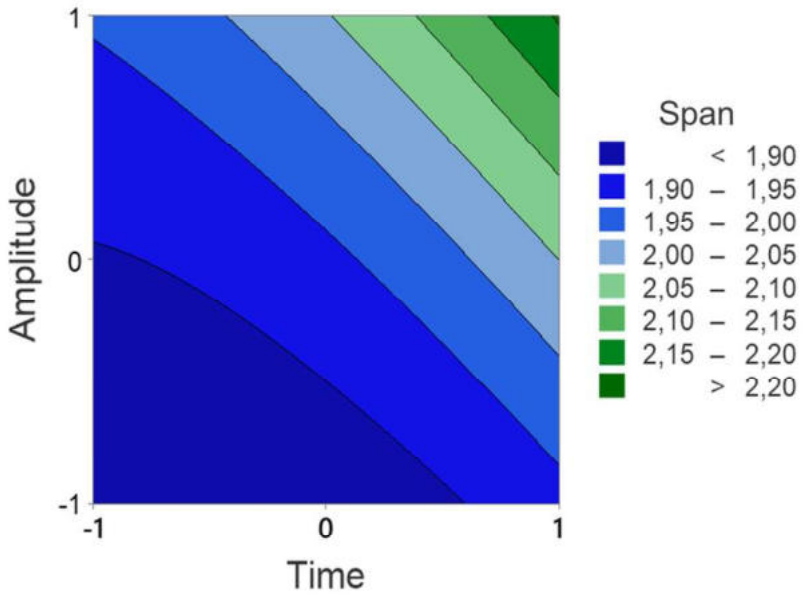

Figure 21. Response surface contours for span estimated from interactions between time and amplitude from ultrasound sonication before crosslinking of the CC PECs (0.5% AO and 0.5% $CaCl_2$).

The desirability function was added to the response surface to optimize these response parameters. The limits were set for each parameter aiming to minimize size and span. The maximum value of desirability was found close to 0.75, as can be visualized on Figure 22. Thus, the optimum conditions that will produce the smallest particle size and span were 3 min and 30% of time and amplitude factors, respectively. Moreover, this experiment also indicated that the CS:SA complex coacervation for açaí oil encapsulation is a stable system because even under stress condition produced by sonication the particles still had size above 300 μm.

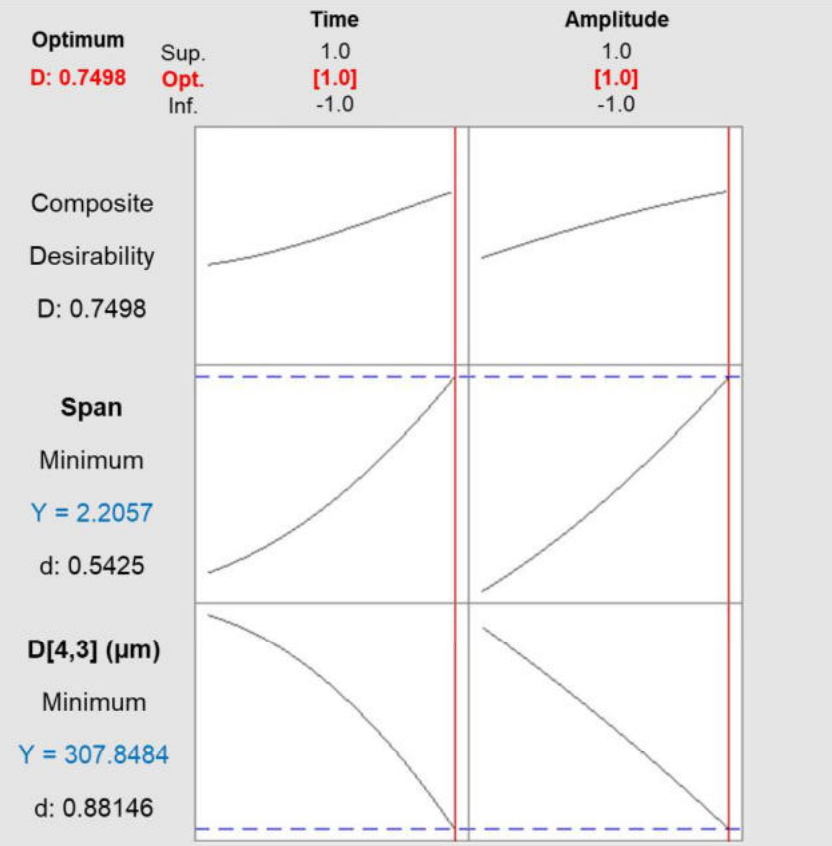

Figure 22. Desirability response graph of the optimized responses, size (D[4,3]) and span, from the ultrasound sonication before crosslinking of the CC PECs (0.5% AO and 0.5% $CaCl_2$).

Ren et al. (2019) studied the effect of an ultrasound treatment on the size and distribution of zein-chitosan complex coacervation for resveratrol encapsulation. These authors also found that the dual-frequency (28/40 kHz) ultrasound treatment significantly reduced particle size from around 1000 to 500 nm. In another work, the ultrasound sonication was used to reduce the size of whey protein/ alginate emulsion

gels from around 7 to 3 μm (LEON et al., 2018). The ultrasound power was found to be an important factor influencing the size reduction from around 1770 to 400 nm, and its distribution of curcumin-loaded zein microspheres (LIU et al., 2016). Furthermore, sonication prior crosslinking had significant effects on particles formation. For this reason, this technique was also used to investigate its effects on particles size after crosslinking.

An overview of the sonication parameters after PECs crosslinking as well as their responses are presented in Table 19.

Table 19. Experimental parameters from ultrasound sonication before and after the addition of crosslinking, and their respective responses.

Sample	Factors				Responses	
	Time (min)	Amplitude (%)	Coded factors		After crosslinking	
			X_{US1}	X_{US2}	D[4,3] (μm)	Span
Control	0	0	0	0	374.32 ± 0.68	1.77 ± 0.01
CC1-20	1	20	-1	-1	374.89 ± 3.04	1.82 ± 0.01
CC2-20	2	20	0	-1	322.43 ± 2.83	1.97 ± 0.02
CC3-20	3	20	+1	-1	364.86 ± 3.11	1.83 ± 0.01
CC1-30	1	30	-1	+1	358.14 ± 1.23	1.77 ± 0.01
CC2-30	2	30	0	+1	316.72 ± 1.28	2.07 ± 0.01
CC3-30	3	30	+1	+1	334.79 ± 2.23	2.07 ± 0.01
CC1-25	1	25	-1	0	362.87 ± 1.55	1.75 ± 0.01
CC2-25*	2	25	0	0	322.61 ± 1.57	1.89 ± 0.01
CC3-25	3	25	+1	0	355.43 ± 1.96	1.80 ± 0.00

Results are expressed as mean ± standard deviation. *Central point with three replications.

It was also noted that size reduced from ~374 to 316 μm, while the span factor increased from around 1.8 to 2.1 with the application of ultrasound sonication after particles crosslinking. The smallest particle size and the highest span was achieved

with the highest sonication conditions, 2 min (T) and 30% (A). This behavior was also observed for the sonication effects prior crosslinking. However, the sonication prior crosslinking produces a lowest particles size than using it after.

The influence on the particle size ($D[4,3]$) and span by using ultrasound sonication after PECs crosslinking was fitted by a second-order polynomial equation (Equation 18 and 19).

$$D[4,3] = 323.58 - 11.82T - 2.79A + 32.64\,T^2 - 4.09A^2 + 4.19(TA) \quad (18)$$

$$Span = 1.9016 + 0.0983T - 0.0092A - 0.0692T^2 + 0.0773A^2 + 0.0138(TA) \quad (19)$$

where, T and A are the factors, time (min) and amplitude (%), respectively, used for ultrasound sonication experiment.

In Table 20 are listed the significant factors of this experiment and its respective responses.

Table 20. Results for regression coefficients and analysis of variance (ANOVA) for dependent variables of the experimental design for ultrasound sonication after PECs crosslinking.

Coefficients	D[4,3] (μm)	Span
Mean		
β_0	323.58*	1.9016*
Linear		
β_1	-11.82*	0.0983*
β_2	-2.79	-0.0092
Quadratic		
β_{11}	32.64*	-0.0692
β_{22}	-4.09	0.0773
Interactions		
β_{12}	4.19	0.0138
R^2	0.9292	0.6921
$F_{calculated}$	18.38*	3.15

*Significant factors ($p \leq 0.05$). β1, β2 are the regression coefficients for the time (T, min) and amplitude (A, %) factors, respectively.

The use of sonication after crosslinking significantly affected size and span ($p<0.05$). The results for the linear regression coefficients show that the size and span of the particles were significantly affected only by time of sonication ($p<0.05$). While the quadratic coefficients of time (β_{11}) had significant effect on size, while no significant effect on span. The models were used to calculate the response surface for each variable response. The estimated response surface contours are shown in Figures 23 and 24.

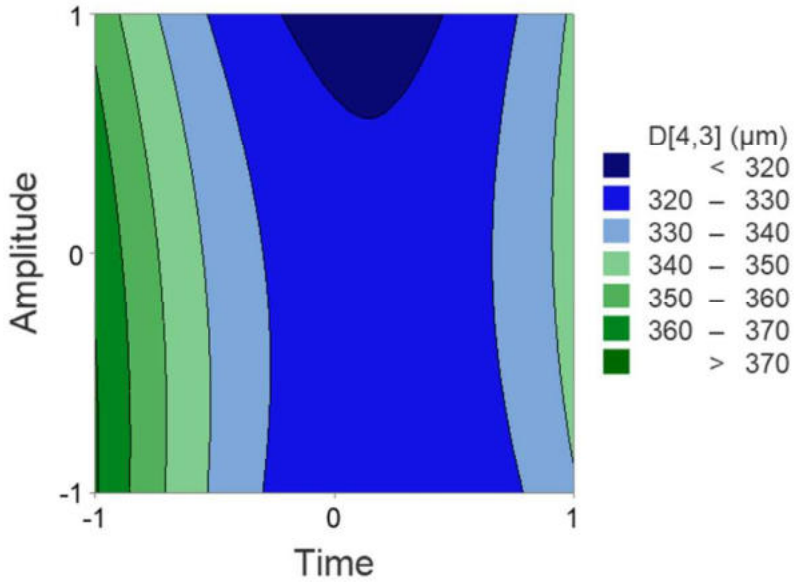

Figure 23. Response surface contours for size [D4,3] (µm) estimated from interactions between time and amplitude from ultrasound sonication after crosslinking of the CC PECs (0.5% AO and 0.5% $CaCl_2$).

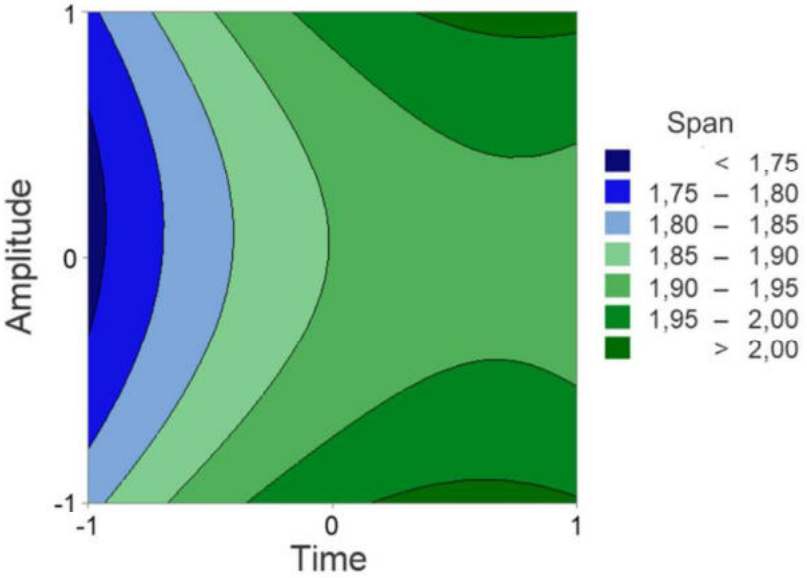

Figure 24. Response surface contours for span estimated from interactions between time and amplitude from ultrasound sonication after crosslinking of the CC PECs (0.5% AO and 0.5% $CaCl_2$).

It can be noted that the smallest particle size can be found using the central point of time and highest amplitude factors, 2 min and 30%, respectively (Figure 23). While the narrowest span can be produced using lowest time and central point of amplitude, 1 min and 25% (Figure 24).

The desirability function was added to the response surface to optimize these response parameters. The limits were set for each parameter aiming to minimize size and span. The maximum value of desirability was found close to 0.96, as can be visualized on Figure 25. Thus, the optimum conditions that will produce the smallest particle size and span were 2 min and 30% of time and amplitude factors, respectively.

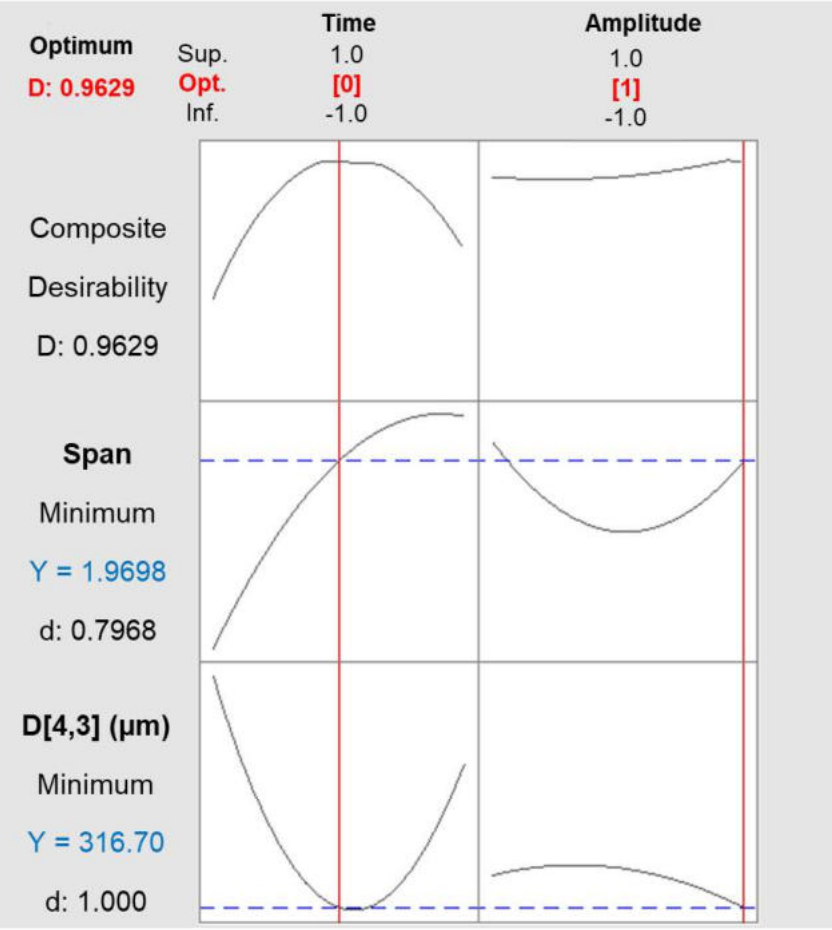

Figure 25. Desirability response graph of the optimized responses, size (D[4,3]) and span, from the ultrasound sonication after crosslinking of the CC PECs (0.5% AO and 0.5% $CaCl_2$).

The use of sonication had significant effects on particles size. As the use of this technique before PECs crosslinking produced the smallest particle size, around 300 μm, the açaí CS:SA PECs were prepared using it prior incorporation of the CS-based films.

5.1.5. Morphological observations of CS:SA PECs

The morphological aspects of the PECs were observed by optical microscopy (OM) and scanning electron microscopy (SEM). The main results of those observations are following presented.

5.1.5.1. Optical microscopy

The morphology of the CS/SA PECs was investigated by optical microscopy and is shown in Figure 26. In this technique, the CC sample (0.5% AO and 0.5% $CaCl_2$) were observed without the use of dyes.

In Figure 26a is presented the morphology of unloaded control CS/SA PECs at 40x magnification. It can be noted that these particles exhibited a less well-defined and more irregular shape than the CC PECs as presented in Figure 26b, which were cross-linked with 0.5% of $CaCl_2$ and 0.5% of açaí oil as core material. It is most likely that the irregular shape of the control PECs is due to the absence of the cross-linking agent. Besides, as these particles are unloaded (without açaí oil), a core is not presented, which makes its optical visualization worse. In a different way, the CC PECs displayed a well-defined rounded shape as presented in Figure 26b. It was possible to note countless spherical particles exhibiting a single core and different sizes.

In other work, Santos, Carvalho, Garcia-Rojas (2021) observed that carboxymethyl tara gum-lactoferrin complex coacervates encapsulated with vitamin D_3 (cholecalciferol) exhibited a comparable spherical well-defined shape. Similarly to their work, it was noted the presence of an innumerable small particles, which appears either as a shadow or as a small dot at 10x magnification objective in Figure 26b.

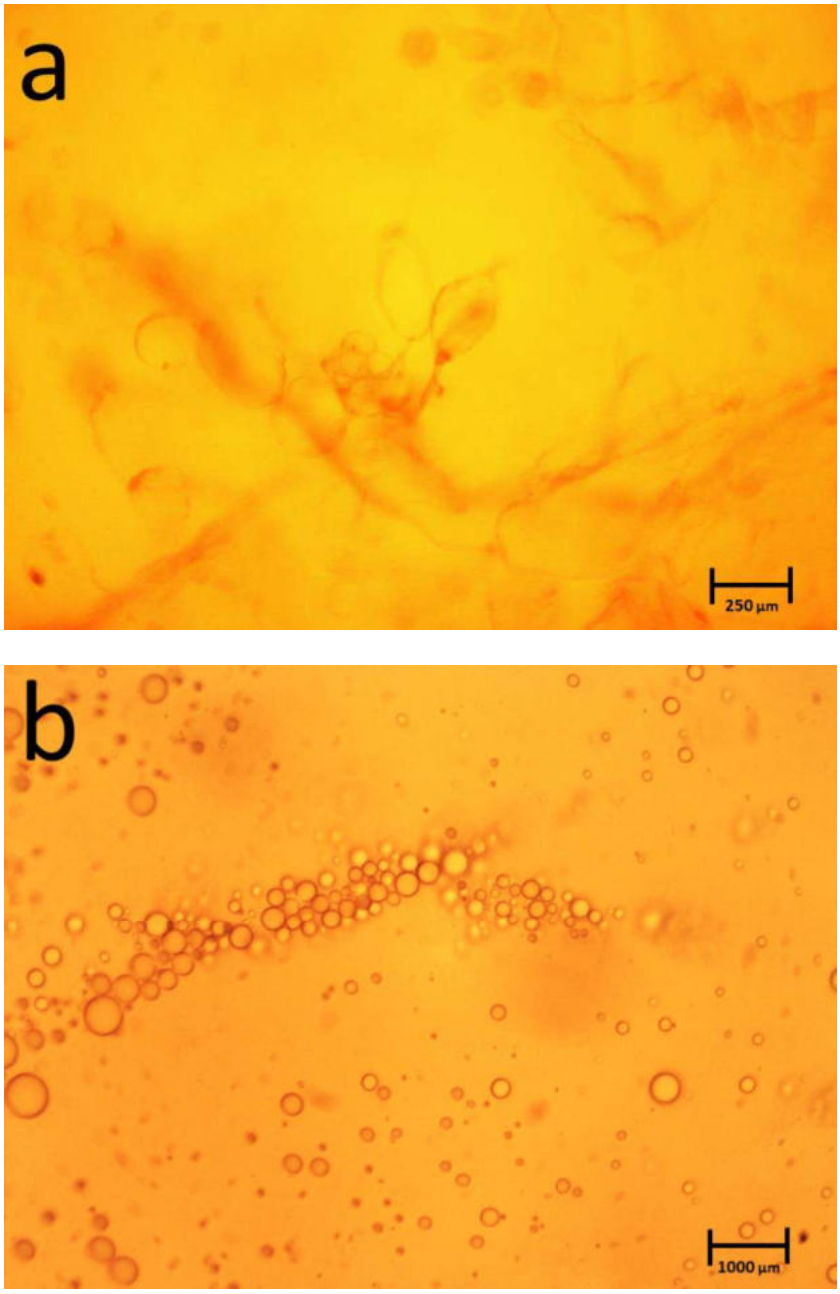

Figure 26. Microphotographs of the unloaded control (a) and CC (0.5% AO and 0.5% $CaCl_2$) (b) PECs observed by optical microscopy at 40x and 10x magnifications, respectively.

5.1.5.2. SEM observation

The structural morphology of the CS:SA PECs with and without açaí oil incorporated was observed by using SEM. In Figures 27 and 28 are presented the SEM observations of unloaded control and the optimized CC PECs. It was observed that the unloaded PECs possibly lost their spherical shape and may coalesced during freeze-drying (Figure 27).

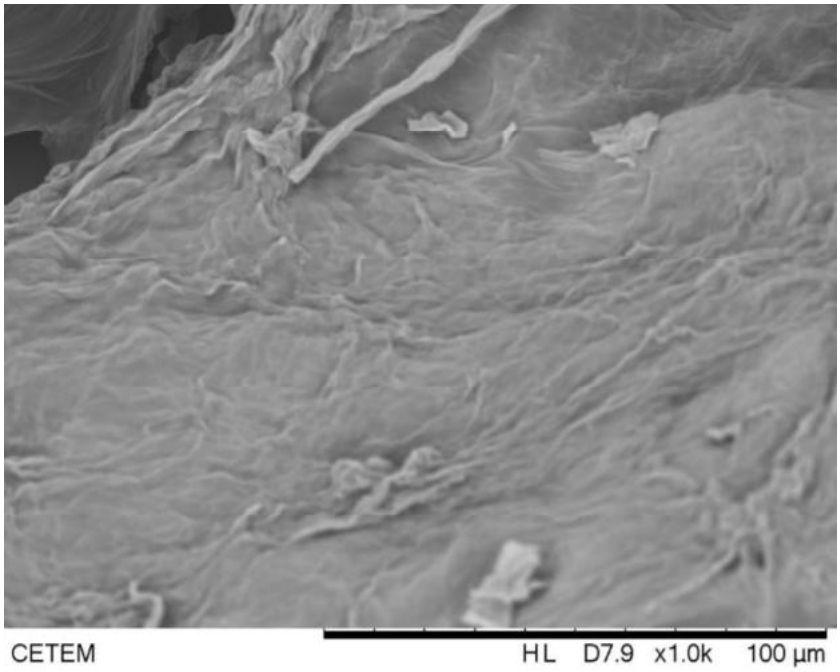

Figure 27. SEM observations of the control (unloaded) CSSA PECs at 1000x magnification.

It is known that ice crystallization during freezing can induce mechanical stress, which could lead to particles destabilization and disruption (RAMPINO et al., 2013). As the control PECs were prepared without $CaCl_2$ as cross-linker, they were less stable than the other particles. Calcium ions had displayed an important effect on binding properties of chitosan-alginate beads, by higher diffusion and more binding CS molecules in SA gel network (GÅSERØD, SMIDSRØD, SKJÅK-BRÆK, 1998). Thus, resulting in a more stable particle because of higher interaction between the polymers. Additionally, this corroborates with the optical microscopy observations for the control sample, in which a less well-defined spherical shape were noted when compared to the other PECs. Differently, the CC PECs displayed a spherical morphology, which were united by a compact coating structure (Figure 28).

It is possible that the PECs aggregated during the freeze-drying due to inter-particle hydrophobic attractions. This behavior was also observed by Khan et al. (2019) in alginate/chitosan-coated with zein for encapsulation of resveratrol. Natrajan et al. (2015) also observed a similar spherical shape of nanocapsules based on CS and SA for turmeric and lemongrass oil. Furthermore, the aggregation of these PECs could

also be linked to the final pH of particles preparation, since Li et al. (2018a) observed that zein-CS nanoparticles were more able to group around pH 7 than pH 4.

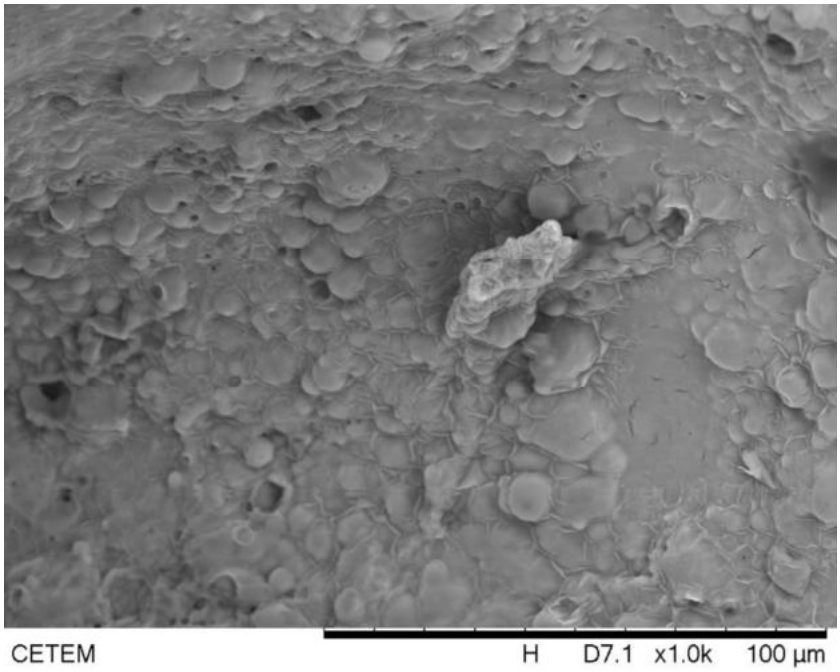

Figure 28. SEM observations of the CC sample (0.5% AO and 0.5% $CaCl_2$) at 1000x magnification.

5.1.6. Infrared spectroscopy of raw materials and açaí PECs

Fournier transform infrared spectroscopy was used to evaluate the molecular structure of AO, CS, SA and their molecular interactions in the PECs. The FTIR spectra for these materials are presented in Figure 29.

Characteristic bands of triglyceride functional groups dominate the FTIR spectrum for AO, as these substances are the major components in oils (ROHMAN, MAN, 2010). Bands around 2921 – 2853 cm^{-1} and at 1744 cm^{-1} can be associated to asymmetrical and symmetrical C–H stretching, and to C=O stretching vibrations of ester carbonyl functional groups, respectively (ROHMAN, MAN, 2010). Bending vibrations of the CH_2 and CH_3 aliphatic groups (scissoring) were observed at 1463 cm^{-1}, C–O stretching and C–H bending vibrations were observed at 1160 cm^{-1} and C–H bending (rocking) vibrations were observed at 722 cm^{-1} (ROHMAN, MAN, 2010).

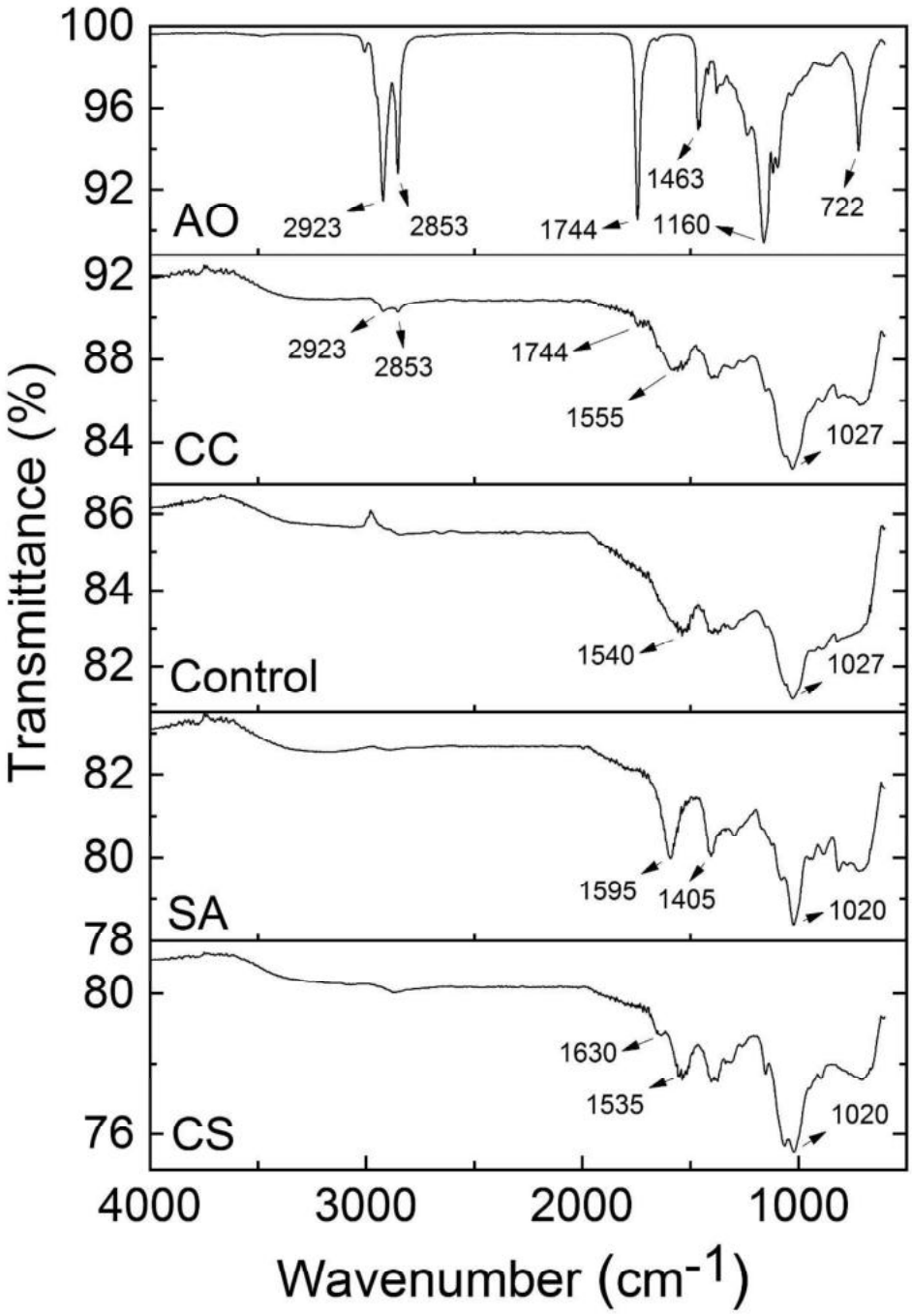

Figure 29. FTIR spectra for CS, SA, AO, control and CC (.5% AO and 0.5% $CaCl_2$) sample.

The spectrum for CS presented bands associated to C=O stretching (amide I) at 1630 cm^{-1}, N−H bending (amide II) at 1535 cm^{-1} and C−O stretching at 1020 cm^{-1} (DEKA et al., 2016; PEREIRA, ANDRADE, 2017). The SA spectrum had characteristic absorption bands at 1595 cm^{-1} and 1405 cm^{-1}, reported as CO_2^- asymmetric and symmetric stretching vibrations, respectively (LAWRIE et al., 2007). Bands at 1020 cm^{-}

^{1} were related to C−O−C antisymmetric stretching and at 815 cm^{-1} associated to C−O stretching vibration of uronic acid residues (DEKA et al., 2016; LAWRIE et al., 2007).

To investigate the PEC formation, the molecular structure of the empty control and the CC PEC were also analyzed using FTIR. For the control, the broad band in the 3500 – 3000 cm^{-1} region, with maximum at 3034 cm^{-1}, was attributed to O–H and N–H stretching in hydrogen-bonded molecules (PEREIRA, ANDRADE, 2017). Absorption bands at 1545 cm^{-1} and 1390 cm^{-1} were associated to C–N stretching and C–N–H bending vibrations (amide II), and carbonyl vibrations of carboxylate groups respectively (DEKA et al., 2016; LAWRIE et al., 2007). For the CC PEC, the C–N stretching vibration was shifted from 1535 cm^{-1} in CS alone to 1555 cm^{-1}. To control PECs, the change from 1535 cm^{-1} in CS alone to 1540 cm^{-1} was also observed. This shift may be an indication of PEC formation between CS and SA (LAWRIE et al., 2007; WANG, KHOR, LIM, 2001). The presence of minor intensity bands of triglyceride functional groups around 2921 − 2853 cm^{-1} and 1744 cm^{-1} in the CC PEC spectrum can be correlated to an effective AO encapsulation by this system.

5.1.7. Rheological properties

The rheological properties for CS and SA stock solutions at 1.0% concentration are shown in Figure 30. The frequency-dependent behavior within the linear viscoelastic range and the Cox-Merz rule were investigated. For these solutions, the dynamic modulus values increased with the increase in frequency. As shown in Figure 30a, the loss modulus values (G") were higher than the storage moduli (G') and no “crossover” (G' = G") was detected within the frequency range studied. Therefore, these stock solutions at 1.0% concentration exhibited a liquid-like behavior. Similar behavior was reported for chitosan solutions at different concentrations (BASTOS et al., 2010), although the authors also noted a shift in frequency for “crossover” points to higher frequency values as the chitosan concentration was decreased from 3.0 to 0.5%.

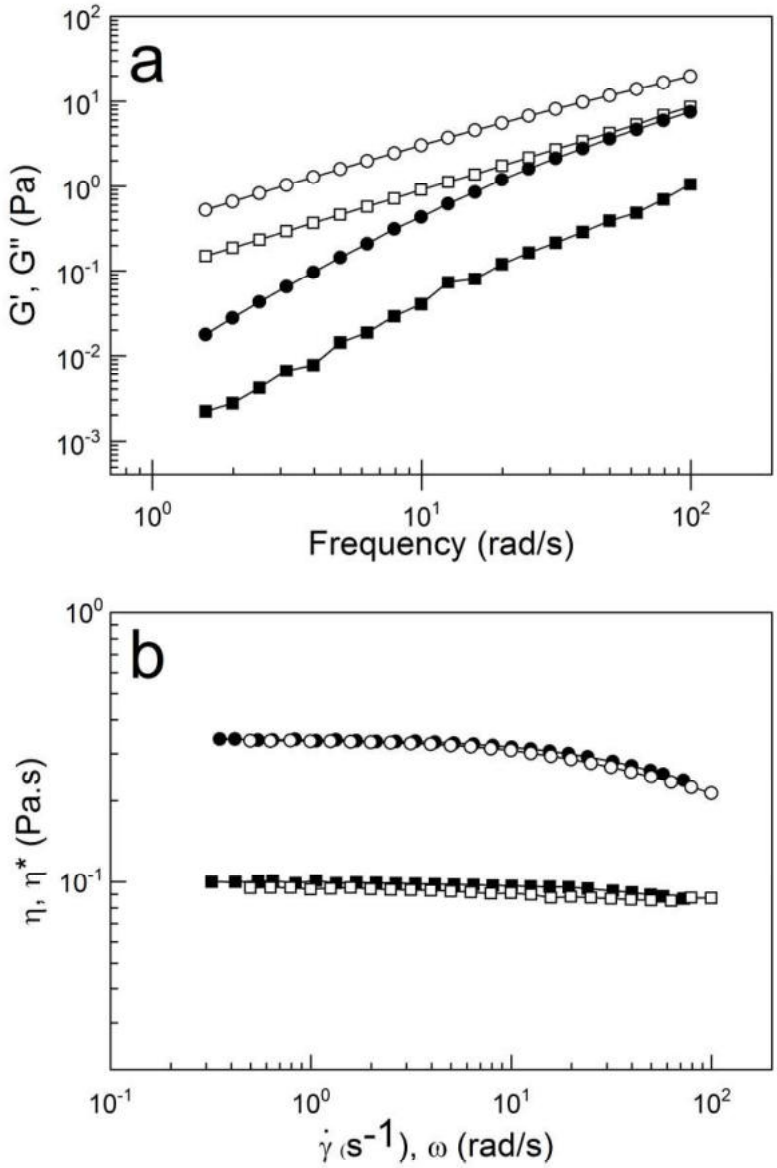

Figure 30. Storage modulus (G', full symbols) and loss modulus (G'', open symbols) as a function of oscillatory frequency (ω) (a), and Cox-Merz plot for CS (squares) and SA (circles) stock solutions at 25ºC (b). Viscosity (η, full symbols) as a function of shear rate ($\dot{\gamma}$), complex viscosity (η*, open symbols) as a function of angular frequency (ω).

Figure 30b shows Cox-Merz plots, in which the variation of the complex viscosity as a function of angular frequency and the shear rate dependence of the apparent viscosity were grafted together. A shear-thinning, pseudoplastic behavior was observed for the SA sample, whereas the CS sample presented a Newtonian response. This result characterizes polymer solutions and dispersions. Complex and apparent viscosities found for the SA sample were higher than those observed for the CS sample. Moreover, the viscosity values observed for the CS solution were slightly

higher than those obtained for complex viscosity, probably because of the better dispersion and hydrogen bonding formation, favored by the steady shear process.

The control and CC PEC dispersions were also investigated for their rheological behavior (Figure 31).

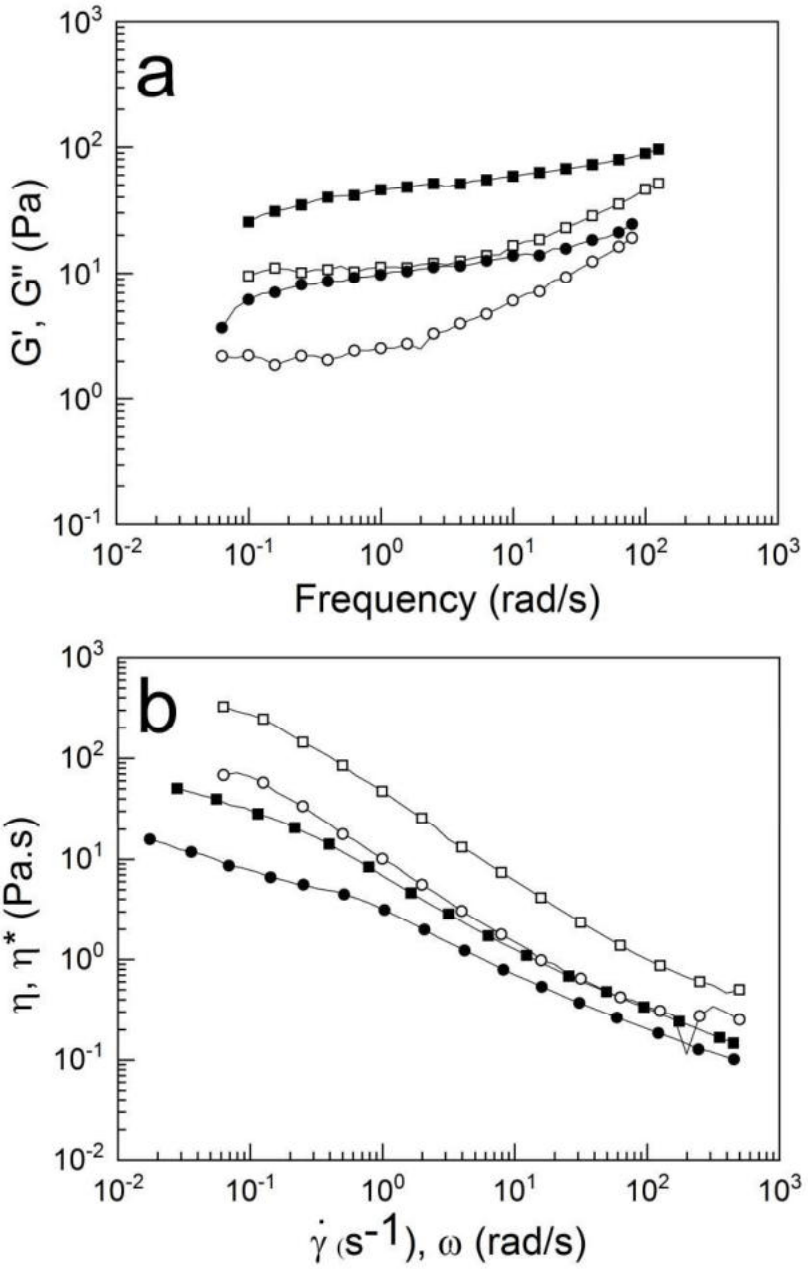

Figure 31. Storage modulus (G', full symbols) and loss modulus (G", open symbols) as a function of oscillatory frequency (ω) (a), and Cox-Merz plot for the control (squares) and CC PECs (circles). Viscosity (η, full symbols) as a function of shear rate ($\dot{\gamma}$), complex viscosity (η*, open symbols) as a function of angular frequency (ω).

Both samples presented increasing dynamic moduli (G', G'') as the frequency was augmented. These PEC dispersions displayed gel-like structures, with G' > G"

(Fig. 5a). A similar G' > G" behavior for CS/SA PECs was also observed by other authors (PHOEUNG et al., 2017). The η and η* values for the control PECs were higher than those observed for the CC PECs, most probably because they are constituted only by interacting CS and SA biopolymers. Despite this, both PECs displayed similar pseudoplastic behavior (Figure 31b), where the η and η* values decreased with the increase in shear rate ($\dot{\gamma}$) and angular frequency (ω), respectively. As can be observed in Figure 28b, both gels did not follow the Cox-Merz rule; η values were lower than η* values, which reveals the disrupting nature of the steady shear.

5.1.8. Thermogravimetric analysis (TGA)

The thermal stability for AO, the control and CC PEC was investigated by TGA. TG and DTG curves are shown in Figure 32. AO presented an initial decomposition temperature (T_{onset}) around 402°C and a maximum peak (T_{peak}) at 440°C (Figure 32a). AO seems to be more thermally stable than palm oil, for which T_{onset} was found between 219ºC and 268°C (LI et al., 2018b). This result may be related to their corresponding fatty acid compositions, which contributes to their oxidative stability (LI et al., 2018b).

The control and CC PECs presented a similar T_{onset}, at 205.6 and 205.8°C, respectively. However, some differences could be observed between their thermal behaviors in the DTG curves (Figure 32b). The control PEC presented three stages of thermal decomposition. The first ranged between 28 – 155ºC and may be associated to the loss of absorbed humidity and decomposition of $-COO^-$ groups in SA (YOU, LIU, ZHAO, 2018). The second and third stages ranged from 155 – 247°C and 247 – 406°C, respectively, attributed to decomposition of CS and SA macromolecules in the PECs.

For the CC PEC, four decomposition stages were observed. The first stage, between 30 and 170°C, associated to water loss. The second stage occurred in the 170 – 255°C range and may be attributed to the degradation of the polymeric chains in alginate as reported by Sarmento et al. (2006), in which the alginate presented an exothermic peak at 250°C. The third mass loss occurred in the 255 – 395 °C range, associated to oxidation and depolymerization reactions of protonated carboxylic groups of chitosan as described by Sarmento et al. (2006). And the last stage occurred

beyond 400°C, reaching a T_{peak} at 450°C. Sarmento et al. (2006) found a peak at 309.6 C for the physical mixture of chitosan/alginate.

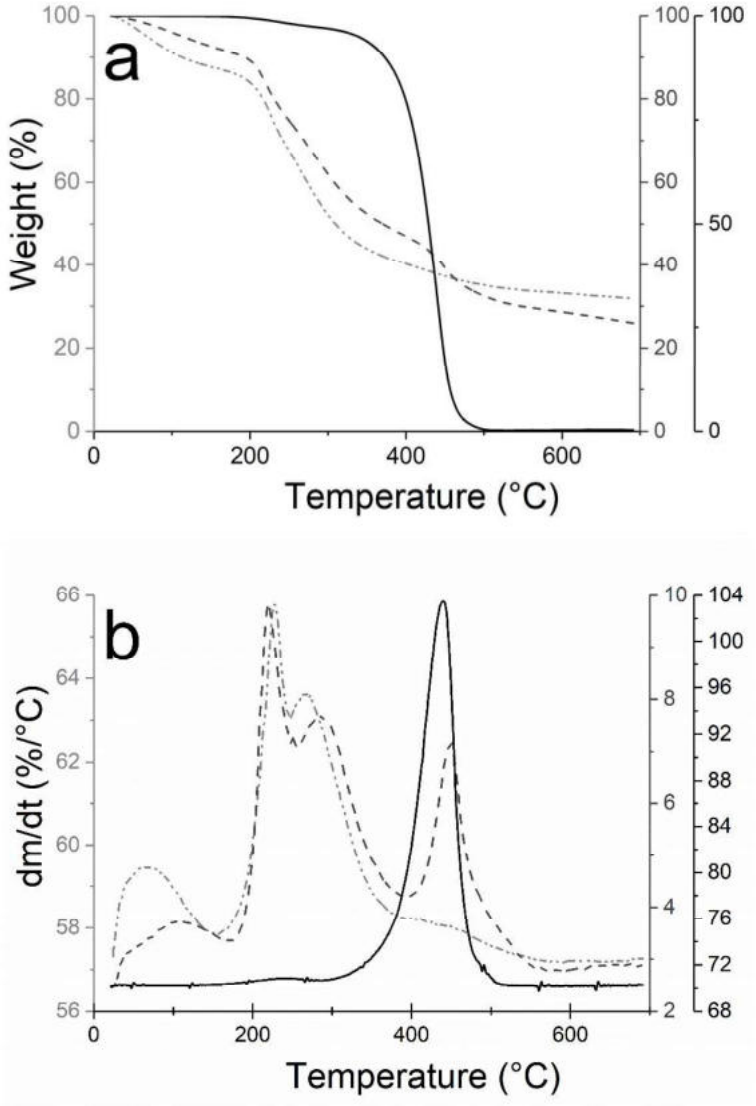

Figure 32. TG (a) and DTG (b) curves for AO (black line), control (dark gray dashed line) and CC (light gray dashed dotted line) PECs.

Overall, these results are in accordance with the literature (OLIVEIRA, PAULA, PAULA, 2014; YOU, LIU, ZHAO, 2018). The fourth decomposition stage was observed beginning at 395ºC up to 560°C and may be correlated to the presence of AO encapsulated in CS/SA PEC. This finding corroborates the FTIR and encapsulation efficiency results and confirms the AO encapsulation in the CC PEC. Moreover, the thermal events registered by TGA and DTG curves of the other CS:SA PECs are listed in Table 21.

Table 21. Thermal events by TGA and DTG curves of the CS:SA 8:2 PECs.

Sample	Stages of thermal degradation	TGA		DTG	
		T_{onset} (°C)	% Residues at 700°C	ΔT (°C)	T_{peak} (°C)
AA	1	216	24.6	25 – 150	483.6
	2			150 – 260	
	3			265 – 360	
	4			360 – 400	
	5			400 – 550	
BA	1	203	14.2	25 – 150	343.2
	2			150 – 250	
	3			250 – 350	
	4			350 – 525	
AB	1	205	22.3	25 – 150	431.5
	2			150 – 275	
	3			275 – 370	
	4			370 – 420	
	5			420 – 580	
BB	1	207	15.6	25 – 180	441.7
	2			180 – 280	
	3			280 – 405	
	4			405 – 525	
CC	1	206	25.9	25 – 170	450.2
	2			170 – 255	
	3			255 – 395	
	4			400 – 550	

ΔT = temperature range; T_{onset} = initial degradation temperature; T_{peak} = peak temperature. *Two replications. AA: 0.25% AO and 0% of $CaCl_2$; BA: 0.75% AO and 0% of $CaCl_2$; AB: 0.25% AO and 1.0% of $CaCl_2$; BB: 0.75% AO and 1.0% of $CaCl_2$; CC: 0.50% AO and 0.50% of $CaCl_2$;

5.1.9. *In vitro* antioxidant activity of the açaí PECs

The antioxidant activity of the selected PEC system (CC) was studied to verify its bioactive behavior. With the aim of better understanding the bioactive behavior of the CC CS/SA/AO system, the empty control PEC was also evaluated as for its antioxidant behavior, as well as AO alone, by the DPPH scavenging assay. The DPPH method is one of the most commonly used to determine radical-scavenging activity in plants, medicinal herbs and several natural compounds, such as phenolics and anthocyanins (LIU, 2010). Recently, this method was successfully applied to determine

the antioxidant activity of PECs/films based on chitosan, alginate and other biopolymers (LIANG et al., 2017; ELGUEA-CULEBRAS et al., 2019). The initial DPPH concentration (mg mL^{-1}) was equivalent to $[(Abs - 0.0059)/100.95]$, where Abs is the absorbance of the methanolic DPPH solutions (R^2 = 0.9927 and $p < 0.05$).

The results of % DPPH radical inhibition for AO, CC (0.50% AO and 0.50% of $CaCl_2$) and the control PECs are shown in Figure 33. As expected, the control PEC displayed the lowest antioxidant activity against DPPH, presenting a value close to 37%. This result could be related to the reaction of amino groups ($-NH_2$) with hydrogen ion to form ammonium groups ($-NH_3^+$) in CS, as reported by other authors (VILELA et al., 2017; RUIZ-NAVAJAS et al., 2013). AO exhibited high antioxidant activity, presenting more than 70.5 ± 0.1% of DPPH inhibition.

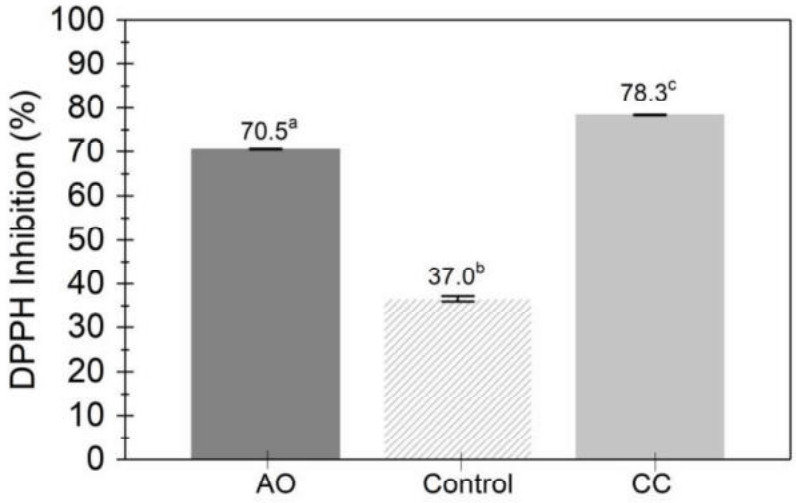

Figure 33. DPPH radical inhibition for AO, the control and CC PEC (0.50% AO and 0.50% of $CaCl_2$).

Other authors also cited a significant antioxidant activity for AO (EC50 = 2057.27 g g^{-1} DPPH), even higher than that for extra virgin olive oil (EC50 = 646.30 g g^{-1} DPPH) (RUFINO et al., 2011). However, the CC sample presented the greatest antioxidant activity, ~ 78% of DPPH inhibition. As the antioxidant activity was higher than that of AO alone, it is reasonable to suggest that the CS/SA optimized PEC may have contributed to the enhancement of antioxidant activity found for the CC sample. The encapsulation process also contributed to protection of the AO unsaturated fatty acids against oxidation, leading to the formation of an oxygen barrier and increasing its stability.

Later, the antioxidant capacity of açaí oil (AO) was determined using other techniques. The results from these experiments are presented on Figure 34. AO exhibited a remarkable antioxidant activity, presenting the highest value by DPPH radical scavenging and by the determination of total polyphenols content (TPC). This notable antioxidant activity can be related to the high amount of phenolic substances, such as procyanidin trimers and dimers, syringic, valinnic and p-hydroxybenzoic acids, present in the assai pulp oil (PACHECO-PALENCIA, MERTENS-TALCOTT, TALCOTT, 2008). These authors suggested that some phenolic substances could be deposited as free or bound compounds onto the nonpolar lipid phase, thus giving a high antioxidant activity to this oil.

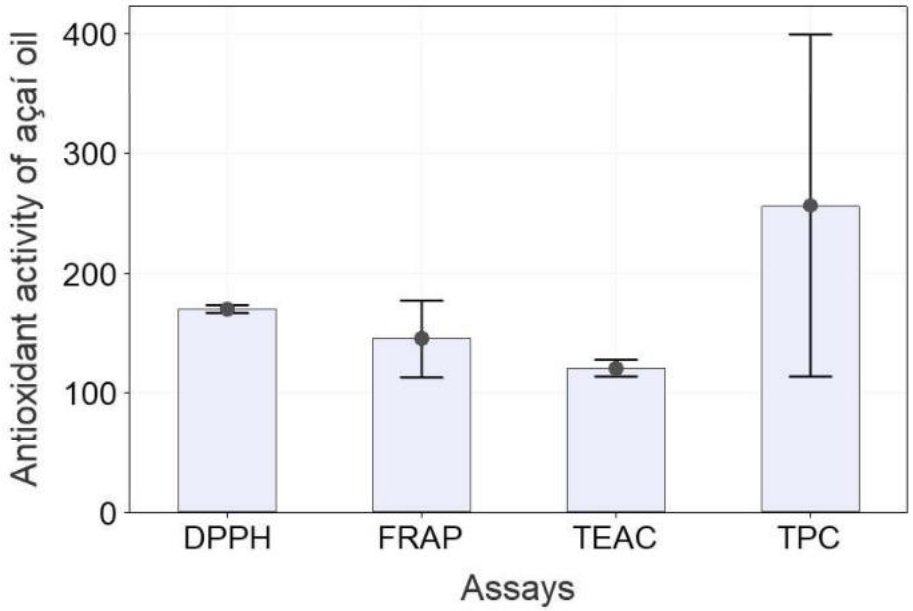

Figure 34. Antioxidant activity of açaí oil by DPPH radical scavenging, FRAP, TEAC and TPC assays. The results as mean (column) ± standard deviation (bar) (n=3) for DPPH, FRAP and TEAC assays are expressed as mg TE L^{-1} of oil, and for TPC as mg GAE L^{-1} of oil.

5.2. Microencapsulation systems based on CS:PPI

Systems using chitosan (CS) and pea protein isolate (PPI) were developed and studied aiming the encapsulation of extra-virgin olive oil (EvO). Different techniques were used in the formulation as well as to the characterization of the microparticles. To study the ideal ratio of CS and PPI in the microparticles, different ratios between these biopolymers were investigated. For this, a central composite design was used to optimize the formulation CS:PPI microparticles with EvO encapsulated.

Statistical tools, such as the response surface methodology and the desirability function, were used to evaluate significant factors affecting the microparticles size and aiming to find an optimum condition to it. The raw materials, EvO, CS and PPI, as well as the formulated complexes coacervates were observed using microscopy techniques to examine its morphological aspects. The complex coacervates were characterized by physicochemical methodologies, such as laser diffraction, Fourier transform infrared spectroscopy, thermogravimetric analysis, and as for the antioxidant properties by spectrophotometric analysis. The results from all these determinations are presented below.

5.2.1. Determination of the zeta-potential of stock solutions

The concentration of biopolymers and their ratio influences the coacervates formation. For this reason, the ζ-potential of CS and PPI stock solutions was investigated as a function of concentration and pH. In this microencapsulation system the concentration of PPI was kept constant at 1.0% (w/v), and the concentration of CS solution changed from 0.05 to 1%. The ζ-potential of the CS solutions as a function of concentration is presented in Table 22.

It was observed that the ζ-potential of the CS solutions significantly decreased from around +64 to +14 mV with the increase in CS concentration from 0.05 to 1% ($p<0.05$). It is known that under acidic environment amino groups of CS are protonated, which leads to electrostatic repulsion between its chains, while interchain hydrogen bonding may occur (FAN et al., 2012). With the increase of CS concentration, the proximity of CS molecules is higher, as well as those electrostatic interactions, which could lead to this shift in ζ-potential values.

Table 22. ζ-potential of CS solutions as a function of concentration

Concentration of biopolymer (%)	ζ-potential (mV)
	CS
0.05	+64.6 ± 1.4[a]
0.5	+50.5 ± 3.7[b]
0.8	+27.8 ± 2.4[c]
1.0	+14.0 ± 1.7[d]

Results are expressed as mean ± standard deviation. Means followed by different superscript lower-case letters in the same column differ statistically by Tukey's post-hoc test ($p<0.05$).

In another work, Solomevich et al. (2021) determined a ζ-potential value around +50 mV for CS solution attributed to its protonated amine groups, which was used to prepare a dextran phosphate-chitosan hydrogel. Carneiro-da-Cunha et al. (2011) found that the ζ-potential was significantly affected by CS concentration. These authors observed that the ζ-potential values increased with the increase of CS concentration, from 0.2 to 0.6% under different salt contents, 0.0 to 0.1% of NaCl.

In Figure 35 the ζ-potential of the 1% PPI aqueous solution as a function of pH is presented.

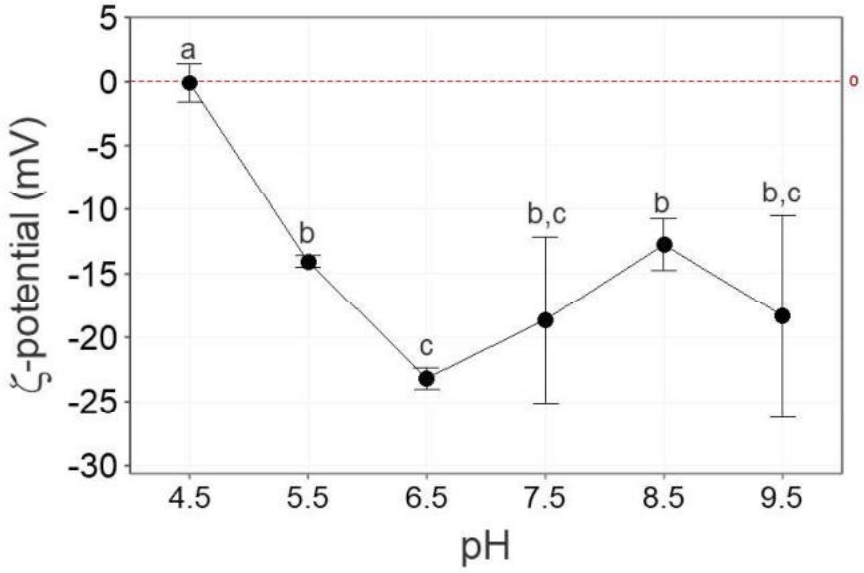

Figure 35. ζ-potential for 1% PPI solution as a function of pH values. Different lowercase (a,b,c) letters within pH range indicates a significant difference among samples by Tukey's test ($p<0.05$).

The ζ-potential of the PPI solution differed significantly as a function of pH. The ζ-potential value ranged from around −0.15 mV at pH 4.5 to −18.5 mV at pH 9.5. The ζ-potential around pH 4.5 reached values close to a neutral charge, suggesting that the isoelectric point (pI) of PPI is in this region. This result is in accordance with the findings of Ladjal-Ettoumi et al. (2016); Wei et al. (2020). These authors determined that the PPI has a pI around pH 4.5. These authors determined that the PPI has a pI around pH 4.5. Moreover, above neutral pH occurs an increase in the negative charge because the unfolding of protein, which provides superior repulsive forces and may result in higher solubility, while in lower pH occurs an increase in positive charges (AMINE et al., 2014; LADJAL-ETTOUMI et al., 2016). When studying the complex coacervation between PPI and CS, Elmer et al. (2011) observed that the ζ-potential of the PPI stock solution (16.5 g mL^{-1}) shifted from a positive value, around 40 mV, at pH 3.5 to negative value, around -10 mV, at pH around 9.

Figure 36 presents a picture of the visual aspects of the 1% PPI solution under different pH values. It is possible to note a higher protein volume at higher pH values, mainly at pH 10, which could be associated to a higher protein unfolding, leading to higher chain volume (AMINE et al., 2014; LADJAL-ETTOUMI et al., 2016).

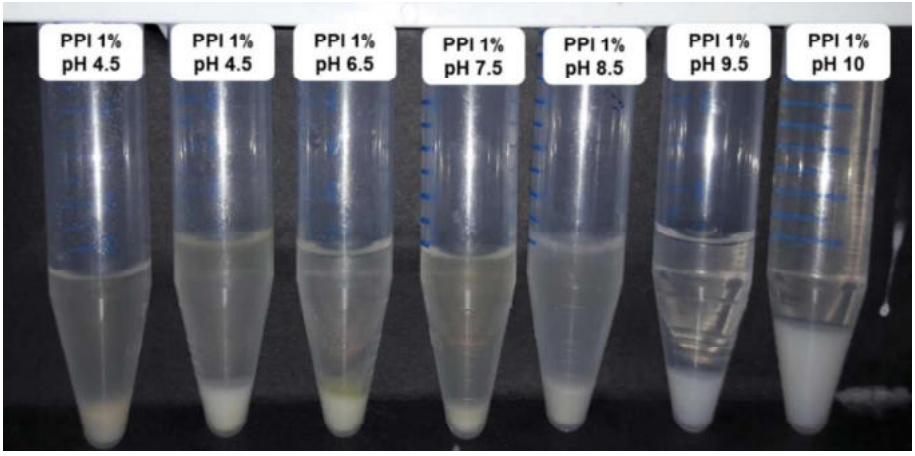

Figure 36. Visual aspects of the 1% PPI solution under different pH values.

5.2.2. Optimization of the CS:PPI microencapsulated systems

As part of the development of microencapsulated systems based on CS:PPI, a high-pressure and a high-speed homogenization were accomplished. The first step of homogenization was performed using the high-pressure Jet Homogenizer from the University of Leeds. In Figure 37 some pictures of the Jet Homogenizer are presented.

The equipment is composed by a chamber (Figure 37A), where the solution cylinder (Figure 37B) is placed with their respective pistons, which are pushed down by a hydraulic ram using compressed air. Figure 37C shows the solution cylinder with the pistons in position prior compression and in the Figure 37D is displayed the mixed solutions collected on an Erlenmeyer glass after high-pressure compressing homogenization. This approach was used for all CS:PPI-EvO systems prior to the high-speed homogenization performed by using the Ultra Turrax T25 homogenizer, following the specific optimization conditions, which are presented below.

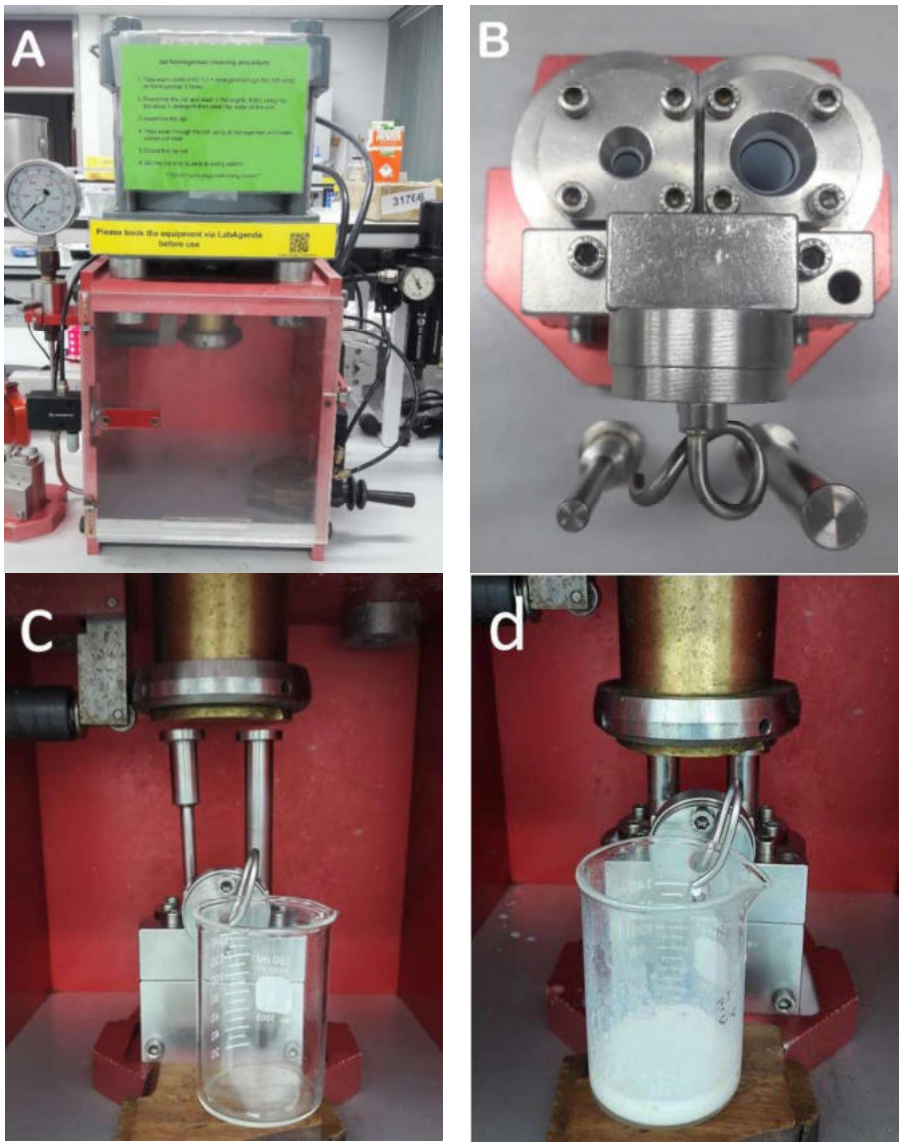

Figure 37. Pictures of the parts and operating procedures of Jet Homogenizer (University of Leeds, UK), (A) compression chamber, (B) solution cylinder, solution cylinder with pistons prior to compression (c) and after compression (d).

As previously discussed, several factors can affect the encapsulation process, e.g., concentration and ratio of biopolymers used as wall materials. For this reason, these parameters were optimized using a two-level-two-factors central composite design to investigate their influence on the characteristics of encapsulation systems based on CS and PPI. EvO at 0.5% (w/w) was used as core material. The PPI solution at 1% concentration and the CS solution with concentration ranging from 0.39 to 1.10% (w/v) were used as wall material. The responses, particle size (D[4,3]) (μm) and span factor were two-times evaluated, at the beginning of microparticles preparation (day 1), when the pH was adjusted to 6.5, and after 10 days of storage (under refrigeration and light protection). The overview of the experimental conditions for the encapsulation of EvO in CS:PPI microcapsules, with the respective results for initial particle size and span are shown in Table 23.

Table 23. Overview of the experimental conditions and the initial responses for the EvO (0.5% w/w) encapsulation in CS:PPI microcapsules.

Sample	Coded levels		Parameters		Initial responses	
	X1	X2	CS (%)	CS:PPI ratio	Size D[4,3] (μm)	Span index
DD	-1	-1	0.5	0.5	7.52 ± 0.1	10.38 ± 0.3
ED	+1	-1	1.0	0.5	6.37 ± 0.09	6.53 ± 0.16
DE	-1	+1	0.5	2.0	3.90 ± 0.15	3.60 ± 0.15
EE	+1	+1	1.0	2.0	5.04 ± 0.74	2.87 ± 0.26
FH	-1.41	0	0.39	1.25	2.44 ± 0.09	2.25 ± 0.14
GH	+1.41	0	1.10	1.25	2.23 ± 0.02	1.50 ± 0.01
HF	0	-1.41	0.75	0.18	6.18 ± 0.28	8.59 ± 0.60
HG	0	+1.41	0.75	2.31	3.67 ± 0.10	1.99 ± 0.05
HH*	0	0	0.75	1.25	5.08 ± 0.27	4.13 ± 0.21

Results are expressed as mean ± standard deviation. *Central point with five replications.

The initial responses, size (D[4,3] μm) and polydispersity index (span) were modelled by fitting a second-order polynomial equation (Equations 20 and 21).

$$Size_{\ Day\ 1}\ D[4,3] = 5.080 - 0.040\beta_1 - 1.062\beta_2 - 0.853\beta_{11} + 0.441\beta_{22} + 0.573\beta_{12} \quad (20)$$

$$Span_{Day\ 1} = 4.134 + 0.0588\beta_1 + 0.0555\beta_2 - 2.0016\beta_{11} - 1.9336\beta_{22} + 0.11\beta_{12} \quad (21)$$

Where β_1, β_2 are the linear regression coefficients, β_{11} e β_{22} quadratic regression coefficients and β_{12} are the interaction coefficients for factors CS (%) and CS:PPI ratio, respectively.

The results for the regression coefficients and the ANOVA of this experimental design are listed in Table 24. The results for the linear regression coefficients show that the particles size was substantially influenced by the CS:PPI ratio, whereas the span factor was not. The results for the quadratic regression coefficients reveals that only the span index was influenced by the CS (%) and the CS:PPI ratio ($p < 0.05$), whereas the size was not. Moreover, the interacion between the two factors, β_{12} (%CS x CS:PPI ratio), has not influenced the responses ($p > 0.05$). Thus, the particle size was significantly affect by a linear term, whereas the span was affected by the quadratic terms of the factors, CS concentration and CS:PPI ratio.

Table 24. Results for regression coefficients and analysis of variance for the initial responses of dependent variables of CS:PPI systems.

Coefficients	D[4,3] (μm)	Span
Mean		
β_0	5.080*	4.13*
Linear		
β_1	-0.040	0.0588
β_2	-1.062*	0.0555
Quadratic		
β_{11}	-0.853	-2.0016*
β_{22}	0.441	-1.9336*
Interactions		
β_{12}	0.573	0.151
R^2	0.6565	0.9918
$F_{calculated}$	2.68	168.64

*Significant factors by ANOVA ($p \leq 0.05$). β1, β2 are the regression coefficients for the factors CS concentration (%) and CS:PPI ratio, respectively.

The size distribution of the CS:PPI-EvO coacervates at day 1 (as soon as they were prepared) can be visualized in Figure 38. It can be noted that all systems displayed a normal size distribution curve. The highest volume particles density (%) ranged around 2 μm in size, although all systems exhibited a very small volume of particles with size up to 200 μm. Huo et al. (2016) found a similar size distribution pattern for antofloxacin-loaded CS microparticles, which displayed size ranging from 2.5 to 9.8 μm. In another work, Adebiyi and Aluko (2011) found that the emulsion droplets stabilized with PPI showed a narrow distribution curve when those systems were kept under neutral pH, while under acidic or alkaline pH values, the samples displayed a broader polydispersity distribution.

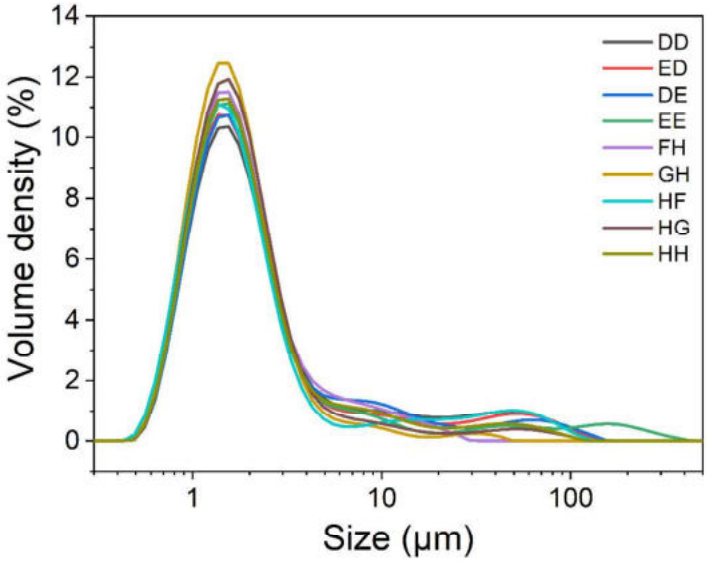

Figure 38. Size distribution curves of the CS:PPI-EvO coacervates at day 1 (pH 6.5).

The models obtained from the experimental design were used to calculate the response surface for each variable. The estimated response surface contours are shown in Figures 39 and 40. It can be noted that the smallest particle size was obtained using the highest CS:PPI ratio, above 1.5, and lowest CS concentration (Figure 39). The narrowest span index was achieved using the mid terms of both factors, CS:PPI ratio, 1.25, and CS concentration, around 0.8% (Figure 40).

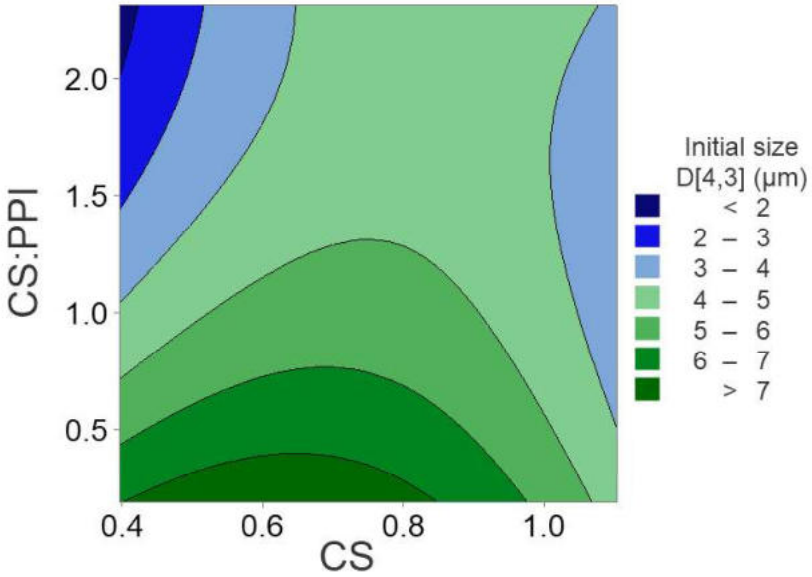

Figure 39. Response surface contours for particle size (D[4,3]) estimated from the interactions between X1 (CS%) and X2 (CS:PPI ratio) for the coacervates prepared at day 1.

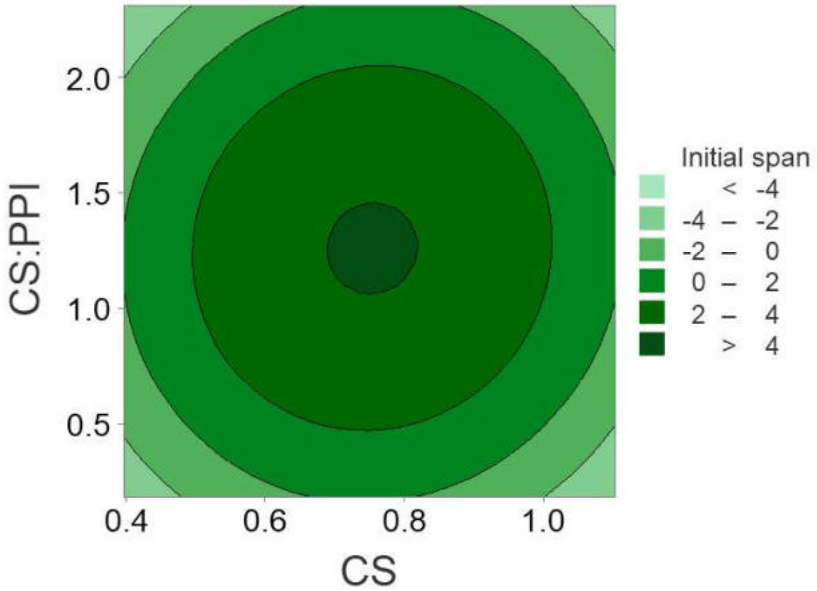

Figure 40. Response surface contours for polydispersity index (span) estimated from the interactions between X1 (CS%) and X2 (CS:PPI ratio) for the coacervates prepared at day 1.

The desirability function was added to the RSM to optimize the response parameters (Figure 41). The limits were set for each parameter aiming to minimize size and span. The maximum desirability value was found close to 0.845, as can be visualized on Figure 41.

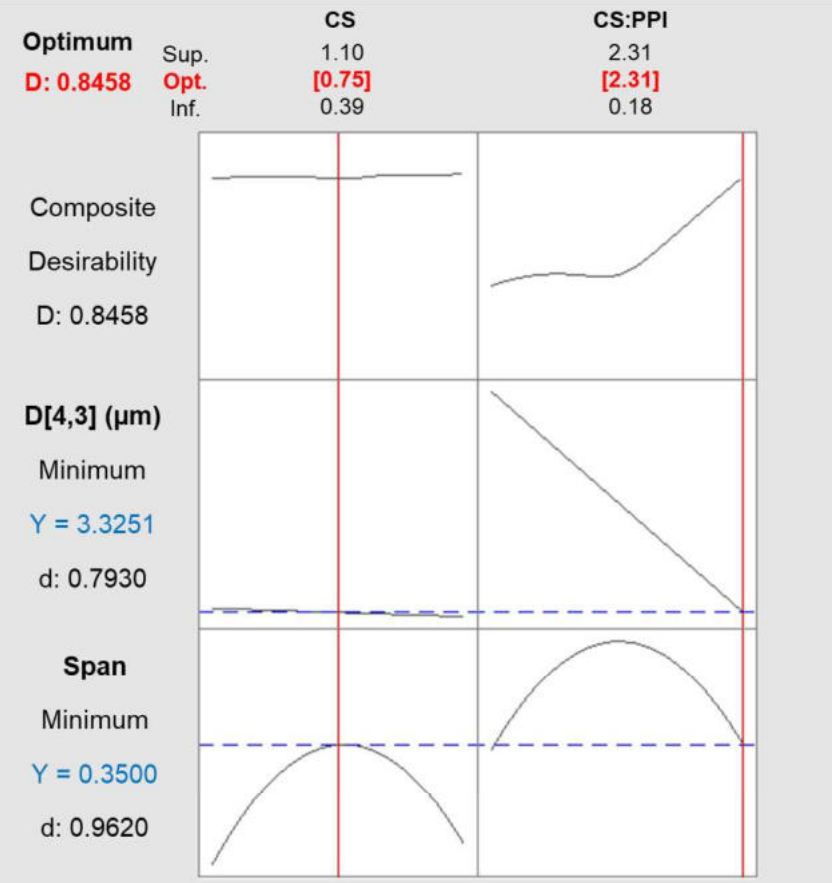

Figure 41. Desirability surface contour for the optimized CS:PPI coacervates.

The optimum conditions that produced the smallest particle size and span were 0.75% of CS, 2.31 of CS:PPI ratio and 0.5% of EvO. The result of *d* values for each response were well fitted, which can be seen by a value close to 0.8 to size and above 0.96 to span. Furthermore, the conditions used in the formulation of sample HG was considered as the optimum terms to EvO encapsulation.

The size and span value of the CS:PPI-EvO microparticles were measured once again after 10 days of its preparation to evaluate any significant changes on these responses. The overview of the experimental conditions for the encapsulation of EvO in CS:PPI microcapsules, with the respective results for final particle size (day 10) and span are shown in Table 25.

It was observed slight changes on size and span. The particles DD (0.5% CS and 0.5 CS:PPI ratio), EE (1.0% CS and 2.0 CS:PPI ratio) and HH (0.75% CS and 1.25 CS:PPI ratio) had a decrease on size, whereas the others had a slight increase. Nevertheless, the particles remained exhibiting small sizes, below 10 µm. The span value was found in a higher range, 1.83 to 15.3, when compared to the values

determined for these particles on the first day, which were in the range of 1.50 to 10.4. The highest changes were observed for the system HF (0.75% CS and 0.18 CS:PPI ratio). This could be an indication of a less stable encapsulation system linked a minor proportion of CS:PPI ratio (0.18), which produced a highest particles polydispersity.

Table 25. Overview of the experimental conditions and the final responses for the EvO (0.5% w/w) encapsulation in CS:PPI microcapsules.

Sample	Coded levels		Parameters		Responses after 10 days	
	X1	X2	CS (%)	CS:PPI	Size D[4,3] (μm)	Span
DD	-1	-1	0.5	0.5	6.82 ± 0.11	8.72 ± 0.19
ED	+1	-1	1.0	0.5	6.49 ± 0.16	6.81 ± 0.30
DE	-1	+1	0.5	2.0	4.13 ± 0.08	3.54 ± 0.06
EE	+1	+1	1.0	2.0	4.24 ± 0.81	3.15 ± 0.35
FH	-1.41	0	0.39	1.25	5.77 ± 0.12	4.62 ± 0.16
GH	+1.41	0	1.10	1.25	3.52 ± 0.05	1.83 ± 0.01
HF	0	-1.41	0.75	0.18	8.84 ± 0.63	15.30 ± 1.76
HG	0	+1.41	0.75	2.31	4.12 ± 0.04	2.21 ± 0.02
HH*	0	0	0.75	1.25	4.52 ± 0.07	3.67 ± 0.07

Results are expressed as mean ± standard deviation. *Central point with five replications.

Once again, these results for size (D[4,3] μm) and polydispersity index (span) (after 10 days) were modelled by fitting a second-order polynomial equation (Equations 22 and 23).

$$Size_{Day\,10}\, D[4,3] = 4.527 - 0.426\beta_1 - 1.451\beta_2 + 0.024\beta_{11} + 0.940\beta_{22} + 0.110\beta_{12} \quad (22)$$

$$Span_{Day\,10} = 2.963 + 0.086\beta_1 - 0.026\beta_2 - 1.420\beta_{11} - 1.294\beta_{22} + 0.171\beta_{12} \quad (23)$$

where β_1, β_2 are the linear regression coefficients, β_{11} e β_{22} quadratic regression coefficients and β_{12} are the interaction coefficients for factors CS (%) and CS:PPI ratio, respectively.

The results for the regression coefficients and the ANOVA of the experimental design are listed in Table 26. After 10 days of storage, the results for the linear regression coefficients showed that the particles size was significantly affected by the CS% and CS:PPI ratio ($p < 0.05$), whereas span factor was not influenced by these same factors ($p > 0.05$). The results for the quadratic regression coefficients revealed that size was influenced by CS:PPI ratio, and span was influenced by both factors, CS (%) and the CS:PPI ratio ($p < 0.05$). Once again, particle size and span were not significantly affect by the interacion between the two factors, β_{12}, CS% x CS:PPI ratio.

Table 26. Results for regression coefficients and analysis of variance for the final responses (after 10 days) of dependent variables of CS:PPI systems.

Coefficients	D[4,3] (μm)	Span
Mean		
β_0	4.527*	2.963*
Linear		
β_1	-0.426*	0.086
β_2	-1.451*	-0.026
Quadratic		
β_{11}	0.024	-1.420*
β_{22}	0.940*	-1.294*
Interactions		
β_{12}	0.110	0.171
R^2	0.9411	0.6784
$F_{calculated}$	22.38	2.95

*Significant factors by ANOVA ($p \leq 0.05$). β1, β2 are the regression coefficients for the factors CS concentration (%) and CS:PPI ratio, respectively.

The size distribution of the CS:PPI-EvO coacervates at the day 10 can be visualized in Figure 42. It was noted that all systems displayed a normal distribution curve, similarly to the results from day 1. The highest volume density (%) of particles also ranged around 2 μm in size, although all systems exhibited an exceedingly small volume of particles with size up to 200 μm.

Differently, Yuan et al. (2017) found a well-defined trimodal distribution with the particles size ranging from 0.05 to 100 μm, when studying a complex coacervation between soy protein and chitosan to algal oil encapsulation. In another recent study, Başyiğit et al. (2021) found a comparable distribution curve with particles ranging from 0.5 to 200 μm. These authors studied different protein systems to encapsulate EvO

and found that the microcapsules prepared with pea protein had the lowest span and the highest homogeneity among the others.

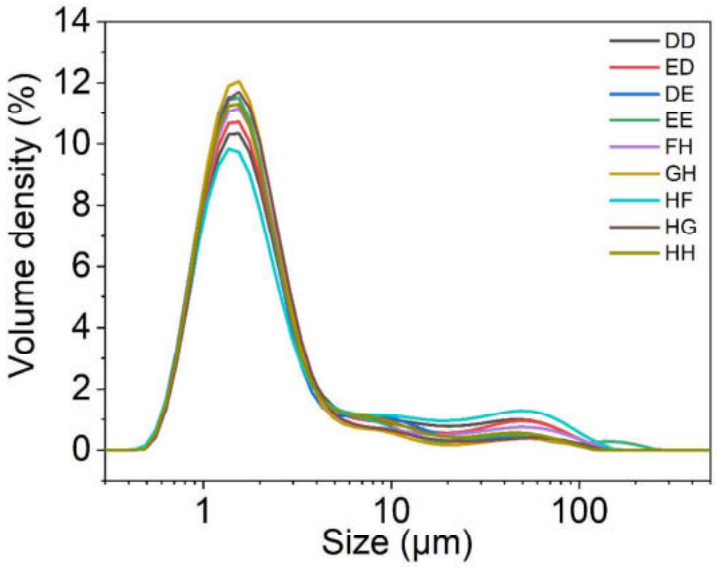

Figure 42. Size distribution of the CS:PPI-EvO coacervates after 10 days.

The fitted models from the experimental design were used to calculate the response surface for each variable. The estimated response surface contours for size and span are shown in Figures 43 and 44. It was observed that the smallest particle size can be found using the highest CS% and CS:PPI ratio, above 0.75% and 1.5, respectively (Figure 43).

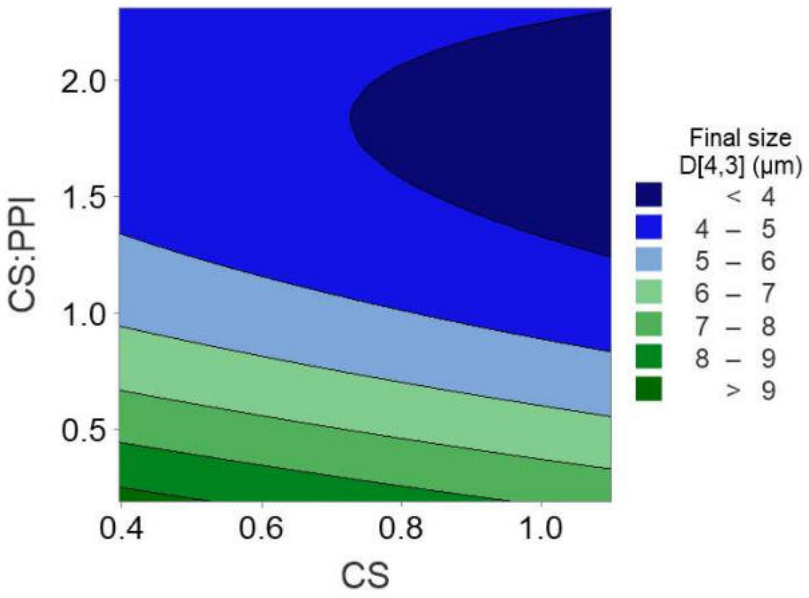

Figure 43. Response surface contours for particle size (D[4,3]) estimated from the interactions between X1 (CS%) and X2 (CS:PPI ratio) for the coacervates at day 10.

This result is in accordance with the findings of Hadidi et al. (2021). These authors studied the effects of the ratio CS:PPI as wall material and the ratio of hyssop essential oil CS:PPI complexes, on the retention rate of hyssop essential oil and on particle size. They found that when the ratio of CS:PPI increases to 1.7 the particle size decreases significantly reaching around 200 nm.

Similarly, the narrowest span was produced using the extremes for both factors, CS:PPI and CS concentration (Figure 44).

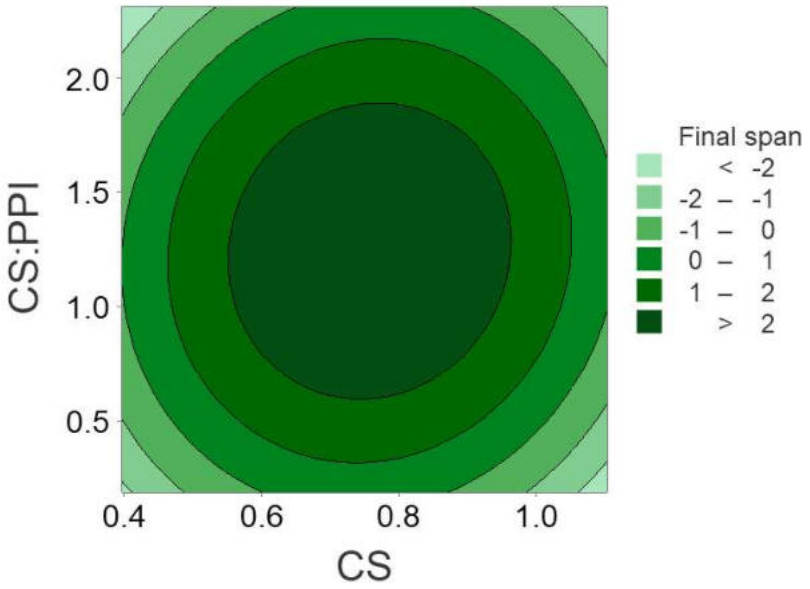

Figure 44. Response surface contours for polydispersity index (span) estimated from the interactions between X1 (CS%) and X2 (CS:PPI ratio) for the coacervates at day 10.

The desirability function was also added to the RSM to optimize these responses, as can be visualized in the Figure 45. Once again, the limits were set for each parameter aiming to minimize size and span. The maximum value of desirability was 0.8805. The optimum conditions that will produce the smallest particle size and span were 0.75% of CS, 2.31 of CS:PPI ratio and 0.5% of EvO.

The result of D values for each response were well fitted, which can be seen by a value above 0.8 for both, size and span. Once again, the sample HG was considered the optimum particle system for these studied conditions. This system exhibited a particle size and a span value around 4 μm and 2, respectively. Hadidi et al. (2021) also determined a desirability value for the optimized CS:PPI complexes and found that the optimum CS:PPI ratio should be of 2.12. Their results are in accordance with the findings of the present work. Moreover, these results indicate that the CS:PPI

complex coacervation for EvO encapsulation is a stable system up to 10 days after its preparation.

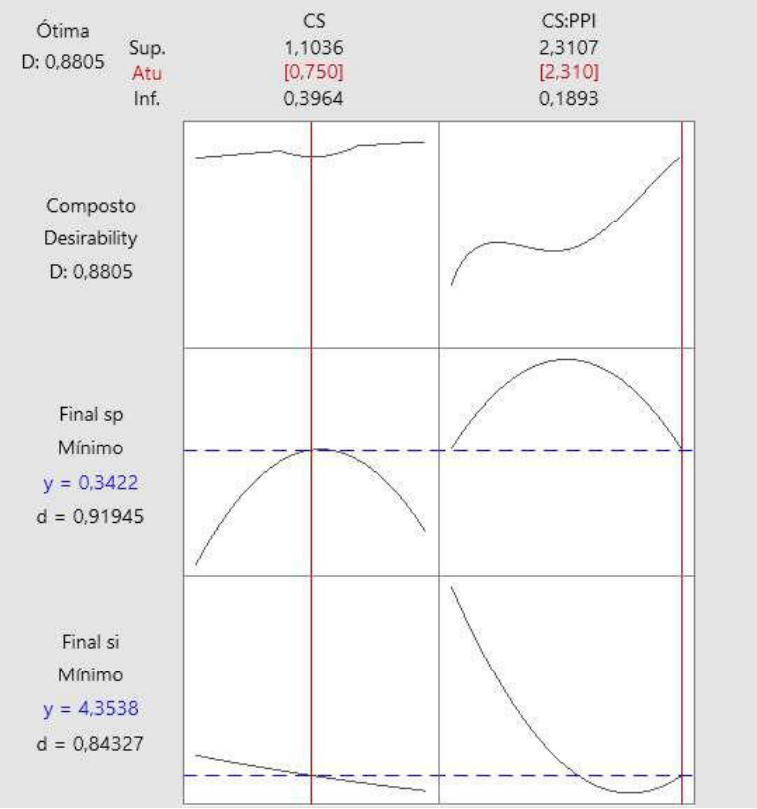

Figure 45. Desirability surface contour for the optimized CS:PPI coacervates at day 10.

5.2.3. Effect of pH on the formation of complex coacervates

Turbidity measurements under different pH values were investigated to verify the formation of CS:PPI coacervates. These results are presented in Figure 46. The samples, DD (0.5% of CS, 0.5 CS:PPI ratio and 0.5% EvO), ED (1.0% of CS, 0.5 CS:PPI ratio and 0.5% EvO), DE (0.5% of CS, 2.0 CS:PPI ratio and 0.5% EvO), EE (1% of CS, 2.0 CS:PPI ratio and 0.5% EvO) and HH (0.75% of CS, 1.25 CS:PPI ratio and 0.5% EvO), were selected to perform this experiment.

The highest turbidity values (%) were found in pH range of 6.5 to 7.5 for all systems. The samples ED and EE exhibited the peak values of turbidity than the other coacervates. The rise in turbidity can be related to an increase in the formation of protein-polysaccharide complexes (GULÃO et al., 2015). Both systems, ED and EE, had superior CS concentration than the others, which could contribute to an increased complexes formation.

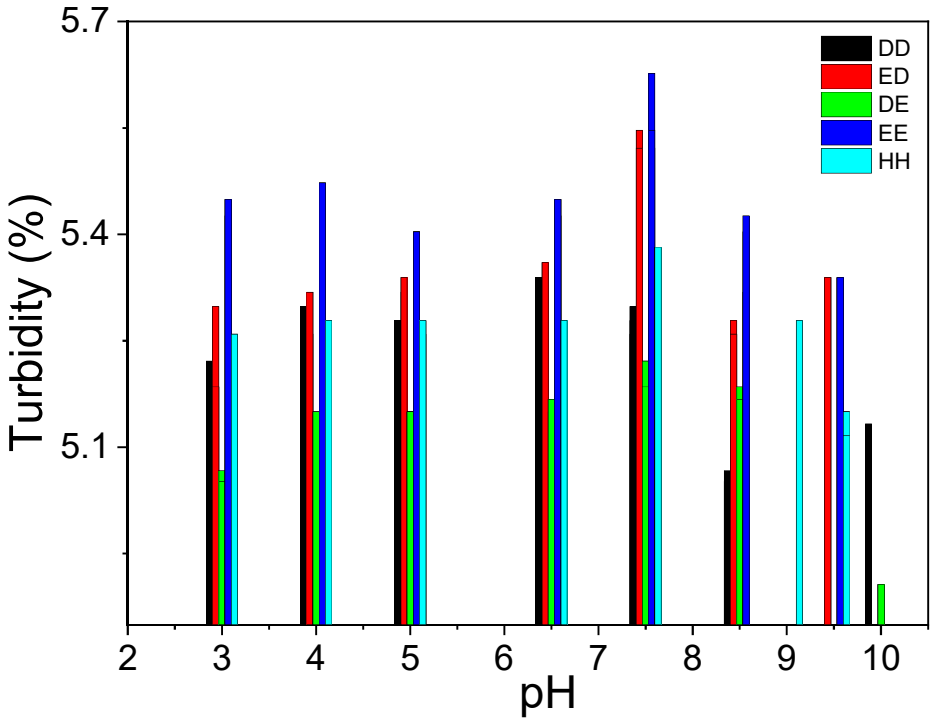

Figure 46. Turbidity (%) as function of pH values of selected CS:PPI complex coacervates. DD = 0.5% of CS, 0.5 CS:PPI ratio, ED = 1.0% of CS, 0.5 CS:PPI ratio, DE = 0.5% of CS, 2.0 CS:PPI ratio, EE = 1% of CS, 2.0 CS:PPI ratio and HH = 0.75% of CS, 1.25 CS:PPI ratio.

Elmer et al. (2011) found a peak optical density in turbidity curves when the PPI:CS ratio was rising. Above pH 8.0 the formation of protein aggregates on the CS:PPI coacervates was observed and the solutions were becoming less opaque, as can be visualized on Figures 43 and 44. This is in accordance with the findings of Liu, Low and Nickerson, (2009), that observed the formation of protein aggregates in PPI:gum Arabic coacervates at mildly alkaline conditions. These authors suggest that above pH 8 the hexameric structure of legumin is favored leading to the formation of those aggregates.

Figure 47 shows the visual aspects of the CS:PPI systems as a function of pH values at day one of preparation. The selected samples were DD (0.5% of CS, 0.5 CS:PPI ratio and 0.5% EvO), ED (% of CS, 0.5 CS:PPI ratio and 0.5% EvO), DE (0.5% of CS, 2.0 CS:PPI ratio and 0.5% EvO), EE (1% of CS, 2.0 CS:PPI ratio and 0.5% EvO) and HH (0.75% of CS, 1.25 CS:PPI ratio and 0.5% EvO). It is observed the presence of aggregates stuck to the sample glasses, especially above pH 7.5, although no phase separation was visibly noted. Moreover, no oil separation was found in any systems under these conditions.

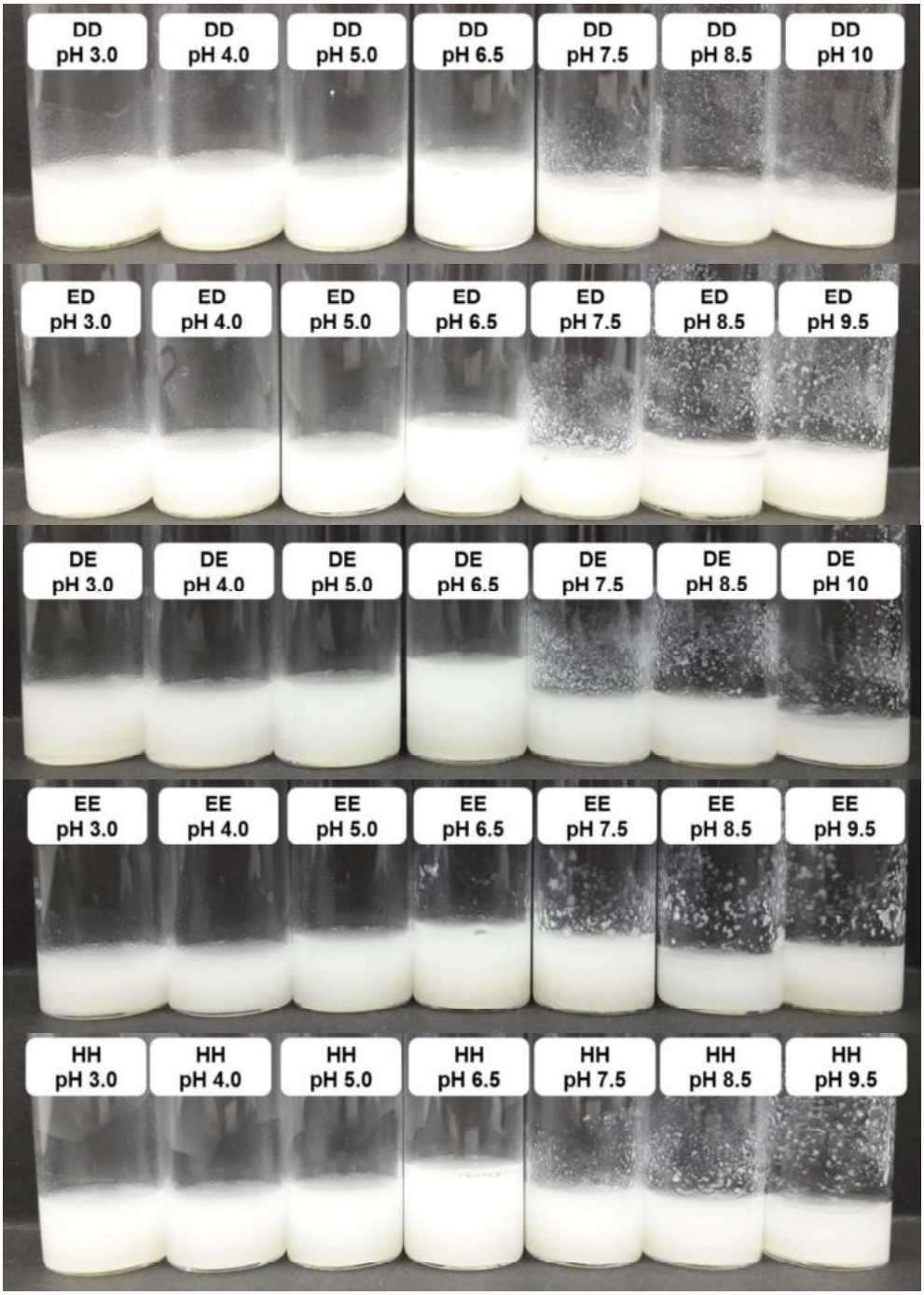

Figure 47. Visual aspects of the CS:PPI-EvO coacervates under different pH values at day 1.

These samples were kept under different pH values for 30 days (stored under refrigeration and protected from light). Then, its visual aspects were observed as is presented in Figure 48.

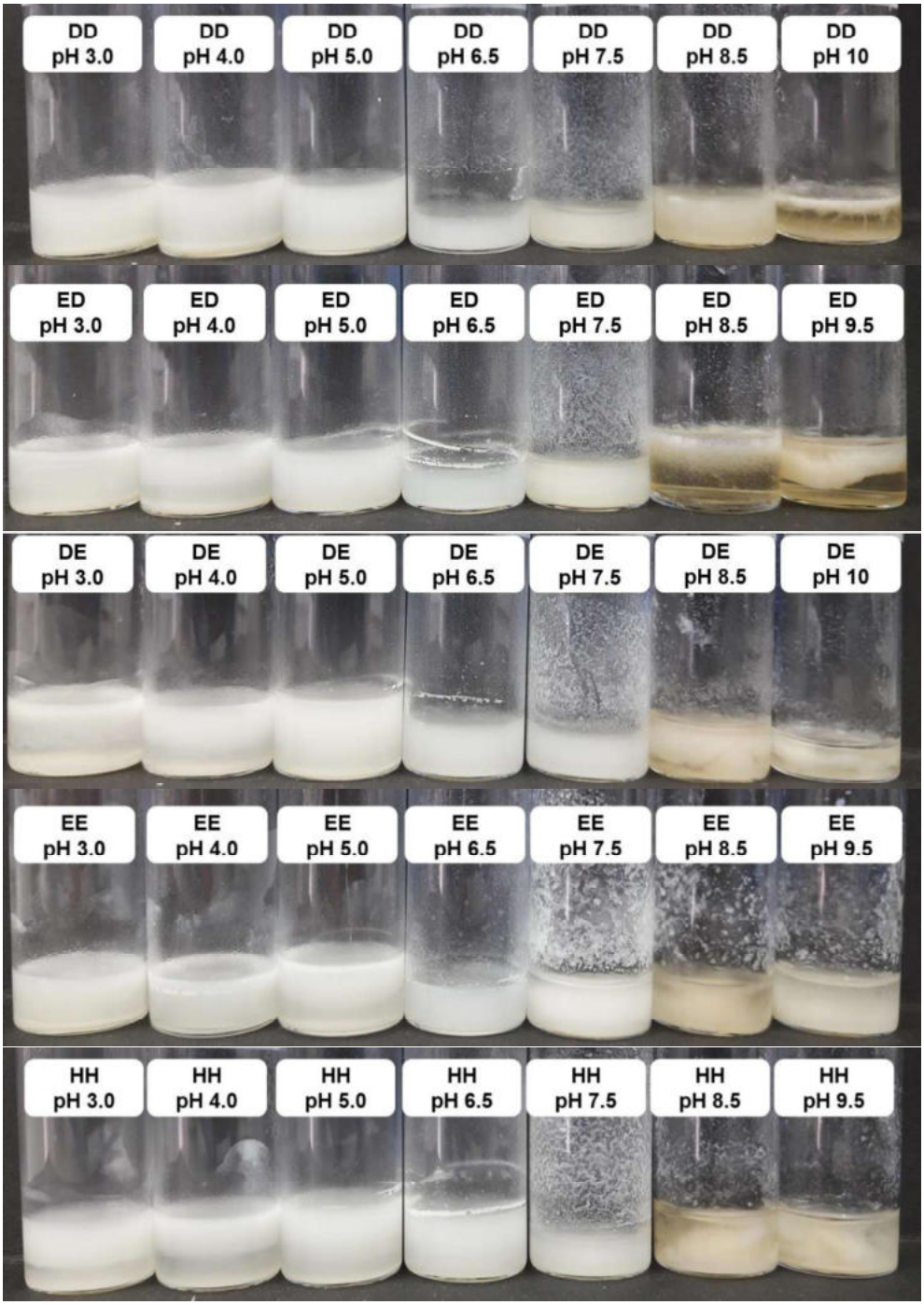

Figure 48. Visual aspects of the CS:PPI-EvO Coacervates under different pH values after 30 days of storage.

It was noted that all samples stored under alkaline conditions, above pH 8.0, exhibited losses on turbidity aspects, changed its color from a cream-white to a gold feature, and displayed phase separation. This can be associated to a decrease in positive charges of $–NH3^{+}$ groups of CS glucosamine units, leading to changes in the complexes interactions and bonding losses between the biopolymers. Under pH 4 and

pH 5, it is also possible to note a very slight phase separation for the samples. This could be linked to a decreased protein solubility on the pH range of 4 to 5.5, as reported by Carpentier et al. (2021).

Furthermore, the samples kept under pH 6.5 and 7.5 does not show any phase separation or oil separation during the 30 days storage period, which is an indication of good stability of those systems (BAŞYIĞIT et al., 2021). This result suggests that under these conditions the systems are kinetically stable, which contributed to a successful microencapsulation process. Moreover, Adebiyi and Aluko (2011) studied the oxidative stability of encapsulated EvO in different proteins microparticles. These authors found that PPI microparticles encapsulated with EvO were more stable to oxidative environment (< 5 mEq O_2 kg^{-1}) than the unloaded EvO (> 25 mEq O_2 kg^{-1}) after 7 days of storage. This corroborates to show the advantages of employing encapsulation techniques to protect bioactive substances from oxidative conditions.

5.2.4. Surface potential charges of the CS:PPI coacervates

The ζ-potential of the CS:PPI-EvO coacervates surface was evaluated and are shown in Figure 49. This coacervates exhibited a positively charged surface for all systems composition. This positive charge can be associated to the presence of CS in the systems since PPI exhibited a negative charge around -20 mV at pH 6.5. Furthermore, this could be an indication of CS and PPI interaction, and that CS is possibly placed on the surface of coacervates. The ζ-potential for this coacervates presented values ranging between 15 and 33 mV.

The particles with the highest ζ-potential values were DE and GH, which had the highest amounts of CS, above 1%, in their formulations. This could be related eighter to net charge of the polymers ratio on the CS:PPI complexes as well as to the excess of CS in the mixture (CARPENTIER et al., 2021). All the other systems had significantly different ζ-potential values ($p < 0.05$). The sample HF exhibited the lowest ζ-potential value, which could be associated to the smallest CS:PPI ratio. Elmer et al. (2011) found the lowest values for ζ-potential of PPI:CS complexes. These authors noted a substantial shift on ζ-potential around 8.5 mV at PPI:CS ratio of 2 to around 5.8 mV when the PPI:CS ratio increased to 20.

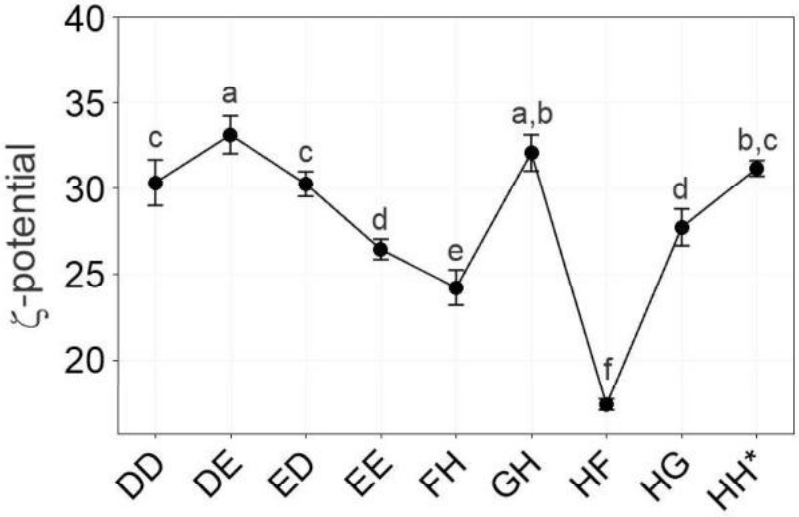

Figure 49. ζ-potential (mV) values for the CS:PPI coacervates at pH 6.5.
DD = 0.5% CS and 0.5 CS:PPI, ED = 1.0% of CS and 0.5 CS:PPI, DE = 0.5% of CS and 2.0 CS:PPI, EE = 1% of CS and 2.0 CS:PPI; FH = 0.39% CS and 1.25 CS:PPI; GH = 1.1% of CS and 1.25 CS:PPI; HF = 0.75% of CS and 0.18 CS:PPI; HG = 0.75% of CS and 2.31 CS:PPI; HH = 0.75% of CS and 1.25 CS:PPI.

The ζ-potential surface charge for the CS:PPI-EvO coacervates after 10 days of storage was re-evaluated and the changes are shown in the Figure 50. The systems presented different behaviors after this period. Four systems, DD (0.5% CS and 0.5 CS:PPI ratio), DE (0.5% CS and 2.0 CS:PPI ratio), ED (1.0% CS and 0.5 CS:PPI ratio) and HH (0.75% CS and 1.25 CS:PPI ratio), exhibited a decrease in ζ-potential values, whereas all the other systems showed an increase in ζ-potential.

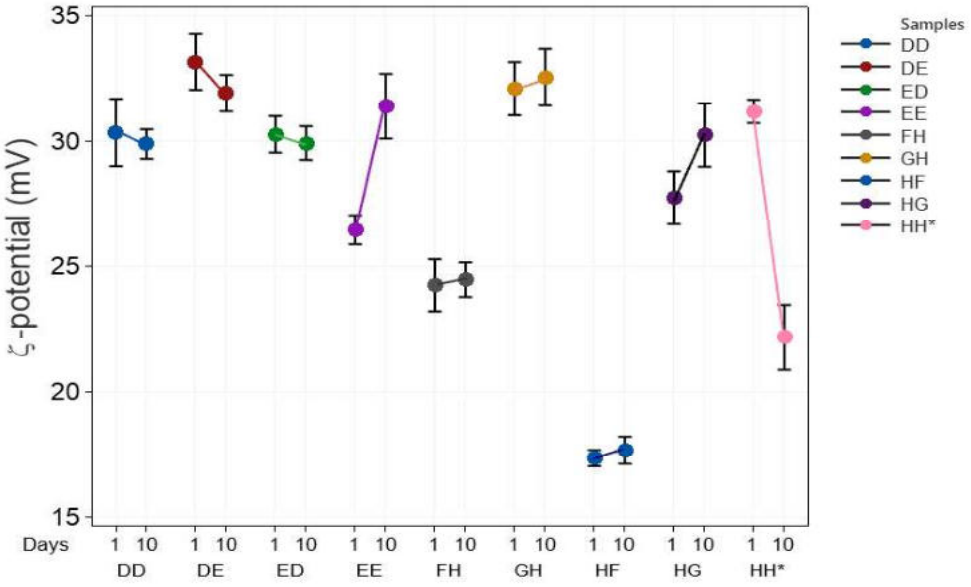

Figure 50. Changes on ζ-potential values of the CS:PPI coacervates after 10 days of storage.

The samples that displayed significant changes were EE and HH ($p > 0.5$), from around 26 to 31 mV and 31 to 22 mV, respectively. After 10 days of storage, samples DE and GH continued showing the highest ζ-potential values, although the sample EE had also achieved a major shift during this period. The optimized sample, HG showed no statistical difference in ζ-potential values ($p>0.05$) after 10 days, which demonstrated its stability under the tested conditions. Microparticles obtained by complex coacervation between CS and soy protein isolate (SPI) (CS:SPI = 0.2) to algal oil encapsulation exhibited a ζ-potential value of 12.2 ± 0.9 (YUAN et al., 2017). In another work, You, Liu and Zhao (2018) found that complex coacervates prepared with the mixture of 0.1% CS and 0.1% of Hsian-Tsao gum (CS:HTG 1:1) showed a positive charge ranging from around 20 to 10 at pH values of 6 - 6.5.

5.2.5. Morphological observations of CS:PPI coacervates by CLSM

The morphological aspects of the CS:PPI coacervates were observed by confocal laser scanning microscopy (CLSM). These observations were performed for selected samples, FH (0.39 % of CS and 1.25 CS:PPI ratio) and HF (0.75% of CS, 0.18 CS:PPI ratio and 0.5% of EvO), and their images are following presented in Figure 51 and Figure 52.

The CS:PPI Coacervates dispersions were stained with 2 drops of a 1 mg mL^{-1} of Nile Red in DMSO solution, and let to react for approximately 3 min, then observed by CLSM. This technique was used to evaluate the incorporation, as well as distribution and morphology of the EvO CS:PPI coacervates. The encapsulated EvO appears as a fluorescence green dye. Nile red was used to dye the olive oil because of its great ability to stain lipid droplets inside biopolymers complexes, which allows a good observation of stained particles by fluorescence (SILVA et al., 2020a).

The CLSM observation of the FH system under different magnification objectives (Figure 51) shows its homogeneity and confirms its small size, mostly below 6 µm. Figure 51a shows the stained FH coacervates at 10x magnification, in which few coacervates aggregates can be noted. In this magnification, the particles appear quite small, which could contribute to a limited visualization of particles. By increasing the

magnification 20x (Figure 51b), the visualization of the FH particles was improved. In this image, countless particles of stained FH coacervates appeared, showing its homogeneity and small size, although the presence of some aggregates may be visualized. Figure 51c shows the same system visualized under higher magnification (63x). In this image, it was possible to confirm the very small size and spheroidal shape of the FH coacervates, as well as to confirm the presence of encapsulated EvO.

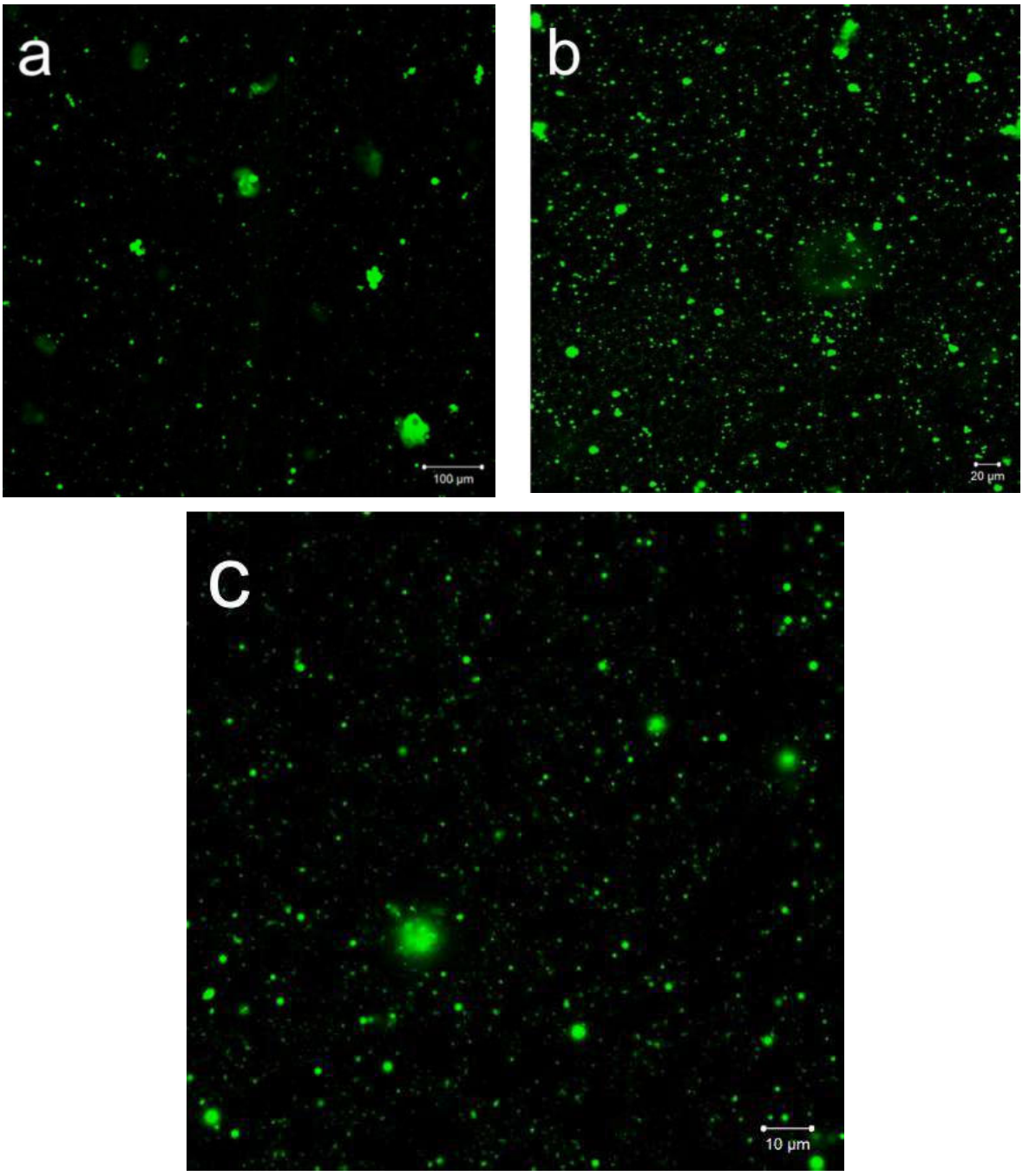

Figure 51. Selected 2D micrographs by CLSM of the CS:PPI-EvO coacervates, sample FH, at 10x (a), 20x (b), and 63x (c) magnifications.

The CLSM observation of the HF system (0.75% of CS, 0.18 CS:PPI ratio and 0.5% of EvO) under different magnification objectives is shown in Figure 52.

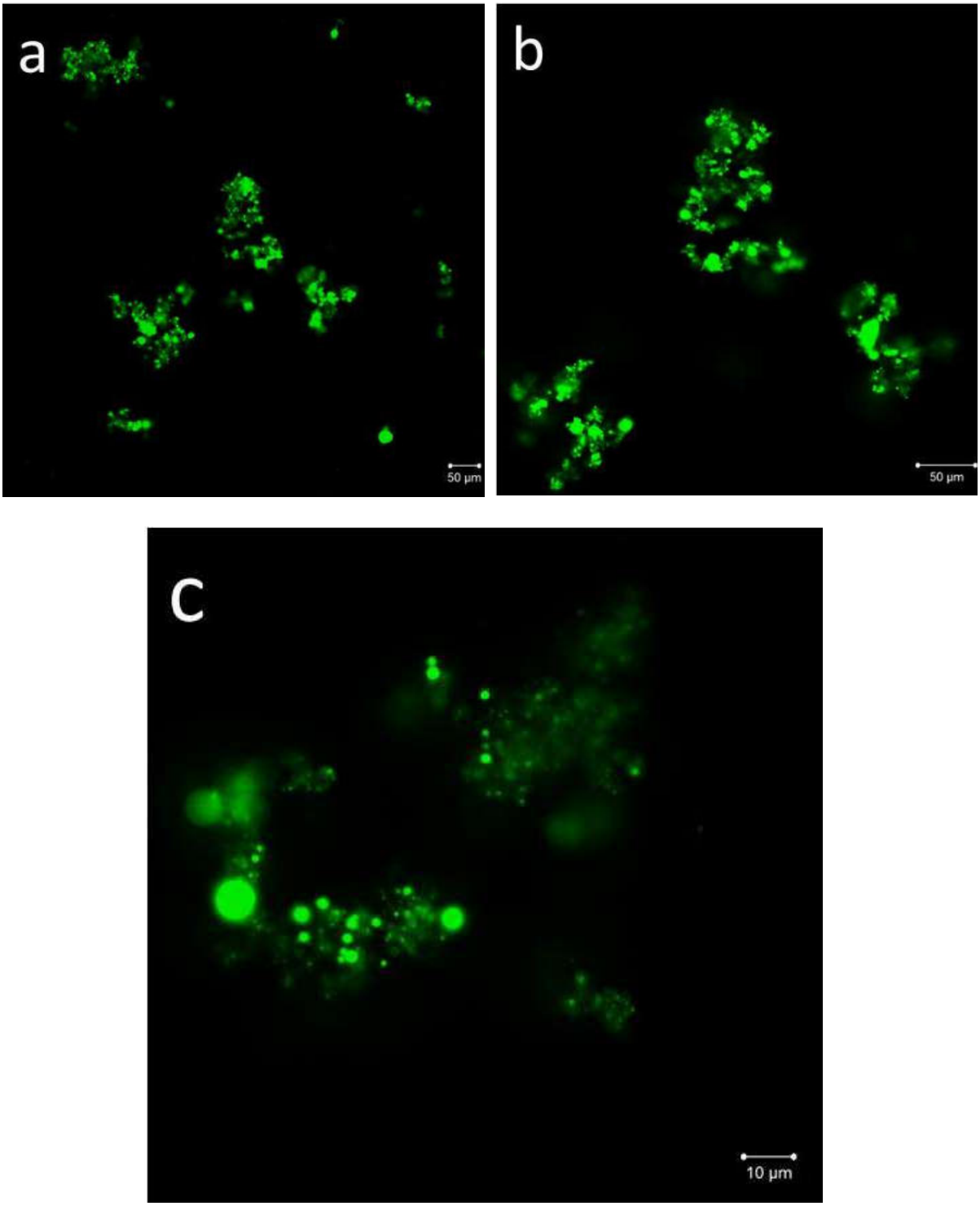

Figure 52. Selected 2D micrographs by CLSM of the CS:PPI-EvO Coacervates , sample HF, at 10x (a), 20x (b), and 63x (c) magnifications.

It was observed particles exhibiting very small sizes and that some aggregates were also formed. Figure 52a shows the stained HF coacervates at 10x magnification, in which aggregates may be observed, even though it is possible to observe smaller particles. By increasing the magnification to 20x (Figure 52b), the visualization of the HG particles becomes clearer, although tiny particles are united forming aggregates. This could be associated to its lowest ζ-potential value and highest particles polydispersity (~15). Figure 52c shows the same system visualized under higher magnification (63x). In this image, it is possible to confirm the very small size, below 10 µm, the circular/spheroidal shape of the HG coacervates, as well as confirm the presence of encapsulated EvO. These systems showed a less homogeneous distribution because it is possible to observe particles with a wide diverse size.

5.2.6. Fournier transform infrared spectroscopy - FTIR

FTIR was used to evaluate the molecular structure of CS, PPI and their molecular interactions in the optimized CS:PPI-EvO coacervates (sample HG - 0.75% of CS, 2.31 CS:PPI ratio and 0.5% EvO). The FTIR spectra of these materials are presented in Figure 53.

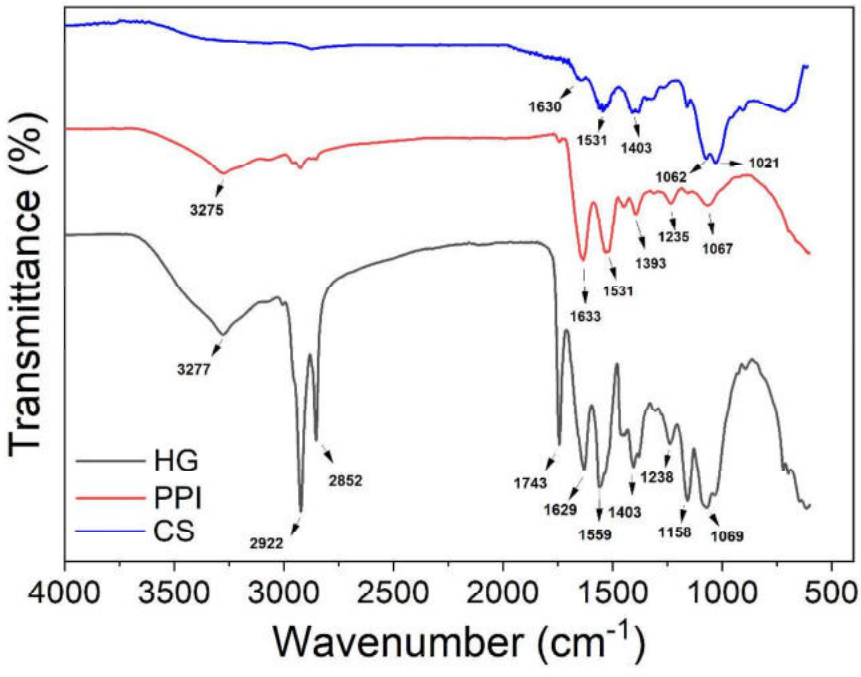

Figure 53. FTIR spectra of CS, PPI, and HG CS:PPI optimized coacervates.

The spectrum for CS presented bands associated to C═O stretching (amide I) at 1630 cm^{-1}, N–H bending (amide II) at 1531 cm^{-1}, C–N stretching (amide III) at 1403 cm^{-1}, asymmetric and symmetric axial deformation of C–O–C bonds at 1062 cm^{-1}, and C–O stretching at 1020 cm^{-1} (DEKA et al., 2016; PEREIRA, ANDRADE, 2017; PEREIRA et al., 2019).

The spectrum for PPI had characteristic absorption bands related to free and associated O–H and N–H bending vibrations around 3275 cm^{-1} and C═O stretching vibration (amide I) around 1633 cm^{-1} (CARPENTIER et al., 2021; HADIDI et al., 2021). This last spectrum band was also reported by Beck, Knoerzer and Arcot (2017), as being a typical band associated to the center of the β-sheet structures of pea protein. Bands related to the N–H stretching (amide II) at 1531 cm^{-1}, to C–N stretching (amide III) due to high content of β-sheet structure at 1235 cm^{-1}, and to C–O stretching at 1067 cm^{-1} (CARPENTIER et al., 2021; HADIDI et al., 2021).

The spectrum for HG optimized CS:PPI coacervates (0.75% of CS, 2.31 CS:PPI ratio and 0.5% EvO) exhibited characteristic bands of triglyceride functional groups related to the presence EvO (ROHMAN, MAN, 2010). The bands around 2922 – 2852 cm^{-1} and at 1743 cm^{-1} were associated to asymmetrical and symmetrical C–H stretching, and to C=O stretching vibrations of ester carbonyl functional groups, respectively, which confirms the EvO encapsulation on the CS:PPI coacervates (ROHMAN, MAN, 2010). Bands related to C═O stretching vibration and N–H stretching shifted to 1629 cm^{-1} and 1559 cm^{-1}, respectively, which can be an indication of coacervates formation between CS and PPI (HADIDI et al., 2021).

This corroborates the findings of Carpentier et al. (2021), who reported that amide peaks shifted to higher values explaining that this is correlated to the formation of electrostatic interactions between PPI and tragacanth gum. Besides this, a shift of wavenumbers on the amide peaks. Moreover, the appearance of a new vibrational band (polar bonds) at 1158 cm^{-1} was found as being related to a typical carbohydrate-protein interaction, as reported by Hadidi et al. (2021). The region between 1100-950 cm^{-1}, known as the fingerprint region, showed a broad band, which can be related to the superposition of PPI and CS spectra on the formation of CS:PPI complexes (CARPENTIER et al., 2021).

5.2.7. Thermogravimetric analysis

The thermogravimetric behavior of CS, PPI and HG CS:PPI coacervates was investigated by TGA and DTG. The TGA and DTG curves for CS are shown in Figure 54. CS presented an initial decomposition temperature (T_{onset}) around 277 °C and a maximum peak temperature (T_{peak}) at 303.3 °C. The residual matter observed for CS was around 31%. It is common to find higher amounts of residual materials at 700 °C in natural polymers. Pereira and Andrade (2017) found around 37% of residual matter for CS films. The DTG curves for CS presented two stages of thermal decomposition. The first ranging from 25 to 120°C and can be associated to loss of absorbed humidity, which is common for natural polymers (PEREIRA, ANDRADE, 2017). The second stage ranged between 220 and 350 °C, associated to the oxidation and depolymerization reactions of protonated carboxylic groups of CS (SARMENTO et al., 2006).

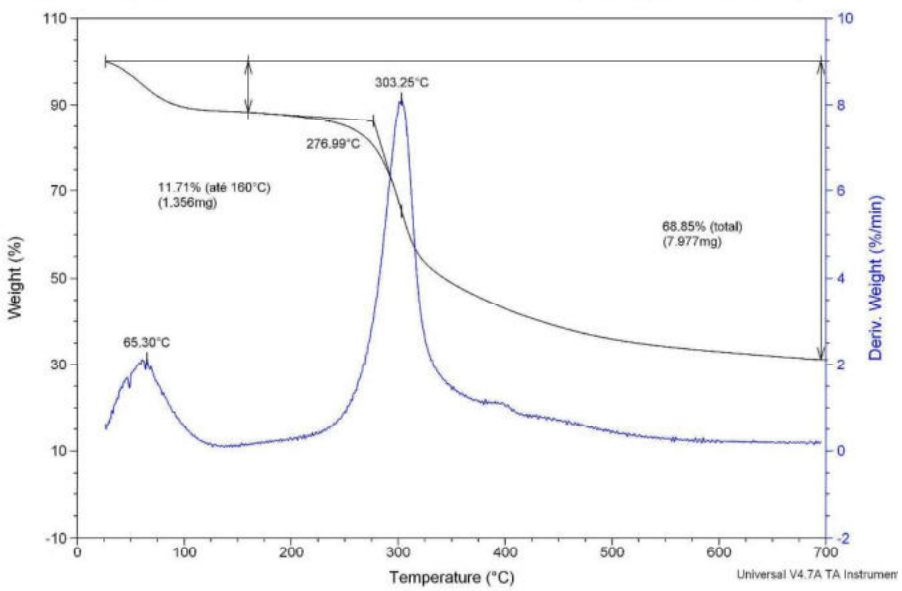

Figure 54. TGA (black line) and DTG (blue line) curves of CS.

The TGA and DTG curves of PPI are shown in Figure 55. PPI displayed T_{onset} around 260 °C and a T_{peak} at 304.8 °C. The DTG curves for PPI also exhibited two stages of thermal decomposition. The first ranging from around 25 to 120°C and can be associated to loss of humidity and low molecular weight compounds (AZEVEDO et al., 2020; BAŞYIĞIT et al., 2021). The second stage ranged between approximately 200 and 500 °C, where was observed the highest weight loss, around 76.5%. Başyiğit

et al. (2021) found a similar thermodegradation behavior for PPI, which exhibited a maximum weight loss close to 66%. This stage of thermo-decomposition can be associated to the oxidation and depolymerization reactions of molecular chains on PPI (SARMENTO et al., 2006).

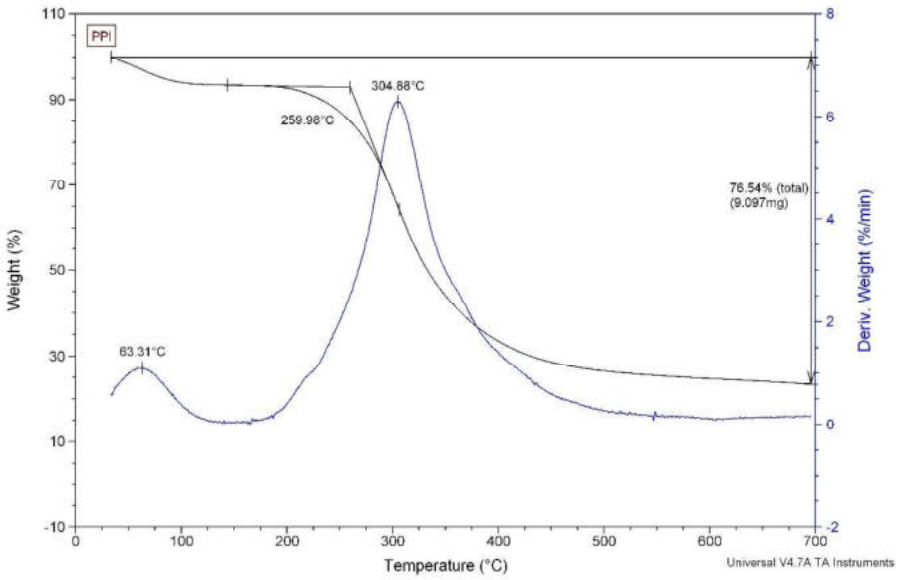

Figure 55. TGA (black line) and DTG (blue line) curves of PPI.

The TGA and DTG curves for the optimized CS:PPI coacervates (sample HG - 0.75% of CS, 2.31 CS:PPI ratio and 0.5% EvO) are shown in Figure 56. The HG microparticles displayed a T_{onset} around 278 °C and a T_{peak} around 358 °C. A shift of T_{peak} for the HG coacervates towards higher temperatures was observed, when compared to the raw materials, CS and PPI alone, which ranged around 305°C. This behavior can be attributed to the presence of encapsulated EvO, since some vegetable oils may display higher T_{peak} values, such as was found for the açaí oil on this work. The olive oil studied by Dweck and Sampaio (2004) exhibited a T_{onset} around 288 °C and a T_{peak} around 413 °C.

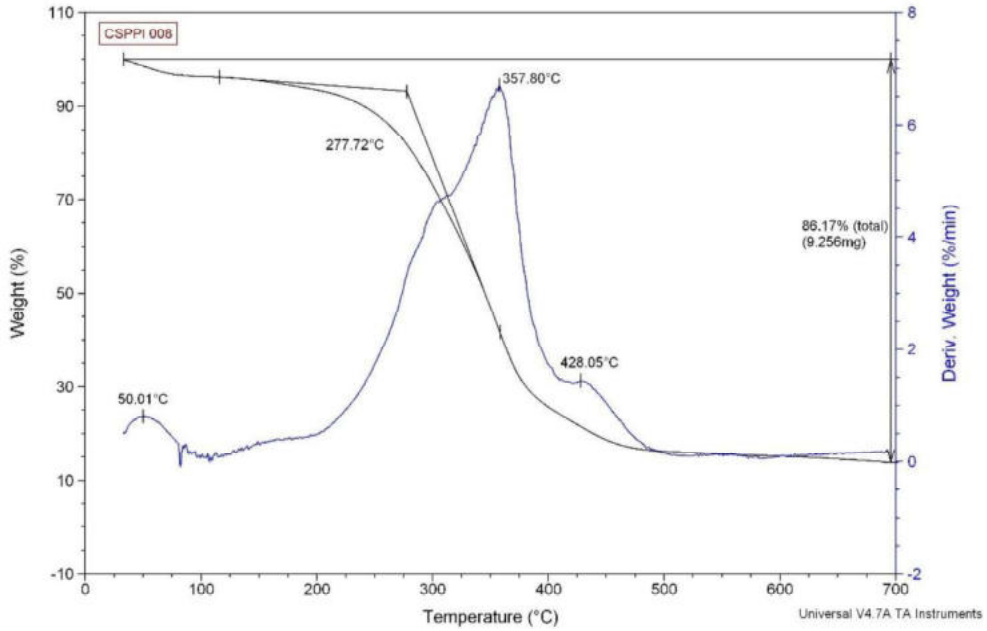

Figure 56. TGA (black line) and DTG (blue line) curves of HG optimized coacervates.

The DTG curves for HG coacervates also exhibited two stages of thermal decomposition. The first ranging from around 25 to 100°C, which can be associated to loss of humidity and low molecular weight compounds, although it can be noted a relatively lower weight loss, which could be due the presence of encapsulated EvO (BAŞYIĞIT et al., 2021; LEI et al., 2018). The second stage ranged between approximately 150 and 500 °C, where was observed the highest weight loss, around 86.2%. Başyiğit et al. (2021) also found a similar thermal behavior for pea protein microcapsules containing encapsulated olive oil, which displayed a T_{peak} around 400 °C.

The thermal events registered by TGA and DTG curves of the other CS:PPI coacervates are listed in Table 27. The thermobehavior of the samples DD (0.5% of CS, 0.5 CS:PPI ratio and 0.5% EvO) and ED (1% of CS, 0.5 CS:PPI ratio and 0.5% EvO) were quite similar to optimized HG CS:PPI coacervates (0.75% of CS, 2.31 CS:PPI ratio and 0.5% EvO). However, the major differences from the other systems were related to the occurrence of three stages of thermal degradation, and an increased $T_{peak,}$ ranging from 450 to 461 °C.

Table 27. Thermal events by TGA and DTG curves of the CS:PPI Coacervates .

Sample	Stage of thermal degradation	TGA		DTG	
		T_{onset} (°C)	% Residues at 700°C	ΔT (°C)	T_{peak} (°C)
DD	1	301.1	13.4	25 – 150	377.2
	2			150 – 500	
ED	1	255.7	25.5	25 – 115	329.3
	2			115 – 390	
	3			390 – 510	
DE	1	224.6	28.4	35 – 100	460.9
	2			100 – 350	
	3			350 – 500	
EE	1	223.4	27.5	25 – 100	449.9
	2			100 – 350	
	3			350 – 500	
FH	1	221.8	27.2	25 – 90	457.1
	2			150 – 350	
	3			350 – 500	
GH	1	228.9	26.6	25 – 100	451.1
	2			200 – 350	
	3			350 – 500	
HF	1	201.8	26.2	25 – 150	451.5
	2			150 – 400	
	3			400 – 510	
HG	1	277.7	23.8	25 – 100	357.4
	2			120 – 500	
HH*	1	221.8 - 222.4	24.8 – 27.4	25 – 100	457.2 – 459.9
	2			100 – 350	
	3			350 – 515	

ΔT = temperature range; T_{onset} = initial degradation temperature; T_{peak} = peak temperature. *Two replications. DD: 0.5% of CS and 0.5 CS:PPI ratio; ED: 1% of CS and 0.5 CS:PPI; DE: 0.5% of CS and 2.0 CS:PPI; EE: 1% of CS and 2.0 CS:PPI; FH: 0.39% of CS and 1.25 CS:PPI; GH: 1.1% of CS and 1.25 CS:PPI; HF: 0.75% of CS and 0.18 CS:PPI; HG: 0.75% of CS and 2.31 CS:PPI; HH: 0.75% of CS and 1.25 CS:PPI. All samples were prepared with 0.5% of EvO.

5.2.8. Determination of total polyphenols and antioxidant activity of CS, PPI, EvO and CS:PPI coacervates

The use of natural bioactive materials to food preservation against oxidative agents has gained significative interest due to its diverse potential application. Many of these bioactive materials are thermosensitive and for this reason their encapsulation in biopolymers matrices has shown to be a good strategy aiming to extend its shelf-life. Different methods are used to physicochemically determine the *in vitro* antioxidant activity of food materials. Mainly, two approaches can be exploited, such as involving hydrogen atom transfer (HAT) and single electron-transfer (SET) reactions, can be exploited to investigate antioxidant materials (PRIOR, WU, SCHAICH, 2005; SHAHIDI, ZHONG, 2015).

In this work, the *in vitro* antioxidant activity of CS, PPI, EvO and the optimized CS:PPI coacervates, HG (0.75% of CS, 2.31 CS:PPI ratio and 0.5% EvO), were determined using SET methods, such as total polyphenols content (TPC), the ferric ion reducing antioxidant power (FRAP), Trolox equivalent antioxidant capacity (TEAC), and DPPH radical scavenging. To this purpose, an aqueous extract at 1% (w/v) concentration of CS and PPI, an aqueous ethanolic extract of optimized HG coacervates (10μL mL^{-1}), and an ethanolic extract of EvO at 10μL $mL^{-}1$, were previously prepared.

The TPC is a valuable assay to assess total antioxidant capacity using the Folin-Ciocalteu reagent and has been widely applied to food extracts. This method is based on the spectrophotometric measure, at 760 nm, of the reduction of the Folin-Ciocalteu reagent, which changes its color from yellow to blue, by phenolics substances under an alkaline environment (PAULA et al., 2018; SHAHIDI, ZHONG, 2015). Thus, when is higher the reducing power of the sample, higher is its antioxidant capacity, and for this, can be considered an antioxidant method. Although many controversy issues are related mainly linked to nonphenolic reducing agents, i.e., reducing sugars, amino acids and others, that can be interferents in the reaction mechanism (PRIOR, WU, SCHAICH, 2005; SHAHIDI, ZHONG, 2015).

The TPC of CS, PPI, EvO and the optimized CS:PPI coacervates (0.75% of CS, 2.31 CS:PPI ratio and 0.5% EvO) was determined employing the Folin-Ciocalteu reagent assay. The results were calculated using a linear regression (Equation 24) obtained from the standard gallic acid curve, expressed as mg of gallic acid equivalent

(GAE) per L of sample. The antioxidant activity by TPC of CS, PPI, EvO and the optimized HG coacervates are presented in the Figure 57. The results were expressed as mean (column) ± standard deviation (bar) (n=3).

$$Total\ polyphenols\ content = \frac{Absorbance_{sample} - 0.0727}{0.0028} \quad R^2 = 0.9984 \quad (24)$$

The CS and PPI exhibited a mild antioxidant activity by TPC, 3.16 ± 0.27 and 19.83 ± 5.13 mg GAE L^{-1}, respectively, whilst the HG coacervates showed a value ranging between both raw materials, 5.48 ± 0.19 mg GAE L^{-1}. The EvO showed the highest antioxidant activity, 82.70 ± 6.5 mg GAE L^{-1}. CS is known for possessing a slightly antioxidant activity due to the interaction of free radicals with the free amino groups from its chain leading to the formation of ammonium groups ($-NH_3^+$) (SIRIPATRAWAN, VITCHAYAKITTI, 2016). Hadidi et al. (2021) determined the antioxidant activity of CS by TPC assay of being around 10 mg GAE g^{-1}.

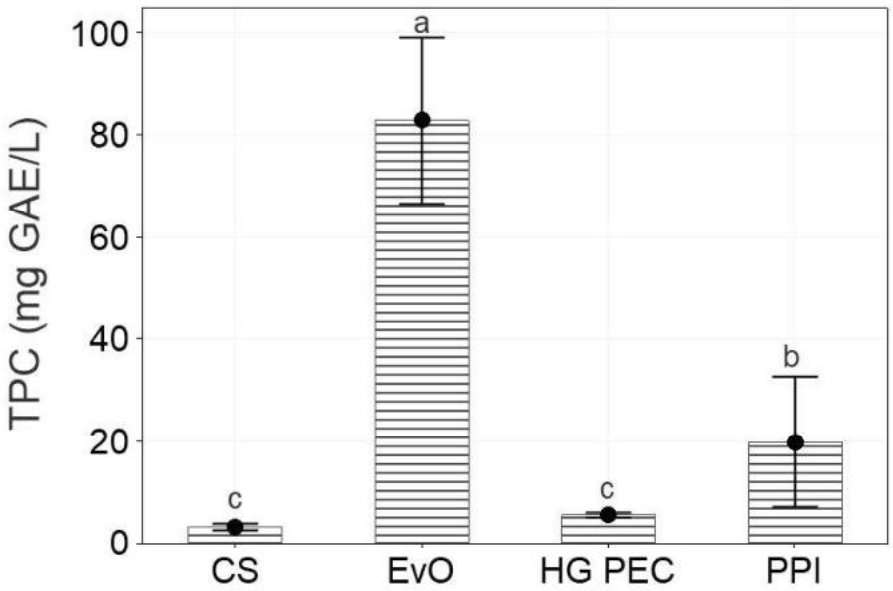

Figure 57. Total polyphenols content (mg GAE L^{-1}) by using the Folin-Ciocalteu reagent assay for the CS, PPI, EvO and optimized HG (0.75% of CS, 2.31 CS:PPI ratio and 0.5% EvO) coacervates. Different lowercase (a,b,c) letters within a column indicates significant difference among samples by Tukey's test ($p<0.05$).

PPI has also demonstrated a moderate antioxidant activity. Agboola et al. (2010) and Hadidi et al. (2021) determined the antioxidant activity of PPI by TPC assay

as 2.84 ± 0.23 mmol GAE 100 g^{-1} (in dry basis) and 4.2 mg GAE g^{-1}, respectively. In the work of Morales-Polanco et al. (2017) the TPC of PPI was 0.47 ± 0.05 mg GAE g^{-1}. The nano-complex based on CS:PPI encapsulated with hyssop essential oil showed an antioxidant activity by TPC assay of 112 mg GAE g^{-1}, as reported by Hadidi et al. (2021).

It has been reported that extra virgin olive oil exhibits good antioxidant properties, due to the presence of different bioactive substances, such as phenolics, i.e., tyrosol and hydroxytyrosol derivatives, and α-tocopherols (FRANKEL et al., 2013; LOZANO-SÁNCHEZ et al., 2011). Picholine variety of olive oils produced by traditional mill in Morocco displayed an antioxidant activity by TPC assay around 60 to 100 μg g^{-1} (EL HAOUHAY et al., 2015). In a recent work, Siano, Picariello, and Vasca (2021) determined the TPC value by Folin-Ciocalteu assay of extra-virgin olive oil from different seasons and found values ranging from 0.10 to 0.82 g GAE kg^{-1} of oil.

The FRAP, as the name suggests, is a spectrophotometric method based on the reduction of ferric ion (Fe^{3+})-ligand complex to ferrous (Fe^{2+}) complex by antioxidants in an acid solution (HUANG, OU, PRIOR, 2005; SHAHIDI, ZHONG, 2015). The reaction is measured at 593 nm by appearance of an intense blue color. Originally, this technique was employed to determine the reducing power of plasma and other biological fluids, but it has been extensively used for food and plant extracts for its simplicity and good cost-effectivity relation (SHAHIDI, ZHONG, 2015).

The FRAP for CS, PPI, EvO and the optimized HG (0.75% of CS, 2.31 CS:PPI ratio and 0.5% EvO) coacervates was determined using a standard curve of Trolox, calculated using a linear regression (Equation 25) and expressed as mg of Trolox equivalent per L of sample. The antioxidant activity these materials determined by FRAP assay are presented in the Figure 58. The results were expressed as mean (column) ± standard deviation (bar) (n=3).

$$FRAP\ (\text{mg TE L}^{-1}) = \frac{Absorbance_{sample} - 1.7515}{0.0033} \quad R^2 = 0.9979 \quad (25)$$

The CS, PPI and the HG PEC exhibited a mild antioxidant activity determined by FRAP, 7.24 ± 1.2, 1.88 ± 0.9, and 9.58 ± 0.2 mg TE L^{-1}, respectively, whereas, the EvO showed the highest antioxidant activity, 214.1 ± 22.1 mg TE L^{-1}. Pu et al. (2019) found that different CS concentrations, 0.01 – 0.3% (w/v), exhibited an antioxidant

activity by FRAP assay ranging from around 0.07 to 0.10 expressed as absorbance. Extra-virgin olive oil from different origins, Moroccan and Spanish, exhibited an antioxidant power around 5 to 10 μM g^{-1} and 0.98 to 3.75 mmol of TE kg^{-1} of EvO, by the studies of El Haouhay et al. (2015) and Borges et al. (2019), respectively.

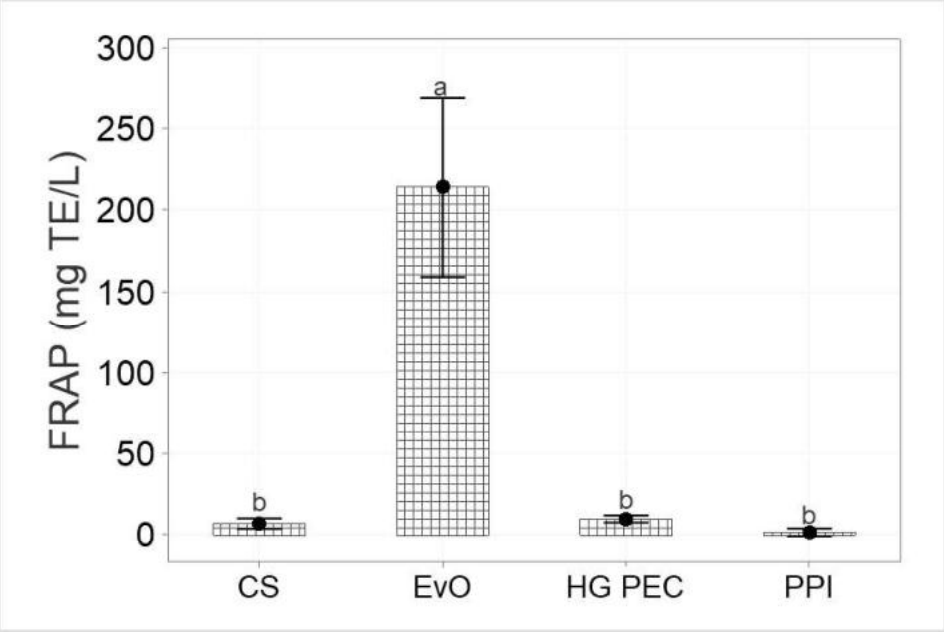

Figure 58. Antioxidant power by FRAP (mg TE L^{-1}) for the CS, PPI, EvO and optimized HG (0.75% of CS, 2.31 CS:PPI ratio and 0.5% EvO) coacervates. Different lowercase (a,b,c) letters within a column indicates significant difference among samples by Tukey's test ($p<0.05$).

The Trolox equivalent antioxidant capacity (TEAC) is a spectrophotometric method that measures at 734 nm of wavelength the capacity of antioxidants to scavenge the ABTS radical. This radical is a blue-green chromophore that loses its color intensity in the presence of antioxidants. The ABTS radical can be neutralized via both electron donation or hydrogen atom donation, thus this method can be either classified as SET and HAT mechanism (SHAHIDI, ZHONG, 2015). The TEAC of CS, PPI, EvO and the optimized CS:PPI coacervates, HG (0.75% of CS, 2.31 CS:PPI ratio and 0.5% EvO), was determined using a Trolox standard curve. The results from this assay were calculated using a liner regression (Equation 26) and expressed as mg of Trolox equivalent per L of sample and are presented in the Figure 59. These results were expressed as mean (column) ± standard deviation (bar) (n=3).

$$TEAC\ (\text{mg TE L}^{-1}) = \frac{Absorbance_{sample} + 0.6783}{0.0019} \quad R^2 = 0.9912 \quad (26)$$

The CS, EvO and the HG coacervates exhibited a moderate antioxidant activity determined by TEAC, 46.0 ± 3.4, 97.4 ± 5.1, and 37.91 ± 5.5 mg TE L^{-1}, respectively, whereas, the PPI showed the highest antioxidant activity, 271.5 ± 3.7 mg TE L^{-1}. Pu et al. (2019) found that different CS concentrations, 0.01 – 0.3% (w/v), exhibited an antioxidant activity by ABTS radical scavenging ranging from around 3 to 50%.

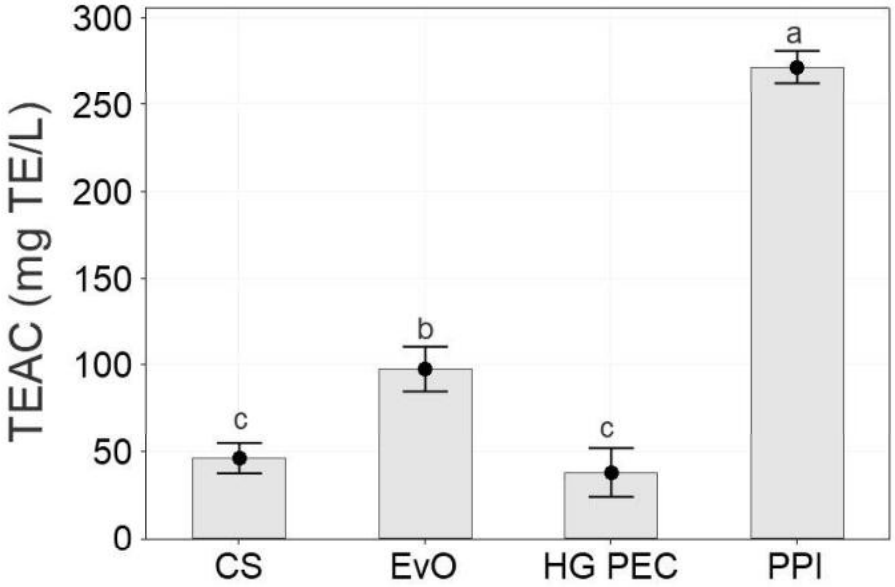

Figure 59. Antioxidant capacity (mg TE L^{-1}) by TEAC assay for the CS, PPI, EvO and optimized HG coacervates (0.75% of CS, 2.31 CS:PPI ratio and 0.5% EvO). Different lowercase (a,b,c) letters within a column indicates significant difference among samples by Tukey's test ($p<0.05$).

The PPI antioxidant capacity by ABTS radical scavenging reported by Morales-Polanco et al. (2017) was of 148.99 ± 9.49 mmol TE g^{-1}. Agboola et al. (2010) determined a value for antioxidant activity of PPI by TEAC of 4.13 ± 0.39 mmol Trolox 100 g^{-1} (in dry basis). Picholine variety olive oils produced by traditional mill in Morocco displayed an antioxidant activity by FRAP assay ranged from 0.2 to 0.8 μM g^{-1} (EL HAOUHAY et al., 2015). Spanish olive oil cultivars on the studies of Borges et al. (2019) showed values of ABTS radical scavenging ranging from 0.48 to 0.80 mmol of TE kg^{-1} of EvO.

The DPPH radical scavenging assay is among the most employed methods to determine antioxidant activity of food and food related products. It is a method based on a SET reaction, although a hydrogen-atom abstraction occurs in a marginal reaction pathway (PRIOR, WU, SCHAICH, 2005). DPPH is a stable organic nitrogen radical that exhibits a dark purple color. The antioxidant capacity against DPPH is measured at 517 nm by its discoloration for an oxidant agent in solution (SHAHIDI, ZHONG, 2015). In this work, the antioxidant capacity against the DPPH radical was determined using a Trolox standard curve, calculated using a liner regression (Equation 27). The results from this assay were expressed as mg of Trolox equivalent per L of sample and are presented in Figure 60.

$$DPPH \cdot \ scavenging\ (\text{mg TE L}^{-1}) = \frac{0.55 - Absorbance_{sample}}{0.0019} \quad R^2 = 0.9992 \quad (27)$$

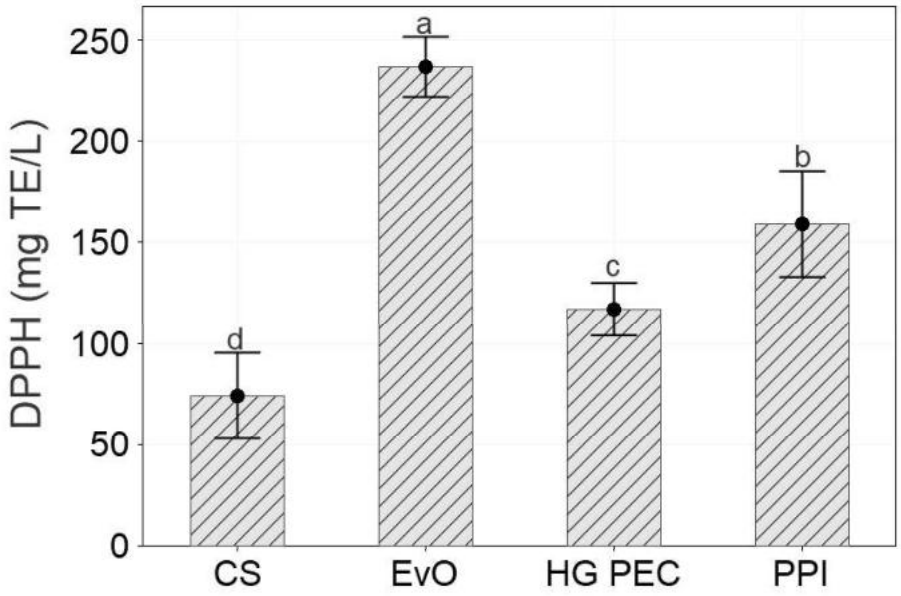

Figure 60. Antioxidant capacity (mg TE L^{-1}) by DPPH assay for the CS, PPI, EvO and optimized HG coacervates (0.75% of CS, 2.31 CS:PPI ratio and 0.5% EvO). Different lowercase (a,b,c) letters within a column indicates significant difference among samples by Tukey's test ($p<0.05$).

The CS and HG coacervates exhibited good antioxidant activity determined by DPPH radical scavenging assay, 74.2 ± 8.5 and 116.9 ± 5.2 mg TE L^{-1}, respectively. PPI and EvO showed the highest values for antioxidant activity, 158.9 ± 10.5 and 236.8

± 5.9 mg TE L^{-1}. Pu et al. (2019) found that different CS concentrations, 0.01 – 0.3% (w/v), exhibited an antioxidant activity by DPPH radical scavenging ranging from around 2 to 30%. Agboola et al. (2010) determined a value for antioxidant activity of PPI by DPPH of 1.89 ± 0.23 mmol TE 100 g^{-1} (in dry basis). In another work, the PPI antioxidant capacity by DPPH radical scavenging reported by Morales-Polanco et al. (2017) was of 13.37 ± 6.66 mmol TE g^{-1}.

Hadidi et al. (2021) found the antioxidant activity of unloaded and loaded hyssop EOs in CS:PPI nano-complexes at different concentrations and found values ranging from 7.7–54.5% and 8.1–66.5%, respectively. These authors also determined the DPPH radical scavenging activities for CS and PPI under different concentrations as being relatively mild, around 10%. Moroccan and Spanish olive oil cultivars exhibited an antioxidant power around 0.2 to 0.4 µM g^{-1} and 0.67 to 1.52 mmol of TE kg^{-1} of EvO, by the studies of El Haouhay et al. (2015) and Borges et al. (2019), respectively.

5.3. Chitosan composite films

5.3.1. Characterization of the CS-composite films

The casting method was used to produce chitosan composite films plasticized with a DES (1:2 ChCl:Gly) and incorporated with different amounts (0-10%) of açaí PECs. The produced films had a visible yellow-gold transparent appearance without any opaque aspect or cracks as can be visualized in Figure 61. The unplasticized chitosan film, F0/0 (0% DES and 0% açaí PECs), was visibly more brittle, transparent, and thinner than the others, as expected (PEREIRA, ANDRADE, 2017).

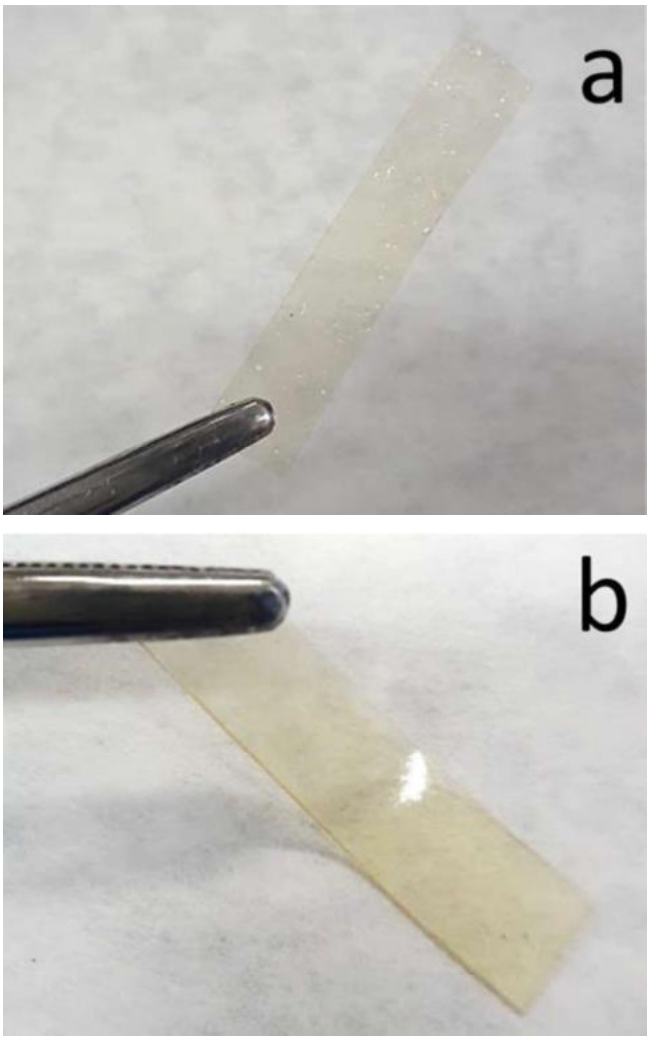

Figure 61. Digital pictures of (a) F0/0 (0% DES and 0% açaí PECs) and (b) F5/0 (5% DES and 0% açaí PECs) films.

The films were stored in a vacuum desiccator under room temperature for more than a year. After this time, the films were removed to observe its visual aspect. The CS-based films did not exhibit any visual appearance of microbial contamination or

signs of deterioration, such as darkening or opaque aspects, cracks, or frostbites (Figure 62). Thus, this result suggests their good stability under storage conditions.

Figure 62. Digital pictures of the CS-DES-based films. F0/0: 0% DES and 0% açaí PECs; F5/0: 5% DES and 0% açaí PECs; F5/0.25: 5% DES and 0.25% açaí PECs; F5/0.5: 5% DES and 0.5% açaí PECs; F5/1: 5% DES and 1% açaí PECs; F5/2: 5% DES and 2% açaí PECs; F5/5: 5% DES and 5% açaí PECs and F5/10: 5% DES and 10% açaí PECs.

5.3.2. Microstructural observations

The OM, SEM and CLSM techniques were used to observe the microstructure of the films and to confirm the presence of the açaí PECs in it, as follows.

5.3.2.1. Optical microscopy - OM

The OM examinations were performed in the film-forming solutions (prior drying) and allowed the visualization of the incorporated açaí PECs (Figure 63a-b). With this simple technique, it was possible to observe the presence and size distribution of the particles, which displayed different sizes as well as its shapes. In Figure 63a, it was observed some particles with irregular shapes, which most probably were crushed by the pressure of top glass slide that covered the film-forming solution during the analyses. Figure 63b shows the rounded and smoothed shapes of the açaí CS:SA PECs.

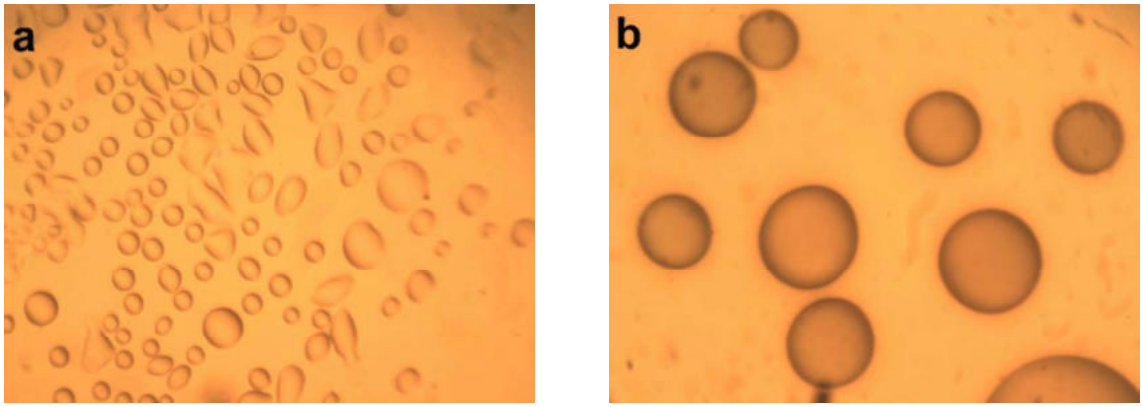

Figure 63. Optical microscopy observations of CS-DES film-forming solution, F5/10 (5% DES and 10% açaí PECs) at 10X (a) and 40X (b) magnification.

5.3.2.2. Scanning electron microscopy - SEM

The SEM cross-sections observations were performed on the cryo-fractured films as presented in Figure 64. The control film, F0/0, were visibly thinner than the others (Figure 64a). This was expected since the addition of plasticizers to biopolymers increases the free volume and intermolecular spaces of its matrix (RIVERO et al., 2016). Except for the films F5/5 (Figure 64g) and F5/10 (Figure 64h), all the others presented a dense continuous and smooth surface (Figure 64b-f), which can be an indication of good miscibility between the components as well as to the CS film-forming ability (PEREIRA, ANDRADE, 2017; RIVERO et al., 2016; SHI et al., 2016).

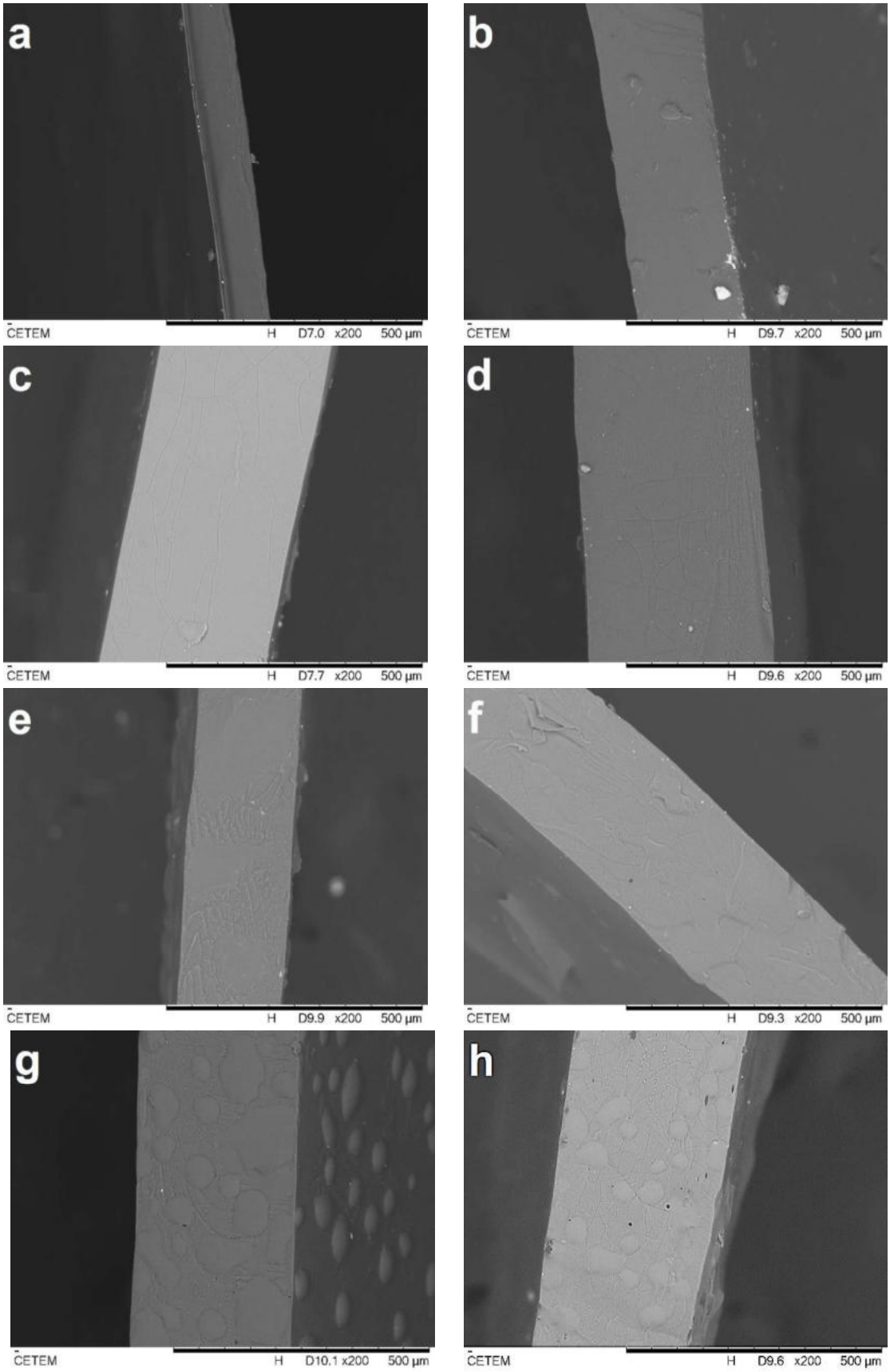

Figure 64. SEM observations from the cross-section of F0/0 (a), F5/0 (b), F5/0.25 (c), F5/0.5 (d), F5/1 (e), F5/2 (f), F5/5 (g) and F5/10 (h) films at 200X magnification.

The presence of the PECs with size < 370 μm may have contributed to the roughness in films F5/5 (Figure 64g) and F5/10 (Figure 64h). It is possible to observe a high distribution of the açaí microparticles in the cross-section of these films, appearing as rounded shades. In these figures, it is also possible to observe larger particles that may have formed during drying by coalescence or aggregation. Dammak et al. (2017) observed a similar behavior in gelatin composite films incorporated with rutin microparticles. These authors revealed that the pure gelatin film (control) had a lower surface roughness, whereas films incorporated with the rutin microparticles presented a rougher surface and some flaws.

5.3.2.3. Confocal laser scanning microscopy - CLSM

The CSLM is widely used to observe compounds and biological cells stained with different fluorescent dyes. Although microscopy analyses are often used to visualize samples surface, the CLSM allows the deep observation inside the bulk of the film due to fluorescent labels (DANG, YOKSAN, 2016). The CLSM examinations at 10X magnification of the CS-DES films incorporated with açaí PECs are displayed in Figure 65. The films were stained with 2 drops of a 1 mg mL^{-1} of Nile Red in DMSO solution, and let to react for approximately 3 min, then observed by CSLM. This technique was used to evaluate the incorporation as well as the distribution of the açaí PECs in the plasticized CS films. It was possible to observe the presence of açaí PECs dyed in fluorescent green incorporated into the CS-DES films, which appeared in black. Nile red was used to dye açaí oil because it has a great ability to stain lipid droplets inside biological cells as well as biopolymers complexes, allowing a good detection of particles by fluorescence (SILVA et al., 2020a).

Figure 62a shows the CS-plasticized unloaded film (F5/0) at 10x magnification. It was observed the absence of fluorescence, which confirms that no particle was incorporated. Besides, this can be considered as a negative control to compare with the other stained films. The frequency of these complexes rises upon their increasing proportions in the films, F5/0 (Figure 65a) < F5/10 (Figure 65f). A more meticulously observation at different focal planes revealed some PECs aggregation and a heterogenous distribution in the films within the increasing amount these particles F5/0.25 (Figure 65b) > F5/10 (Figure 65f). This behavior could be the result of water evaporation during drying, leading the particles to aggregate.

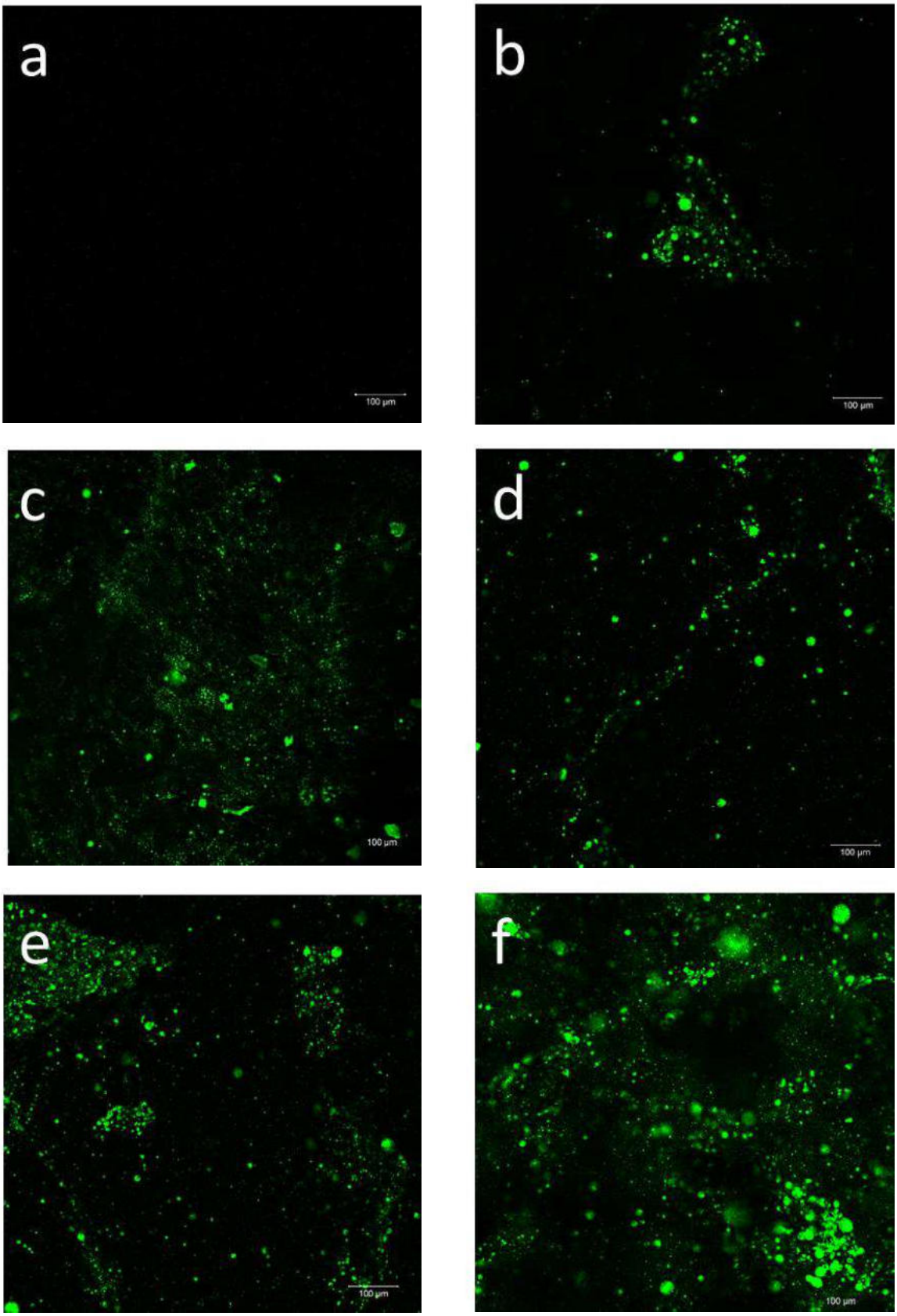

Figure 65. Selected 2D micrographs by CSLM for CS-DES films, F5/0 (a), F5/0.25 (b), F5/0.5 (c), F5/2 (d), F5/5 (e) and F5/10 (f) at 10X magnification. The encapsulated açaí oil in the PECs appears in green whereas the CS-DES based matrix appears in black.

Furthermore, it was also possible to observe particles standing upon each other in different layers of the film, resulting in a more condensed and overloaded image of them (SILVA et al. 2020a). Moreover, other magnifications at 20x and 40x were selected to better observe the particles morphology on the CS-composite films with higher incorporation of açaí PECs, as can be visualized in Figure 66.

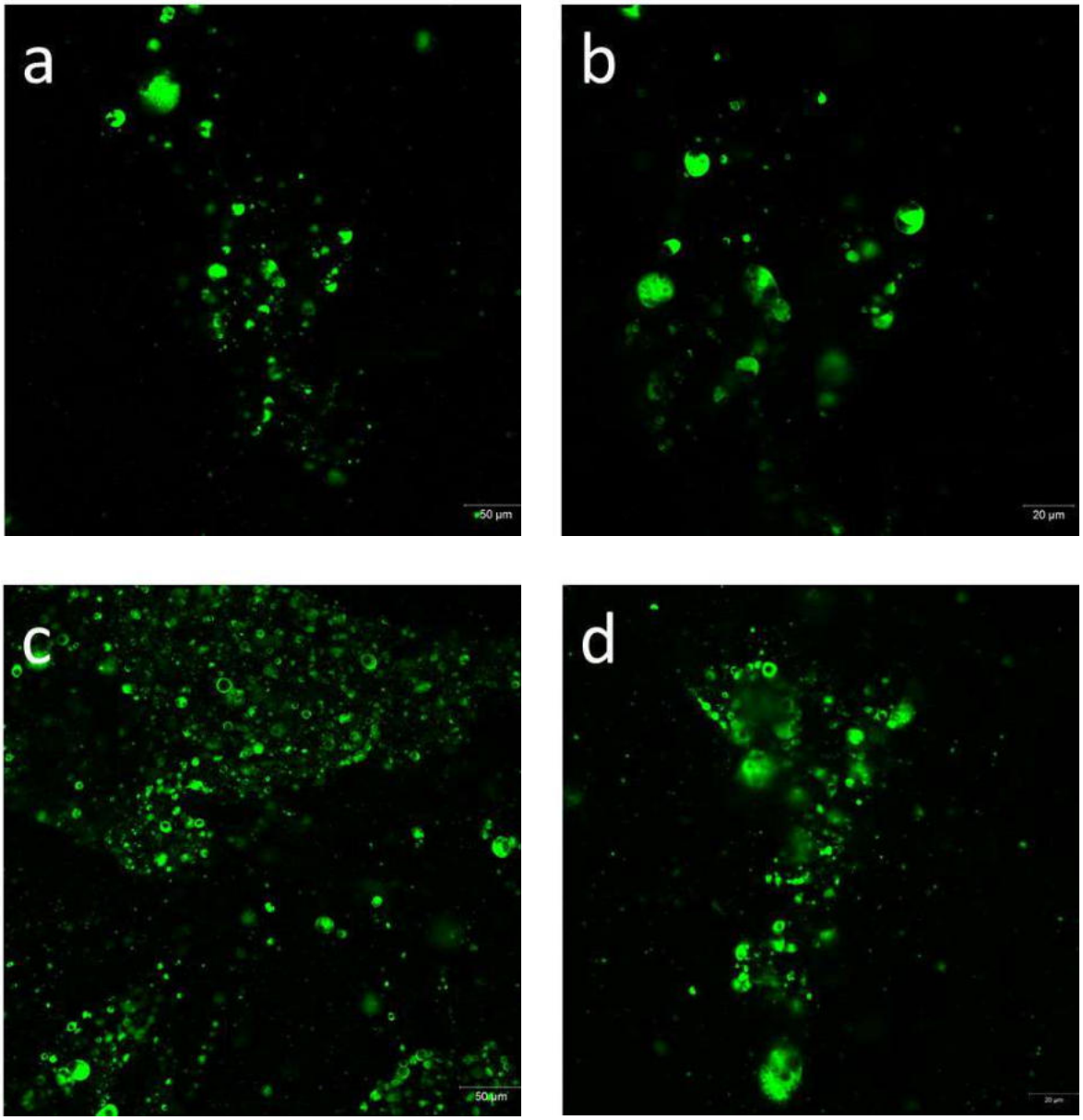

Figure 66. Selected 2D micrographs from CSLM from CS-DES films, (a) F5/2 at 20x, (b) F5/2 at 40x, (c) F5/5 at 20x, and (d) F5/10 at 40x magnifications. The açaí oil encapsulated in the PECs appears in green whereas the CS-DES based films appear in black.

It was noted from Figure 66a-d that the PECs exhibited spherical-like structures, similarly to vacuoles containing the açaí oil (stained in green), which is a typical

behavior of coacervates (MOSCHAKIS, BILIADERIS, 2017). Similar observations were found by Silva et al. (2020a) when studying by CSLM the morphology of stained chitosan/virgin coconut oil-based emulsion films. These authors found that at lower oil concentration, the CS films exhibited a more homogenous distribution of the lipid droplets. Furthermore, they observed that as the coconut oil concentration increased, the occurrence of aggregates or bigger oily particles also increased, possibly because of changes in interfacial tension of the emulsion droplets during film drying.

5.3.3. Thickness and water vapor permeability (WVP) of the films

The WVP of biobased films is linked to the exchange of moisture that goes from the environment or the coated food through the films. For this reason, the film thickness is an important factor that influences WVP. The thickness and the WVP of the CS-DES based films incorporated with different contents of bioactive açaí PECs are present in Table 28.

Table 28. Thickness and WVP for CS-DES films incorporated with açaí PECs.

Sample	Thickness (μm)	WVP (g m^{-1} s^{-1} Pa^{-1})
F0/0	0.16 ± 0.02^{c}	$1.1\times10^{-10} \pm 1.0\times10^{-11c}$
F5/0	0.19 ± 0.03^{bc}	$1.9\times10^{-10} \pm 9.9\times10^{-12bc}$
F5/0.25	0.36 ± 0.02^{a}	$3.9\times10^{-10} \pm 3.2\times10^{-11a}$
F5/0.5	0.34 ± 0.01^{a}	$3.4\times10^{-10} \pm 2.3\times10^{-11ab}$
F5/1	0.33 ± 0.01^{a}	$3.9\times10^{-10} \pm 5.3\times10^{-11a}$
F5/2	0.27 ± 0.05^{abc}	$4.2\times10^{-10} \pm 9.9\times10^{-11a}$
F5/5	0.28 ± 0.04^{abc}	$2.9\times10^{-10} \pm 5.0\times10^{-12ab}$
F5/10	0.29 ± 0.06^{ab}	$3.4\times10^{-10} \pm 4.0\times10^{-11ab}$

Results are expressed as mean ± standard deviation. Different superscript letters within a column indicate a significant difference among samples by Tukey's test ($p<0.05$).

The WVP rises with the increase in PECs content in the films. The films without PECs presented the lowest WVP when compared to the others. The F0/0 film formulated without DES or PECs exhibited the lowest WVP, 1.1×10^{-10} g m^{-1} s^{-1} Pa^{-1} ($p<0.05$). This result is similar to the value of 1.08×10^{-10} g m^{-1} s^{-1} Pa^{-1} found by Rivero et al. (2016) for unplasticized chitosan films. These same authors found that the

addition of 0.25% of plasticizer in CS films significantly increased its WVP. However, at the present work, the CS film plasticized with 5% of DES, sample F5/0, did not present significant difference ($p<0.05$) in WVP when compared to the F0/0 film.

The WVP for the films incorporated with the PECs were significantly higher than the films without it. This may be explained by increment in the thickness and PECs, which could modify the polymer network, decreasing the density or local viscosity, and giving more mobility to diffusing molecules through the films (WANG, QIAN, DING, 2018; DAMMAK et al., 2017). Furthermore, the reduction of film barrier properties may happen with the incorporation of vegetable oils (MUJTABA et al., 2019). Films based on polysaccharides and lipids are reported to display WVP values ranging from 0.7 to 4.0 $\times 10^{-10}$ g m^{-1} s^{-1} Pa^{-1}, which is the range of our findings (DAMMAK et al., 2017).

5.3.4. Fourier transform infrared spectroscopy (FTIR)

Infrared spectroscopy was used to investigate the molecular structure of the CS-based films, as well as the interactions occurring between CS, DES and açaí PECs incorporated in them. The FTIR spectra of these materials are displayed in Figure 67 and Figure 68a-b and the wavenumber of their respective bands are listed in Table 29.

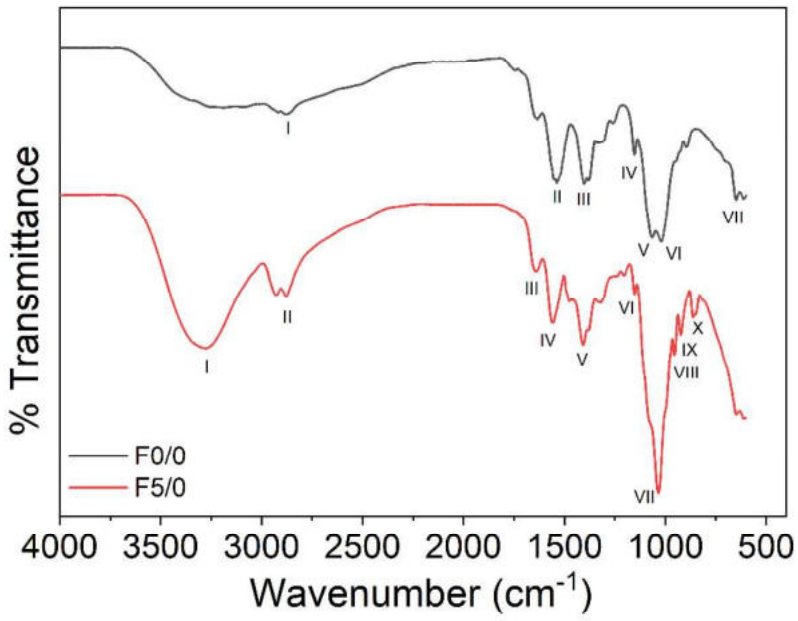

Figure 67. FTIR spectra for pure CS (F0/0) and CS-DES (F5/0) films.

The spectrum for pure CS film, F0/0, presented high intensity bands associated to N−H bending (amide II), C−O symmetric stretching vibrations, C–O–C antisymmetric stretching, C−O stretching and C–H bending (rocking) vibrations, as associated to the bands at 1538 cm^{-1}, 1403 cm^{-1}, 1066 cm^{-1}, 1021 cm^{-1} and 649 cm^{-1}, respectively (Figure 67, black line) (LAWRIE et al., 2007; PEREIRA, ANDRADE, 2017). In the F5/0 film, it was noteworthy that the addition of DES (Gly:ChCl) to the CS films produced broad bands around 3290 cm^{-1} and 1034 cm^{-1} related to O−H and C−O stretching, respectively (Figure 67, red line). These changes can be attributed to the formation of hydrogen bonds between CS and DES or also by the –O-H···Cl− bonds between Gly and ChCl in DES (SOKOLOVA et al., 2018).

The FTIR spectrum of the CS-composite films displayed in Figure 68a-b are quite similar to the patterns of F5/0 film. These results are in accordance with the literature (SOKOLOVA et al., 2018; PEREIRA, ANDRADE, 2017). It is worth saying that the bands attributed to amide I and amide II were changed from 1650 cm^{-1} and 1590 cm^{-1} to lower wavenumbers, around 1640 cm^{-1} and 1558 cm^{-1}, which suggest an interaction between the components of the CS-composite films. This behavior was also observed by Pereira and Andrade (2017) in the CS-DES-curcumin films. Moreover, some notation in F5/2 film can be point out as it presented slighted different bands when compared to the others (Table 29).

Table 29. List of prominent FTIR bands of the CS-based films.

Sample	Bands at wavenumber (cm^{-1})										
	I	II	III	IV	V	VI	VII	VIII	IX	X	XI
F0/0	2876	1538	1403	1153	1066	1021	649	-	-	-	-
F5/0	3279	2878	1640	1557	1407	1151	1034	955	923	863	-
F5/0.25	3280	2928	1642	1559	1408	1152	1035	955	923	863	-
F5/0.5	3277	2879	1640	1556	1408	1152	1033	955	923	863	-
F5/1	3281	2929	1642	1559	1408	1035	955	923	863	-	-
F5/2	3281	2879	1743	1641	1558	1408	1153	1035	955	923	863
F5/5	3282	2925	1641	1559	1408	1152	1034	955	923	863	-
F5/10	3278	2926	1641	1556	1407	1152	1034	955	923	863	-

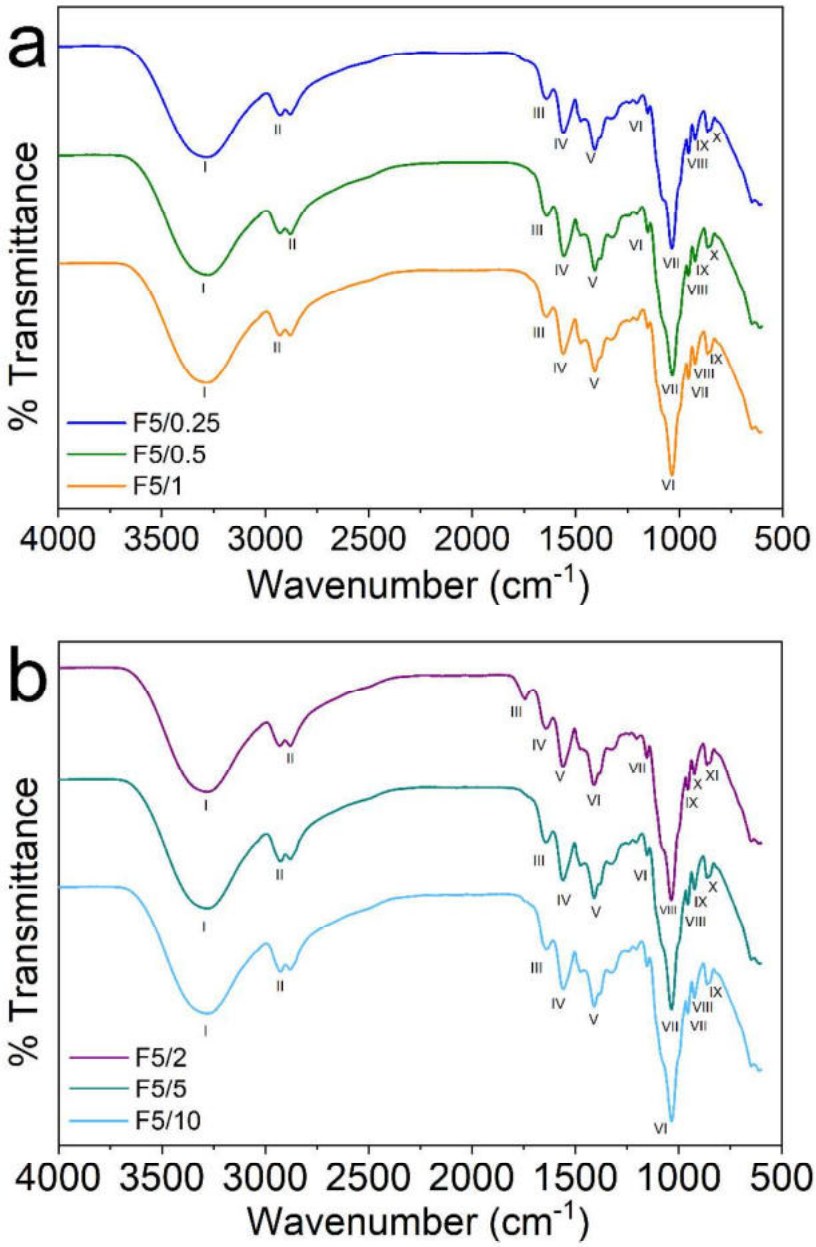

Figure 68. FTIR spectra for CS-composite films, (a) F5/0.25, F5/0.5 and F5/1, and (b) F5/2, F5/5 and F5/10.

In the F5/2 film, the low intensity band that appeared around 1743 cm^{-1} may be associated to C=O stretching vibration of ester carbonyl functional groups from the açaí oil or to the presence of DES. The association of this band to the açaí oil can be recognized as it is frequently linked to triglycerides (ROHMAN, MAN, 2010). Even though, the presence of this band was also reported by Sokolova et al. (2018) in the plasticized CS-DES films with malonic acid and ChCl, which were linked to the mol excess of malonic acid over CS. Likewise, Delgado-Mellado et al. (2018) have also

reported a band around 1715 – 1734 cm^{-1} in the FTIR/ATR spectra of different DES mixtures.

5.3.5. X-ray diffraction (XRD)

The XRD analyses were performed to evaluate the changes in the amorphous and crystalline structures of the CS composite films Figure 69. The diffractograms showed that the CS composite films display a semicrystalline structure. Pure chitosan film, F0/0, showed three strong reflections around 2θ values of 11.5°, 18.4° and 23.3° (Figure 69a). The peak around 11.5° confirms that CS films presented a semicrystalline structure, which may be related to the hydrated crystalline structure of CS due to the integration of water molecules in its crystal lattice (MOALLA et al., 2021; PEREIRA, ANDRADE, 2017; QIAO et al., 2021). The peaks around 2θ values of 18.4° and 23.3° can be assigned to the crystal lattice and to the amorphous structure of CS, respectively (MADIAN, MOHAMED, 2020). This last peak was cited as being a typical fingerprint in chitosan films by Sun et al. (2017).

XRD patterns for the CS films have changed with the addition of DES. The main characteristic observed in these diffractograms is the decrease in crystallinity in the plasticized CS films when compared to the unplasticized, F0/0. The peak in the region 2θ = 11.5° was significantly weakened with the addition of DES, as can be visualized in the diffractogram for plasticized CS films (Figure 69). This phenomenon can be justified by the loss of hydrogen bonds between amino and hydroxyl groups in CS due to complexation with the plasticizer, which results in the increase in the amorphous structure of CS-DES films. Wong et al. (2018) also observed that the addition of DES to chitosan-carboxymethylcellulose films significantly reduced the intensity of the reflection at 2θ = 12.9°. The F5/0 film exhibited only one broad peak around 2θ values of 20.4° (Figure 69a). This behavior was also observed in the other films, which displayed only one broad peak at 2θ = ~20°, as can be visualized in Figure 69b-c.

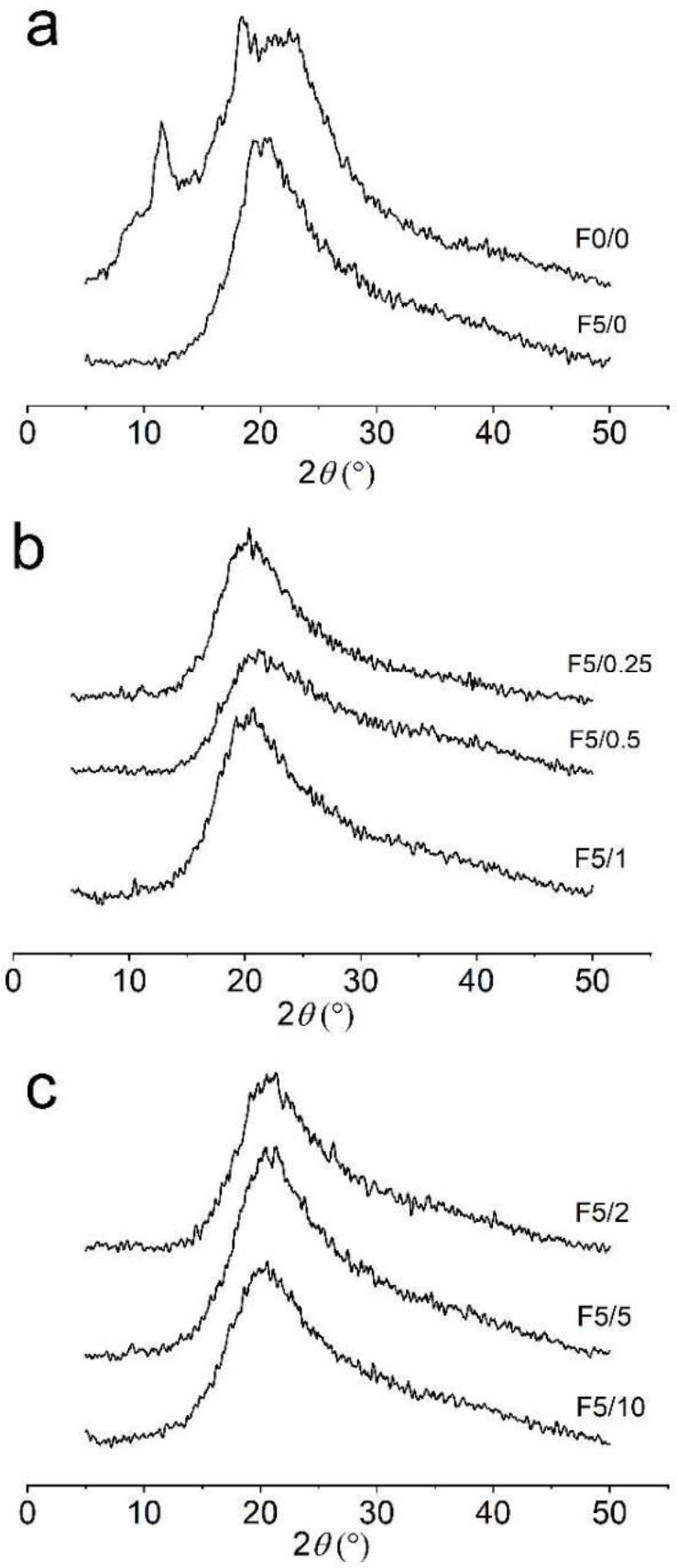

Figure 69. XRD patterns of the CS composite films.

The crystallinity degree (CrD) of the films was estimated as the ratio percentage of crystalline and amorphous areas, and the results are listed in Table 30. The pure CS film displayed an estimated CrD close to 8%. This result is close to the CrD value of ~7% determined for chitosan-based films by Silva et al. (2020b). These authors also found a much higher value of CrD around 44% for chitosan powder. Escárcega-Galaz et al., (2018) found that CS films at 2% concentration showed a degree of crystallinity around 9.2% and, when glycerol was added, this value changed to 8%. In other works, CS-based films exhibited higher values of crystallinity degree ranging from 37.8 to 46%, which presented a DA of 85 and 88%, respectively (LIU et al., 2013; REN et al., 2017).

Table 30. Estimated crystallinity degree (%) of chitosan composite films.

Sample	Estimated CrD (%)
F0/0	7.95
F5/0	4.35
F5/0.25	4.45
F5/0.5	4.13
F5/1	3.93
F5/2	4.94
F5/5	5.23
F5/10	5.74

The estimated CrD decreased with the addition of plasticizer and the açaí PECs. The film F5/1 presented the lowest crystallinity degree, close to 4%. As the composition in plasticizer was kept constant at 5% in the CS-DES films, it was possible to suggest that the addition of açaí PECs influenced their CrD. Furthermore, it was notable that the addition of 2, 5 and 10% (F5/2, F5/5 and F5/10) of açaí PECs in the films may have contributed to increase the CrD up to ~6%, although this is a lower value than the CrD of F0/0. This result corroborates the hypothesis that açaí PECs may interact with the CS matrix, resulting in a more organized structure and enhanced crystallinity. Moreover, this hypothesis is also supported by the results of mechanical properties

found for those same film samples, which displayed a lower elasticity as discussed in the following topics.

5.3.6. Mechanical properties

The mechanical properties, tensile strength (TS), elongation at break (EB or ε_{max}) and Young's modulus (YM or *E*), of the CS-DES based films incorporated with açaí PECs at different ratios are shown in Table 31. The TS and EB are the most important mechanical characteristics for film applications (VAN DEN BROEK et al., 2015). TS is correlated to the maximum tensile stress sustained by the film (SUN et al., 2020). The control film, F0/0 displayed a TS value around 11 MPa. Benbettaïeb, Karbowiak, Debeaufort (2017) reported a TS value for pure chitosan film around 16 MPa.

Table 31. TS, EB and YM of CS-DES based films.

Sample	Tensile strength (MPa)	Elongation at break (%)	Young's Modulus (MPa)
F0/0	11.0 ± 1.5^{a}	0.60 ± 0.1^{d}	2927 ± 154^{a}
F5/0	0.74 ± 0.07^{b}	36.4 ± 1.9^{c}	1.7 ± 0.1^{b}
F5/0.25	1.20 ± 0.04^{b}	89.2 ± 3.7^{a}	1.7 ± 0.4^{b}
F5/0.5	1.26 ± 0.16^{b}	99.3 ± 4.5^{a}	1.6 ± 0.4^{b}
F5/1	1.13 ± 0.24^{b}	83.0 ± 9.6^{a}	1.7 ± 0.2^{b}
F5/2	1.47 ± 0.31^{b}	103.6 ± 8.4^{a}	1.7 ± 0.2^{b}
F5/5	0.63 ± 0.16^{b}	52.0 ± 7.1^{b}	1.4 ± 0.3^{b}
F5/10	0.66 ± 0.08^{b}	$49.3 \pm 2.3^{b,c}$	1.35 ± 0.06^{b}

Results are expressed as mean ± standard deviation (n = 3). Different superscript letter within a column indicates a significant difference among samples by Tukey's test ($p<0.05$).

The addition of DES significantly affected the mechanical properties of the films when comparing to the F0/0 and the F5/0 (Figure 70). This behavior was expected since it is well known that plasticizers change the mechanical properties of films by increasing the matrix free volume and reducing the interchain interactions along the polymers chains (MKANDAWIRE, ARYEE, 2018; RIVERO et al., 2016). This performance was also observed by Almeida et al. (2018) when studying CS-based

films plasticized with DES (ChCl:Lactic acid 1:1) and incorporated with curcumin. These authors observed that the TS decrease from ~43.3 to 13.2 in CS-based films with the addition of up to 30% of DES. In the work of Pereira and Andrade (2017), the addition of DES as plasticizer in chitosan-based films decreased the TS from ~24 to ~20 MPa, although a significant decrease in TS was obtained using glycerol. In general, the addition of DES as well as the açaí-PECs decreased the TS when compared to the unplasticized control film, F0/0. Observing only the plasticized CS-based films, it was noted that the incorporation of açaí PECs had no significant effect on TS ($p>0.05$). In the work of Ma et al. (2015), the incorporation of 0-3% of cinnamon:soybean oil microemulsions in chitosan films decreased TS from ~627 to ~27 MPa.

EB is the maximum length variation (%) before rupture of the film under stress and is an important information related to its stretchability and deformation. The EB for the unplasticized film, F0/0, was around 0.6% and significantly increased to ~36% with the addition of DES, F5/0 ($p<0.05$) (Figure 70a). The increase in deformation of chitosan-based films plasticized with ChCl:LA DES was also observed by Almeida et al. (2018). The authors noted an increase in EB value from around 2 to 20, when the DES concentration was of 30%. Moreover, the incorporation of açaí PECs positively affected the EB, which reached the highest value around 104% for the F5/2 film ($p<0.05$) (Figure 70b). It was also seen that beyond 2% of PECs incorporation, the films exhibited a lower EB value (Figure 70c). This effect can be related to a higher interference on CS-DES continuous network by the highest amount of PECs. Above 2%, the addition of PECs seems to disrupt the matrix continuity and promote fragility.

The YM value is related to the ratio between stress and strain, and it measures the rigidity of films through the ability to resist variations in length under tension or compression (KAMDEM, SHEN, NABINEJAD, 2019). The YM of pure chitosan films was close to 3000 MPa, whereas the CS-DES films exhibited significantly lower values, less than 2 MPa ($p<0.05$). Thus, the addition of DES produced fewer rigid films than pure chitosan. It was observed that between the plasticized films, the YM decreased with the increase of PECs, although no significant difference was observed ($p>0.05$). This result is in accordance with the previously presented EB values, which suggested that CS-DES films incorporated with açaí PECs were more flexible than those of pure chitosan.

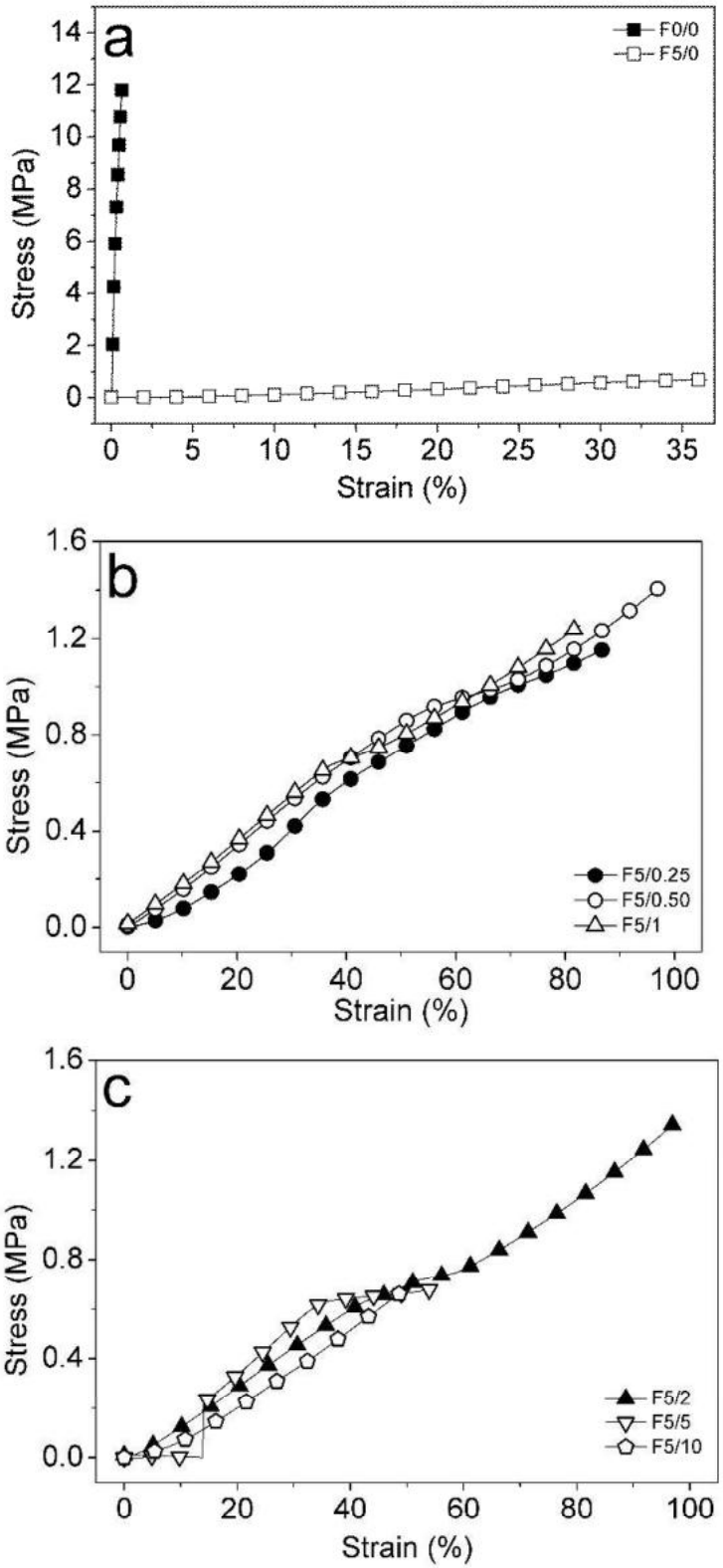

Figure 70. Stress versus strain curves for films: (a) F0/0 (full squares) and F5/0 (open squares); (b)F5/0.25 (full circles), F5/0.5 (circles), F5/1 (triangles); (c) F5/2 (full triangles), F5/5 (upside down triangles) and F5/10 (lozenges).

5.3.7. Dynamic mechanical analyses (DMA)

The DMA was used to investigate the dynamic mechanical performance of the pure CS and the plasticized composite CS films in a temperature ranging from -50 to 300°C. DMA investigates the viscoelastic behavior of polymeric films. The results from this can be either expressed by the loss modulus (E'') and the storage modulus (E'), or as the loss factor or tan delta (tan δ) versus temperature. Moreover, E' represents the elastic behavior, whereas E'' symbolizes the viscous behavior of the film. In turn, tan δ can be defined as the ratio between the E''/ E', where δ is the angle between in- and out-of-phase components of the modulus in cyclic motion (GUERRERO et al., 2019). The DMA patterns of the films expressed as the variation of the tan δ as a function of temperature are shown in Figure 71.

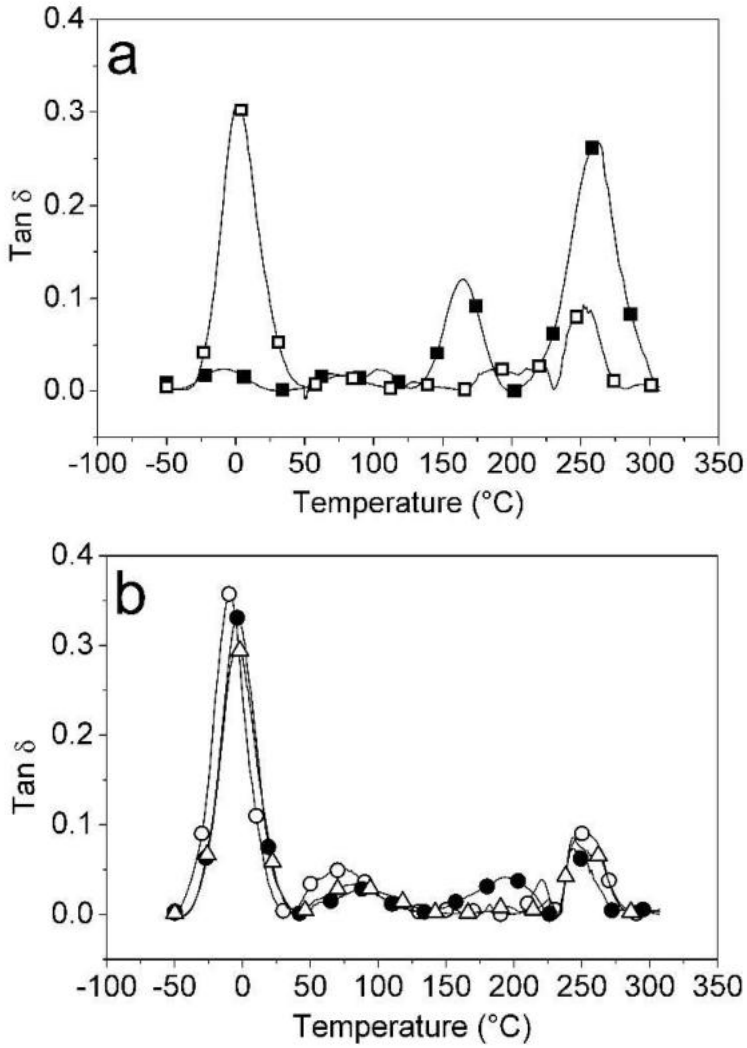

Figure 71. Variation of tan delta with temperature for films: (a) F0/0 (full squares) and F5/0 (open squares); (b) F5/0.5 (open circles), F5/2 (full circles) and F5/10 (open triangles).

The F0/0 film (pure CS film) presented three peaks attributed to the γ, β and α transitions, which are associated to conformational relaxations of the amorphous phase (Figure 71a). The first transition, γ, generally occurs at low temperature with the polymer in the glass state and is associated to the relaxation of small side and terminal groups. It is possible to observe that the DES addition promoted a shift in the γ transition from -8°C in F0/0 (pure CS) to 2°C in the F5/0 films, associated to the plasticizing effect in the CS structure. The β transition temperature in the F0/0 was observed around 165 °C, while in the CS-DES films this peak was weakened and became wider. This could be associated to the interactions of CS and DES which suppressed the orderliness of CS molecular chains and reduced its crystallinity. This effect was also observed by Tuhin et al. (2012) in the CS-starch-Gly-mustard oil films.

The maximum temperature of the peak of tan *δ* in the F0/0 film was close to 263 °C, whereas in the plasticized CS-composite films ranged from -9.2 to 2.2 °C (Figure 71b). This result confirms the plasticizing effect of the DES on the CS-composite films, as the tan *δ* shifted in the CS-DES films because of an increased amorphous structure of CS. Moreover, the tan δ value and the E' at 25°C of the films are listed in the Table 32.

Table 32. E' (MPa) at 25 °C and Tan *δ* (°C) of the CS-based films.

Sample	E' (MPa) at 25 °C	Tan *δ* (°C)		
		$Peak_1$	$Peak_2$	$Peak_3$
F0/0	211.3	-8.1	165.3	263
F5/0	2.65	2.2	188	254
F5/0.5	1.13	-9.2	72	252
F5/2	0.91	-4.5	88.5	254
F5/10	0.98	-3.4	86.3	254

In these results is possible to note an intense decreasing effect on the E' values at 25 °C with the addition of DES in the CS films. This indicates the relaxations of the CS chains promoted by the plasticizer, which are also in accordance with the findings of XRD analyses, which showed a decrease in CS crystallinity with the DES addition to the films. Pereira and Andrade (2017) also found three peaks of tan δ at −1.5 °C, 73.9 °C and 166.8 °C for pure CS film.

5.3.8. Thermogravimetric analysis (TGA)

The TGA and its derivative (DTG) curves investigated under nitrogen atmosphere and temperature ranging from 25 to 700 °C were used to evaluate the thermal behavior of the CS-based films. The TGA and DTG curves are shown in Figure 72 and Figure 73a-c. The TGA and DTG data, initial temperature of degradation (T_{onset}), maximum temperature of degradation (T_{peak}) and percentage of residue at 700 °C for the CS-based films, are listed in Table 33.

Table 33. TGA and DTG data of CS-based films.

Sample	T_{onset} (°C)	T_{peak} (°C)	Residue (%) at 700°C
F0/0	241.3	294.2	32.44
F5/0	169.9	281.4	16.40
F5/0.25	201.8	256.1	12.59
F5/0.5	173.9	253.5	11.49
F5/1	192.8	252.9	10.98
F5/2	171.3	254.8	13.22
F5/5	174.6	246.3	12.38
F5/10	182.2	251.8	12.64

From these results, it is possible to observe that the F0/0 film presented a thermal degradation behavior occurring in two steps (Figure 72). The first step of weight loss ranged from around 100 to 200°C, which can be attributed to water evaporation (KAMDEM, SHEN, NABINEJAD, 2019; SOKOLOVA et al., 2018). The second mass loss ranged from around 200 up to 400 °C, which is correlated to the thermal decomposition of chitosan, through the dehydration of glycosidic rings and its chain depolymerization (PEREIRA, ANDRADE, 2017; SARMENTO et al., 2006). T_{peak} of F0/0 was close to the value of ~290 °C and ~300 °C observed by Kamdem, Shen, Nabinejad (2019) and Sokolova et al. (2018), respectively, in pure CS films.

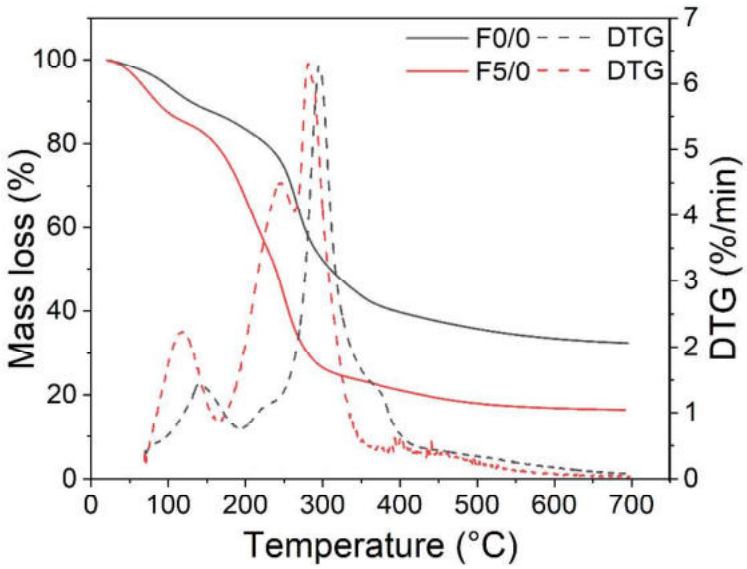

Figure 72. TGA (continuous lines) and DTG (dashed lines) curves for CS-based films, F0/0 - F5/0.

It is noteworthy that the T_{onset} in the plasticized CS film, F5/0, occurred at a lower temperature due to the influence of DES on the CS chain mobility, resulting in a decreased thermal stability of the film (Figure 72). This plasticizing behavior reflects on T_{onset} of the CS-composite films, which decreased from ~240°C in F0/0 to ~170°C in F5/0 films. Observing the DTG curve for F5/0 film, it was noted a bimodal behavior as a shoulder, on the main peak ranged from around 170 – 350°C due to the overlapping of CS decomposition region with the DES. This effect was also observed by Sokolova et al. (2018) in CS films plasticized with different proportions of DES, malonic acid:ChCl.

Thermal degradation behavior of the CS-DES films occurred mainly in two steps, as can be visualized in Figure 73a-c. The decreasing in the thermal behavior was also observed to the CS-composite films incorporated with açaí PECs, which displayed the second event at T_{onset} ranging from 201 to 182°C in F5/0.25 and F5/10 films, respectively (Figure 73a-c). This result suggests that the CS-composite films degrade at higher temperatures than the F5/0 film. The improvement of the thermal stability observed for the composite films indicates the effect of AO microcapsules, since the DES content was kept constant. The T_{peak} in the composite films was slightly different, ranging from 256 to ~251 °C.

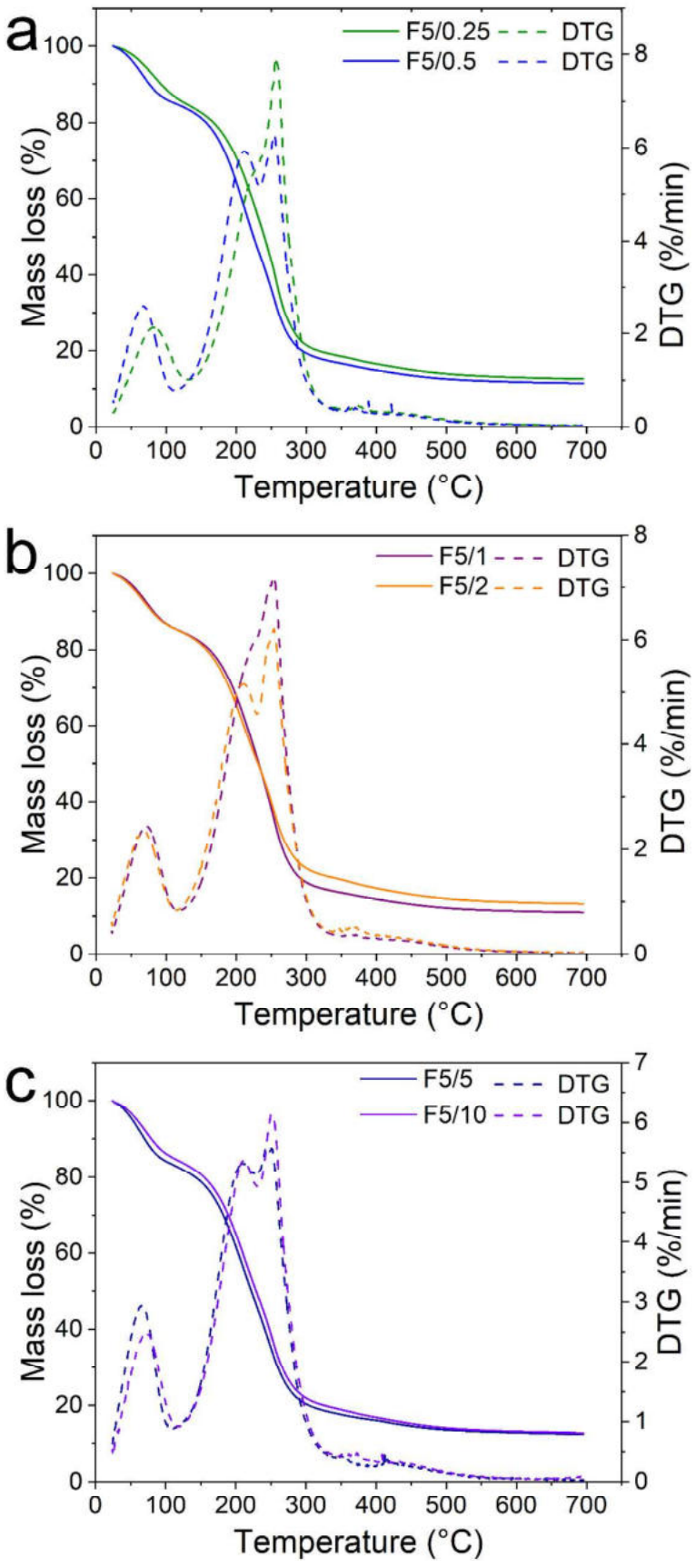

Figure 73. TGA (straight) and DTG (dash) curves of CS-based films, F5/0.25 - F5/0.5 (a), F5/1 - F5/2 (b), and F5/5 - F5/10 (c).

5.3.9. Determination of total polyphenols and antioxidant activity of the films

The *in vitro* evaluation of bioactive compounds to food application has gained attention due to potential applicability to preservation against oxidative agents. In this work, the *in vitro* antioxidant activity of CS-based films was determined using SET methods, such as TPC by using Folin-Ciocalteu reagent, the FRAP, TEAC by using ABTS reagent, and DPPH radical scavenging assays. To these determinations, an aqueous ethanolic (40:60 v/v) extract from the film samples (~10 mg mL^{-1}) were prepared, and the results were expressed as mg g^{-1} of film.

The TPC of CS-based films was determined employing the Folin-Ciocalteu reagent assay. The results were calculated using a linear regression (Equation 28) obtained from the standard gallic acid curve, expressed as mg of gallic acid equivalent (GAE) per g^{-1} of film.

$$Total\ polyphenols\ content = \frac{Absorbance_{sample} - 0.0696}{0.0031} \quad R^2 = 0.9988 \qquad (28)$$

The result from the antioxidant activity by TPC for the CS-based films expressed as mean (column) ± standard deviation (bar) (n=3) is presented in the Figure 74.

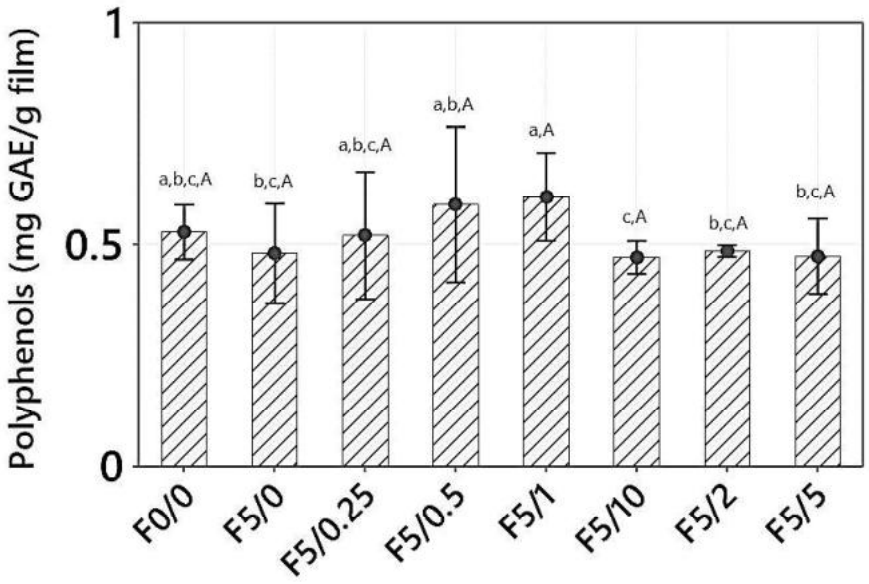

Figure 74. Total polyphenols content for the CS-based films. Different lowercase (a,b,c) or uppercase (A,B,C) letters within a column indicates significant difference among samples by Tukey's test or Dunnett's test, respectively ($p<0.05$).

The CS-based films exhibited a low value of TPC, ranging from 0.47 to 0.61 mg of GAE g^{-1} of film. It was noted that the film F5/1 presented the highest TPC value, followed by F5/0.5. However, no significant statistical difference was observed among all films, either by the Tukey or Dunnett's test ($p>0.05$), as can be observed in Figure 74. Likewise, this result reflects the efficient açaí oil encapsulation addition on the CS-composite films on preserving its bioactivity to be further released in a potential food application. Moreover, it has been reported that CS films display a low value of TPC, < 2 mg GAE g^{-1} (RUIZ-NAVAJAS et al., 2013; SIRIPATRAWAN, HARTE, 2010; SIRIPATRAWAN, VITCHAYAKITTI, 2016). This mild scavenging property is due to the interaction of free radicals with the residual free amino groups ($-NH_2$) from CS forming ammonium groups ($-NH_3^+$) (SIRIPATRAWAN, VITCHAYAKITTI, 2016). The AO exhibited an antioxidant activity determined by TPC of 256.05 ± 57.45 mg GAE L^{-1}. This value was approximately three time higher than EvO, which was around 83 mg GAE L^{-1}.

The FRAP of the CS-based films was determined using a standard curve of Trolox, calculated using a linear regression (Equation 29) and expressed as mg of Trolox equivalent per g of sample. The antioxidant activity of the CS-based films determined by FRAP assay are presented in the Figure 75. The results were expressed as mean (column) ± standard deviation (bar) (n=3).

$$FRAP\ (\text{mg TE g}^{-1}) = \frac{Absorbance_{sample} - 1.7515}{0.0033} \quad R^2 = 0.9979 \quad (29)$$

The antioxidant power of CS-based films ranged from ~0.5 to 1.0 mg TE g^{-1} of film. The control sample, F0/0 presented an antioxidant value around 0.5 mg TE g^{-1} of film, whereas the F5/10 presented a value two times higher. These results are in accordance with the studies of Ruiz-Navajas et al. (2013), that found an antioxidant power by FRAP of 0.21 mg TE g^{-1} in pure CS film. Besides, it was observed that the antioxidant power of the films significantly increased with the increase in incorporated açaí PECs ($p<0.05$). When taking the F0/0 film as control, the films F5/0.5, F5/1, F5/2, F5/5 and F5/10 were statistically different ($p<0.05$ by Dunnett's test).

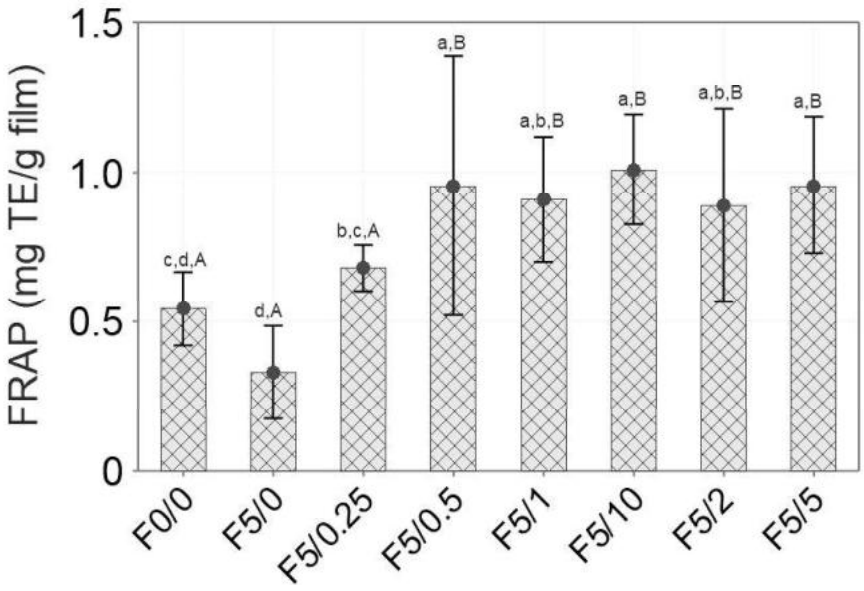

Figure 75. Antioxidant power (mg TE g^{-1} film) by FRAP assay of the CS-based films. Different lowercase (a,b,c) or uppercase (A,B,C) letters within a column indicates significant difference among samples by Tukey's test or Dunnett's test, respectively ($p<0.05$).

Cuevas-Acuña et al. (2020) studied the antioxidant properties of chitosan-gelatin composite films by FRAP, and found values ranging from ~300 to 600 µmol TE mg^{-1} of film. In another study, conjugated chitosan grafted with stearic acid and gallic acid exhibits an antioxidant activity by FRAP assay, expressed as $IC_{50,}$ ranging from ~141 to 367 µg mL^{-1} (YANG, LIU, LIN, 2017). As the antioxidant activity of a particular material is measured by a specific assay, their results are the reflection of the chemical reactivity under conditions applied in those cases (SHAHIDI, ZHONG, 2015). Because of this, it is a hard task to compare and generalize data, since researchers are free to express their results by different means, i.e., as mg of TE g^{-1}, mg TE L^{-1}, IC_{50}, and as percentage of inhibition and antioxidant capacity (%).

The TEAC for the CS-based films using the ABTS radical reagent was determined using a Trolox standard curve. The results from this assay were calculated using a liner regression (Equation 30) and expressed as mg of Trolox equivalent per g of film and are presented in the Figure 76. These results were expressed as mean (column) ± standard deviation (bar) (n=3).

$$TEAC\ (\mathrm{mg\ TE\ g^{-1}}) = \frac{Absorbance_{sample} + 0.6783}{0.0019} \quad R^2 = 0.9912 \qquad (30)$$

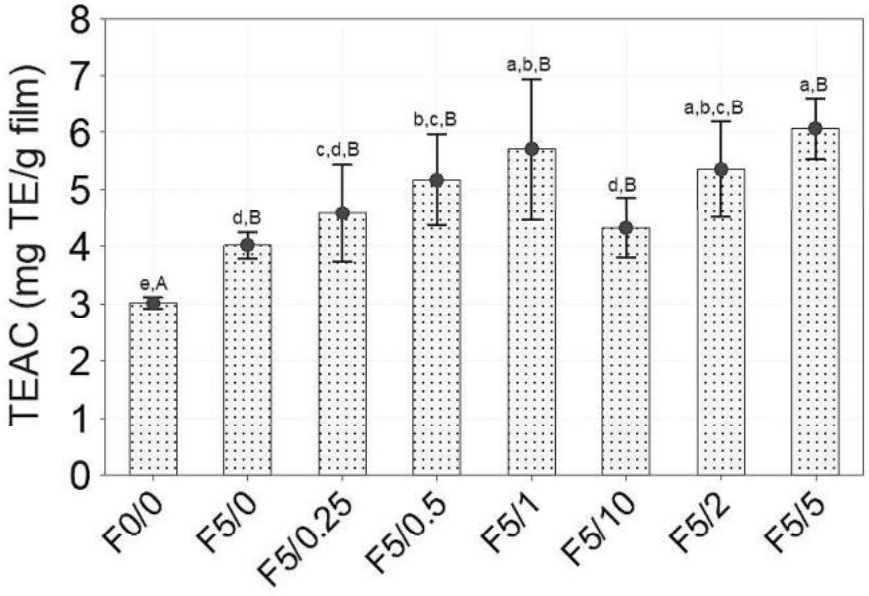

Figure 76. Antioxidant capacity (mg TE g^{-1} film) by TEAC assay for the CS-based films. Different lowercase (a,b,c) or uppercase (A,B,C) letters within a column indicates significant difference among samples by Tukey's test or Dunnett's test, respectively ($p<0.05$).

The antioxidant activity for the CS-based films ranged from around 3 to 6 mg TE g^{-1} of film. The CS-composite films incorporated with açaí PECs were almost two times higher than the control, F0/0, exhibiting a significant difference between them ($p<0.05$ Dunnett's test). The film F5/5 exhibited the highest antioxidant capacity, followed by F5/1 and F5/2. Thus, it is possible to suggest that the açaí PECs contributed to increase the antioxidant activity of the CS-based films. Different researchers have studied antioxidant properties of CS-based films incorporated with different bioactive substances. Some recent works related to antioxidant capacity of CS-based films against ABTS radical are presented below.

Cuevas-Acuña et al. (2020) studied the antioxidant properties of chitosan-gelatin composite films using the ABTS radical scavenging assay, and found values ranging from ~200 to 900 µmol TE mg^{-1} of film. In another work, CS film incorporated with mango leaf extract presented an antioxidant capacity by ABTS radical scavenging assay ranging from ~2 to 8 µg GAE g^{-1} film (RAMBABU et al., 2019). CS/gelatin composite films incorporated with gallic acid presented an antioxidant capacity against ABTS radical ranging from 20 to 60% (RUI et al., 2017).

In this work, the antioxidant capacity against the DPPH radical was determined using a Trolox standard curve, calculated using a liner regression (Equation 31). The

results from this assay were expressed as mg of Trolox equivalent per g of film and are presented in Figure 77.

$$DPPH \cdot\ scavenging\ (\text{mg TE}\ g^{-1}) = \frac{Absorbance_{sample} - 0.3622}{0.0011} \quad R^2 = 0.9991 \quad (31)$$

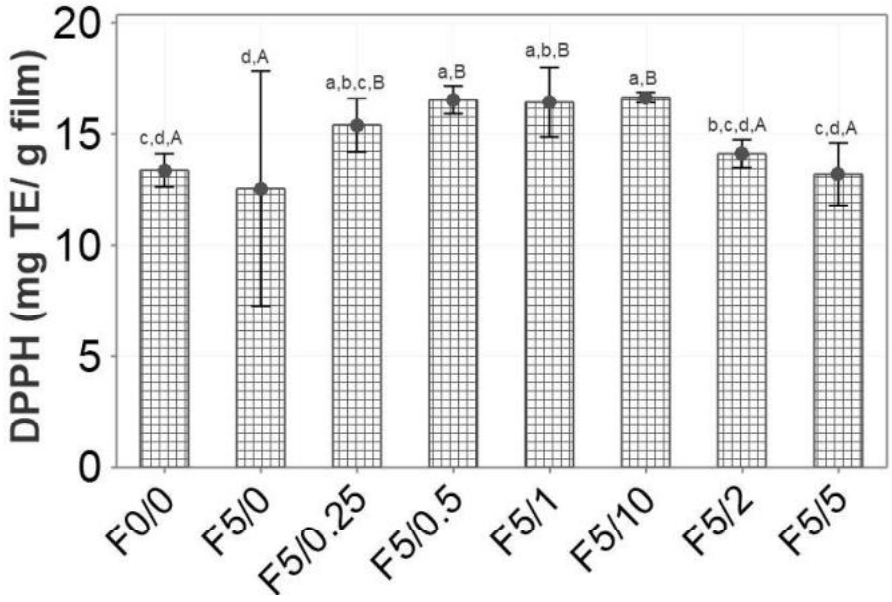

Figure 77. Antioxidant capacity (mg TE g^{-1} film) by DPPH assay for the CS-based films. Different lowercase (a,b,c) or uppercase (A,B,C) letters within a column indicates significant difference among samples by Tukey's test or Dunnett's test, respectively ($p<0.05$).

The CS-based films displayed an antioxidant activity against the DPPH radical ranging from around 13 to 17 mg TE g^{-1} of film. These values were higher than the findings of antioxidant power by DPPH assay of 0.003 mg TE g^{-1} in pure CS film by Ruiz-Navajas et al. (2013). Additionally, it was noted that the CS-composite films with higher açaí PECs exhibited highest antioxidant activity against DPPH. The F5/10 film was significantly more antioxidant than the control, F0/0 ($p<0.05$ by Tukey and Dunnett's test). In another work, MORADI et al. (2012) found that CS film displayed an antioxidant capacity against DPPH radical around 10%. Rui et al. (2017) found that CS film presents a DPPH radical antioxidant capacity around 15% and by ABTS assay around 20%. Riaz et al. (2018) determined the antioxidant activity of CS-based films incorporated with apple peel polyphenols by DPPH and ABTS radical scavenging, which ranged from 20 to 95 %. Another work that incorporated young apple

polyphenols in CS films found values of DPPH radical scavenging activity ranging from 35 to 95% (SUN et al., 2017).

In the work of Siripatrawan and Vitchayakitti (2016) the antioxidant activity by DPPH assay for CS-based films incorporated with propolis exhibited values ranging from around 5 to 55%. When incorporated with green tea extract, CS-based films displayed a DPPH scavenging activity ranging from around 2 to 50% (SIRIPATRAWAN, HARTE, 2010). Furthermore, the açaí oil studied in this work displayed an antioxidant activity against the DPPH radical of 101.8 ± 8.2 mg TE L^{-1} oil. Another study by Rufino et al. (2011) found that açaí oil has an antioxidant activity around 2056.25 g of oil g^{-1} of DPPH, expressed as EC_{50}. Thus, the antioxidant activity determined for the CS-composite films incorporated with açaí PECs may have contributed to the bioactivity of films.

6. CONCLUSIONS

The present study obtained different active lipid carriers based on the formation of complexes between chitosan and alginate (CS:SA), and chitosan and pea protein isolate (CS:PPI) to encapsulate açaí oil (AO) and extra-virgin olive oil (EvO), respectively. These materials are biobased, biocompatible, environmentally friendly, generally recognized as safe to food application and are obtained from renewable sources. The formulation of these microparticles was optimized using central composite experimental designs and response surface methodology. The formation of these complexes was significantly influenced by their composition, amount of core material and cross-linking agent, concentration of polysaccharide, ratio between polysaccharide:protein. The microparticles based on CS and SA were efficiently formed to encapsulation of AO, displaying up to 99.9% of encapsulation efficiency. The optimized system CS:SA-AO PECs, 0.5% AO and 0.5% $CaCl_2$, exhibited good rheological and stability properties, as well as a high antioxidant activity, up to 78% by the DPPH radical scavenging. Similarly, the microparticles based on CS and PPI were obtained to encapsulate EvO, although this lipid carriers displayed an exceedingly small size than the other systems. The optimum CS:PPI-EvO systems, 0.75% of CS, 2.31 CS:PPI ratio and 0.5% EvO, also showed high in vitro antioxidant properties determined by the DPPH radical scavenging assay, around 120 mg TE L^{-1}. Both microencapsulation systems have demonstrated to be an effective approach to encapsulate bioactive lipids. The açaí loaded microparticles were selected and incorporated in chitosan-composite films. Chitosan based films are naturally biodegradable, a cost-effective alternative and produces environmentally friendly food packaging. Chitosan films were obtained by casting their film-forming solutions, plasticized with a deep eutectic solvent based on chlorine chloride:glycerol and incorporated with different amounts of açaí loaded microparticles. These films were physicochemically characterized and exhibited good vapor barrier properties, flexibility, thermostability and antioxidant properties against the DPPH radical, around 17 mg TE g^{-1} of film. Thus, their potential application as active food packaging can be suggested.

7. REFERENCES

ABBOTT, A. P.; BOOTHBY, D.; CAPPER, G.; DAVIES, D. L.; RASHEED, R. K. Deep eutectic solvents formed between choline chloride and carboxylic acids: versatile alternatives to ionic liquids. **Journal of the American Chemical Society**, 126, p. 9142–9147, 2004.

ABBOTT, A. P.; HARRIS, R. C.; RYDER, K. S.; D'AGOSTINO, C.; GLADDEN, L. F.; MANTLE, M. D. Glycerol eutectics as sustainable solvent systems. **Green Chemistry**, 13, p. 82–90, 2011.

ABDEL-RAHMAN, R. M.; HRDINA, R.; ABDEL-MOHSEN, A. M.; FOUDA, M. M. G.; SOLIMAN, A. Y.; MOHAMED, F. K.; MOHSIN, K.; PINTO, T. D. Chitin and chitosan from Brazilian Atlantic coast: Isolation, characterization and antibacterial activity. **International Journal of Biological Macromolecules**, 80, p.107–120, 2015.

ABUGOCH, L. E.; TAPIA, C.; VILLAMÁN, M. C.; YAZDANI-PEDRAM, M.; DÍAZ-DOSQUE, M. Characterization of quinoa protein–chitosan blend edible films. **Food Hydrocolloids**, 25, p. 879–886, 2011.

ACQUAH, C.; ZHANG, Y.; DUBÉ, M. A.; UDENIGWE, C. C. Formation and characterization of protein-based films from yellow pea (*Pisum sativum*) protein isolate and concentrate for edible applications. **Current Research in Food Science**, 2, p. 61–69, 2020.

ADEBIYI, A. P.; ALUKO, R. E. Functional properties of protein fractions obtained from commercial yellow field pea (*Pisum sativum* L.) seed protein isolate. **Food Chemistry**, 128, p. 902–908, 2011.

AFZAL, S.; MASWAL, M.; DAR, A. A. Rheological behavior of pH responsive composite hydrogels of chitosan and alginate: Characterization and its use in encapsulation of citral. **Colloids and Surfaces B: Biointerfaces**, 169, p. 99–106, 2018.

AGBOOLA, S. O.; MOFOLASAYO, O. A.; WATTS, B. M.; ALUKO, R. E. Functional properties of yellow field pea (*Pisum sativum* L.) seed flours and the in vitro bioactive properties of their polyphenols. **Food Research International**, 43, p. 582–588, 2010.

AGÜERO, L.; ZALDIVAR-SILVA, D.; PEÑA, L.; DIAS, M. Alginate microparticles as oral colon drug delivery device: A review. **Carbohydrate Polymers**, 168, p. 32–43, 2017.

ALMEIDA, C. M. R.; MAGALHÃES, J. M. C. S.; SOUZA, H. K. S.; GONÇALVES, M. P. The role of choline chloride-based deep eutectic solvent and curcumin on chitosan films properties. **Food Hydrocolloids**, 81, p. 456–466, 2018.

ALOMAR, M. K.; HAYYAN, M.; ALSAADI, M. A.; AKIB, S.; HAYYAN, A.; HASHIM, M. A. Glycerol-based deep eutectic solvents: Physical properties. **Journal of Molecular Liquids**, 215, p. 98–103, 2016.

AMINE, C.; DREHER, J.; HELGASON, T.; TADROS, T. Investigation of emulsifying properties and emulsion stability of plant and milk proteins using interfacial tension and interfacial elasticity. **Food Hydrocolloids**, 39, p. 180–186, 2014.

ANNU, P.; RAJA, A. N. Recent development in chitosan-based electrochemical sensors and its sensing application. **International Journal of Biological Macromolecules**, 164, p. 4231–4244, 2020.

ANSORENA, M. R.; ZUBELDÍA, F.; MARCOVICH, N. E. Active wheat gluten films obtained by thermoplastic processing. **LWT - Food Science and Technology**, 69, p. 47–54, 2016.

ANVISA - Agência Nacional de Vigilância Sanitária. *In* **Alegações de propriedade funcional aprovadas pela ANVISA**. Available at https://www.gov.br/agricultura/pt-br/assuntos/inspecao/produtos-vegetal/legislacao-1/biblioteca-de-normas-vinhos-e-bebidas/alegacoes-de-propriedade-funcional-aprovadas_anvisa.pdf/view Accessed on May 10, 2021.

AS YOU SOW. 2021. Press-releases – **After dialogue with As You Sow, Keurig Dr Pepper agrees to 20% cut in virgin plastic use**. Available at <https://www.asyousow.org/press-releases/2021/4/12/after-dialogue-with-as-you-sow-keurig-dr-pepper-agrees-to-20-cut-in-virgin-plastic-use?utm_medium=email&utm_source=rasa_io&PostID=28618185&MessageRunDetailID=4922559192> accessed on April 26, 2021.

ASSAD I.; BHAT, S. U.; GANI, A.; SHAH, A. Protein based packaging of plant origin: Fabrication, properties, recent advances and future perspectives. **International Journal of Biological Macromolecules**, 164, p. 707–716, 2020.

ASTM (2016). American Society for Testing and Materials. Standard E096M-16, **Standard Test Methods for Water Vapor Transmission of Materials 1**. West Conshohocken, PA, USA: ASTM International, 2016, pp. 1–10, Available at <https://doi.org/10.1520/E0096_E0096M-16>, accessed on June 2020.

ASTM. American Society for Testing and Materials. Standard D 996 – 04, **Standard Terminology of Packaging and Distribution Environments**. Philadelphia, PA, USA: ASTM International, 2004, pp. 1-12.

AUGUSTIN, M. A.; HEMAR, Y. Nano- and micro-structured assemblies for encapsulation of food ingredients. **Chemical Society Reviews**, 38, p. 902–912, 2009.

AZEVEDO, V. M.; BORGES, S. V.; MARCONCINI, J. M.; YOSHIDA, M. I.; NETO, A. R. S.; PEREIRA, T. C.; PEREIRA, C. F. G. Effect of replacement of corn starch by whey protein isolate in biodegradable film blends obtained by extrusion. **Carbohydrate Polymers**, 157, p. 971–980, 2017.

AZEVEDO, V. M.; DE OLIVEIRA, A. C. S.; BORGES, S. V.; RAGUZZONI, J. C.; DIAS, M. V.; COSTA, A. L. R. Pea protein isolate nanocomposite films for packaging applications: effect of starch nanocrystals on the structural, morphological, thermal, mechanical and barrier properties. **Emirates Journal of Food and Agriculture**, 13, p. 495-504, 2020.

BARAC, M.; CABRILO, S.; PESIC, M.; STANOJEVIC, S.; ZILIC, S.; MACEJ, O.; RISTIC, N. Profile and functional properties of seed proteins from six pea (*Pisum sativum*) genotypes. **International Journal of Molecular Sciences**, 11, p. 4973–4990, 2010.

BARRETO, C.; OLIVEIRA, E. Para além de potes e panelas: cerâmica e ritual na Amazônia antiga. **Habitus**, 14, p. 51-72, 2016. Available at <https://doi.org/10.18224/hab.v14.1.2016.51-72>, accessed on April 22, 2021.

BASTARRACHEA, L.; DHAWAN, S.; SABLANI, S. S. Engineering Properties of Polymeric-Based Antimicrobial Films for Food Packaging: A Review. **Food Engineering Reviews**, 3, p. 79–93, 2011.

BASTOS, D. S.; BARRETO, B. N.; SOUZA, H. K. S.; BASTOS, M.; ROCHA-LEÃO, M. H. M.; ANDRADE, C. T.; GONÇALVES, M. P. Characterization of a chitosan sample extracted from Brazilian shrimps and its application to obtain insoluble complexes with a commercial whey protein isolate. **Food Hydrocolloids**, 24, p. 709–718, 2010.

BAŞYIĞIT, B.; YÜCETEPE, M.; KARAASLAN, A.; KARAASLAN, M. High efficiency microencapsulation of extra virgin olive oil (EVOO) with novel carrier agents: Fruit proteins. **Materials Today Communications**, 28, n. 102618, p. 1-10, 2021.

BATISTA, C. C. R.; OLIVEIRA, M. S.; ARAÚJO, M. E.; RODRIGUES, A. M. C.; BOTELHO, J. R. S.; SILVA SOUZA FILHO, A. P.; MACHADO, N. T.; CARVALHO, R. N. Supercritical CO_2 extraction of açaí (*Euterpe oleracea*) berry oil: Global yield, fatty acids, allelopathic activities, and determination of phenolic and anthocyanins total compounds in the residual pulp. **The Journal of Supercritical Fluids**, 107, p. 364–369, 2016.

BAYBAŞ, D.; SERDAROĞLU, G.; SEMERCI, B. The composite microbeads of alginate, carrageenan, gelatin, and poly(lactic-co-glycolic acid): Synthesis, characterization and density functional theory calculations. **International Journal of Biological Macromolecules**, 181, p. 322–338, 2021.

BECK, S. M.; KNOERZER, K.; ARCOT, J. Effect of low moisture extrusion on a pea protein isolate's expansion, solubility, molecular weight distribution and secondary structure as determined by Fourier Transform Infrared Spectroscopy (FTIR). **Journal of Food Engineering**, 214, p. 166–174, 2017.

BEDADE, D. K.; SUTAR, Y. B.; SINGHAL, R. S. Chitosan coated calcium alginate beads for covalent immobilization of acrylamidase: Process parameters and removal of acrylamide from coffee. **Food Chemistry**, 275, p. 95–104, 2019.

BENBETTAÏEB, N.; KARBOWIAK, T.; DEBEAUFORT, F. Bioactive edible films for food applications: Influence of the bioactive compounds on film structure and properties. **Critical Reviews in Food Science and Nutrition**, 8398, p. 1–17, 2017.

BERGER, K. R.; WELT, B. A Brief History of Packaging. *In* **EDIS - Electronic Data Information Source of University of Florida.** Institute of Food and Agricultural Sciences, University of Florida, Issue 17, 2005, pp. 1–5. Available at <https://doi.org/10.32473/edis-ae206-2002> accessed on April 21, 2021.

BONILLA, F.; CHOULJENKO, A.; REYES, V.; BECHTEL, P. J.; KING; J. M.; SATHIVEL, S. Impact of chitosan application technique on refrigerated catfish fillet quality. **LWT - Food Science and Technology**, 90, p. 277–282, 2018

BORGES, T. H.; SERNA, A.; LÓPEZ, L. C.; LARA, L.; NIETO, R.; SEIQUER, I. Composition and antioxidant properties of Spanish extra virgin olive oil regarding cultivar, harvest year and crop stage. **Antioxidants**, 8, n. 217, p. 1-16, 2019.

BRAND-WILLIAMS, W.; CUVELIER, M. E.; BERSET, C. Use of a Free Radical Method to Evaluate Antioxidant Activity. **LWT - Food Science and Technology**, 28, p. 25–30, 1995.

BRODY, A. L.; BUGUSU, B.; HAN, J. H.; SAND, C. K.; MCHUGH, T. H. Innovative Food Packaging Solutions. **Journal of Food Science**, 73, p. 107–116, 2008.

BRUGNEROTTO, J.; DESBRIÈRES, J.; ROBERTS, G.; RINAUDO, M. Characterization of chitosan by steric exclusion chromatography. **Polymer**, 42, p. 09921–09927, 2001.

BRUNTON, N. P.; MASON, C.; COLLINS, M. J. Rapid microwave assisted preparation of fatty acid methyl esters for the analysis of fatty acid profiles in foods. **Journal of Analytical Chemistry**, 70, p. 1218–1224, 2015.

BURGER, T. G.; ZHANG, Y. Recent progress in the utilization of pea protein as an emulsifier for food applications. **Trends in Food Science & Technology**, 86, p. 25–33, 2019.

BUSCHMANN, A. H.; CAMUS, C.; INFANTE, J.; NEORI, A.; ISRAEL, Á.; HERNÁNDEZ-GONZÁLEZ, M. C.; PEREDA, S. V.; GOMEZ-PINCHETTI, J. L.; GOLBERG, A.; TADMOR-SHALEV, N.; CRITCHLEY, A. T. Seaweed production: overview of the global state of exploitation, farming and emerging research activity. **European Journal of Phycology,** 52, p. 391–406, 2017.

CALDERÓN-OLIVER, M.; PEDROZA-ISLAS, R.; ESCALONA-BUENDÍA, H. B.; PEDRAZA-CHAVERRI, J.; PONCE-ALQUICIRA, E. Comparative study of the microencapsulation by complex coacervation of nisin in combination with an avocado antioxidant extract. **Food Hydrocolloids,** 62, p. 49–57, 2017.

CAMPOS, C. A.; GERSCHENSON, L. N.; FLORES, S. K. Development of Edible Films and Coatings with Antimicrobial Activity. **Food and Bioprocess Technology**, 4, p. 849–875, 2011.

CAMPOS, E.; BRANQUINHO, J.; CARREIRA, A. S.; CARVALHO, A.; COIMBRA, P.; FERREIRA, P.; GIL, M. H. Designing polymeric microparticles for biomedical and industrial applications. **European Polymer Journal**, 49, p. 2005–2021, 2013.

CARDOSO, G. P.; DUTRA, M. P.; FONTES, P. R.; RAMOS, A. L. S.; GOMIDE, L. A. M.; RAMOS, E. M. Selection of a chitosan gelatin-based edible coating for color preservation of beef in retail display. **Meat Science**, 114, p. 85–94, 2016.

CARINA, D.; SHARMA, S.; JAISWAL, A. K.; JAISWAL, S. Seaweeds polysaccharides in active food packaging: A review of recent progress. **Trends in Food Science & Technology**, 110, p. 559–572, 2021.

CARNEIRO-DA-CUNHA, M. G.; CERQUEIRA, M. A.; SOUZA, B. W. S.; TEIXEIRA, J. A.; VICENTE, A. A. Influence of concentration, ionic strength and pH on zeta potential and mean hydrodynamic diameter of edible polysaccharide solutions envisaged for multinanolayered films production. **Carbohydrate Polymers**, 85, p. 522–528, 2011.

CAROCHO, M.; HELENO, S.; RODRIGUES, P.; BARREIRO, M. F.; BARROS, L.; FERREIRA, I. C. F. R. A novel natural coating for food preservation: Effectiveness on microbial growth and physicochemical parameters. **LWT - Food Science and Technology**, 104, p. 76–83, 2019.

CARPENTIER, J.; CONFORTO, E.; CHAIGNEAU, C.; VENDEVILLE, J.-E.; MAUGARD, T. Complex coacervation of pea protein isolate and tragacanth gum: Comparative study with commercial polysaccharides. **Innovative Food Science & Emerging Technologies**, 69, n. 102641, p. 1-12, 2021.

CARVALHO, A. V.; SILVEIRA, T. F. F.; MATTIETTO, R. A.; OLIVEIRA, M. DO S. P.; GODOY, H. T. Chemical composition and antioxidant capacity of açaí (*Euterpe oleracea*) genotypes and commercial pulps. **Journal of the Science of Food and Agriculture**, 97, p. 1467–1474, 2017.

CAZÓN, P.; VELAZQUEZ, G.; RAMÍREZ, J. A.; VÁZQUEZ, M. Polysaccharide-based films and coatings for food packaging: A review. **Food Hydrocolloids**, 68, p. 136–148, 2017.

CHAKRAVARTULA, S. S. N.; SOCCIO, M.; LOTTI, N.; BALESTRA, F.; DALLA ROSA, M.; SIRACUSA, V. Characterization of composite edible films based on pectin/alginate/whey protein concentrate. **Materials**, 12, n. 2454, p. 1-19, 2019.

CHEN, C.; PENG, X.; ZENG, R.; CHEN, M.; WAN, C.; CHEN, J. *Ficus hirta* fruits extract incorporated into an alginate-based edible coating for Nanfeng mandarin preservation. **Scientia Horticulturae**, 202, p. 41–48, 2016.

CHEVALIER, E.; CHAABANI, A.; ASSEZAT, G.; PROCHAZKA, F.; OULAHAL, N. Casein/wax blend extrusion for production of edible films as carriers of potassium sorbate — A comparative study of waxes and potassium sorbate effect. **Food Packaging and Shelf Life**, 16, p. 41–50, 2018.

COCA-COLA. The Coca-Cola Company®. 2019. **News – DASANI boots sustainability credentials with launch of recyclable, reusable and package-less innovations**. Available at < https://www.coca-colacompany.com/news/dasani-boosts-sustainability-credentials> accessed on April 26, 2021.

COCA-COLA. The Coca-Cola Company®. 2021. Sustainable Business – **Sustainable Packaging Design. Make 100% of our packaging recyclable globally by 2025**. Available at <https://www.coca-colacompany.com/sustainable-business/packaging-sustainability/design> accessed on April 26, 2021.

COMUNIAN, T. A.; FAVARO-TRINDADE, C. S. MICROENCAPSULATION using biopolymers as an alternative to produce food enhanced with phytosterols and omega-3 fatty acids: A review. **Food Hydrocolloids**, 61, p. 442–457, 2016.

CONZATTI, G.; FAUCON, D.; CASTEL, M.; AYADI, F.; CAVALIE, S.; TOURRETTE, A. Alginate/chitosan polyelectrolyte complexes: A comparative study of the influence of the drying step on physicochemical properties. **Carbohydrate Polymers**, 172, p. 142–151, 2017.

COSTA, H. C. B.; SILVA, D. O.; VIEIRA, L. G. M. Physical properties of açai-berry pulp and kinetics study of its anthocyanin thermal degradation. **Journal of Food Engineering**, 239, p. 104–113, 2018.

COSTA, J. C. M.; MIKI, K. S. L.; RAMOS, A. S.; TEIXEIRA-COSTA, B. E. Development of biodegradable films based on purple yam starch/chitosan for food application. **Heliyon**, 6, p. 1–10, 2020.

COSTA, M. J.; MARQUES, A. M.; PASTRANA, L. M.; TEIXEIRA, J. A.; SILLANKORVA, S. M.; CERQUEIRA, M. A. Physicochemical properties of alginate-based films: Effect of ionic crosslinking and mannuronic and guluronic acid ratio. **Food Hydrocolloids**, 81, p. 442–448, 2018.

CRINI, G. Historical review on chitin and chitosan biopolymers. **Environmental Chemistry Letters**, 17, p. 1623–1643, 2019.

CROGUENNEC, T.; TAVARES, G. M.; BOUHALLAB, S. Heteroprotein complex coacervation: A generic process. **Advances in Colloid and Interface Science**, 239, p. 115–126, 2017.

CUEVAS-ACUÑA, D. A.; RUIZ-CRUZ, S.; ARIAS-MOSCOSO, J. L.; LOPEZ-MATA, M. A.; ZAMUDIO-FLORES, P. B.; BURRUEL-IBARRA, S. E.; CARMEN SANTACRUZ-ORTEGA, H. Effects of the addition of ultrasound-pulsed gelatin to chitosan on physicochemical and antioxidant properties of casting films. **Polymer International**, 69, p. 423–428, 2020.

DAMMAK, I.; BITTANTE, A. M. Q. B.; LOURENÇO, R. V.; SOBRAL, P. J. DO A. Properties of gelatin-based films incorporated with chitosan-coated microparticles charged with rutin. **International Journal of Biological Macromolecules**, 101, p. 643–652, 2017.

DANG, K. M.; YOKSAN, R. Morphological characteristics and barrier properties of thermoplastic starch/chitosan blown film. **Carbohydrate Polymers**, 150, p. 40–47, 2016.

DEKA, C.; DEKA, D.; BORA, M. M.; JHA, D. K.; KAKATI, D. K. Synthesis of peppermint oil-loaded chitosan/alginate polyelectrolyte complexes and study of their antibacterial activity. **Journal of Drug Delivery Science and Technology**, 35, p. 314–322, 2016.

DEL POZO-INSFRAN, D.; BRENES, C. H.; TALCOTT, S. T. Phytochemical composition and pigment stability of açai (*Euterpe oleracea* Mart.). **Journal of Agricultural and Food Chemistry**, 52, p. 1539–1545, 2004.

DELGADO-MELLADO, N.; LARRIBA, M.; NAVARRO, P.; RIGUAL, V.; AYUSO, M.; GARCÍA, J.; RODRÍGUEZ, F. Thermal stability of choline chloride deep eutectic solvents by TGA/FTIR-ATR analysis. **Journal of Molecular Liquids**, 260, p. 37–43, 2018.

DEVI, N.; KAKATI, D. K. Smart porous microparticles based on gelatin/sodium alginate polyelectrolyte complex. **Journal of Food Engineering**, 117, p. 193–204, 2013.

DEVI, N.; SARMAH, M.; KHATUN, B.; MAJI, T. K. Encapsulation of active ingredients in polysaccharide–protein complex coacervates. **Advances in Colloid and Interface Science**, 239, p. 136–145, 2017.

DHALL, R. K.; ALAM, M. S. Biodegradable Packaging. *In* **Encyclopedia of Renewable and Sustainable Materials,** Elsevier Inc., 2020, p. 26–43.

DJEMAOUNE, Y.; CASES, E.; SAUREL, R. The effect of high-pressure microfluidization treatment on the foaming properties of pea albumin aggregates. **Journal of Food Science**, 84, p. 2242–2249, 2019.

DOMÍNGUEZ, R.; BARBA, F. J.; GÓMEZ, B.; PUTNIK, P.; BURSAĆ KOVAČEVIĆ, D.; PATEIRO, M.; SANTOS, E. M.; LORENZO, J. M. Active packaging films with natural antioxidants to be used in meat industry: A review. **Food Research International,** 113, p. 93–101, 2018.

DRAGET, K. I.; SMIDSRØD, O.; SKJÅK-BRÆK, G. Alginates from Algae. *In* A. STEINBUNCHEL; S. K. RHEE (Eds.), **Polysaccharides and polyamides in the food industry. Properties, production and patents.** Wiley-VCH Verlar GmbH & Co., pp. 1–30, 2005.

DUAN, C.; MENG, X.; MENG, J.; KHAN, M. I. H.; DAI, L.; KHAN, A.; AN, X.; ZHANG, J.; HUQ, T.; NI, Y. Chitosan as a preservative for fruits and vegetables: A review on chemistry and antimicrobial properties. **Journal of Bioresources and Bioproducts**, 4, p. 11–21, 2019.

DUBEY, N. K.; DUBEY, R. Edible films and coatings: An update on recent advances. *In* K. PAL; I. BANERJEE; P. SARKAR; D. KIM; W.-P. DENG; N. K. DUBEY; K. MAJUMDER (Eds.), **Biopolymer-Based Formulations: Biomedical and Food Applications** Elsevier Inc., pp. 675–695, 2020.

DUCEL, V.; RICHARD, J.; SAULNIER, P.; POPINEAU, Y.; BOURY, F. Evidence and characterization of complex coacervates containing plant proteins: application to the microencapsulation of oil droplets. **Colloids and Surfaces A: Physicochemical and Engineering Aspects**, 232, p. 239–247, 2004.

DWECK, J.; SAMPAIO, C. M. S. Analysis of the thermal decomposition of commercial vegetable oils in air by simultaneous TG/DTA. **Journal of Thermal Analysis and Calorimetry**, 75, p. 385–391, 2004.

EGHBAL, N.; CHOUDHARY, R. Complex coacervation: Encapsulation and controlled release of active agents in food systems. **LWT - Food Science and Technology**, 90, p. 254–264, 2018.

EL HAOUHAY, N.; SAMANIEGO-SÁNCHEZ, C.; ASEHRAOU, A.; VILLALÓN-MIR, M.; LÓPEZ-GARCÍA DE LA SERRANA, H. Microbiological characterization of Picholine variety olives and analysis of olive oil produced in traditional oil mills in Morocco. **CyTA - Journal of Food**, 13, p. 107–115, 2015.

ELGUEA-CULEBRAS, G. O. DE; BOURBON, A. I.; COSTA, M. J.; MUÑOZ-TEBAR, N.; CARMONA, M.; MOLINA, A.; SÁNCHEZ-VIOQUE, R.; BERRUGA, M. I.; VICENTE, A. A. Optimization of a chitosan solution as potential carrier for the incorporation of *Santolina chamaecyparissus* L. solid by-product in an edible vegetal coating on 'Manchego' cheese. **Food Hydrocolloids**, 89, p. 272–282, 2019.

ELMER, C.; KARACA, A. C.; LOW, N. H.; NICKERSON, M. T. Complex coacervation in pea protein isolate–chitosan mixtures. **Food Research International**, 44, p. 1441–1446, 2011.

EPA - Environmental Protection Agency of United States. *In* **Safer Chemical Ingredients List**. Available at <https://www.epa.gov/saferchoice/safer-ingredients#pop9012764> accessed on May 10, 2021.

ESCÁRCEGA-GALAZ, A. A.; SÁNCHEZ-MACHADO, D. I.; LÓPEZ-CERVANTES, J.; SANCHES-SILVA, A.; MADERA-SANTANA, T. J.; PASEIRO-LOSADA, P. Characterization data of chitosan-based films: Antimicrobial activity, thermal analysis, elementary composition, tensile strength and degree crystallinity. **Data in Brief**, 21, p. 473–479, 2018.

ESPADAS-ALDANA, G.; VIALLE, C.; BELAUD, J.-P.; VACA-GARCIA, C.; SABLAYROLLES, C. Analysis and trends for Life Cycle Assessment of olive oil production. **Sustainable Production and Consumption**, 19, p. 216–230, 2019.

ESPINOSA-ANDREWS, H.; ENRÍQUEZ-RAMÍREZ, K. E.; GARCÍA-MÁRQUEZ, E.; RAMÍREZ-SANTIAGO, C.; LOBATO-CALLEROS, C.; VERNON-CARTER, J. Interrelationship between the zeta potential and viscoelastic properties in coacervates complexes. **Carbohydrate Polymers**, 95, p. 161–166, 2013.

ESPITIA, P. J. P.; AVENA-BUSTILLOS, R. J.; DU, W.-X.; TEÓFILO, R. F.; SOARES, N. F. F.; MCHUGH, T. H. Optimal antimicrobial formulation and physical–mechanical properties of edible films based on açaí and pectin for food preservation. **Food Packaging and Shelf Life**, 2, p. 38–49, 2014.

EUROPEAN BIOPLASTICS ORG. Nova-Institute (2020). *In* **Applications for bioplastics**. Available at < https://www.european-bioplastics.org/market/applications-sectors/> accessed on April 26, 2021.

FAKHOURI, F. M.; MARTELLI, S. M.; CAON, T.; VELASCO, J. I.; BUONTEMPO, R. C.; BILCK, A. P.; MEI, L. H. I. The effect of fatty acids on the physicochemical properties of edible films composed of gelatin and gluten proteins. **LWT - Food Science and Technology**, 87, p. 293–300, 2018.

FAKHOURI, F. M.; MARTELLI, S. M.; CAON, T.; VELASCO, J. I.; MEI, L. H. I. Edible films and coatings based on starch/gelatin: Film properties and effect of coatings on quality of refrigerated Red Crimson grapes. **Postharvest Biology and Technology**, 109, p. 57–64, 2015.

FAN, W.; YAN, W.; XU, Z.; NI, H. Formation mechanism of monodisperse, low molecular weight chitosan nanoparticles by ionic gelation technique. **Colloids and Surfaces B: Biointerfaces,** 90, p. 21–27, 2012.

FAOSTAT. Food and Agriculture Organization of the United Nations (FAO). Statistics Division. **Commodity balances - Livestock and fish primary equivalent**. Rome, Italy. 2021. Available at <http://www.fao.org/faostat/en/#home> accessed on April 26, 2021.

FAOSTAT. Food and Agriculture Organization of the United Nations (FAO). Statistics Division. **Crops**. Rome, Italy. 2020. Available at < http://www.fao.org/faostat/en/#data/QC/visualize> accessed on May 25, 2021.

FERREIRA, M. S. L.; FAI, A. E. C.; ANDRADE, C. T.; PICCIANI, P. H.; AZERO, E. G.; GONÇALVES, É. C. B. A. Edible films and coatings based on biodegradable residues applied to acerolas (*Malpighia punicifolia* L.). **Journal of the Science of Food and Agriculture**, 96, p. 1634–1642, 2016.

FERREIRA, W. H.; ANDRADE, C. T. Characterization of glycerol-plasticized starch and graphene oxide extruded hybrids. **Industrial Crops and Products**, 77, p. 684–690, 2015.

FISCHER, E.; CACHON, R.; CAYOT, N. *Pisum sativum* vs *Glycine max*, a comparative review of nutritional, physicochemical, and sensory properties for food uses. **Trends in Food Science & Technology**, 95, p. 196–204, 2020.

FOSCOLOU, A.; CRITSELIS, E.; PANAGIOTAKOS, D. Olive oil consumption and human health: A narrative review. **Maturitas**, 118, p. 60–66, 2018.

FRANKEL, E., BAKHOUCHE, A.; LOZANO-SÁNCHEZ, J.; SEGURA-CARRETERO, A.; FERNÁNDEZ-GUTIÉRREZ, A. Literature review on production process to obtain extra virgin olive oil enriched in bioactive compounds. Potential use of byproducts as alternative sources of polyphenols. **Journal of Agricultural and Food Chemistry**, 61, p. 5179–5188, 2013.

FRIEDMAN, M.; JUNEJA, V. K. Review of antimicrobial and antioxidative activities of chitosans in food. **Journal of Food Protection**, 73, p. 1737–1761, 2010.

FUJIWARA, Y.; MAEDA, R.; TAKESHITA, H.; KOMOHARA, Y. Alginates as food ingredients absorb extra salt in sodium chloride-treated mice. **Heliyon**, 7, n. e06551, pp. 1-7, 2021.

GARRIDO, T.; ETXABIDE, A.; LECETA, I.; CABEZUDO, S.; DE LA CABA, K.; GUERRERO, P. Valorization of soya by-products for sustainable packaging. **Journal of Cleaner Production**, 64, p. 228–233, 2014.

GÅSERØD, O.; SMIDSRØD, O.; SKJÅK-BRÆK, G. Microcapsules of alginate-chitosan - I. A quantitative study of the interaction between alginate and chitosan. **Biomaterials**, 19, p. 1815–1825, 1998.

GENSKOWSKY, E.; PUENTE, L. A.; PÉREZ-ÁLVAREZ, J. A.; FERNANDEZ-LOPEZ, J.; MUÑOZ, L. A.; VIUDA-MARTOS, M. Assessment of antibacterial and antioxidant properties of chitosan edible films incorporated with maqui berry (*Aristotelia chilensis*). **LWT - Food Science and Technology**, 64, p. 1057–1062, 2015.

GHASEMI, S.; JAFARI, S. M.; ASSADPOUR, E.; KHOMEIRI, M. Nanoencapsulation of D-limonene within nanocarriers produced by pectin-whey protein complexes. **Food Hydrocolloids**, 77, p. 152–162, 2018.

GIANNAKAS, A.; PATSAOURA, A.; BARKOULA, N.-M.; LADAVOS, A. A novel solution blending method for using olive oil and corn oil as plasticizers in chitosan based organoclay nanocomposites. **Carbohydrate Polymers**, 157, p. 550–557, 2017.

GOH, C. H.; HENG, P. W. S.; CHAN, L. W. Alginates as a useful natural polymer for microencapsulation and therapeutic applications. **Carbohydrate Polymers**, 88, p. 1–12, 2012.

GONÇALVES, R. P.; FERREIRA, W. H.; GOUVÊA, R. F.; ANDRADE, C. T. Effect of chitosan on the properties of electrospun fibers from mixed poly(vinyl alcohol)/chitosan solutions. **Materials Research**, 20, p. 984–993, 2017.

GONZÁLEZ-ESPINOSA, Y.; SABAGH, B.; MOLDENHAUER, E.; CLARKE, P.; GOYCOOLEA, F. M. Characterisation of chitosan molecular weight distribution by multi-detection asymmetric flow-field flow fractionation (AF4) and SEC. **International Journal of Biological Macromolecules**, 136, 911–919, 2019.

GORJI, E. G.; WAHEED, A.; LUDWIG, R.; TOCA-HERRERA, J. L.; SCHLEINING, G.; GORJI, S. G. Complex coacervation of milk proteins with sodium alginate. **Journal of Agricultural and Food Chemistry, 66**, p. 3210–3220, 2018.

GOUVÊA, R. F.; FERREIRA, W. H.; SOUTO, L. F. C.; GONÇALVES, R. P.; SOARES, B. G.; ANDRADE, C. T. Flexible dielectric ZnO-doped reduced graphene oxide bionanocomposites from solution blending for potential application in bio-related devices. **Journal of Applied Polymer Science**, December 2020, 1–12, 2021.

GROH, K. J.; BACKHAUS, T.; CARNEY-ALMROTH, B.; GEUEKE, B.; INOSTROZA, P. A.; LENNQUIST, A.; LESLIE, H. A.; MAFFINI, M.; SLUNGE, D.; TRASANDE,

L.; WARHURST, A. M.; MUNCKE, J. Overview of known plastic packaging-associated chemicals and their hazards. **Science of The Total Environment**, 651, p. 3253–3268, 2019.

GROSS, R. A.; KALRA, B. Biodegradable polymers for the environment. **Science**, 297, p. 803–807, 2002.

GUERRERO, P.; MUXIKA, A.; ZARANDONA, I.; DE LA CABA, K. Crosslinking of chitosan films processed by compression molding. **Carbohydrate Polymers**, 206, p. 820–826, 2019.

GULÃO, E. D. S.; DE SOUZA, C. J. F.; ANDRADE, C. T.; GARCIA-ROJAS, E. E. Complex coacervates obtained from peptide leucine and gum arabic: Formation and characterization. **Food Chemistry**, 194, p. 680–686, 2015.

GUO, Z.; JIA, X.; ZHENG, Z.; LU, X.; ZHENG, Y.; ZHENG, B.; XIAO, J. Chemical composition and nutritional function of olive (*Olea europaea* L.): a review. **Phytochemistry Reviews**, 17, p. 1091–1110, 2018.

HADIDI, M.; MOTAMEDZADEGAN, A.; JELYANI, A. Z.; KHASHADEH, S. Nanoencapsulation of hyssop essential oil in chitosan-pea protein isolate nano-complex. **LWT - Food Science and Technology**, 144, n. 111254, p. 1-9, 2021.

HAGHIGHI, H.; LICCIARDELLO, F.; FAVA, P.; SIESLER, H. W.; PULVIRENTI, A. Recent advances on chitosan-based films for sustainable food packaging applications. **Food Packaging and Shelf Life**, 26, n. 100551, p. 1-16, 2020.

HAI, L. VAN; ZHAI, L.; KIM, H. C.; PANICKER, P. S.; PHAM, D. H.; KIM, J. Chitosan Nanofiber and Cellulose Nanofiber Blended Composite Applicable for Active Food Packaging. **Nanomaterials**, 10, p. 1752-1766, 2020.

HALONEN, N.; PÁLVÖLGYI, P. S.; BASSANI, A.; FIORENTINI, C.; NAIR, R.; SPIGNO, G.; KORDAS, K. BIO-Based Smart Materials for Food Packaging and Sensors – A Review. **Frontiers in Materials**, 7, p. 1–14, 2020.

HAMEDI, H.; KARGOZARI, M.; SHOTORBANI, P. M.; MOGADAM, N. B.; FAHIMDANESH, M. A novel bioactive edible coating based on sodium alginate and galbanum gum incorporated with essential oil of *Ziziphora persica*: The antioxidant and antimicrobial activity, and application in food model. **Food Hydrocolloids**, 72, p. 35–46, 2017.

HAMZAH, H. M.; OSMAN, A.; TAN, C. P.; GHAZALI, F. M. Carrageenan as an alternative coating for papaya (*Carica papaya* L. cv. Eksotika). **Postharvest Biology and Technology**, 75, p. 142–146, 2013.

HAN, M.; CLAUSEN, M. P.; CHRISTENSEN, M.; VOSSEN, E.; VAN HECKE, T.; BERTRAM, H. C. Enhancing the health potential of processed meat: the effect of chitosan or carboxymethyl cellulose enrichment on inherent microstructure, water mobility and oxidation in a meat-based food matrix. **Food & Function**, 9, p. 4017–4027, 2018.

HARDY, A.; SEGUIN, C.; BRION, A.; LAVALLE, P.; SCHAAF, P.; FOURNEL, S.; BOUREL-BONNET, L.; FRISCH, B.; DE GIORGI, M. β-cyclodextrin-functionalized chitosan/alginate compact polyelectrolyte complexes (CoPECs) as functional biomaterials with anti-inflammatory properties. **ACS Applied Materials & Interfaces**, 10, p. 29347–29356, 2018.

HOELL, I. A.; VAAJE-KOLSTAD, G.; EIJSINK, V. G. H. Structure and function of enzymes acting on chitin and chitosan. **Biotechnology and Genetic Engineering Reviews**, 27, p. 331–366, 2010.

HONG, T.; ZHANG, Y.; XU, D.; WU, F.; XU, X. Effect of sodium alginate on the quality of highland barley fortified wheat noodles. **LWT - Food Science and Technology,** 140, p. p. 110719-110728, 2021.

HOUGHTON, D.; WILCOX, M. D.; BROWNLEE, I. A.; CHATER, P. I.; SEAL, C. J.; PEARSON, J. P. Acceptability of alginate enriched bread and its effect on fat digestion in humans. **Food Hydrocolloids**, 93, p. 395–401, 2019.

HU, C.; LU, W.; MATA, A.; NISHINARI, K.; FANG, Y. Ions-induced gelation of alginate: Mechanisms and applications. **International Journal of Biological Macromolecules**, 177, p. 578–588, 2021.

HUANG, D.; OU, B.; PRIOR, R. L. The chemistry behind antioxidant capacity assays. **Journal of Agricultural and Food Chemistry**, 53, p. 1841–1856, 2005.

HUANG, G. Q.; SUN, Y. T.; XIAO, J. X.; YANG, J. Complex coacervation of soybean protein isolate and chitosan. **Food Chemistry**, 135, p. 534–539, 2012.

HUANG, H.; LIAO, D.; ZOU, Y.; CHI, H. The effects of chitosan supplementation on body weight and body composition: a systematic review and meta-analysis of randomized controlled trials. **Critical Reviews in Food Science and Nutrition**, 60, p. 1815–1825, 2020.

HUO, W.; XIE, G.; ZHANG, W.; WANG, W.; SHAN, J.; LIU, H.; ZHOU, X. Preparation of a novel chitosan-microcapsules/starch blend film and the study of its drug-release mechanism. **International Journal of Biological Macromolecules**, 87, p. 114–122, 2016.

IFEDUBA, E. A.; AKOH, C. C. Microencapsulation of stearidonic acid soybean oil in Maillard reaction-modified complex coacervates**. Food Chemistry**, 199, p. 524–532, 2016.

IMRE, B.; GARCÍA, L.; PUGLIA, D.; VILAPLANA, F. Reactive compatibilization of plant polysaccharides and biobased polymers: Review on current strategies, expectations and reality. **Carbohydrate Polymers**, 209, p. 20–37, 2019.

INTRADO GLOBE NEWSWIRE. **Bioplastic market size to reach $13.1 billion by 2027** | CAGR: 13.8%: AMR. 2020 Available at <https://www.globenewswire.com/news-release/2020/11/19/2130218/0/en/Bioplastic-Market-Size-to-Reach-13-1-Billion-by-2027-CAGR-13-8-AMR.html> accessed on April 24, 2021.

ISO. International Organization for Standardization. Standard ISO 16620-1:2015, **Plastics — Biobased content — Part 1: General principles**. Vernier, Geneva, Switzerland, 2015. <Available at https://www.iso.org/obp/ui/#iso:std:iso:16620:-1:ed-1:v1:en> accessed on April 12, 2021.

JÄGER, J. K.; PISCICELLI, L. Collaborations for circular food packaging: The set-up and partner selection process. **Sustainable Production and Consumption**, 26, p. 733–740, 2021.

JAHROMI, M.; NIAKOUSARI, M.; GOLMAKANI, M. T.; MOHAMMADIFAR, M. A. Physicochemical and structural characterization of sodium caseinate based film-forming solutions and edible films as affected by high methoxyl pectin. **International Journal of Biological Macromolecules**, 165, p. 1949–1959, 2020.

JIANG, Y.; LAN, W.; SAMEEN, D. E.; AHMED, S.; QIN, W.; ZHANG, Q.; CHEN, H.; DAI, J.; HE, L.; LIU, Y. Preparation and characterization of grass carp collagen-chitosan-lemon essential oil composite films for application as food packaging. **International Journal of Biological Macromolecules**, 160, p. 340–351, 2020.

JOST, V.; LANGOWSKI, H. C. Effect of different plasticizers on the mechanical and barrier properties of extruded cast PHBV films. **European Polymer Journal**, 68, p. 302–312, 2015.

JURIĆ, S.; JURIĆ, M.; REŽEK JAMBRAK, A.; VINCEKOVIĆ, M. TAILORING alginate/chitosan microparticles loaded with chemical and biological agents for agricultural application and production of value-added foods. **Applied Sciences**, 11, p. 4061-4096, 2021.

KAMDEM, D. P.; SHEN, Z.; NABINEJAD, O. Development of biodegradable composite chitosan-based films incorporated with xylan and carvacrol for food packaging application. **Food Packaging and Shelf Life**, 21, n. 100344, p. 1-7, 2019.

KARACA, A. C.; LOW, N.; NICKERSON, M. Emulsifying properties of chickpea, faba bean, lentil and pea proteins produced by isoelectric precipitation and salt extraction. **Food Research International**, 44, p. 2742–2750, 2011.

KASAAI, M. R. A review of several reported procedures to determine the degree of N-acetylation for chitin and chitosan using infrared spectroscopy. **Carbohydrate Polymers**, 71, 497–508, 2008.

KASAAI, M. R. Calculation of Mark-Houwink-Sakurada (MHS) equation viscometric constants for chitosan in any solvent-temperature system using experimental reported viscometric constants data. **Carbohydrate Polymers**, 68, 477–488, 2007.

KAYITMAZER, A. B. Thermodynamics of complex coacervation. **Advances in Colloid and Interface Science**, 239, p. 169–177, 2017.

KERCH, G.; KORKHOV, V. Effect of storage time and temperature on structure, mechanical and barrier properties of chitosan-based films. **European Food Research and Technology,** 232, p. 17–22, 2011.

KHAN, M. A.; YUE, C.; FANG, Z.; HU, S.; CHENG, H.; BAKRY, A. M.; LIANG, L. Alginate/chitosan-coated zein nanoparticles for the delivery of resveratrol. **Journal of Food Engineering,** 258, p. 45–53, 2019.

KHAYROVA, A.; LOPATIN, S.; VARLAMOV, V. Obtaining chitin, chitosan and their melanin complexes from insects. **International Journal of Biological Macromolecules**, 167, p. 1319–1328, 2021.

KHOSHAKHLAGH, K.; KOOCHEKI, A.; MOHEBBI, M.; ALLAFCHIAN, A. Development and characterization of electrosprayed *Alyssum homolocarpum* seed gum nanoparticles for encapsulation of *D*-limonene. **Journal of Colloid and Interface Science**, 490, p. 562–575, 2017.

KLINMALAI, P.; HAGIWARA, T.; SAKIYAMA, T.; RATANASUMAWONG, S. Chitosan effects on physical properties, texture, and microstructure of flat rice noodles. **LWT - Food Science and Technology**, 76, p. 117–123, 2017.

KOWALCZYK, D.; SZYMANOWSKA, U.; SKRZYPEK, T.; BASIURA-CEMBALA, M.; ŁUPINA, K.; BIENDL, M. Edible films based on gelatin, carboxymethyl cellulose, and their blends as carriers of potassium salts of iso-α-acids: Structural, physicochemical and antioxidant properties. **Food Hydrocolloids**, 115, n. 106574, p. 1-11, 2021.

KUMAR, M.; TOMAR, M.; POTKULE, J.; VERMA, R.; PUNIA, S.; MAHAPATRA, A.; BELWAL, T.; DAHUJA, A.; JOSHI, S.; BERWAL, M. K.; SATANKAR, V.; BHOITE, A. G.; AMAROWICZ, R.; KAUR, C.; KENNEDY, J. F. Advances in the plant protein extraction: Mechanism and recommendations. **Food Hydrocolloids**, 115, n. 106595, p. 1-17, 2021. Available at <https://doi.org/10.1016/j.foodhyd.2021.106595>, accessed on May 27, 2021.

LADJAL-ETTOUMI, Y.; BOUDRIES, H.; CHIBANE, M.; ROMERO, A. Pea, chickpea and lentil protein isolates: Physicochemical characterization and emulsifying properties. **Food Biophysics**, 11, p. 43–51, 2016.

LAGOS, J. B.; VARGAS, F. C.; OLIVEIRA, T. G.; MAKISHI, G. L. DA A.; SOBRAL, P. J. DO A. Recent patents on the application of bioactive compounds in food: A short review. **Current Opinion in Food Science**, 5, p. 1–7, 2015.

LAWRIE, G.; KEEN, I.; DREW, B.; CHANDLER-TEMPLE, A.; RINTOUL, L.; FREDERICKS, P.; GRØNDAHL, L. Interactions between alginate and chitosan biopolymers characterized using FTIR and XPS. **Biomacromolecules**, 8, p. 2533–2541, 2007.

LECETA, I.; GUERRERO, P.; CABEZUDO, S.; CABA, K. DE LA. Environmental assessment of chitosan-based films. **Journal of Cleaner Production**, 41, p. 312–318, 2013.

LEI, M.; JIANG, F.; CAI, J.; HU, S.; ZHOU, R.; LIU, G.; WANG, Y.-H.; WANG, H.-B.; HE, J.-R.; XIONG, X.-G. Facile microencapsulation of olive oil in porous starch granules: Fabrication, characterization, and oxidative stability. **International Journal of Biological Macromolecules**, 111, p. 755–761, 2018.

LEKJING, S. A chitosan-based coating with or without clove oil extends the shelf life of cooked pork sausages in refrigerated storage. **Meat Science**, 111, p. 192–197, 2016.

LEON, A. M.; MEDINA, W. T.; PARK, D. J.; AGUILERA, J. M. Properties of microparticles from a whey protein isolate/alginate emulsion gel. **Food Science and Technology International**, 24, p. 414–423, 2018.

LEÓN-ZAPATA, M. A. D.; SÁENZ-GALINDO, A.; ROJAS-MOLINA, R.; RODRÍGUEZ-HERRERA, R.; JASSO-CANTÚ, D.; AGUILAR, C. N. Edible candelilla wax coating with fermented extract of tarbush improves the shelf life and quality of apples. **Food Packaging and Shelf Life**, 3, p. 70–75, 2015.

LI, J.; LIU, J.; SUN, X.; LIU, Y. The mathematical prediction model for the oxidative stability of vegetable oils by the main fatty acids composition and thermogravimetric analysis. **LWT - Food Science and Technology**, 96, 51–57, 2018b.

LI, M.-F.; CHEN, L.; XU, M.-Z.; ZHANG, J.-L.; WANG, Q.; ZENG, Q.-Z.; WEI, X.-C.; YUAN, Y. The formation of zein-chitosan complex coacervated particles: Relationship to encapsulation and controlled release properties. **International Journal of Biological Macromolecules**, 116, p. 1232–1239, 2018a.

LI, Y.; MCCLEMENTS, D. J. Controlling lipid digestion by encapsulation of protein-stabilized lipid droplets within alginate–chitosan complex coacervates. **Food Hydrocolloids**, 25, p. 1025–1033, 2011.

LIANG, J.; YAN, H.; ZHANG, J.; DAI, W.; GAO, X.; ZHOU, Y.; WAN, X.; PULIGUNDLA, P. Preparation and characterization of antioxidant edible chitosan films incorporated with epigallocatechin gallate nanocapsules. **Carbohydrate Polymers,** 171, p. 300–306, 2017.

LIOUPI, A.; NENADIS, N.; THEODORIDIS, G. Virgin olive oil metabolomics: A review. **Journal of Chromatography B,** 1150, p. 122161, 2020.

LIU, G.; WEI, D.; WANG, H.; HU, Y.; JIANG, Y. Self-assembly of zein microspheres with controllable particle size and narrow distribution using a novel built-in ultrasonic dialysis process. **Chemical Engineering Journal**, 284, p. 1094–1105, 2016.

LIU, J.; MENG, C.; LIU, S.; KAN, J.; JIN, C. Preparation and characterization of protocatechuic acid grafted chitosan films with antioxidant activity. **Food Hydrocolloids**, 63, p. 457–466, 2017.

LIU, K.; YUAN, C.; CHEN, Y.; LI, H.; LIU, J. Combined effects of ascorbic acid and chitosan on the quality maintenance and shelf life of plums. **Scientia Horticulturae**, 176, p. 45–53, 2014.

LIU, M.; ZHOU, Y.; ZHANG, Y.; YU, C.; CAO, S. Preparation and structural analysis of chitosan films with and without sorbitol. **Food Hydrocolloids**, 33, p. 186–191, 2013.

LIU, S.; LOW, N. H.; NICKERSON, M. T. Effect of pH, salt, and biopolymer ratio on the formation of pea protein isolate - gum Arabic complexes. **Journal of Agricultural and Food Chemistry,** 57, 1521–1526, 2009.

LIU, Z. Q. Chemical methods to evaluate antioxidant ability. **Chemical Reviews**, 110, p. 5675–5691, 2010.

LOPEZ-SANTAMARINA, A.; MONDRAGON, A. DEL C.; LAMAS, A.; MIRANDA, J. M.; FRANCO, C. M.; CEPEDA, A. Animal-origin prebiotics based on chitin: an alternative for the future? A critical review. **Foods**, 9, 782-802, 2020.

LOTITO, S. B.; FREI, B. The increase in human plasma antioxidant capacity after apple consumption is due to the metabolic effect of fructose on urate, not apple-derived antioxidant flavonoids. **Free Radical Biology and Medicine**, 37, p. 251–258, 2004.

LOZANO-SÁNCHEZ, J.; GIAMBANELLI, E.; QUIRANTES-PINÉ, R.; CERRETANI, L.; BENDINI, A.; SEGURA-CARRETERO, A.; FERNÁNDEZ-GUTIÉRREZ, A. Wastes generated during the storage of extra virgin olive oil as a natural source of phenolic compounds. **Journal of Agricultural and Food Chemistry**, 59, p. 11491–11500, 2011.

LUO, Y.; WANG, Q. Recent development of chitosan-based polyelectrolyte complexes with natural polysaccharides for drug delivery. **International Journal of Biological Macromolecules**, 64, p. 353–367, 2014.

MA, Q.; ZHANG, Y.; CRITZER, F.; DAVIDSON, P. M.; ZIVANOVIC, S.; ZHONG, Q. Physical, mechanical, and antimicrobial properties of chitosan films with microemulsions of cinnamon bark oil and soybean oil. **Food Hydrocolloids**, 52, p. 533–542, 2015.

MA, T.; ZHAO, H.; WANG, J.; SUN, B. Effect of processing conditions on the morphology and oxidative stability of lipid microcapsules during complex coacervation. **Food Hydrocolloids**, 87, p. 637–643, 2019.

MA, Z.; GARRIDO-MAESTU, A.; JEONG, K. C. Application, mode of action, and in vivo activity of chitosan and its micro- and nanoparticles as antimicrobial agents: A review. **Carbohydrate Polymers**, 176, p. 257–265, 2017.

MADIAN, N. G.; MOHAMED, N. Enhancement of the dynamic mechanical properties of chitosan thin films by crosslinking with greenly synthesized silver nanoparticles. **Journal of Materials Research and Technology**, 9, p. 12970–12975, 2020.

MARKUS, F.; RAMANI, N. Biodegradable Plastic as Integral Part of the Solution to Plastic Waste Pollution of the Environment. **Current Opinion in Green and Sustainable Chemistry**, In press (April), n. 100490, 2021. Available at < https://doi.org/10.1016/j.cogsc.2021.100490> accessed on April 8, 2021.

MARYAM ADILAH, Z. A.; JAMILAH, B.; NUR HANANI, Z. A. Functional and antioxidant properties of protein-based films incorporated with mango kernel extract for active packaging. **Food Hydrocolloids**, 74, p. 207–218, 2018.

MATTA, F. V.; XIONG, J.; LILA, M. A.; WARD, N. I.; FELIPE-SOTELO, M.; ESPOSITO, D. Chemical composition and bioactive properties of commercial and non-commercial purple and white açaí berries. **Foods**, 9, p. 1-17, 2020.

MBOUS, Y. P.; HAYYAN, M.; WONG, W. F.; LOOI, C. Y.; HASHIM, M. A. Unraveling the cytotoxicity and metabolic pathways of binary natural deep eutectic solvent systems. **Scientific Reports**, 7, p. 41257-41271, 2017.

MCCARTHY, N. A.; KENNEDY, D.; HOGAN, S. A.; KELLY, P. M.; THAPA, K.; MURPHY, K. M.; FENELON, M. A. Emulsification properties of pea protein isolate using homogenization, microfluidization and ultrasonication. **Food Research International**, 89, p. 415–421, 2016.

MENCONI, A.; HERNANDEZ-, X.; LATORRE, J. D.; KALLAPURA, G.; PUMFORD, N. R.; MORGAN, M. J.; HARGIS, B. M.; TELLEZ, G. Effect of chitosan as a biological sanitizer for *Salmonella typhimurium* and aerobic gram negative spoilage bacteria present on chicken skin. **International Journal of Poultry Science**, 12, 318–321, 2013.

MERTENS-TALCOTT, S. U.; RIOS, J.; JILMA-STOHLAWETZ, P.; PACHECO-PALENCIA, L. A.; MEIBOHM, B.; TALCOTT, S. T.; DERENDORF, H. Pharmacokinetics of anthocyanins and antioxidant effects after the consumption of anthocyanin-rich açai juice and pulp (*Euterpe oleracea* mart.) in human healthy volunteers. **Journal of Agricultural and Food Chemistry**, 56, p. 7796–7802, 2008.

MILLER, K. S.; KROCHTA, J. M. Oxygen and aroma barrier properties of edible films: A review. **Trends in Food Science & Technology**, 8, p. 228–237, 1997. Available at < https://doi.org/10.1016/S0924-2244(97)01051-0>, accessed on April 22, 2021.

MKANDAWIRE, M.; ARYEE, A. N. Resurfacing and modernization of edible packaging material technology. **Current Opinion in Food Science**, 19, p. 104–112, 2018.

MOALLA, S.; AMMAR, I.; FAUCONNIER, M.-L.; DANTHINE, S.; BLECKER, C.; BESBES, S.; ATTIA, H. Development and characterization of chitosan films carrying *Artemisia campestris* antioxidants for potential use as active food packaging materials. **International Journal of Biological Macromolecules**, 183, p. 254–266, 2021.

MOHAMED, S. A. A.; EL-SAKHAWY, M.; EL-SAKHAWY, M. A.-M. Polysaccharides, protein and lipid-based natural edible films in food packaging: A review. **Carbohydrate Polymers**, 238, p. 116178-116182, 2020.

MORADI, M.; TAJIK, H.; RAZAVI ROHANI, S. M.; OROMIEHIE, A. R.; MALEKINEJAD, H.; ALIAKBARLU, J.; HADIAN, M. Characterization of antioxidant chitosan film incorporated with *Zataria multiflora* Boiss essential oil and grape seed extract. **LWT - Food Science and Technology,** 46, p. 477–484, 2012.

MORALES-POLANCO, E.; CAMPOS-VEGA, R.; GAYTÁN-MARTÍNEZ, M.; ENRIQUEZ, L. G.; LOARCA-PIÑA, G. Functional and textural properties of a dehulled oat (*Avena sativa* L) and pea (*Pisum sativum*) protein isolate cracker. **LWT - Food Science and Technology**, 86, p. 418–423, 2017.

MORELLI, S.; HOLDICH, R. G.; DRAGOSAVAC, M. M. Chitosan and Poly(Vinyl Alcohol) microparticles produced by membrane emulsification for encapsulation and pH controlled release. **Chemical Engineering Journal,** 288, p. 451–460, 2016.

MORENO, O.; ATARÉS, L.; CHIRALT, A. Effect of the incorporation of antimicrobial/antioxidant proteins on the properties of potato starch films. **Carbohydrate Polymers**, 133, p. 353–364, 2015.

MORIN-CRINI, N.; LICHTFOUSE, E.; TORRI, G.; CRINI, G. Applications of chitosan in food, pharmaceuticals, medicine, cosmetics, agriculture, textiles, pulp and paper, biotechnology, and environmental chemistry. **Environmental Chemistry Letters**, 17, p. 1667–1692, 2019.

MOSCHAKIS, T.; BILIADERIS, C. G. Biopolymer-based coacervates: Structures, functionality and applications in food products. **Current Opinion in Colloid and Interface Science**, 28, p. 96–109, 2017.

MUJTABA, M.; MORSI, R. E.; KERCH, G.; ELSABEE, M. Z.; KAYA, M.; LABIDI, J.; KHAWAR, K. M. Current advancements in chitosan-based film production for food technology; A review. **International Journal of Biological Macromolecules,** 121, p. 889–904, 2019.

MUNHOZ, D. R.; MOREIRA, F. K. V.; BRESOLIN, J. D.; BERNARDO, M. P.; DE SOUSA, C. P.; MATTOSO, L. H. C. Sustainable production and in vitro biodegradability of edible films from yellow passion fruit coproducts via continuous casting. **ACS Sustainable Chemistry and Engineering**, 6, p. 9883–9892, 2018.

MUÑOZ-BONILLA, A.; CERRADA, M. L.; FERNÁNDEZ-GARCÍA, M. Antimicrobial Activity of Chitosan in Food, Agriculture and Biomedicine. *In* MUÑOZ-BONILLA, A.; CERRADA, M. L.; FERNÁNDEZ-GARCÍA, M. (Eds.). **Polymeric Materials with Antimicrobial Activity: From Synthesis to Applications**. 1st edition. The Royal Society of Chemistry, pp. 22–53, 2014.

MUXIKA, A.; ETXABIDE, A.; URANGA, J.; GUERRERO, P.; DE LA CABA, K. Chitosan as a bioactive polymer: Processing, properties and applications. **International Journal of Biological Macromolecules**, 105, p. 1358–1368, 2017.

NATRAJAN, D.; SRINIVASAN, S.; SUNDAR, K.; RAVINDRAN, A. Formulation of essential oil-loaded chitosan–alginate nanocapsules. **Journal of Food and Drug Analysis**, 23, p. 560–568, 2015.

NEHCHIRI, N.; AMIRI, S.; RADI, M. Improving the water barrier properties of alginate packaging films by submicron coating with drying linseed oil. **Packaging Technology and Science**, 34, p. 283–295, 2021.

NIU, F.; KOU, M.; FAN, J.; PAN, W.; FENG, Z. J.; SU, Y.; YANG, Y.; ZHOU, W. Structural characteristics and rheological properties of ovalbumin-gum arabic complex coacervates. **Food Chemistry**, 260, p. 1–6, 2018.

NOGUEIRA, G. F.; OLIVEIRA, R. A. DE; VELASCO, J. I.; FAKHOURI, F. M. Methods of incorporating plant-derived bioactive compounds into films made with agro-based polymers for application as food packaging: A brief review. **Polymers**, 12, p. 2518-2552, 2020.

NOVA-INSTITUTE. **Renewable Carbon Publications**. *In* Nova-Institute (Germany), OWS (Belgium), Hydra Marine Science (Italy/Germany), IKT Stuttgart (Germany) in cooperation with DIN CERTCO and TÜV Austria, Biodegradable Polymers in Various Environments According to Established Standards and Certification Schemes – Graphic. Sustainability and Health, **NOVA-INSTITUT GmbH**, Hürth, Germany. 2021. Available at <https://renewable-carbon.eu/publications/product/biodegradable-polymers-in-various-environments-according-to-established-standards-and-certification-schemes-graphic-pdf/> accessed on April 05, 2021.

OBERLINTNER, A.; BAJIĆ, M.; KALČÍKOVÁ, G.; LIKOZAR, B.; NOVAK, U. Biodegradability study of active chitosan biopolymer films enriched with Quercus polyphenol extract in different soil types. **Environmental Technology & Innovation**, 21, n. 101318, p. 1-12, 2021.

ODENDAAL, A. Y.; SCHAUSS, A. G. Potent antioxidant and anti-inflammatory flavonoids in the nutrient-rich Amazonian palm fruit, açaí (*Euterpe* spp.). *In* R. R. WATSON; V. R. PREEDY; S. ZIBADI (Eds.), **Polyphenols in Human Health and Disease**, Vol. 1. Elsevier Inc., 2014, pp. 219–239.

OLIVEIRA, E. F.; PAULA, H. C. B.; PAULA, R. C. M. Alginate/cashew gum nanoparticles for essential oil encapsulation**. Colloids and Surfaces B: Biointerfaces**, 113, p. 146–151, 2014.

OLIVEIRA, H. C.; GOMES, B. C. R.; PELEGRINO, M. T.; SEABRA, A. B. Nitric oxide-releasing chitosan nanoparticles alleviate the effects of salt stress in maize plants. **Nitric Oxide**, 61, p. 10–19, 2016.

OSMOKROVIC, A.; JANCIC, I.; VUNDUK, J.; PETROVIC, P.; MILENKOVIC, M., OBRADOVIC, B. Achieving high antimicrobial activity: Composite alginate hydrogel beads releasing activated charcoal with an immobilized active agent. **Carbohydrate Polymers**, 196, p. 279–288, 2018.

OTONI, C. G.; AVENA-BUSTILLOS, R. J.; AZEREDO, H. M. C.; LOREVICE, M. V.; MOURA, M. R.; MATTOSO, L. H. C.; MCHUGH, T. H. Recent Advances on Edible Films Based on Fruits and Vegetables - A Review. **Comprehensive Reviews in Food Science and Food Safety**, 16, p. 1151–1169, 2017.

OZKAN, G.; FRANCO, P.; MARCO, I. D.; XIAO, J.; CAPANOGLU, E. A review of microencapsulation methods for food antioxidants: Principles, advantages, drawbacks and applications. **Food Chemistry**, 272, p. 494–506, 2019.

PACHECO-PALENCIA, L. A.; MERTENS-TALCOTT, S.; TALCOTT, S. T. Chemical composition, antioxidant properties, and thermal stability of a phytochemical enriched oil from açai (*Euterpe oleracea* Mart.). **Journal of Agricultural and Food Chemistry**, 56, p. 4631–4636, 2008.

PAGE, B. Rigid metal packaging. *In:* EMBLEM, A.; EMBLEM H. (Eds.). **Packaging Technology - Fundamentals, Materials and Processes**. Woodhead Publishing Limited, 2012, p. 122–162. Available at <https://doi.org/10.1533/9780857095701.2.122> accessed on April 21, 2021.

PALA, D.; BARBOSA, P. O.; SILVA, C. T.; DE SOUZA, M. O.; FREITAS, F. R.; VOLP, A. C. P.; MARANHÃO, R. C.; FREITAS, R. N. Açai (*Euterpe oleracea* Mart.) dietary intake affects plasma lipids, apolipoproteins, cholesteryl ester transfer to high-density lipoprotein and redox metabolism: A prospective study in women. **Clinical Nutrition**, 37, p. 618–623, 2018.

PARREIDT, T. S.; MÜLLER, K.; SCHMID, M. Alginate-Based Edible Films and Coatings for Food Packaging Applications. **Foods**, 7, n. 170, p. 1-38, 2018.

PAULA, R. DE; FERNANDES, P.; TRINDADE, M. A.; MELO, M. P. DE. Natural Antioxidants and Food Applications: Healthy Perspectives. *In* A. M. HOLBAN; A. M. GRUMEZESCU (Eds.). **Alternative and Replacement Foods**. 1st. edition. Elsevier Inc., 2018, pp. 31–64.

PAVINATTO, A.; DE ALMEIDA MATTOS, A. V.; MALPASS, A. C. G.; OKURA, M. H.; BALOGH, D. T.; SANFELICE, R. C. Coating with chitosan-based edible films for mechanical/biological protection of strawberries. **International Journal of Biological Macromolecules**, 151, p. 1004–1011, 2020.

PAVLATH, A. E.; ORTS, W. Edible Films and Coatings: Why, What, and How? *In*. HUBER K. C.; EMBUSCADO, M. E. (Eds.). **Edible Films and Coatings for Food Applications**, Springer New York, 2009, p. 1–23. Available at <https://doi.org/10.1007/978-0-387-92824-1>, accessed on April 20, 2021.

PEÑA-CHÁIDEZ, J. E.; ROSAS-FLORES, W.; SALAZAR-MONTOYA, J. A.; MORALES-CONTRERAS, B. E.; GALLEGOS-INFANTE, J. A.; MORALES-CASTRO, J.; MEDRANO-ROLDÁN, H. Rheological and thermal characterization of pinto saltillo bean (*Phaseolus vulgaris* L.) protein isolates/sodium alginate gels. **LWT - Food Science and Technology**, 146, n. 111419, p. 1-8, 2021.

PENG, Y.; WU, Y.; LI, Y. Development of tea extracts and chitosan composite films for active packaging materials. **International Journal of Biological Macromolecules**, 59, p. 282–289, 2013.

PEREDA, M.; AMICA, G.; MARCOVICH, N. E. Development and characterization of edible chitosan/olive oil emulsion films. **Carbohydrate Polymers**, 87, p. 1318–1325, 2012.

PEREIRA, A. S.; DINIZ, M. M.; DE JONG, G.; GAMA FILHO, H. S.; ANJOS, M. J.; FINOTELLI, P. V.; FONTES-SANT'ANA, G. C.; AMARAL, P. F. F. (2019). Chitosan-alginate beads as encapsulating agents for *Yarrowia lipolytica* lipase:

Morphological, physico-chemical and kinetic characteristics. **International Journal of Biological Macromolecules**, 139, 621–630, 2019.

PEREIRA, P. F.; ANDRADE, C. T. Optimized pH-responsive film based on a eutectic mixture-plasticized chitosan. **Carbohydrate Polymers**, 165, p. 238–246, 2017.

PEREIRA, R.; CARVALHO, A.; VAZ, D. C.; GIL, M. H.; MENDES, A.; BÁRTOLO, P. DEVELOPMENT of novel alginate based hydrogel films for wound healing applications. **International Journal of Biological Macromolecules**, 52, p. 221–230, 2013.

PETKOSKA, A. T.; DANILOSKI, D.; D'CUNHA, N. M.; NAUMOVSKI, N.; BROACH, A. T. Edible packaging: Sustainable solutions and novel trends in food packaging. **Food Research International**, 140, n. 109981, p. 1-15, 2021.

PHILIBERT, T.; LEE, B. H.; FABIEN, N. Current status and new perspectives on chitin and chitosan as functional biopolymers. **Applied Biochemistry and Biotechnology**, 181, p. 1314–1337, 2017.

PHOEUNG, T.; SPANEDDA, M. V.; ROGER, E.; HEURTAULT, B.; FOURNEL, S.; REISCH, A.; MUTSCHLER, A.; PERRIN-SCHMITT, F.; HEMMERLÉ, J.; COLLIN, D.; RAWISO, M.; BOULMEDAIS, F.; SCHAAF, P.; LAVALLE, P.; FRISCH, B. Alginate/chitosan compact polyelectrolyte complexes: a cell and bacterial repellent material. **Chemistry of Materials**, 29, p. 10418–10425, 2017.

PORSE, H.; RUDOLPH, B. The seaweed hydrocolloid industry: 2016 updates, requirements, and outlook. **Journal of Applied Phycology**, 29, p. 2187–2200, 2017.

PRAVINATA, L.; AKHTAR, M.; BENTLEY, P. J.; MAHATNIRUNKUL, T.; MURRAY, B. S. Preparation of alginate microgels in a simple one step process via the Leeds Jet Homogenizer. **Food Hydrocolloids**, 61, p. 77–84, 2016.

PREUSS, H.; KAATS, G. Chitosan as a dietary supplement for weight loss: A review. **Current Nutrition & Food Science**, 2, p. 297–311, 2006.

PRIOR, R. L.; WU, X.; SCHAICH, K. Standardized methods for the determination of antioxidant capacity and phenolics in foods and dietary supplements. **Journal of Agricultural and Food Chemistr**y, 53, p. 4290–4302, 2005.

PU, S.; LI, J.; SUN, L.; ZHONG, L.; MA, Q. An in vitro comparison of the antioxidant activities of chitosan and green synthesized gold nanoparticles. **Carbohydrate Polymers**, 211, p. 161–172, 2019.

QIAO, C.; MA, X.; WANG, X.; LIU, L. Structure and properties of chitosan films: Effect of the type of solvent acid. **LWT - Food Science and Technology**, 135, n. 109984, p. 1-6, 2021.

QIN, Y.; JIANG, J.; ZHAO, L.; ZHANG, J.; WANG, F. Applications of Alginate as a Functional Food Ingredient. *In* A. M. GRUMEZESCU; A. M. HOLBAN (Eds.), **Biopolymers for Food Design**. Elsevier, pp. 409–429, 2018.

QUIRÓS-SAUCEDA, A. E.; AYALA-ZAVALA, J. F.; OLIVAS, G. I.; GONZÁLEZ-AGUILAR, G. A. Edible coatings as encapsulating matrices for bioactive compounds: a review. **Journal of Food Science and Technology**, 51, p. 1674–1685, 2014.

RABELO, C. A. S.; TAARJI, N.; KHALID, N.; KOBAYASHI, I.; NAKAJIMA, M.; NEVES, M. A. Formulation and characterization of water-in-oil nanoemulsions loaded with açaí berry anthocyanins: Insights of degradation kinetics and stability evaluation of anthocyanins and nanoemulsions. **Food Research International**, 106, p. 542–548, 2018.

RACHTANAPUN, C.; TANTALA, J.; KLINMALAI, P.; RATANASUMAWONG, S. Effect of chitosan on Bacillus cereus inhibition and quality of cooked rice during storage. **International Journal of Food Science & Technology**, 50, p. 2419–2426, 2015.

RAI, P.; MEHROTRA, S.; PRIYA, S.; GNANSOUNOU, E.; SHARMA, S. K. Recent advances in the sustainable design and applications of biodegradable polymers. **Bioresource Technology**, 325, n. 124739, p. 1-12, 2021.

RAJAEI, A.; HADIAN, M.; MOHSENIFAR, A.; RAHMANI-CHERATI, T.; TABATABAEI, M. A coating based on clove essential oils encapsulated by chitosan-myristic acid nanogel efficiently enhanced the shelf-life of beef cutlets. **Food Packaging and Shelf Life**, 14, p. 137–145, 2017.

RAMBABU, K.; BHARATH, G.; BANAT, F; SHOW, P.L.; COCOLETZI, H. H. Mango leaf extract incorporated chitosan antioxidant film for active food packaging. **International Journal of Biological Macromolecules**, 126, p. 1234–1243, 2019.

RAMPINO, A.; BORGOGNA, M.; BLASI, P.; BELLICH, B.; CESÀRO, A. Chitosan nanoparticles: Preparation, size evolution and stability. **International Journal of Pharmaceutics**, 455, p. 219–228, 2013.

RE, R.; PELLEGRINI, N.; PROTEGGENTE, A.; PANNALA, A.; YANG, M.; RICE-EVANS, C. Antioxidant activity applying an improved ABTS radical cation decolorization assay. **Free Radical Biology and Medicine**, 26, p. 1231–1237, 1999.

REN, L.; YAN, X.; ZHOU, J.; TONG, J.; SU, X. Influence of chitosan concentration on mechanical and barrier properties of corn starch/chitosan films. **International Journal of Biological Macromolecules**, 105, p. 1636–1643, 2017.

REN, X.; HOU, T.; LIANG, Q.; ZHANG, X.; HU, D.; XU, B.; CHEN, X.; CHALAMAIAH, M.; MA, H. Effects of frequency ultrasound on the properties of zein-chitosan complex coacervation for resveratrol encapsulation. **Food Chemistry**, 279, p. 223–230, 2019.

RIAZ, A.; LEI, S.; AKHTAR; H. M. S.; WAN, P.; CHEN, D.; JABBAR, S.; ABID, M.; HASHIM, M. M.; ZENG, X. Preparation and characterization of chitosan-based antimicrobial active food packaging film incorporated with apple peel polyphenols. **International Journal of Biological Macromolecules**, 114, p. 547–555, 2018.

RIBEIRO-SANTOS, R.; ANDRADE, M.; MELO, N. R. DE; SANCHES-SILVA, A. Use of essential oils in active food packaging: Recent advances and future trends. **Trends in Food Science and Technology**, 61, p. 132–140, 2017.

RISCH, S. J. Food Packaging History and Innovations. **Journal of Agricultural and Food Chemistry**, 57, p. 8089–8092, 2009.

RIVERO, S.; DAMONTE, L.; GARCÍA, M. A.; PINOTTI, A. An insight into the role of glycerol in chitosan films. **Food Biophysics**, 11, p. 117–127, 2016.

ROCCA-SMITH, J. R.; MARCUZZO, E.; KARBOWIAK, T.; CENTA, J.; GIACOMETTI, M.; SCAPIN, F.; VENIR, E.; SENSIDONI, A.; DEBEAUFORT, F. Effect of lipid incorporation on functional properties of wheat gluten based edible films. **Journal of Cereal Science**, 69, p. 275–282, 2016.

RODRIGUES, D. C.; CUNHA, A. P.; BRITO, E. S.; AZEREDO, H. M. C.; GALLÃO, M. I. Mesquite seed gum and palm fruit oil emulsion edible films: Influence of oil content and sonication. **Food Hydrocolloids**, 56, p. 227–235, 2016.

RODRÍGUEZ, J.; MARTÍN, M. J.; RUIZ, M. A.; CLARES, B. Current encapsulation strategies for bioactive oils: From alimentary to pharmaceutical perspectives. **Food Research International**, 83, p. 41–59, 2016.

ROHMAN, A.; MAN, Y. B. C. Fourier transform infrared (FTIR) spectroscopy for analysis of extra virgin olive oil adulterated with palm oil. **Food Research International**, 43(3), p. 886–892, 2010.

RUFINO, M. DO S. M.; PÉREZ-JIMÉNEZ, J.; ARRANZ, S.; ALVES, R. E.; DE BRITO, E. S.; OLIVEIRA, M. S. P.; SAURA-CALIXTO, F. Açaí (*Euterpe oleraceae*) 'BRS Pará': A tropical fruit source of antioxidant dietary fiber and high antioxidant capacity oil. **Food Research International,** 44, 2100–2106, 2011.

RUFINO, M. S. M.; ALVES, R. E.; BRITO, E. S.; PEREZ-JIMENEZ, J.; SAURA-CALIXTO, F. D. Total phenolic content and antioxidant activity in acerola, açaí, mangaba and uvaia fruits by DPPH method. **Acta Horticulturae**, 841, p. 459–462, 2009.

RUI, L.; XIE, M.; HU, B.; ZHOU, L.; YIN, D.; ZENG, X. A comparative study on chitosan/gelatin composite films with conjugated or incorporated gallic acid. **Carbohydrate Polymers**, 173, p. 473–481, 2017.

RUIZ-NAVAJAS, Y.; VIUDA-MARTOS, M.; SENDRA, E.; PEREZ-ALVAREZ, J. A.; FERNÁNDEZ-LÓPEZ, J. In vitro antibacterial and antioxidant properties of chitosan edible films incorporated with *Thymus moroderi* or *Thymus piperella* essential oils. **Food Control**, 30, p. 386–392, 2013.

RUTZ, J. K.; BORGES, C. D.; ZAMBIAZI, R. C.; CRIZEL-CARDOZO, M. M.; KUCK, L. S.; NOREÑA, C. P. Z. Microencapsulation of palm oil by complex coacervation for application in food systems. **Food Chemistry**, 220, p. 59–66, 2017.

RUTZ, J. K.; BORGES, C. D.; ZAMBIAZI, R. C.; DA ROSA, C. G.; DA SILVA, M. M. Elaboration of microparticles of carotenoids from natural and synthetic sources for applications in food. **Food Chemistry**, 202, p. 324–333, 2016.

SABERI, B.; THAKUR, R.; VUONG, Q. V.; CHOCKCHAISAWASDEE, S.; GOLDING, J. B.; SCARLETT, C. J.; STATHOPOULOS, C. E. Optimization of physical and optical properties of biodegradable edible films based on pea starch and guar gum. **Industrial Crops and Products**, 86, p. 342–352, 2016.

SADAHIRA, M. S.; RODRIGUES, M. I.; AKHTAR, M.; MURRAY, B. S.; NETTO, F. M. Influence of pH on foaming and rheological properties of aerated high sugar system with egg white protein and hydroxypropylmethylcellulose. **LWT - Food Science and Technology**, 89, p. 350–357, 2018.

SÆTHER, H. V.; HOLME, H. K.; MAURSTAD, G.; SMIDSRØD, O.; STOKKE, B. T. Polyelectrolyte complex formation using alginate and chitosan. **Carbohydrate Polymers**, 74, p. 813–821, 2008.

SAHARIAH, P.; MÁSSON, M. Antimicrobial chitosan and chitosan derivatives: A review of the structure-activity relationship. **Biomacromolecules**, 18, p. 3846–3868, 2017.

SALGADO, P. R.; ORTIZ, C. M.; MUSSO, Y. S.; DI GIORGIO, L.; MAURI, A. N. Edible films and coatings containing bioactives. **Current Opinion in Food Science**, 5, p. 86–92, 2015.

SANCHEZ-SALVADOR, J. L.; BALEA, A.; MONTE, M. C.; NEGRO, C.; BLANCO, A. Chitosan grafted/cross-linked with biodegradable polymers: A review. **International Journal of Biological Macromolecules,** 178, p. 325–343, 2021.

SANTOS, G. A.; CARVALHO, A. A. C.; OLIVEIRA, A. P.; NAOZUKA, J.; MATTA, F. V.; FELIPE-SOTELO, M.; WARD, N. I.; CORRÊA, N. C. F.; NOMURA, C. S. Bioaccessibility of essential elements in açaí (*Euterpe oleracea* mart.) pulp. **ACS Food Science & Technology**, *online,* 2021 Available at<https://doi.org/10.1021/acsfoodscitech.1c00070> accessed on Jun 06, 2021.

SANTOS, M. B.; CARVALHO, M. G.; GARCIA-ROJAS, E. E. Carboxymethyl tara gum-lactoferrin complex coacervates as carriers for vitamin D3: Encapsulation and controlled release. **Food Hydrocolloids**, 112, n. 106347, p. 1-10, 2021.

SANTOS, M. B.; DA COSTA, N. R.; GARCIA-ROJAS, E. E. Interpolymeric Complexes Formed Between Whey Proteins and Biopolymers: Delivery Systems of Bioactive Ingredients. **Comprehensive Reviews in Food Science and Food Safety**, 17, p. 792–805, 2018.

SARMENTO, B.; FERREIRA, D.; VEIGA, F.; RIBEIRO, A. Characterization of insulin-loaded alginate nanoparticles produced by ionotropic pre-gelation through DSC and FTIR studies. **Carbohydrate Polymers**, 66, p. 1–7, 2006.

SHAHBAZI, Y. The properties of chitosan and gelatin films incorporated with ethanolic red grape seed extract and *Ziziphora clinopodioides* essential oil as biodegradable materials for active food packaging. **International Journal of Biological Macromolecules**, 99, p. 746–753, 2017.

SHAHIDI, F.; ZHONG, Y. Measurement of antioxidant activity. **Journal of Functional Foods**, 18, p. 757–781, 2015.

SHARMA, S.; RAO, T. V. R. Xanthan gum based edible coating enriched with cinnamic acid prevents browning and extends the shelf-life of fresh-cut pears. **LWT - Food Science and Technology,** 62, p. 791–800, 2015.

SHEVKANI, K.; SINGH, N.; KAUR, A.; RANA, J. C. Structural and functional characterization of kidney bean and field pea protein isolates: A comparative study. **Food Hydrocolloids**, 43, p. 679–689, 2015.

SHI, W.-J.; TANG, C.-H.; YIN, S.-W.; YIN, Y.; YANG, X.-Q.; WU, L.-Y.; ZHAO, Z.-G. Development and characterization of novel chitosan emulsion films via pickering emulsions incorporation approach. **Food Hydrocolloids**, 52, p. 253–264, 2016.

SHISHIR, M. R. I.; XIE, L.; SUN, C.; ZHENG, X.; CHEN, W. Advances in micro and nano-encapsulation of bioactive compounds using biopolymer and lipid-based transporters. **Trends in Food Science and Technology**, 78, p. 34–60, 2018.

SIANO, F.; PICARIELLO, G.; VASCA, E. Coulometrically determined antioxidant capacity (CDAC) as a possible parameter to categorize extra virgin olive oil. **Food Chemistry**, 354, n. 129564, p. 1-9, 2021.

SILVA, M. P.; CUNHA, V. M. B.; SOUSA, S. H. B.; MENEZES, E. G. O.; BEZERRA, P. D. N.; FARIAS NETO, J. T.; FILHO, G. N. R.; ARAÚJO, M. E.; CARVALHO JR., R. N. Supercritical CO_2 extraction of lyophilized açaí (*Euterpe oleracea* Mart.) pulp oil from three municipalities in the state of Pará, Brazil. **Journal of CO_2 Utilization**, 31, p. 226–234, 2019.

SILVA, S. S.; RODRIGUES, L. C.; FERNANDES, E. M.; GOMES, J. M.; VILAS-BOAS, Â.; PIRRACO, R. P.; REIS, R. L. Approach on chitosan/virgin coconut oil-based emulsion matrices as a platform to design superabsorbent materials. **Carbohydrate Polymers**, 249, n. 116839, p. 1-10, 2020a.

SILVA, T. N.; REYNAUD, F.; PICCIANI, P. H. S.; HOLANDA E SILVA, K. G.; BARRADAS, T. N. Chitosan-based films containing nanoemulsions of methyl salicylate: Formulation development, physical-chemical and in vitro drug release characterization. **International Journal of Biological Macromolecules**, 164, p 2558–2568, 2020b.

SILVA-WEISS, A.; IHL, M.; SOBRAL, P. J. A.; GÓMEZ-GUILLÉN, M. C.; BIFANI, V. Natural Additives in Bioactive Edible Films and Coatings: Functionality and Applications in Foods. **Food Engineering Reviews**, 5, p. 200–216, 2013.

SINGLETON, V. L.; ORTHOFER, R.; LAMUELA-RAVENTÓS, R. M. Analysis of total phenols and other oxidation substrates and antioxidants by means of Folin-Ciocalteu reagent, In ABELSON, J.; SIMON, M.; VERDINE, G.; PYLE, A. (Eds.)

Methods in Enzymology. ISSN: 0076-6879. Academic Press: 299, 1999. p.152-178.

SIRACUSA, V.; LOTTI, N. Biobased Plastics for Food Packaging. *In* **Reference Module in Food Science**. Elsevier Inc, 2018, p. 1–19.

SIRIPATRAWAN, U.; HARTE, B. R. Physical properties and antioxidant activity of an active film from chitosan incorporated with green tea extract. **Food Hydrocolloids**, 24, p. 770–775, 2010.

SIRIPATRAWAN, U.; VITCHAYAKITTI, W. Improving functional properties of chitosan films as active food packaging by incorporating with propolis. **Food Hydrocolloids**, 61, p. 695–702, 2016.

SLATNAR, A.; MIKULIC-PETKOVSEK, M.; STAMPAR, F.; VEBERIC, R.; SOLAR, A. HPLC-MS n identification and quantification of phenolic compounds in hazelnut kernels, oil and bagasse pellets. **Food Research International**, 64, p. 783–789, 2014.

SMITH, E. L.; ABBOTT, A. P.; RYDER, K. S. Deep eutectic solvents (DESs) and their applications. **Chemical Reviews**, 114, p. 11060–11082, 2014.

SOARES, J.; MIGUEL, I.; VENÂNCIO, C.; LOPES, I.; OLIVEIRA, M. Public views on plastic pollution: Knowledge, perceived impacts, and pro-environmental behaviours. **Journal of Hazardous Materials**, 412, n. 125227, p. 1-8, 2021.

SOHAIL, M.; SUN, D.-W.; ZHU, Z. Recent developments in intelligent packaging for enhancing food quality and safety. **Critical Reviews in Food Science and Nutrition**, 58, p. 2650–2662, 2018.

SOKOLOVA, M. P.; SMIRNOV, M. A.; SAMAROV, A. A.; BOBROVA, N. V.; VOROBIOV, V. K.; POPOVA, E. N.; FILIPPOVA, E.; GEYDT, P.; LAHDERANTA, E.; TOIKKA, A. M. Plasticizing of chitosan films with deep eutectic mixture of malonic acid and choline chloride. **Carbohydrate Polymers**, 197, p. 548–557, 2018.

SOLOMEVICH, S. O.; DMITRUK, E. I.; BYCHKOVSKY, P. M.; SALAMEVICH, D. A.; KUCHUK, S. V.; YURKSHTOVICH, T. L. Biodegradable polyelectrolyte complexes of chitosan and partially crosslinked dextran phosphate with potential for biomedical applications. **International Journal of Biological Macromolecules,** 169, p. 500–512, 2021.

SOUSA, A. M. M.; SOUZA, H. K. S.; LATONA, N.; LIU, C. K.; GONÇALVES, M. P.; LIU, L. Choline chloride based ionic liquid analogues as tool for the fabrication of agar films with improved mechanical properties. **Carbohydrate Polymers**, 111, p. 206–214, 2014.

STONE, A. K.; KARALASH, A.; TYLER, R. T.; WARKENTIN, T. D.; NICKERSON, M. T. Functional attributes of pea protein isolates prepared using different extraction methods and cultivars. **Food Research International**, 76, p. 31–38, 2015.

SUN, L.; SUN, J.; CHEN, L.; NIU, P.; YANG, X.; GUO, Y. Preparation and characterization of chitosan film incorporated with thinned young apple polyphenols as an active packaging material. **Carbohydrate Polymers**, 163, p. 81–91, 2017.

SUN, Q.; SUN, C.; XIONG, L. Mechanical, barrier and morphological properties of pea starch and peanut protein isolate blend films. **Carbohydrate Polymers,** 98, p. 630–637, 2013.

SUN, Y.; LIU, Z.; ZHANG, L.; WANG, X.; LI, L. Effects of plasticizer type and concentration on rheological, physico-mechanical and structural properties of chitosan/zein film. **International Journal of Biological Macromolecules**, 143, p. 334–340, 2020.

TAMM, F.; HERBST, S.; BRODKORB, A.; DRUSCH, S. Functional properties of pea protein hydrolysates in emulsions and spray-dried microcapsules. **Food Hydrocolloids**, 58, p. 204–214, 2016.

TAVASSOLI-KAFRANI, E.; SHEKARCHIZADEH, H.; MASOUDPOUR-BEHABADI, M. Development of edible films and coatings from alginates and carrageenans. **Carbohydrate Polymers**, 137, p. 360–374, 2016.

TIMILSENA, Y. P.; AKANBI, T. O.; KHALID, N.; ADHIKARI, B.; BARROW, C. J. Complex coacervation: Principles, mechanisms and applications in microencapsulation. **International Journal of Biological Macromolecules,** 121, p. 1276–1286, 2019.

TIMILSENA, Y. P.; WANG, B.; ADHIKARI, R.; ADHIKARI, B. Advances in microencapsulation of polyunsaturated fatty acids (PUFAs)-rich plant oils using complex coacervation: A review. **Food Hydrocolloids**, 69, p. 369–381, 2017.

TRIVEDI, V.; SATIA, M.; DESCHAMPS, A.; MAQUET, V.; SHAH, R.; ZINZUWADIA, P.; TRIVEDI, J. Single-blind, placebo controlled randomised clinical study of chitosan for body weight reduction. **Nutrition Journal**, 15, p. 1-12, 2016

TUHIN, M. O.; RAHMAN, N.; HAQUE, M. E.; KHAN, R. A.; DAFADER, N. C.; ISLAM, R.; NURNABI, M.; TONNY, W. Modification of mechanical and thermal property of chitosan–starch blend films. **Radiation Physics and Chemistry**, 81, p. 1659–1668, 2012.

TULBEK, M. C.; LAM, R. S. H.; WANG, Y. C.; ASAVAJARU, P.; LAM, A. Pea: A sustainable vegetable protein crop. *In* S. R. NADATHUR; J. P. D. WANASUNDARA; L. SCANLIN (Eds.), **Sustainable Protein Sources**. Elsevier Inc., pp. 145–164, 2017.

TWEDE, D. The packaging technology and science of ancient transport amphoras. **Packaging Technology and Science**, 15, p. 181–195, 2002.

UNILEVER. Press releases - **Unilever announces ambitious new commitments for a waste-free world**. 2019. Available at <

https://www.unilever.com/news/press-releases/2019/unilever-announces-ambitious-new-commitments-for-a-waste-free-world.html> accessed on April 26, 2021.

VALERO, D.; DÍAZ-MULA, H. M.; ZAPATA, P. J.; GUILLÉN, F.; MARTÍNEZ-ROMERO, D.; CASTILLO, S.; SERRANO, M. Effects of alginate edible coating on preserving fruit quality in four plum cultivars during postharvest storage. **Postharvest Biology and Technology**, 77, p. 1–6, 2013.

VAN DEN BROEK, L. A. M.; KNOOP, R. J. I.; KAPPEN, F. H. J.; BOERIU, C. G. Chitosan films and blends for packaging material. **Carbohydrate Polymers**, 116, p. 237–242, 2015.

VAN DEN OEVER, M.; MOLENVELD, K.; VAN DER ZEE, M.; BOS, H. Bio-based and biodegradable plastics: facts and figures: focus on food packaging in the Netherlands. **Wageningen Food & Biobased Research**, 1722, 65p., 2017. Available at <https://doi.org/10.18174/408350> accessed on April 8, 2021.

VERLEE, A.; MINCKE, S.; STEVENS, C. V. Recent developments in antibacterial and antifungal chitosan and its derivatives. **Carbohydrate Polymers**, 164, p. 268–283, 2017.

VERMA, M. K.; SHAKYA, S.; KUMAR, P.; MADHAVI, J.; MURUGAIYAN, J.; RAO, M. V. R. Trends in packaging material for food products: historical background, current scenario, and future prospects. **Journal of Food Science and Technology**, p. 1-14, 2021.

VILELA, C.; PINTO, R. J. B.; COELHO, J.; DOMINGUES, M. R. M.; DAINA, S.; SADOCCO, P.; SANTOS, S. A. O.; FREIRE, C. S. R. Bioactive chitosan/ellagic acid films with UV-light protection for active food packaging. **Food Hydrocolloids**, 73, p. 120–128, 2017.

VITAL, A. C. P.; GUERRERO, A.; ORNAGHI, M. G.; KEMPINSKI, E. M. B. C.; SARY, C.; MONTESCHIO, J. D. O.; MATUMOTO-PINTRO, P. T.; RIBEIRO, R. P.; PRADO, I. N. Quality and sensory acceptability of fish fillet (*Oreochromis niloticus*) with alginate-based coating containing essential oils. **Journal of Food Science and Technology**, 55, p. 4945–4955, 2018.

WANG, H.; DING, F.; MA, L.; ZHANG, Y. Edible films from chitosan-gelatin: Physical properties and food packaging application. **Food Bioscience**, 40, n. 100871, p. 1-17, 2021.

WANG, H.; QIAN, J.; DING, F. Emerging chitosan-based films for food packaging applications. **Journal of Agricultural and Food Chemistry**, 66, p. 395–413, 2018.

WANG, H.; WAN, Y.; WANG, W.; LI, W.; ZHU, J. Effect of calcium ions on the III steps of self-assembly of SA investigated with atomic force microscopy. **International Journal of Food Properties**, 21, 1995–2006, 2018.

WANG, L.; KHOR, E.; LIM, L.-Y. Chitosan–alginate–$CaCl_2$ system for membrane coat application. **Journal of Pharmaceutical Sciences**, 90, p. 1134–1142, 2001.

WANG, X.; ZENG, Q.; DEL MAR CONTRERAS, M.; WANG, L. Profiling and quantification of phenolic compounds in Camellia seed oils: Natural tea polyphenols in vegetable oil. **Food Research International**, 102, p. 184–194, 2017.

WANG, Y.; KIMURA, K.; DUBIN, P. L.; JAEGER, W. Polyelectrolyte−micelle coacervation: effects of micelle surface charge density, polymer molecular weight, and polymer/surfactant ratio. **Macromolecules**, 33, p. 3324–3331, 2000.

WANI, T. A.; MASOODI, F. A.; GANI, A.; BABA, W. N.; RAHMANIAN, N.; AKHTER, R.; WANI, I. A.; AHMAD, M. Olive oil and its principal bioactive compound: Hydroxytyrosol – A review of the recent literature. **Trends in Food Science & Technology**, 77, p. 77–90, 2018.

WEI, Y.; CAI, Z.; WU, M.; GUO, Y.; TAO, R.; LI, R.; WANG, P.; MA, A.; ZHANG, H. Comparative studies on the stabilization of pea protein dispersions by using various polysaccharides. **Food Hydrocolloids**, 98, n. 105233, p. 1-15, 2020.

WONG, C. Y.; WONG; W. Y.; WALVEKAR, R.; LOH, K. S.; KHALID, M.; LIM, K. L. Effect of deep eutectic solvent in proton conduction and thermal behaviour of chitosan-based membrane. **Journal of Molecular Liquids**, 269, p. 675–683, 2018.

WU, T.; HUANG, J.; JIANG, Y.; HU, Y.; YE, X.; LIU, D.; CHEN, J. Formation of hydrogels based on chitosan/alginate for the delivery of lysozyme and their antibacterial activity. **Food Chemistry**, 240, p. 361–369, 2018.

XIAO, J.; WANG, W.; HUANG, Q.; LI, Y. Edible Delivery Systems Based on Favorable Interactions for Encapsulation of Phytochemicals. **Reference Module in Food Science**, 1, p. 1–6, 2018.

YAMAGUCHI, K. K. DE L.; PEREIRA, L. F. R.; LAMARÃO, C. V.; LIMA, E. S.; VEIGA-JUNIOR, V. F. D. Amazon acai: Chemistry and biological activities: A review. **Food Chemistry**, 179, p. 137–151, 2015.

YANG, J.; ZAMANI, S.; LIANG, L.; CHEN, L. Extraction methods significantly impact pea protein composition, structure and gelling properties. **Food Hydrocolloids**, 117, n. 106678, p. 1-13, 2021.

YANG, T. S.; LIU, T. T.; LIN, I. H. Functionalities of chitosan conjugated with stearic acid and gallic acid and application of the modified chitosan in stabilizing labile aroma compounds in an oil-in-water emulsion. **Food Chemistry**, 228, p. 541–549, 2017.

YAROSLAVOV, A. A.; EFIMOVA, A. A.; KRASNIKOV, E. A.; TROSHEVA, K. S.; POPOV, A. S.; MELIK-NUBAROV, N. S.; KRIVTSOV, G. G. Chitosan-based multi-liposomal complexes: Synthesis, biodegradability and cytotoxicity. **International Journal of Biological Macromolecules**, 177, p. 455–462, 2021.

YOU, G.; LIU, X. L.; ZHAO, M. M. Preparation and characterization of hsian-tsao gum and chitosan complex coacervates. **Food Hydrocolloids**, 74, p. 255–266, 2018.

YOUNES, I.; RINAUDO, M. Chitin and chitosan preparation from marine sources. Structure, properties and applications. **Marine Drugs**, 13, 1133–1174, 2015.

YUAN, Y.; KONG, Z. Y.; SUN, Y. E.; ZENG, Q. Z.; YANG, X. Q. Complex coacervation of soy protein with chitosan: Constructing antioxidant microcapsule for algal oil delivery. **LWT - Food Science and Technology**, 75, p. 171–179, 2017.

ZANETTI, M.; CARNIEL, T. K.; DALCANTON, F.; DOS ANJOS, R. S.; RIELLA, H. G.; DE ARAÚJO, P. H. H.; DE OLIVEIRA, D.; FIORI, M. A. Use of encapsulated natural compounds as antimicrobial additives in food packaging: A brief review**.** **Trends in Food Science and Technology**, 81, p. 51–60, 2018.

ZDANOWICZ, M.; WILPISZEWSKA, K.; SPYCHAJ, T. Deep eutectic solvents for polysaccharides processing. A review. **Carbohydrate Polymers**, 200, p. 361–380, 2018.

ZHAO, Y.; KHALID, N.; SHU, G.; NEVES, M. A.; KOBAYASHI, I.; NAKAJIMA, M. Complex coacervates from gelatin and octenyl succinic anhydride modified kudzu starch: Insights of formulation and characterization. **Food Hydrocolloids**, 86, p. 70–77, 2019.

ZHONG, Y.; LI, Y. Effects of storage conditions and acid solvent types on structural, mechanical and physical properties of kudzu starch (*Pueraria lobata*)-chitosan composite films. **Starch - Stärke**, 63, p. 579–586, 2011.

ZHOU, W.; HE, Y.; LIU, F.; LIAO, L.; HUANG, X.; LI, R.; ZOU, Y.; ZHOU, L.; ZOU, L.; LIU, Y.; RUAN, R.; LI, J. Carboxymethyl chitosan-pullulan edible films enriched with galangal essential oil: Characterization and application in mango preservation. **Carbohydrate Polymers**, 256, n. 117579, p. 1-9, 2021.

8. SUPPLEMENTARY MATERIAL

SUPPLEMENT 1 – Fatty acids profile from açaí oil

Table S1. Fatty acids composition of açaí oil.

FAMEs (%)	Açaí oil			
	In this work*	BATISTA et al., 2016	RUFINO et al., 2011	SILVA et al., 2019
Saturated				
Myristic acid - C14:0	Traces	0.13 – 0.42	ND	0.07 – 0.19
Palmitic acid - C16:0	18.9 ± 4.3	23.47 – 90.86	25.3	21.15 – 21.79
Stearic acid - C18:0	61.8 ± 0.3	0.8 – 5.35	1.4	ND
Arachidic acid - C20:0	0.2 ± 0.1	0.08 – 0.10	ND	0.08 -0.18
Monounsaturated				
Palmitoleic acid C18:1	8.5 ± 0.6	0.23 – 65.81	56.9	3.43 – 3.90
Gondoic acid C20:1	0.14 ± 0.02	ND	ND	ND
Erucic acid C22:1	Traces	ND	ND	ND
Polyunsaturated				
Linoleic acid - C18:2	8.6 ± 1.2	ND – 15.54	10.6	9.45 – 12.31
SFA	81 ± 4	26.22 – 99.67	26.7	22.18 – 23.01
MUFA	8.7 ± 0.6	0.31 – 70.46	62.3	65.2 – 67.7
PUFA	8.6 ± 1.2	ND – 15.54	11.1	9.54 – 12.48
PUFA/SFA	0.1	<0.16	0.4	0.41 – 0.56

*Results are expressed as mean ± standard deviation (n = 2). ND = Not determined.

SUPPLEMENT 2 – MS chromatograms of the phenolic compounds from açaí oil

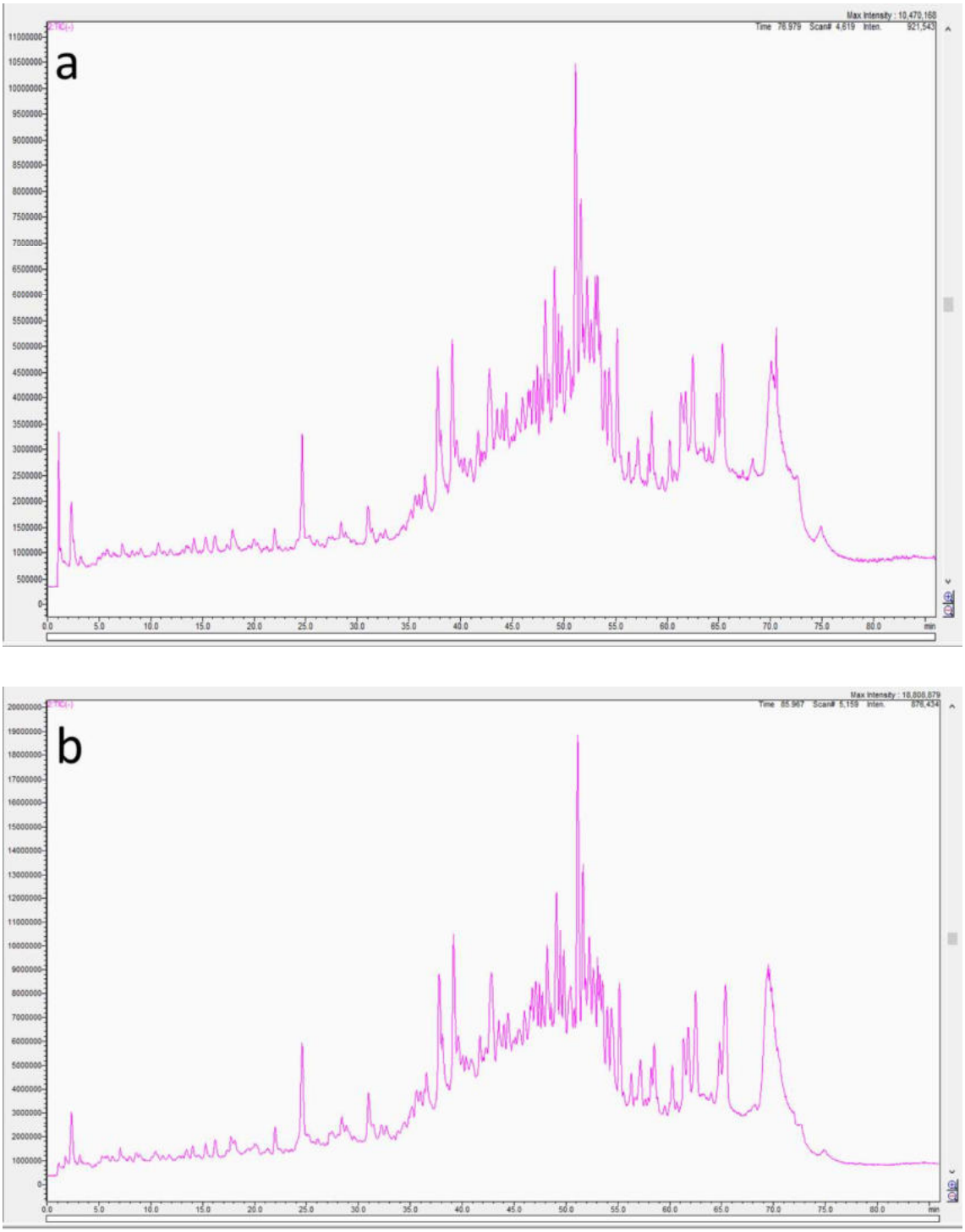

Figure S1. MS chromatograms obtained for açaí oil extracts at, (a) 1 mg mL^{-1} and (b) at 2 mg mL^{-1} concentrations by ESI on negative mode.

SUPPLEMENT 3 – DSC curves of CS:SA-AO

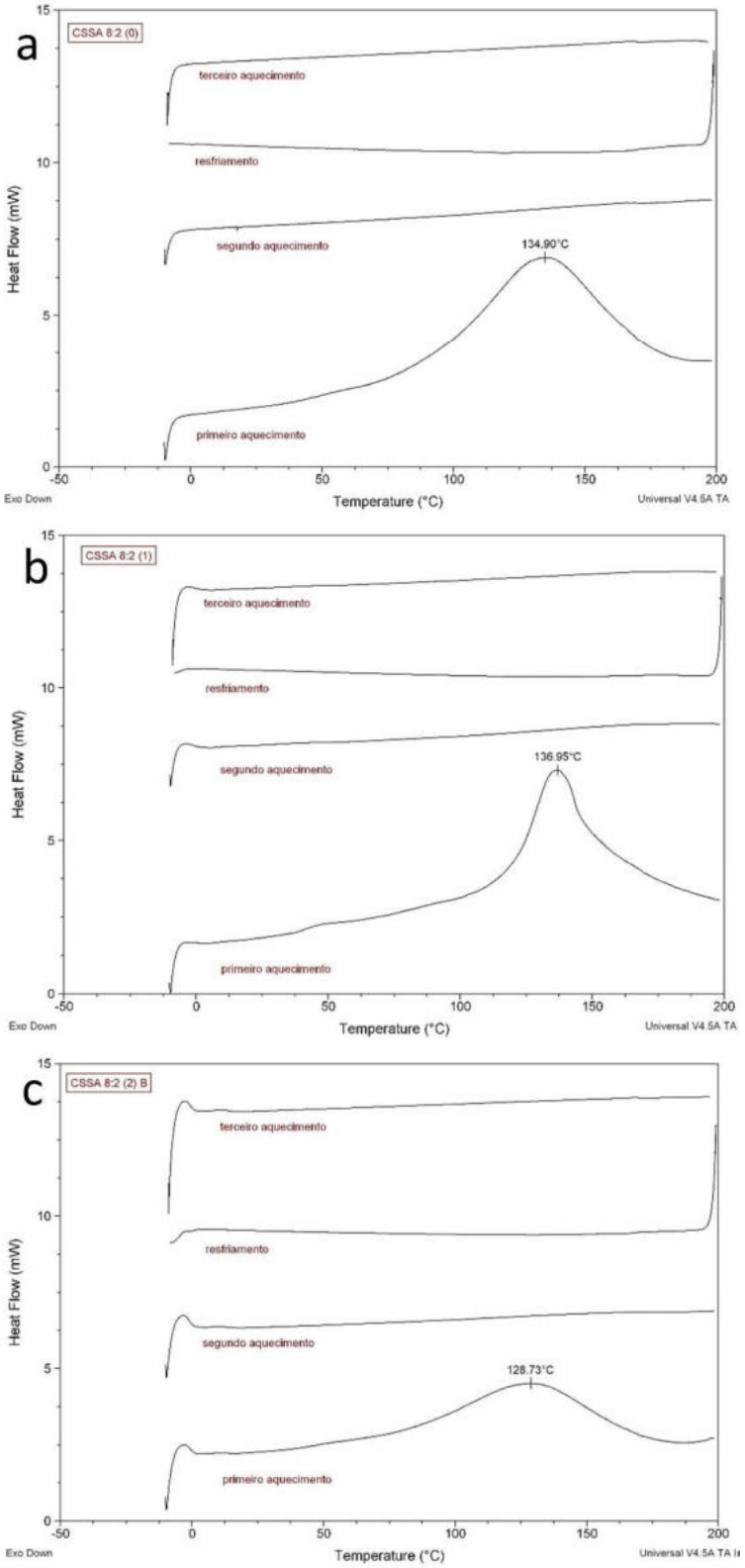

Figure S2. DSC curves of CS:SA-AO for samples (a) control sample (unloaded), (b) AA (0.25% AO and 0% $CaCl_2$) and (c) BA (0.75% AO and 0% $CaCl_2$).

SUPPLEMENT 4 – DSC curves of CS:SA-AO

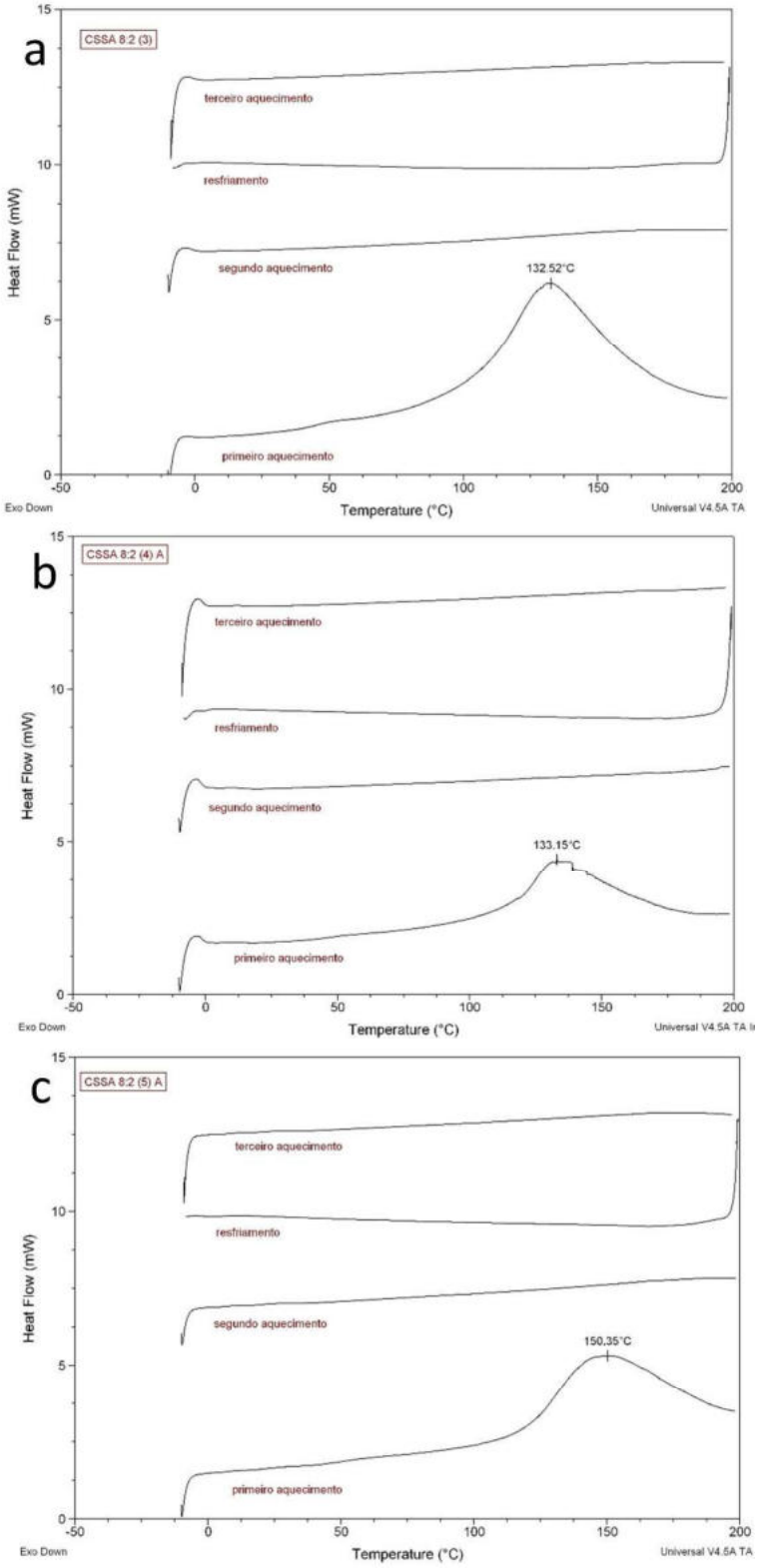

Figure S3. DSC curves of CS:SA-AO for samples (a) AB (0.25% AO and 1.0% $CaCl_2$), (b) BB (0.75% AO and 1.0% $CaCl_2$) and (c) CC (0.5% AO and 0.5% $CaCl_2$).

SUPPLEMENT 5 – Digital pictures of CS-DES-AO films

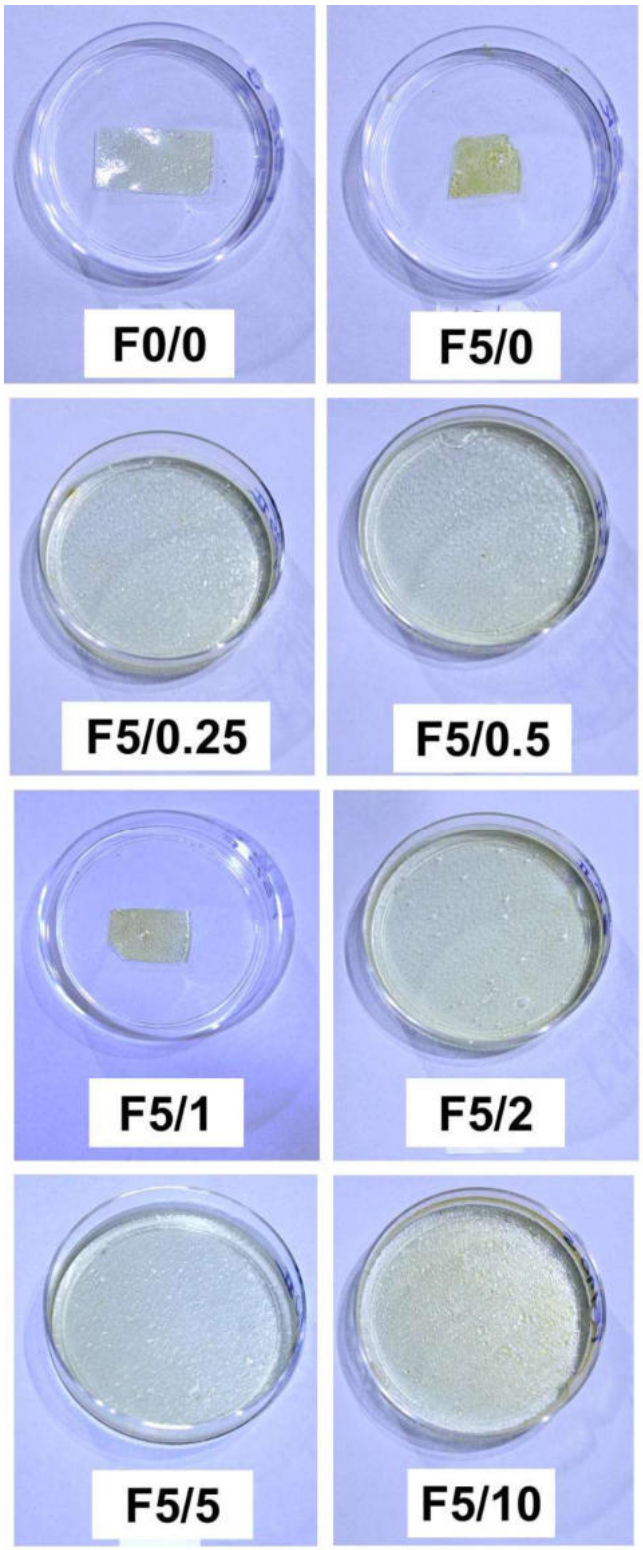

Figure S4. Digital pictures of the CS-DES-AO films after more than one year of storage.